IMPERIAL COLLEGE OF SCIENCE, TECHNOLOGY
AND MEDICINE
(University of London)

THE ANALYSIS AND IDENTIFICATION OF FRICTION JOINT PARAMETERS IN THE DYNAMIC RESPONSE OF STRUCTURES

by

REN YING

A thesis submitted to the University of London for the degree of Doctor of Philosophy.

Department of Mechanical Engineering
Imperial College, London SW7 2AZ
U.K.

March 1992

To my parents and my wife Qin

ABSTRACT

This thesis is on the application of friction in joints for controlling the dynamic response of structures. It is in three parts.

Part one is concerned with modelling the friction joint when relative motion occurs between components in the tangential direction. When the friction joint is subjected to a tangential load, it usually deforms nonlinearly. The methods available to model the friction joints are investigated and summarised as using 1) a dry friction element, 2) a bilinear element, and 3) a microslip element. A new microslip element is proposed and verified using the experimental data, and is found to be more representative than other models.

Part two is concerned with the prediction of the response of a structure with nonlinear joints. The most commonly used methods are numerical integration in the time domain. The methods available are discussed and two of these methods are found to be particularly useful. The most attractive property of these two methods is that both are unconditionally stable. One of the methods is also explicit, hence it is computationally efficient. Because the ordinary start up process for the explicit method can be erroneous unless the time step length is very small, a new start up process incorporating the implicit method is proposed. Methods for reducing the size of the problem are also investigated.

Even if the condensation method to reduce the size of the problem is applied, the time domain solution can still be expensive. If the excitation is periodic and only the steady state response is of interest, some cheap, but approximate methods can be used. The most commonly used method, the Harmonic Balance (HB) Method, is investigated. In order to improve the accuracy, a new Higher-order Harmonic Balance Method (HHB) is developed. Two perturbation approaches and the Newton-Raphson algorithm are found to be effective in solving the nonlinear equations. Linear and quadratic approximation methods for the initial estimation of a newly perturbed system are developed.

Part three consists of substructure coupling and joint identification. Both approaches use the Frequency Response Function data (FRF).

A new generalized coupling method is developed and is found to be computationally efficient and simple to program. It is also general and can be widely applied. The method is particularly effective and efficient in detecting the linear-dependent joint coordinates.

Two new generalized joint identification methods are developed, and techniques to improve the accuracy of the identified joint parameters are investigated. The nature of the joint identification problem is also studied.

Both of the approaches discussed in part three are verified by experiment.

ACKNOWLEDGMENTS

The author would like to express his gratitude to Dr. C.F. Beards, for his help, encouragement and guidance throughout the duration of this work, and for his sustained advice in the preparation of the manuscript.

Special thanks are due to Professor D.J. Ewins and Professor P. Grootenhuis for their kindness and help during some difficult periods of this research.

Many members of the staff are also acknowledged, particularly Mr. D.A. Robb, Mr. D. Hitchins and Dr. M. Imregun for their helpful guidance in the conducting of experimental and computing work.

For their friendly cooperation and useful discussion, the author also expresses his sincere gratitude to many former and present colleagues in the Dynamics Section, particularly to R.M. Lin, A Nobari and H. Jung.

The author is also very grateful to Professor K. Willams (Visiting professor from Saskachewan University, Canada) and Ms. J. Pugh (from the British College of Optometrists) for their valuable comments on some parts of the thesis.

The author is indebted to the British Council and the Chinese Government for providing the financial support.

Finally, very special thanks to my wife, Qin, for sharing all the good and bad moments and for her love and sacrifice. Without her full support and encouragement, this thesis would not have been brought to completion.

NOMENCLATURE

The following is a list of the principal symbols used in this thesis. Because of the several branches covered, some symbols might denote different meanings, these symbols are defined where they occur in the text.

A	area of the cross section
$A_1,A_2,....,A_n$	real parts of the harmonics of the force F in joint
a	parameter for modelling a joint (Cp2)
	parameter in algorithm two(Cp3)
$a_1,a_2,....,a_n$	real parts of the harmonics of the displacement x(Cp4)
a_e	effective parameter in algorithm two(Cp3)
$B_1,B_2,....,B_n$	imaginary parts of the harmonics of the force F in joint(Cp4)
b	parameter for modelling a joint (Cp2)
$b_1,b_2,....,b_n$	imaginary parts of the harmonics of the displacement x(Cp4)
c	viscous damping
E	energy dissipation per cycle(Cp2)
	Young's modulus (Cp2)
f	function
	frequency
	force
F, F(t)	force (in time domain)
$F_1,F_2,...,F_n$	amplitudes of harmonics of the force in a joint
F_i	force of initial loading
F_n	nonlinear force
F_r	reloading force
F_u	unloading force
g	function
h	receptance element in [H]
	stiffness area(Cp2)
	height
I	second moment of area
k	stiffness
	initial stiffness of the joint in the tangential direction
L	length
M	torque
	mass
N	normal clamping force
P, p(t)	excitation force (in time domain)
$P_1,P_2,...,P_n$	amplitudes of harmonics of the excitation force
r	radius

s	stress over the stiffness area
T	period of vibration(Cp4)
	tangential force(Cp2)
T_{max}	maximum tangential shear force
t	time
u	deformation at a joint
u_i	deformation of an initial loading
u_r	deformation of a reloading
u_u	deformation of an unloading
v	velocity
x	displacement
	coordinate
x(t)	displacement (in time domain)
x_0	displacement before x_1
x_1	displacement at last time point
$X_1, X_2, \ldots, X_n$	amplitude of harmonics of displacement
x_2	displacement at current time point
W,w	width
[C]	viscous damping matrix
[D]	hysteretic damping matrix
$[H_A]$	receptance matrix of an assembly
$[H_{\alpha\beta}]$	receptance matrix between coordinates α and β (α,β=a,b,c,g,n,m i, j)
$[H_{ii}]$	receptance matrix between joint coordinates
$[H_{ij}]$	receptance matrix between excitation and joint coordinates
$[H_S]$	receptance matrix of a substructure
[K]	stiffness matrix
[M]	mass matrix
[T]	transformation matrix
$[Z_A]$	impedance matrix of an assembly
$[Z_{\alpha\beta}]$	impedance matrix between coordinates α and β.(α,β=a,b,c,g,n,m i, j)
$\{f_A\}$	force vector of an assembly
$\{f_\alpha\}$	force vector at coordinates α (α=a,b,c,g,n,m i, j)
$\{f_S\}$	force vector of substructure
{q}	generalized displacement vector(Cp3)
{x}	displacement vector
$\{x_A\}$	displacement vector of an assembly
$\{x_\alpha\}$	displacement vector at coordinates α (α=a,b,c,g,n,m i, j)
$\{x_S\}$	displacement vector of a substructure

α_j	joint increment
α_p	excitation increment
β	parameter for Newmark-β method
Δ	time interval
Φ	normalised mode shape
ϕ	phase
γ	parameter for Newmark-β method
μ	friction coefficient
θ	angular displacement
τ	shear stress per unit width
τ_{max}	shear stress limit per unit width
ω	angular frequency
ω_r	resonance frequency

operators

$\|\|A\|\|$	Euclidean norm of a matrix [A]
$\|A\|$	magnitude of A
Real (x)	real part of a complex number (vector, matrix) x
Imag (x)	imaginary part of a complex number (vector, matrix) x
EXP(x)	natural exponential function
Max(a,b,..)	maximum value in a,b,....
Min(a,b,..)	minimum value in a,b,....
$\{\ \}^T$, $[\ ]^T$	transpose
$[\ ]^{-1}$	standard inverse
$[\ ]^+$	pseudo inverse
$[\ ]^*$	complex conjugate
$[\ ]^H$	complex conjugate transpose
{a+b+c}	{a}+{b}+{c}
[A+B+C]	[A]+[B]+[C]
y(i)	i'th element in {y}
Y(i,j)	the element of the i'th row and j'th column in matrix [Y]

$$\frac{\partial\{y\}}{\partial\{x\}} = \begin{bmatrix} \frac{\partial y(1)}{\partial x(1)} & \frac{\partial y(1)}{\partial x(2)} & \cdots & \frac{\partial y(1)}{\partial x(n)} \\ \frac{\partial y(2)}{\partial x(1)} & \frac{\partial y(2)}{\partial x(2)} & & \frac{\partial y(2)}{\partial x(n)} \\ \vdots & \vdots & \ddots & \vdots \\ \frac{\partial y(n)}{\partial x(1)} & \frac{\partial y(n)}{\partial x(2)} & \cdots & \frac{\partial y(n)}{\partial x(n)} \end{bmatrix}$$

$\dot{}$	derivative with respect to time

Abbreviations

AFT	alternating frequency time domain method
ARVF	averge-relative value factor
CP	corner point
DOF	degree-of-freedom
DFT	discrete Fourier transform
ECP	effective corner point
ESD	equivalent stiffness and damping method
FE	finite element
FEM	finite element method or finite element modelling
FFT	fast Fourier transform
FRF	frequency response function
GIC	generalized impedance coupling
GRC	generalized receptance coupling
HB	harmonic balance method
HHB	higher-order harmonic balance method
IHB	incremental harmonic balance method
LESD	local equivalent stiffness and damping method
MTC	multi-step two-coordinate coupling
P-P	peak to peak value
PPC	pseudo coordinate coupling
RC	receptance coupling
RJCF	relative joint correlation factor
SDOF	single degree of freedom system
SVD	singular value decomposition
S-area	stiffness area
S-S area	slipped stiffness area
WA	weight after method
WB	weight before method
WBG	weight before, group equation method
WBS	weight before, single equation method

superscript(left)

(n)	number of perturbation (Cp4), e.g. ${}^{(n)}X$

superscript (right)

(n)	number of iteration

subscript (left)

A, B	substructures A, B

subscript (right)

a	assembly
	master coordinate on substructure
b	interface coordinate on substructure
c	interface coordinate on substructure
i	joint coordinate on substructure
j	joint coordinate on assembly or joint
m	master coordinate on substructure
n	master coordinate on assembly
s	substructure

TABLE OF CONTENTS

CHAPTER [4] APPROXIMATE METHODS FOR CALCULATION OF THE STEADY-STATE RESPONSE OF A NONLINEAR STRUCTURE

APPENDICES

CHAPTER 1

INTRODUCTION

§1.1 GENERAL INTRODUCTION

Studies on vibration phenomena can be dated back to a few centuries ago. It has long been observed that when a structure is subjected to a periodic load, it can vibrate violently. Consequently, high levels of stress and noise are built up. Unlike static deformation, the vibration magnitude of a structure is determined by both the magnitude and the period (or frequency) of the excitation. For each structure, there are always some special frequencies; if the frequency of an excitation load happens to coincide with (or be close to) one of these special frequencies, the structure will vibrate at an exceedingly high level. These special frequencies are called the natural frequencies and they are inherent properties of the structure.

Usually, corresponding to kinetic energy, potential energy and energy dissipation, the properties of a structure can be defined by mass, stiffness and damping. However, it is also worth mentioning that if some parts of the structure are rotating, other forces such as centrifugal force can be involved. Accordingly, other properties should be used. In this thesis, the effects of rotation are excluded, hence only the mass, stiffness and damping effects are considered.

The final purpose of the structural dynamic study is to control the vibration of structures at a desirable level. In most cases, without significantly affecting the performance and the cost of the structure, the vibration level should be kept as low as possible. In practice, due to the complexity of the working load, the excitation can only be reduced, but it is almost impossible for it to be eliminated completely. Therefore, an engineering structure must be so designed that the response of a structure under external excitation does not exceed a permitted level.

The main tasks in structural dynamics can be summarised as:

1) to predict the response of a structure under certain excitation at the design stage and the effects of modifications.

2) to suggest effective measures to solve vibration problems for existing structures.

The basic requirements to fulfil these tasks are the abilities to

i) model a structure;

ii) predict the response of a structure under an excitation; and

iii) measure the response.

§1.2 MODELLING A STRUCTURE

It is essential to have a theoretical model to represent a structure in order to study its dynamic properties. Theoretical modelling methods can be categorised into two groups; those based on the stress-strain relations in the structure (continuous model), and those on the discretalization of the structure (finite element model).

A continuous model is often used for studying simple structures such as a uniform beam, or a plate; usually it is characterised by a partial differential equation with respect to the coordinates (x, y, z) and time (t). An analytical solution can often be obtained and the dynamic characteristics of the structure can be represented accurately. However, a continuous model is often extremely difficult to use in engineering problems because of the complexity of real-life engineering structures.

In contrast to a continuous model, a finite element model consists of many small elements, each element is constructed on some idealised assumptions (e.g. assumed deformation shape of the element). Therefore, a finite element model is always an approximation. However, high accuracy can usually be achieved by using a sufficiently small element. A finite element model is characterised by the stiffness, mass and damping matrices, and it is most suitable for analysis by numerical methods.

For a linear structure (see §1.3), besides theoretical modelling, the model can also be established by using experimental measures. The most commonly used experimentally established models are the response model and the modal model. A response model is characterised by the ratio of the excitation of a sinusoidal force to the response of the structure. The ratio is referred to as the frequency response function(FRF). The structure can also be characterised by a set of vibration modes and their corresponding natural frequencies, this model is referred to as the modal model.

The spatial model, modal model and response model are interchangeable. For theoretical analysis, it usually starts from a spatial model, while for experimental study, the response model is often first established. More details about these three models and their relations can be found in [1].

§1.3 NONLINEAR PROBLEM

Most analysis techniques in structural dynamics are based on the assumption that the structure to be analysed is linear. A structure is said to be linear if the relationship between the response of the structure and the external force is proportional. When a structure is linear, the principle of superposition holds, which means that doubling the excitation will double the levels of the response. When a structure is subjected to more than one excitation, the response is the same as the sums of the response due to each excitation. If a structure is linear, the response of the structure is purely sinusoidal when the excitation is sinusoidal, in other words, no energy can transfer between different frequencies.

If the relationship between the response of a structure and the excitation is not proportional, then the structure is said to be nonlinear. When a structure is nonlinear, the superposition principle is no longer valid, and the spatial properties change all the time when the structure is excited. Therefore, the modal model is not appropriate and the response model is also very difficult to define uniquely.

From the physical point of view, vibration energy can transfer from one frequency to another in a nonlinear structure, sometimes, the energy transfer can even make the structure unstable.

Most engineering structures are not absolutely linear. For structures made from solid materials, the relationship between the response and external force is substantially proportional under a small deformation, and it is reasonable to assume that the structure is linear. However, for other structures, the relationship cannot be approximated to be proportional even if under a small deformation, and they must be considered to be nonlinear structures.

The nonlinearity can be categorised into two groups [2]; the material type nonlinearity, and the large deformation nonlinearity. A spring with cubic stiffness and a pendulum with large angular response are examples of these two groups of nonlinearity respectively. The material nonlinearity is often localized, i.e. only some parts of the structure are nonlinear; while the large deformation nonlinearity is often global.

In this thesis, the property of a friction joint is studied. It will be shown later that nonlinearity of a friction joint is of the material type. Therefore, unless specified, the nonlinearity in this thesis is the material type.

§1.4 BASIC STRATEGY FOR REDUCTION OF THE VIBRATION OF A STRUCTURE

At any time, the excitation force must be balanced by the restoring, damping and inertia forces in the structure. Because the magnitude of the damping force is usually much smaller than other forces, the effects of the damping force are often insignificant at most frequencies. However, at or close to a natural frequency of a structure, the restoring force and inertia force cancel each other out, and the excitation must be balanced by the damping force. Therefore, at or close to a resonance frequency, the damping in the structure is very important.

Accordingly, the basic strategies of vibration control should be

1)to avoid exciting a structure at its resonance; and

2)to increase the damping levels in the structure when resonance is unavoidable.

If resonance can be avoided, there is little use for mechanical damping. Unfortunately, avoiding resonances becomes more and more difficult nowadays due to higher excitations over a wider frequency range. This situation is exacerbated by using low weight and flexible structural components such as beams and a thin plates, and by using all welded construction methods. As a result, the assembled structure has more resonances with a lower inherent damping level. When a structure with low inherent damping is excited at one of its natural frequencies, violent vibration is inevitable which causes various problems which can lead to the ultimate failure of the structure. Consequently, the damping in an engineering structure is more important than ever before.

§1.5 EFFECTS OF A JOINT

§1.5.1 The Joint, A Problem in the Finite Element Model (FEM)

A **joint** in this thesis is defined as any connection between two distinct parts of a structure. A **friction joint** is a type of joint with two surfaces directly pressed together by a normal force applyed through bolts, rivets or other clamping mechanisms.

In the last section, it has been explained that the basic strategy in controlling vibration is to avoid the structure being excited at a resonance. In order to avoid a structure being

excited at a resonance, the properties of the structure must be predicted accurately. This means that each part of the structure should be modelled accurately.

Nowadays, although the FEM is so developed that the accuracy of modelling a solid structure is usually satisfactory, there are still some parts on the structure which cannot be modelled accurately, or even reasonably. One of these is the joint. So, quite often, the flexibility of a joint is ignored in the analysis of an assembled structure, i.e. the joint is assumed rigid. In practice, however, the joint effects can be very significant on the response of a fabricated structure. As pointed out by Beards[3], up to 60% of the deformation and 90% of the damping in a fabricated structure can arise from various joints. Neglecting these effects can make the prediction on the property of the whole structure inaccurate or even unreasonable. Clearly, establishment of accurate joint models is of great importance in accurate prediction of the dynamic behaviour of the structure.

§1.5.2 Friction Joint; A Great Source for Vibration Reduction

Apart from the problems caused by the joint in the FEM, the joint is also interesting because of its capacity for controlling vibration.

It has been discussed in §1.3 that it is not always possible to avoid all the resonance frequencies of a structure. Thus, the effect of damping becomes important. To increase the damping level in a structure, the following three measures can be taken:

1) the introduction of high damping materials,

2) the introduction of energy dissipation equipment (e.g dashpot), and

3) the utilisation of the damping capacity of various joints (mainly friction joint).

Use of measures 1) and 2) requires additional components, which means extra cost to manufacture the structure. Sometimes, these measures are difficult to apply because of the practical limit on these additional components such as the size and shape. In addition, it is often found that although the damping levels of these material can be very high, they are usually expensive, and there are also some physical limits on these materials, for example, the damping materials are often only effective under large strain and within some frequency and temperature ranges; outside these limits, the damping level drops dramatically.

In contrast to the first two measures, because the joint is an original part of a structure, using the damping capacity does not have these disadvantages. The effects of friction joints on the reduction of vibration levels have attracted great interests [4-19] (see the next section). It has been found that a friction joint has a great potential for reducing the vibration levels of a structure. By controlling the clamping force at the joint so that it

allows slip at interfaces, the vibration magnitude(FRF) of a structure can often be reduced by 20dB or more [4], which is equivalent to reducing the vibration level to one-tenth of its original value.

§1.6. REVIEW OF PREVIOUS WORK ON FRICTION JOINTS

The observation and utilisation of friction force can be traced back many thousand years when ancient people discovered the method of making fire by drilling wood and to move heavy objects by using round logs.

The concept of friction force was first introduced in 1519 by Lenardo da Vinci and the eighteen century saw the breakthrough in the study of friction. In 1750, Euler concluded that it was not possible to give the inclined plane inclinations such that the descent would be as slow as desired. Either the body would not slide at all, or it would slide very fast. In 1785, Coulomb verified experimentally that the friction force was proportional to the normal force and also made a distinction between static and kinetic friction force. Various studies have been carried out and summarised by Martins *et al* in [20]. Almost all of them were in the fields of tribology.

In contrast to the developments in tribology, the developments of structural dynamics were insignificant until 1931. Before that, the effect of a friction force on the response of a structure was simply approximated by an equivalent "viscous" damping which dissipated the same energy as the friction force in each cycle. In 1931 Den Hartog [21] analytically solved the steady state response problem of an SDOF system with combined Coulomb and viscous friction. An important discovery was that the system with only friction damping can be excited into unbounded response at resonance. The analytical method was later extended to a 2-DOF system by Yeh [22]

Since 1970, the effects of slip between a friction joint interface on the control of vibration of mechanical structures attracted the attentions of many researchers such as Earles [5-7], Beards [8-13], Dowell [14-15] and Menq [16-17]. Various structures have been tested and the great potential for a friction joint to reduce vibration level has been observed.

The problems in utilising a friction joint as a tool to control the vibration of a fabricated structure were summarised by Beards[3] as:

1) fretting corrosion at joint interface;

2) loss of static stiffness of the structure; and

3) difficulty in design and analysis due to problems of nonlinearity.

Beards [8][12] has shown that fretting damage can be minimised by providing a layer of low modulus or yield strength material between the joint interfaces; non-metallic or metal coatings can also be used to prevent the fretting caused crack from propagating through the whole joint; many surface preparations such as shot peening, blasting and metal sprays reduce the fretting damage, and inexpensive cyanide hardening and electro-discharge machining were very effective and suggested for surface treatment.

Beards [3] also pointed out that any loss of static stiffness of a structure did not necessarily affect the integrity of the structure if the joints were carefully located.

Accordingly, the major obstacle in the application of the friction joint in vibration control is the problem of nonlinearity. In dealing with this nonlinear problem, attention was paid to the following:

1) modelling the properties of a joint.

2) calculating the response of a fabricated structure when the properties of all the joints are known.

Quasi-static experiments have been carried out on various friction joints [23-34]. It has been found that the relationships between the load and deformation in the directions normal and parallel to the interface are not linear. In the direction parallel to the interface, energy is dissipated when a cyclic load is applied. When the deformation magnitude is small, Coulomb's dry friction law is not adequate, and it is believed that microslip mechanism is responsible for the characteristics of the friction joint. Several theoretical models have been developed to represent the nonlinear behaviour of a friction joint [35-51,16]. Some of these models were adopted primarily for mathematical convenience [35-38], while others had physical significance [39-51,16]. Although some of these physically motivated models are based upon the so called nonlocal and nonlinear friction law [39,40], most of them are constructed on the basis of Coulomb's dry friction law [41-51,16].

Coulomb's dry friction was assumed for most of the studies in predicting the response of a structure with friction joint/s attached[5-17, 52-74]. The most commonly used method in analysing the response of a structure is an approximation method--the Harmonic Balance method [5-17, 52-62], which effectively linearises the dry friction force at a joint. Recently, effort has also been devoted to obtaining results which are balanced in multi-harmonics[63-65]. In most cases, only one joint is involved. Numerical integration methods [66-73] have also been used in calculation of the transient response of the structure and an analog computer method has been developed for modelling the bilinear type hysteresis [74].

Various structures have been studied including fabricated beams(e.g.[2][3]), plates(e.g.[9][13]), frame structures(e.g.[10][11]), turbine blades(e.g.[19][58][59]) and turbine discs(e.g.[56][67]). SDOF systems [63][65], lumped parameter systems [56][64], finite element systems [35][57], continuous systems [19], response systems (in FRFs)[5-12] and modal systems [53-55] have all been used to model these structures.

The effects of the joint mass [69] and variable normal load [58][59]][62] on the property of the joint have also attracted the attention of some researchers. Two-dimensional motion at the joint has recently been investigated [60][61]. The effects of a friction force on the stability of a structure have also been studied [56][68][71][73]. For most of the analyses on friction joint related problems, only qualitative agreements between the theoretical analysis and the experiment have been achieved. Quantitative agreement is still lacking.

To summarise; many efforts have been devoted to the study of the friction joint, nevertheless, the understanding on the friction joint is still limited. Here, Jones's comments in 1988 [75] are summarised to conclude this review:

So we might ask, what developments have taken place with respect to our understanding of damping of built-up structures? The answer seems, surprisingly, or perhaps not, very little! ... it would be difficult to find any recent studies which have advanced our ability to predict joint damping or to predict the response of built-up jointed structures better than was achieved in 1960's. The only major change has been in computer power, software including finite element codes, test instrumentation and electronic analyzers. The difficulty remains in the modelling of the damping, and in the variability of manufactured structures, even when the process is automated.

§1.7 PREVIEW OF THE THESIS

As discussed in the last section, despite developments on the study of friction joints in the past, the friction joint has seldom been deliberately used to reduce the vibration of engineering structures. The nonlinear problem is believed to be the major obstacle in utilising the capacity of damping in a friction joint, and how to model a friction joint accurately is the root of the problem. The research presented in this thesis is intended to seek new developments on model and identification of friction joints, and also on prediction of the response of a structure containing nonlinear friction joints.

The most basic requirement, and probably the most difficult task in the study of friction joint, is to model the joint. This problem is dealt with in Chapter 2. The most commonly used friction joint models have been presented and methods to derive joint models summarised. The problems of these models are also discussed. Based on the new concept of stiffness area, a new microslip element is developed for modelling a friction joint and models constructed from the new element are verified by using experimental data. The

new element and the joint models are found to be more representative than other available models. For a friction joint with complicated geometric shape and surface, an approach utilising both the FE method and the new element is proposed.

In Chapter 3 and Chapter 4, efforts are devoted to selecting proper available techniques and developing new techniques for predicting the response of a structure with nonlinear friction joints attached.

In Chapter 3, time-domain methods are investigated. Stability, accuracy and efficiency of the methods are discussed. The ability to calculate the friction force from the deformation of the joint is essential. Two simple algorithms based on Masing's rule are developed to calculate the corresponding friction force from the response. A new method of condensation has also been studied.

In Chapter 4, the frequency-domain methods are investigated. The Harmonic Balance method is studied and some new algorithms to find the solution for the Harmonic Balance method (HB) are proposed, and the advantages and disadvantages of the HB method are discussed. In order to achieve the desirable accuracy for the predicted response, a new Higher-order Harmonic Balance method(HHB) is suggested. An incremental approach is developed to find the solution for the HHB method. Comparison between the numerical results from the HHB method and time-domain method demonstrates the accuracy and efficiency of the HHB method.

There are two extreme cases for a friction joint; one is the case when the joint is unclamped, the other is when the joint is tightly clamped. These two cases usually set the lower and upper bounds for the natural frequencies of a structure. It is possible to predict the property of the structure with tightly clamped joints by using that with unclamped joints. The most commonly used methods are only for coupling two structures. In Chapter 5, some of the commonly used FRF coupling methods are reviewed and their advantages and shortcomings are discussed. Then a new generalised coupling method is developed. Based on the new generalised FRF coupling method, another computationally efficient coupling algorithm is proposed. The effects of measurement errors on the coupling results are investigated by using the simulated experimental data.

Although properties of some friction joints can be found from a static test, it is believed that an accurate model for most joints in an engineering structure can only be established from a dynamic test. In order to develop techniques for modelling a nonlinear friction joint, a full understanding of the methods for establishing a linear joint model from the dynamic experimental data is essential. In Chapter 6, joint identification techniques using FRF data are investigated systematically. A brief review on the joint identification techniques is presented and two new joint identification techniques are developed. The effects of measurement errors on the accuracy of the identified joint model are

discussed and techniques to improve the accuracy of the identification method are presented. The nature of the identification problem has also been discussed.

In chapter 7, the newly developed coupling and joint identification techniques are investigated by using experimental data. The joint identification technique is also applied to identify a nonlinear friction joint by using newly improved control technique in the experiment. Satisfactory results are obtained.

Finally, all the new developments presented in this thesis are reviewed and suggestions for future studies are presented.

CHAPTER 2

MODELLING THE FORCE-DEFORMATION CHARACTERISTICS OF FRICTION JOINTS IN THE TANGENTIAL DIRECTION

§2.1 INTRODUCTION

The definition of a joint given in Chapter 1 is very general; the clamped edge of a panel is a joint, and the root of a turbine blade is also a joint. The contact surface of a joint is called the **interface**. The connection part of a component which forms a joint is referred as the **joint component**.

The properties of a friction joint are interesting because joints are always an essential part of any real fabricated engineering structure and dissipate vibrational energy. A joint may be desirable in the sense that it dissipates the vibration energy; it can also be undesirable because the slip between the interfaces of a joint can cause problems such as fretting corrosion at the interfaces and a reduction in total static stiffness of the structure; the slip at the joint can also make the properties of a structure nonlinear [3], which makes the analysis of a structure with a friction joint very difficult.

The undesirable effects can be reduced by using high normal force at the interfaces. However, even when a joint is tightly clamped, the dynamic characteristics of the joint are still different from the properties of the solid materials from which the joint component is made. This difference is often one of the main sources of mis-prediction of the dynamic behaviour of a structure using the finite element method which usually does not include the effects of the various joints.

Should the energy dissipation mechanism in a friction joint be used deliberately to reduce the vibration levels of a structure, the joint clamping force should be reduced to allow some slip mechanisms to act. Unfortunately, this will usually exaggerate the undesirable effects. The energy dissipation mechanism is closely related to the slip between the interfaces which is also responsible for the undesirable effects. Therefore, the desirable and the undesirable effects of a joint are inseparable. As discussed in chapter one, fretting corrosion and the reduction of total static stiffness can be controlled by special preparation on the interface and carefully choosing the joint in which slip is allowed. However, in

order to deal with the nonlinear problem quantitatively, it is essential to be capable of modelling the dynamic behaviour of all the joints accurately. In other words, a quantitative mathematical model must be established for every joint. In this chapter, the major effort is devoted to obtaining a quantitative analytical model for a friction joint.

§2.2 BASIC CONCEPTS IN MODELLING A FRICTION JOINT

§2.2.1 Types of Nonlinearity

The basic requirement to characterise a friction joint is to find the relationship between an external excitation force (load) and the response (displacement, velocity and acceleration) at the joint caused by the external load.

For a linear component, the excitation-response relation can be expressed by:

$$F=kx+c\dot{x} \tag{2.1}$$

under any circumstance. However, for the nonlinear element, the relation is much more complicated. Usually, a general form of the force-response relation of a nonlinear element is:

$$F=F(x,\dot{x},t) \tag{2.2}$$

If the nonlinear element is independent of the velocity, then

$$F=F(x,t) \tag{2.3}$$

and the excitation-response relation becomes the force-deformation relation.

For some nonlinear elements, the relationship is only determined by the deformation at the current state and can be presented by a single formula

$$F=F(x) \tag{2.4}$$

For other nonlinear elements, however, the relationship is not only related to the current response state, but the loading history too. Usually, this type of nonlinearity can not be presented by a single formula and is the most difficult to analyse. This type of nonlinearity is often referred as **nonlinearity with memory (or multi-value nonlinearity)**; the nonlinear property which can be characterised by equation(2.4) is referred as the **single-value nonlinearity.**

§2.2.2 Types of Loading on a Friction Joint

It will be shown in the next section that the force-deformation relation of the friction joint is not only nonlinear, but actually dependent upon the loading history. Different loading

periods are characterised by different properties. However, the relationship in several loading period are often similar or the same, and accordingly, the loading is often categorized as:

1) **Initial loading**: The loading period with increasing load from the free rest state (zero load).

2) **Unloading**: Any loading period with decreasing load.

3) **Reloading**: Any loading period with increasing load except for the initial loading.

For a nonlinear element, there is only one initial loading, however, there can be many unloadings (and reloadings). The force-deformation relation of all the unloadings (and reloadings) are similar, and sometimes, can be modelled by the same analytical formula. This will be discussed later in this chapter.

§2.3 THE BEHAVIOUR OF A FRICTION JOINT IN THE NORMAL AND THE TANGENTIAL DIRECTIONS

There are two basic types of force-deformation relations for a friction joint; one is in the direction normal to the interfaces, the other is in the direction parallel or tangential to the interfaces.It has been shown experimentally [76][29] that the force-deformation relations in both directions are not linear (figure 2.1 and figure 2.2).However, the force-deformation relations in the two directions are different in their nature.

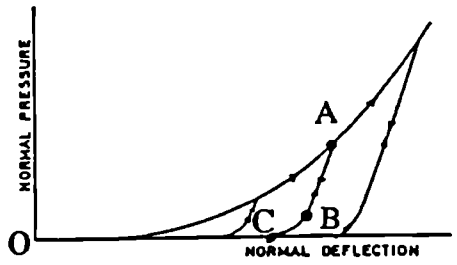

Figure 2.1 The loading relation in the normal direction
(after Thornley et al [76])

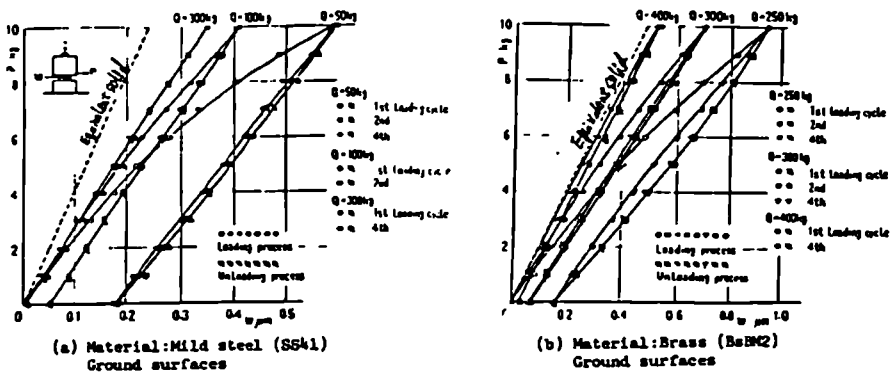

Figure 2.2 The loading curves in the tangential direction
(After Masuko et al[29])

§2.3.1 Behaviour of a Friction Joint in the Normal Direction

For the force-deformation relation in the normal direction, as shown in figure 2.1, although the initial loading (OA) is different from the subsequent loading(e.g. ABC), the relation in the subsequent cyclic loading are the same, i.e. the force-deformation curve after initial loading OA follows the path ABC. Except for the initial loading, the unloading and the reloading curves are overlaid. Usually it is the behaviour after the initial loading that is of interest, therefore, the properties of the friction joint in the normal direction is effectively a type of single value nonlinearity.

In practice, a certain level of pre-load will be applied in the normal direction, and when the joint is subjected to a cyclic load in the normal direction, the joint will deform along the path ABC. Because the magnitude of the cyclic load is usually much smaller than that of the pre-load, the joint is more likely to deform in the range of AB. Since the force-deformation relation in path AB is effectively linear, the behaviour of a friction joint in the normal direction is substantially linear.

§2.3.2 Behaviour of a Friction Joint in the Tangential Direction

For the force-deformation relation in the tangential direction, however, the path of subsequent cyclic unloadings and reloadings are different, in other words, the behaviour of a friction joint in the tangential direction is a kind of nonlinearity with memory. It can also be noted that the path ABA forms a loop. This indicates that energy is dissipated when the joint is subjected to a cyclic load. This kind of loop (energy dissipation) does not exist under loading in the normal direction.

One feature which can be noted is that the loop is effectively symmetrical with respect to the centre point of the loop. Therefore, it must be possible to represent the unloading and reloading properties in some similar mathematical formulae.

Because energy dissipation (and also effective nonlinearity) does not exist under cyclic loading in a normal direction, it will not be investigated further in this thesis. In this chapter, we shall deal with the properties of the joint in the tangential direction only.

§2.4 THE DRY FRICTION MODEL

In this section, the simplest and also the most important model is discussed. Most of the other friction models are based on, or closely related to this model.

The most well known theory about the friction force is Coulomb's dry friction law which may be stated as follows:

The friction force at the interface is

1) affected by the material properties in contact and the surface preparation;

2) proportional to the normal clamping force;

3)substantially independent of the sliding speed and the apparent area of contact; and

4) greater just prior to the occurrence of the relative motion than after sliding

The first three points are generally well accepted, while disagreement exists between different researchers for the fourth point (Some details have been discussed by Martins *et al* [20]). However, if the duration time of two components being pressed together is insignificant, it is generally accepted that the difference between the friction force at smooth metal contact surfaces just prior to the sliding and after the sliding, if it exists at all, is usually not significant. Accordingly, the difference is often ignored.

The mathematical expression for Coulomb's law can be presented as follows:

$$F=\begin{cases} -N\mu & v>0 \\ -P & v=0 \\ N\mu & v<0 \end{cases} \qquad (2.5)$$

where v is the relative motion at the joint interface, N is the normal clamping force, μ is the friction coefficient and P is the external force with a magnitude less than the product of the normal force and the friction coefficient ($N\mu$).

From equation (2.5), it is known that if the external force is smaller than the friction limit ($N\mu$), the two interfaces of a joint will remain locked; the friction force at the interface has the same magnitude as the external force but acts in the opposite direction. Once sliding occurs, the friction force is equal to the friction limit and the direction of the friction force

is always opposite to the direction of motion; no tangential force greater than the friction limit can be transmitted through the interface.

The direct use of the dry friction law leads to the simplest joint model -- the point contact dry friction model (element); since the friction force is independent of the area and shape of the interface and is also independent of the pressure at the interface, the joint property will be the same as the joint with only one contact point as shown in figure 2.3. In other words, the joint can be considered as contacting at one point only. An implication of the dry friction law is that before sliding is initiated, the deformation of the joint is zero.

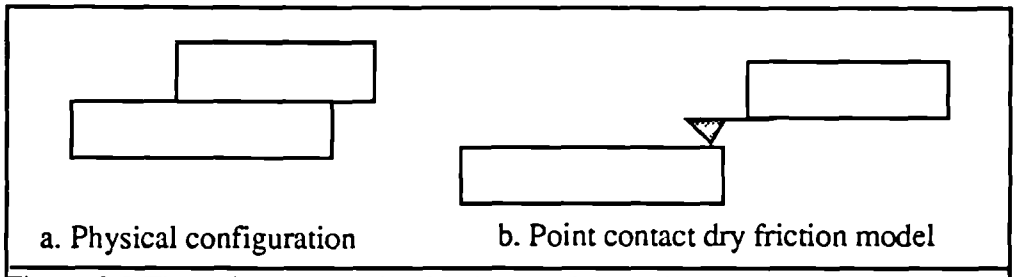

Figure 2.3 The point contact dry friction model and its physical configuration

The point dry friction model has been used by many researchers (e.g. [10][53][54]) in the analysis of vibration problems. However, the analyses are usually less satisfactory in quantitative study than in qualitative study, especially when the vibration magnitude is small [3]. Nowadays, it is generally accepted that for most of the engineering joints, the elasticity of the joint components and the interfaces plays an important role in the behaviour of the whole joint; slip may occur over some parts of the interface before the two components slide against each other. The force-deformation relation under such a partial slip state usually cannot be represented by the point contact dry friction model. This kind of partial slip is called **micro-slip**. When slip occurs all over the interfaces, it is called **macro-slip** or **sliding**.

Clearly other more refined models are required to represent the behaviour of the microslip joint.

§2.5 MASING'S RULE

Before going any further with the microslip models, it may be appropriate to introduce a rule which represents the properties of a joint by the initial loading relation, this being Masing's rule. Masing's rule can be expressed as follows:

If a joint consists of only linear components and the dry friction elements, the properties of the joint are fully defined by the force-deformation relation of the initial loading, i.e. the unloading and the reloading relationship can be obtained directly from the initial loading.

As shown in figure 2.4 if an interface is subjected to an initial load F, and the deformation u follows a path

$$F=f(u) \tag{2.6}$$

to a point $A(u_i,F_i)$, then an unloading path from the point A to a point $B(u_u,F_u)$ can be expressed as:

$$\begin{cases} F_u=F_i-2\,f(\frac{u_i-u_u}{2}) & u_u \geq -u_i \\ F_u=-f(-u_u) & u_u<-u_i \end{cases} \tag{2.7}$$

Similarly, a reloading path from the point $B(u_u, F_u)$ to a point $C(u_r, F_r)$ is

$$\begin{cases} F_r=F_u+2f(\frac{u_r-u_u}{2}) & |u_r| \leq \max(|u_u|,|u_i|) \\ F_r=f(u_r) & |u_r|>\max(|u_u|,|u_i|) \end{cases} \tag{2.8}$$

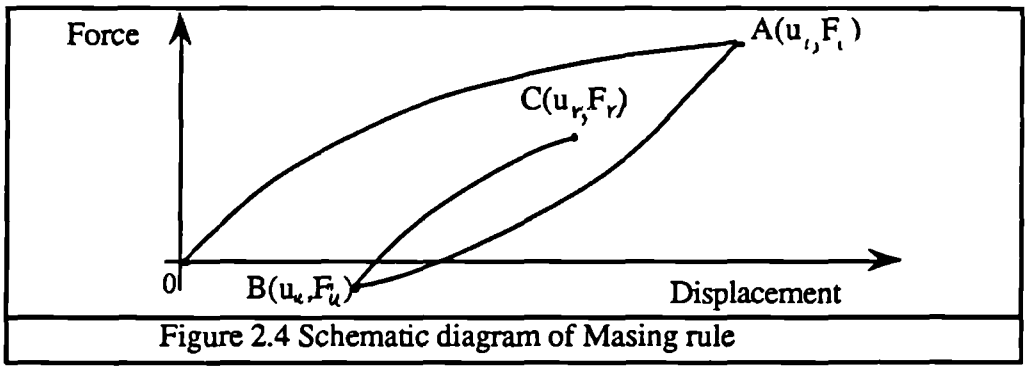

Figure 2.4 Schematic diagram of Masing rule

The proof of Masing's rule is not published in English [77], and to the author's knowledge, no proof in English was available. Therefore, Masing's rule is proved independently and forms Appendix A of this thesis.

The application of Masing's rule can simplify the analysis of the force-deformation relation significantly. If a joint model consists of only linear components and dry friction components, once the initial loading is known, further unloading and reloading can be deduced from the initial loading relation, in other words, a friction joint is completely characterised by the initial loading relation. Some other properties of the joint can also be detected from the relationship of the initial loading.

One of the important properties of a friction joint is the energy dissipation under a cyclic load. The energy dissipated each cycle is the area of the loop, which can obtained from integration as:

$$E=\int_{u_u}^{u_r}(F_r-F_u)du \tag{2.9}$$

Substituting equations (2.7) and (2.8) into equation(2.9) leads to

$$E=\int_{u_u}^{u_r}\{F_i-2f(\frac{u_r-u_u}{2})+2f(\frac{u-u_u}{2}) - (F_i-2f(\frac{u_r-u}{2}))\}du$$

$$=8\int_0^{(u_r-u_u)/2}f(y)dy - 4\frac{u_r-u_u}{2}f(\frac{u_r-u_u}{2}) \qquad (2.10)$$

From equation(2.10), it is proved that the energy dissipated each cycle is a function of the peak to peak value (P-P value) of the deformation and is independent of the absolute value of the maximum deformation.

The energy dissipated per cycle can also be calculated from

$$E=\int_{F_u}^{F_r}(u_u-u_r)dF$$

$$=8\int_0^{(Fr-Fu)/2}f^{-1}(y)dy - 4(\frac{F_r-F_u}{2})f^{-1}(\frac{F_r-F_u}{2}) \qquad (2.11)$$

Therefore, the energy dissipated per cycle is also a function of the P-P value of the cyclic load.

§2.6 FRICTION BILINEAR ELEMENT AND ASSEMBLY

Another most important element in modelling the friction joint is the friction bilinear element which consists of a linear spring and a dry friction element, the physical configuration of a friction bilinear element is shown in figure 2.5a.

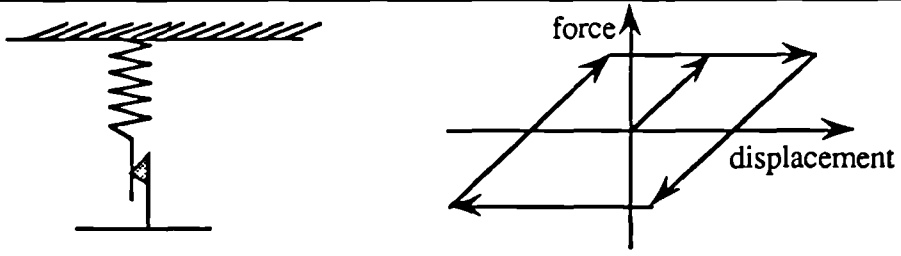

(a) Mathematical model (b) hysteresis loop

Figure2.5 Mathematical model and hysteresis loop of a bilinear element

The element has the following properties

1) if the deformation u is less than the limit u_0, the force-deformation relation of the element is effectively linear, i.e. f=ku

2) if the deformation x exceeds the limit u_0, the force is a constant ku_0.

When the element is subjected to a cyclic load, a hysteresis loop is formed as shown in figure 2.5b. For the simplicity, the friction bilinear element is known as the **bilinear element** only.

The bilinear element is actually an extension of the dry friction element with additional flexibility. The dry friction model is a special case of the bilinear element with the linear spring having infinite stiffness.

For a dry friction element, the force at the zero deformation state is not determined, but for a bilinear element, the force is determined under any circumstance.

Bilinear elements can be connected in series, parallel or in a parallel-series combination as shown in figure 2.6 to yield different force-deformation relations. This kind of bilinear assembly model was originally introduced to model the yielding behaviour of continuous and composite materials [44][78].

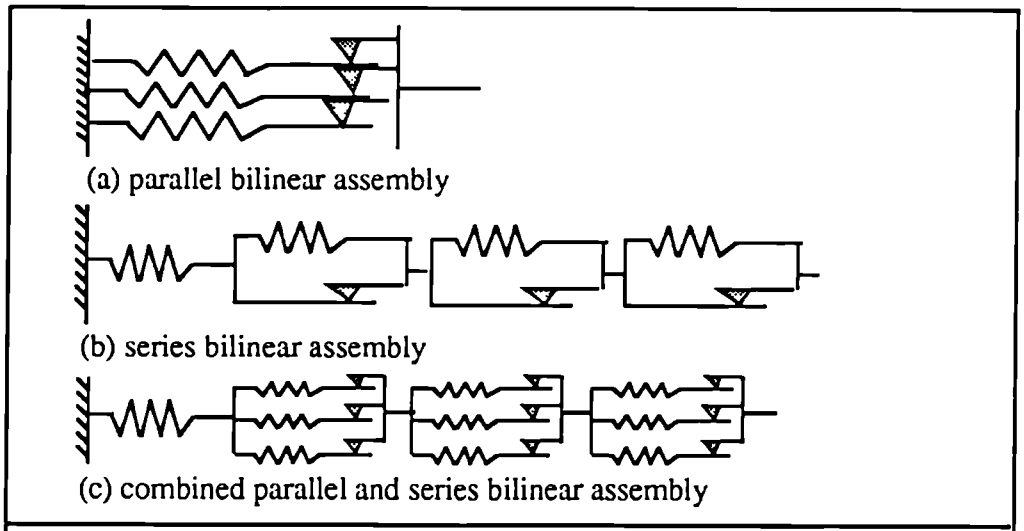

Figure 2.6 different bilinear assembly models

No matter how complicated the bilinear assembly is, two basic properties for the bilinear assembly are held:

1) Masing's rule can be applied, and

2) The slope of a force-deformation curve represents the stiffness contributed from stiffness of the elastic components and the bilinear elements in which slip has not initiated. A reduction of the slope indicates an increase in the number of slipped bilinear elements.

A typical parallel-series bilinear assembly loading curve is shown in figure 2.7

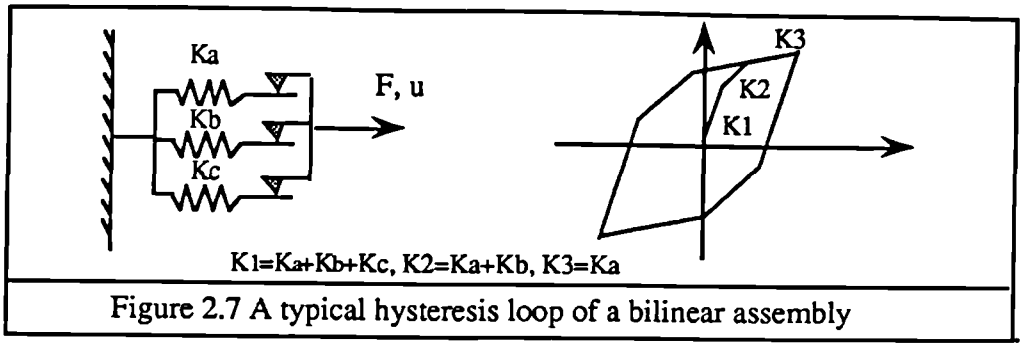

Figure 2.7 A typical hysteresis loop of a bilinear assembly

§2.7 MICROSLIP WITH CONSIDERATION ON THE ELASTICITY OF THE JOINT COMPONENT ONLY

§2.7.1 Review of the Microslip Models Based on the Dry Friction Element

In the next few sections, microslip caused by the elasticity of the joint components are considered and the properties discussed.

Experimental results [30] show that the variation of the force-displacement relation is insignificant in the frequency range up to 200Hz, this covers the frequency range of interest in most structural engineering problems. As a result, it is commonly assumed that the friction force under cyclic excitation is independent of the excitation frequency. To simplify the problem, the difference between the friction force just prior to and just after slip is also ignored.

The microslip phenomenon was first discovered on a spherical contact rig by Mindlin *et al* analytically [79] in 1949 and experimentally [24] in 1951. Analytically, Mindlin assumed that the dry friction law was held at an infinitely small area and he found that if slip did not occur at some parts of the interfaces, the shear stress at these areas would be infinite. Therefore, slip must occur at these parts of the interfaces.

After Mindlin, a series of theoretical analyses on different joints with different configurations were developed (e.g.Pian and Hallowell [41],Goodman and Klumpp [80], Earles and Philpot [26] and Metherell and Diller [45]). These models are all based on Mindlin's assumption that the dry friction law held at any point on the interface.

The methods used to calculate the force-deformation relation for these dry friction element based models are similar; the procedure is in two stages:

1) detect the slip area, and

2) calculate the deformation of the joint component due to the external force and friction shear stress at the interface.

To illustrate the basic procedure, a new bending microslip model is developed and presented in the next section.

§2.7.2 A Bending Joint Model -- New Development

The joint model presented in this section is shown in figure 2.8. The joint is effectively the root of a clamp ;r beam with unit width. This kind of joint can be found in many engineering structures such as the root of a turbine blade. To the author's knowledge, it has not been analysed based on this physical configuration.

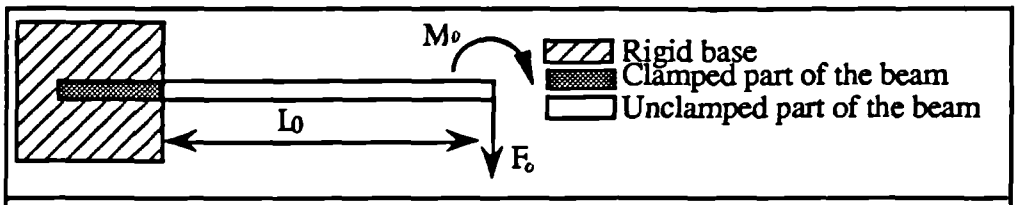

Figure 2.8 The diagram for the bending joint model

Assume that the structure is subjected to an external force and moment at the free end of the beam. The root of the beam is clamped by a uniformly distributed pressure and the surface conditions of the interface are the same. The friction shear stress limit per unit width is the product of the pressure per unit width and the friction coefficient, i.e. $\tau_{max}=p\mu$.

Based on the dry friction law, if slip does not occur, the external force and moment at the root must be balanced by the force and moment at point A, which means the shear force and moment at point A must be infinite. Because the shear stress cannot exceed the friction limit, slip must occur in some regions of the root.

The shear stress direction must be opposite to the direction of motion, hence the component of shear stress in the horizontal direction is much smaller than that in the vertical direction. If the thickness of the beam is small, the shear stress in the horizontal direction can be neglected. To balance both the external moment and the external force, two slip regions must occur at the root with the shear stress in opposite directions as shown in figure 2.9.

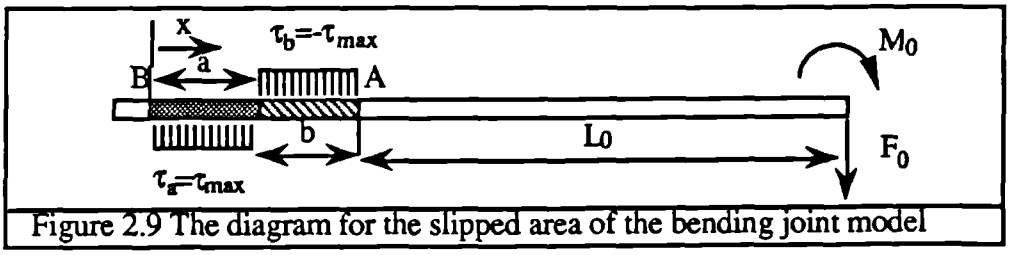

Figure 2.9 The diagram for the slipped area of the bending joint model

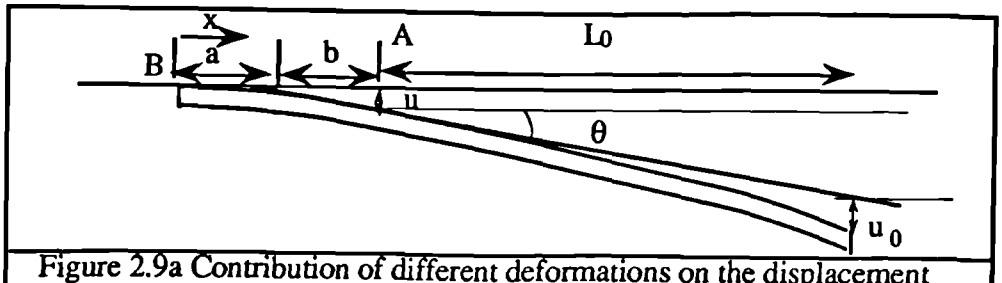

Figure 2.9a Contribution of different deformations on the displacement at the tip of the beam

The equilibrium equations for the force and moment at point B are

$$F-b\tau_{max}+a\tau_{max}=0, \text{ and} \tag{2.12}$$

$$M+F(a+b)+\frac{1}{2}\tau_{max}a^2=\tau_{max}b(a+\frac{b}{2}) . \tag{2.13}$$

Solving equations(2.12) and (2.13) leads to

$$a=\frac{1}{\tau_{max}}\sqrt{\frac{2M\tau_{max}+F^2}{2}}, \tag{2.14}$$

$$\text{and } b=\frac{1}{\tau_{max}}(F+\sqrt{\frac{2M\tau_{max}+F^2}{2}}), \tag{2.15}$$

where $F=F_0$ and $M=M_0+F_0L_0$

Once the slipped area has been detected, the second step is to determine the deformation level with the knowledge of the external force and the slipped area. When the thickness of the beam is small, Euler beam theory can be used. The governing equilibrium equation for a bending beam is [81]:

$$-\frac{\partial^2}{\partial x^2}[EI(x,t)\frac{\partial^2 u(x,t)}{\partial x^2}]+f(x,t)=m(x)\frac{\partial^2 u(x,t)}{\partial t^2} \tag{2.16}$$

For a case of a quasi-static load on a uniform cross-section beam root, the inertia force can be ignored, then equation(2.16) becomes

$$-EI\frac{d^4u(x)}{dx^4}+f(x)=0 \tag{2.17}$$

$$\text{where } f(x)=\begin{cases}\tau_{max} & x\le a\\ -\tau_{max} & x>a\end{cases} \tag{2.18}$$

The boundary conditions at the left and right ends of the beam are

$$\text{left end: } u(0)=0 \text{ and} \frac{du(0)}{dx}=0, \tag{2.19a,b}$$

$$\text{right end: } EI\frac{d^2u(L)}{dx^2}=M \text{ and } EI\frac{d^3u(L)}{dx^3}=-F. \tag{2.20a,b}$$

$$\text{at } x=a: u(a^+)=u(a^-) \tag{2.21a}$$

$$\therefore \frac{du(a^+)}{dx}=\frac{du(a^-)}{dx} \tag{2.21b}$$

$$: EI\frac{d^2u(a^+)}{dx^2} = EI\frac{d^2u(a^-)}{dx^2} = M_b \tag{2.21c}$$

$$: EI\frac{d^3u(a^+)}{dx^3} = EI\frac{d^3u(a^-)}{dx^3} = -F_b \tag{2.21d}$$

where $L=a+b$, a^+ and a^- represent the position on the right and left of the position $x=a$

Also $$F_a = F - \tau_{max} b \tag{2.22}$$

and $$M_a = M + Fb - \frac{1}{2} b \tau_{max}^2 \tag{2.23}$$

are the shear force and the shear moment at $x=a$.

From equations(2.17) to (2.23), the translational and angular displacement at the point M can be easily worked out :

$$\begin{cases} u(x) = -\dfrac{\tau_{max}(x-a)^4}{24EI} + d_3(x-a)^3 + d_2(x-a)^2 + d_1(x-a) + d_0 & x > a \\ u(x) = \dfrac{\tau_{max} x^4}{24EI} - c_3 x^3 + \dfrac{1}{2} c_2 x^2 & x \le a \end{cases} \tag{2.24,2.25}$$

where $$c_3 = -\frac{(F_a + \tau_{max} a)}{6EI} \tag{2.26a}$$

$$c_2 = \frac{1}{2}\left(\frac{M_a}{EI} - \frac{\tau_{max} a^2}{2EI} - \frac{a(F_a + \tau_{max} a)}{EI}\right) \tag{2.26b}$$

$$d_3 = -\frac{F_a}{6EI} \tag{2.26c}$$

$$d_2 = \frac{M_a}{2EI} \tag{2.26d}$$

$$d_1 = \frac{du(a)}{dx} \tag{2.26e}$$

and $$d_0 = u(a). \tag{2.26f}$$

Therefore

$$u(L) = -\frac{\tau_{max} b^4}{24EI} + d_3 b^3 + d_2 b^2 + d_1 b + d_0, \tag{2.27}$$

$$\theta(L) = \frac{du(L)}{dx} = -\frac{\tau_{max} b^3}{6EI} + d_3 b^2 + d_2 b + d_1. \tag{2.28}$$

The displacement at the tip of the free end is the sum of the displacement due to slip at the clamped end of the beam and the elastic deformation of the un-clamped part of the beam, i.e

$$u_{Total}=u(L)+u_0+\theta(L)L_0 \tag{2.29}$$

For a cantilever beam with a force F_0 applied to its free end, the displacement at the tip can be found as:

$$u_0=\frac{F_0L_0^3}{3EI} \tag{2.30}$$

and the moment at point M due to the force F is

$$M=F_0L_0 \tag{2.31}$$

If equations(2.19) and (2.20) are substituted into equation(2.18), the force-deformation relation can be calculated. It can be noted that the loading relation can be written in the form

$$u_{total}=f(EI,L_0,\tau_{max},F_0) \tag{2.32}$$

Figure 2.10 shows the force-deformation relation at the free end of a uniform beam

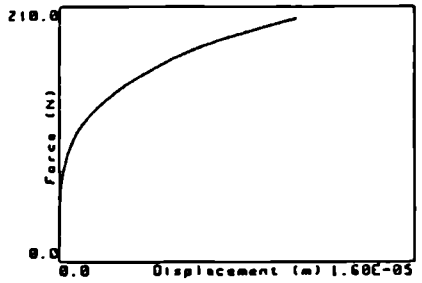

L_0=0m
M=0Nm
τ_{max}=5000N/m
E=2.06× 10^{11}N/m^2
I=4.17 × $10^{-9}m^4$

Figure 2.10 Initial loading curve of the bending joint model

It should be noted that the derived formulae are only valid for a beam with small thickness. When the thickness of the beam is significant, more accurate Timoshenko beam theory [82] should be used. However, the principle of the method is still applicable except that the formula deduction may be more tedious.

Since the only nonlinear element is the dry friction shear stress at the interfaces, the unloading and reloading relation can be found using Masing's rule.

§2.7.3 Features of Joint Models Based on the Dry Friction Element

Figure 2.11 shows the physical configurations and stress distributions over the interfaces for two of the published joint models. Some common points can be noted. First of all, all

these joints have very simple geometry, and uniform stress distribution over the interfaces and uniform surface conditions are assumed. Because the only nonlinearity is the dry friction shear stress at the interface, Masing's rule is applicable and the model is fully defined by the force-deformation relation of the initial loading.

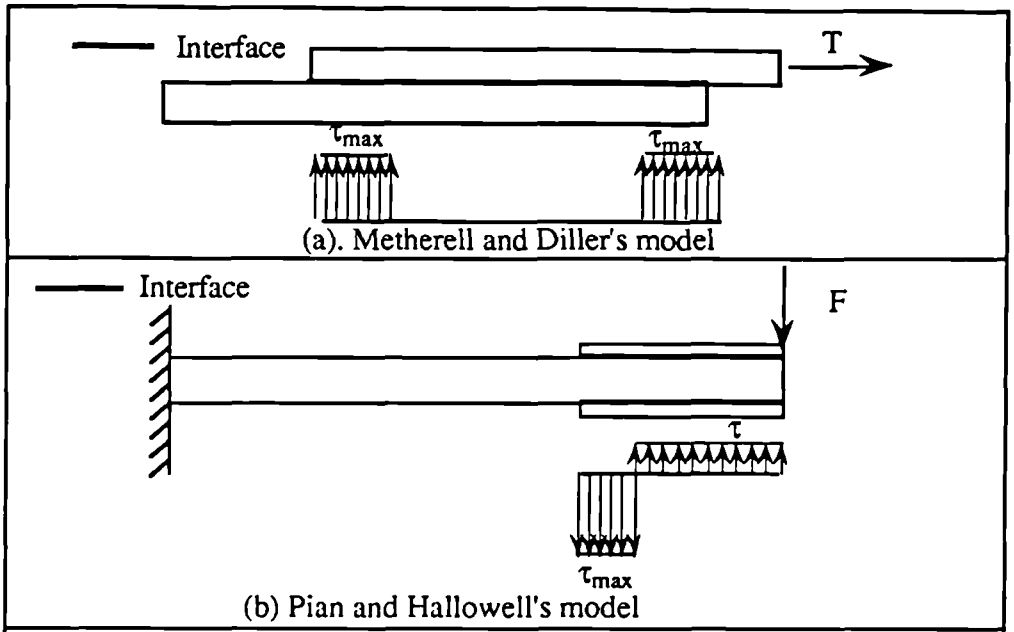

Figure 2.11. Two examples of dry friction element based joint models and their stress distributon over the interface

However, there are some significant differences between these models, apart from the difference in the geometry. It can be noted that for some of the models (e.g. figure 2.11a), the shear stress at the interface must be either the friction shear limit or zero. In other words, the external force and moment are completely balanced by the friction force in the slipped regions. For other models (e.g. figure 2.11b), however, the stress can be below the friction limit. For some models, the slip only occurs at one area; for the others, there can be several slipped areas and the slipped areas can have shear stress in both directions.

§2.8 MICROSLIP MODEL BASED ON THE BILINEAR ELEMENT

§2.8.1 Asperity at Interfaces and Its Effects on the Behaviour of a Joint

For the joint models discussed in the foregoing sections, the basic assumption is that Coulomb's friction law is held at infinitesimal area and under infinitesimal deformation. However, this basic assumption may not be realistic. Indeed, when Coulomb presented his research results, he had never intended to extend his theory to the contact problem with very small areas and with very small deformation.

A problem arises when the elasticity of the asperity on the interface is significant: under the microscope, even the finest machined surfaces are not actually smooth [83], instead, it

appears a very rough surface consisting of many tiny bumps known as **asperities**. A relevant quotation about the contact of interfaces is [83]:

Putting two solids together is rather like turning Switzerland upside down and standing it on Austria--the area of intimate contact will be small

The asperities are not rigid. When two surfaces are pressed together, the asperities will deform until the normal pressure is balanced by the internal normal stress in the asperities. The deformation of the asperities causes more contact area and hence the stiffness in the normal direction will increase when the normal clamping force increases. The increase of normal stiffness with normal clamping force, an indication of the effects of asperities, have been found by many researchers [29][32]. Since the initial loading and unloading curves in the normal direction are different, plastic deformation of asperities must occur.

When force is applied in the tangential direction, the asperities will also deform until the shear stress between the asperities exceeds the limit, then the asperities will break up and rub against each other. If it is reasonable to model the rub mechanism between the asperities by the dry friction law, it is certainly not appropriate to use the law to model the deformation of the asperities before they break up.

Clearly, the asperities on the interfaces play an important role in the behaviour of the joint, particularly when the motion between the asperities is small compared with the size of the asperities. How to model these asperities is of great importance

§2.8.2 A Microslip Model Based on the Friction Bilinear Element

Menq *et al* [59] suggested that the force-deformation relation of an asperity is linear before slipping. Accordingly, he suggested that the contact interface in a small area can be approximated by a linear spring until the contact is broken. After breaking up, the relationship between the friction force and deformation at the interfaces can be modelled using the dry friction law. This assumed relationship between the friction force and the deformation at the contact interface is the typical property of a friction bilinear element.

If the bilinear element is used to replace the dry friction contact element in the microslip models discussed in the foregoing sections, the resultant models can be more realistic.

The method used to derive the force-deformation relation of a joint model based on the bilinear element is similar to the method in §2.7. However, because the tangential force can transfer through the un-slipped area as well as the slipped area, the slipped area corresponding to external loading is usually very difficult to detect, therefore, it is better to start with an assumed slipped area, the corresponding force and deformation is then calculated from the information in the slipped area.

Menq *et al* [59] proposed a new translational microslip model based on the bilinear element. Menq's model is actually an extension of the dry friction element based translational microslip model by Metherell and Diller [45] with one bar being rigid. The model consists of a elastic bar and a rigid base as shown in figure 2.12, the left end of the elastic bar is connected to the rigid base through a linear spring β. This model will be used in this section to illustrate the general method for deriving a joint model based on the friction bilinear element.

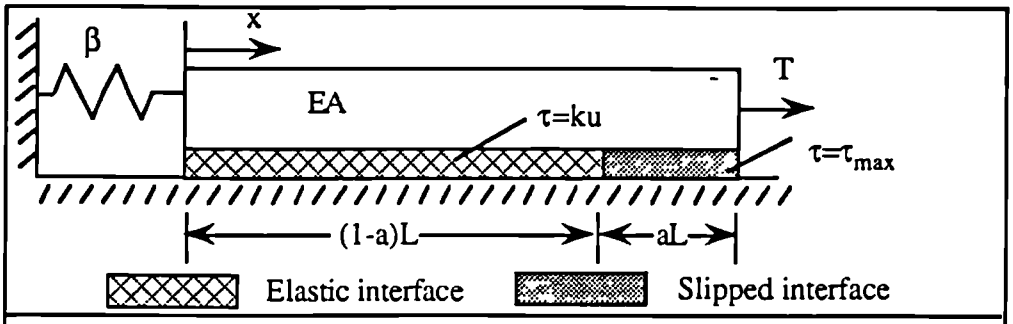

Figure 2.12 Diagram for Menq's model

The force-deformation relation consists of three ranges; the elastic range, the microslip range and the macroslip range. Only the relationship in the microslip range is presented below. Detailed formulae derivation is given in [59].

First assume slip has occurred in the area aL from the right end of the bar as shown in figure 2.12. The governing equilibrium equation in the non-slipped area & slipped area for the elastic bar are

For non-slipped area (x<(1-a)L)

$$EA\frac{\partial^2 u}{\partial x^2} - ku=0 \qquad (2.33)$$

For slipped area (x≥(1-a)L)

$$EA\frac{\partial^2 u}{\partial x^2} - \tau_{max}=0 \qquad (2.34)$$

The boundary conditions at both ends of the bar are

$$EA\frac{\partial u(0)}{\partial x} - \beta u(0)=0 \text{ and } EA\frac{\partial u(L)}{\partial x} =T \qquad (2.35, 2.36)$$

The continuity condition at x=(1-a)L must be satisfied too, i.e.

$$u^-=u^+,\ \frac{du^-}{dx}=\frac{du^+}{dx} \qquad (2.37,\ 2.38)$$

where superscripts + and - denote limiting values from the right and left of the transition point (x=(1-a)L) respectively.

Solving equation(2.33) and (2.34) with the boundary conditions leads to the force at the left end and displacement in a parametric form as:

$$T=\tau_{max}L\{a+\frac{[\eta+\lambda\tanh\lambda(1-a)]}{\lambda[\eta\tanh\lambda(1-a)+\lambda]}\} \qquad (2.39)$$

$$u(x)=\begin{cases}\dfrac{\tau_{max}}{k}\dfrac{\eta\sinh\lambda\frac{x}{L}+\lambda\cosh\lambda\frac{x}{L}}{\eta\sinh\lambda(1-a)+\lambda\cosh\lambda(1-a)} & 0<x\le(1-a)L\\ \dfrac{\tau_{max}}{k}+\dfrac{\tau_{max}}{EA}[x(\frac{x}{2}-L)+\frac{L^2}{2}(1-a^2)]+\dfrac{T}{EA(x-L+aL)} & (1-a)L<x\le L\end{cases} \qquad (2.40)$$

where $\lambda=\sqrt{\frac{kL^2}{EA}}$ (2.41)

and $\eta=\frac{\beta L}{EA}$ (2.42)

Substituting x=L into equation(2.40) leads to the displacement at the right hand side of the bar:

$$u(L)=\frac{\tau_{max}}{k}\{1+\lambda^2a[\frac{a}{2}+\frac{1}{\lambda}[\eta+\lambda\tanh\lambda(1-a)][\eta\tanh\lambda(1-a)+\lambda]\} \qquad (2.43)$$

Equations(2.39) and (2.43) represent a set of two parametric equations which define the relationship between the force and deformation at the right hand end of the bar. Unlike other models discussed in foregoing sections, it is extremely difficult, if possible at all, to find the deformation directly from the magnitude of the external force (or vice versa). Therefore, microslip models based on the bilinear element are usually more complicated to derive than models based on the dry friction element.

§2.8.3 Comments on Two Basic Groups of Joint Models

Two groups of microslip models have been discussed so far, one is based on the group of models using the dry friction element and the other is the group of models based on the

bilinear element. These two groups of joint models are most commonly used. Usually a closed-form analytical model is obtained.

The models based on dry friction elements are usually easier to derive than the models based on the bilinear elements. Indeed, because of the difficulties in deriving the bilinear element based joint models, only two models with very simple configuration have been developed; one is the model developed by Menq *et al* [59], and the other will be presented in §2.15.1. On the other hand, since the models based on the bilinear element effectively include the effects of elasticity of the asperities at the interfaces, it is more realistic than the models based on the dry friction element.

However, there are two problems which need to be considered carefully when modelling a friction joint:

1) The assumptions made during derivations of the dry friction element or bilinear element based models.

Because of the effects of the asperities, the dry friction element is clearly not realistic when the magnitude of the motion is small; replacement of the dry friction element by the bilinear element in modelling the friction joint is an effort to make the model more realistic. However, the bilinear element itself is still an idealised assumption. The assumption of a bilinear element effectively means that all of the asperities are elastic and the same in all the properties. Clearly, this assumption is not realistic either. If the force-deformation relation of a joint is to be modelled accurately, the force-deformation relation at very small area must first be modelled accurately. The ability to represent the relationship between the force (stress) and deformation (strain) at a very small area is clearly of the utmost importance in accurate modelling of friction joints.

2) Joints with complicated configurations.

All the models mentioned so far are represented in a closed-form analytical formulae. However, in order to achieve these closed-forms, the configuration of the joint, the pressure distribution and surface conditions over the interface must be simple. Unfortunately, real engineering joints are usually much more complicated. Accordingly, practical applications of these closed-form analytical models are severely limited.

In the remaining parts of this chapter, these two problems are dealt with. First, the relationship between the force and deformation at a small interface area is investigated and a new element is developed; then the method to find the overall behaviour of a joint with complicated configuration and interface conditions is investigated.

§2.9 MECHANISMS OF MICROSLIP

In the foregoing sections, the microslip caused by the elasticity of a joint component is studied. However, this is not the only possible cause of microslip, microslip can also be caused by other mechanisms.

In practice, asperities are different both in size and in shape, therefore, when two interfaces are pressed together, big asperities contact and deform first. Accordingly, the pressure in asperities is different. When a tangential force is applied, asperities deform in the tangential direction and due to the difference of the asperities, the nature of the deformation of the asperities are different; some asperities deform elastically, some plastically and others may break up completely. These different types of deformation will clearly introduce a nonlinear relation between the load and deformation. Therefore, even if there is no deformation on the joint component, microslip can still occur.

Another mechanism for microslip to take place is when the shear stress limits over the interface are different. This can be caused by different surface conditions due to different surface treatment, it can also be the results of uneven pressure at the interface due to concentrated normal loads, waviness of the contact surface, etc.

If the joint component is soft, the motion at different part of the interface will be significant, in other words, if part of the interface is subjected to a large motion, most of the asperities will break up and slip against each other. Therefore, a dry friction model (also the bilinear contact model in slipped range) will be a good assumption; if at some other parts of the interface, the deformation level is much smaller, asperities act elastically, hence the bilinear element is representative. However, if the joint component is stiff, various parts of the interface are subjected to similar motion, and the difference between asperities will play a significant role. The assumption of dry friction or bilinear friction is not appropriate under these circumstances.

From the above discussion, it can be stated that microslip can be affected by the following:

i) different properties of the asperities at the interface

ii) different pressure over the interface caused by concentrated normal load, flatness of interface etc.

iii) different deformation over the interface of the joint caused by either deformation of a component or rotation of a component.

The microslip due to i) occurs on a micro-scale and this type of microslip is referred as the **micro-microslip**; the microslip effects due to ii) and iii) only become

significant over a large interface, therefore, they are called the **macro-microslip** in the following analysis.

§2.10 TYPES OF MICRO-MICROSLIP MODELS (MICROSLIP ELEMENTS)

Although microslip due to asperities (micro-microslip) was first recorded a long time ago, the real mechanism of microslip has never been fully understood, and surprisingly very few theoretical models have been developed to quantitatively simulate micro-microslip at the metal interface. To the author's knowledge, there are only two physically meaningful micro-microslip models (microslip element), namely Burdekin's model [48] and Shoukry's model [49]. In both of the cases, Masing's rule holds.

§2.10.1 Burdekin's Model

Burdekin *et al* [48] proposed a microslip element in 1978. To the author's knowledge, this is the first analytical model which considers the effects of asperities. Each asperity is represented as a prismatic rod with the same stiffness and each rod is modelled as a bilinear element. After assuming a linear height distribution of rods, the initial loading relation is found as:

$$\begin{cases} T = au + bu^2 & 0 < u < -\dfrac{a}{2b} \\ T = -\dfrac{a^2}{4b} & u \geq -\dfrac{a}{2b} \end{cases} \tag{2.44}$$

where a and b are parameters determined by the apparent contact area, normal and shear stiffness of the asperities, normal displacement, friction coefficient and a constant relating the number of contacts to the normal displacement of the surfaces.

§2.10.2 Shoukry's Model

Shoukry [49] developed another microslip element using Mindlin's spherical contact element [79] as the basic element. Therefore, microslip can occur at each asperity. After assuming exponential distribution of peak height of spherical contact element, the force-deformation relation was found to be :

$$T = \mu N\left(1 - e^{-\frac{\gamma u}{\sigma}}\right) \tag{2.45}$$

where μ, N are the friction coefficient and normal force respectively,

σ is the standard deviation of the peak height distribution, and

γ is a constant which is equal to $\dfrac{2(1-\nu)}{\mu(2-\nu)}$ where ν is Poission' ratio.

Unlike Burdekin s model, the joint parameters of Shoukry's model can be measured directly.

It is interesting to point out that before Shoukry's work, Rogers *et al* [30] had proposed a mathematical expression for the loading relation of a metal interface joint in the tangential direction based on the shape of the experimental loading curve, the formula was written as:

$$T=Ts(1-e^{-\frac{Ku}{Ts}}) \tag{2.46}$$

where Ts is the friction limit which is equal to μN in Shoukry's expression.
and K is the initial stiffness, i.e. $K=\frac{dT}{du}|_{u-0}$

It can be found from equations (2.45) and (2.46) that these two formulae are the same with

$$K=\frac{dT}{du}_{|x=0}=\frac{\mu N\gamma}{\sigma} \tag{2.47}$$

and $$\frac{K}{Ts}=\frac{K}{\mu N}=\frac{\gamma}{\sigma} \tag{2.48}$$

However, the formula used by Shoukry is physically more significant, not only because the formula is derived from a physically meaningful model, but the joint parameters in a loading curve (e.g. initial stiffness, friction limit) are related to other physical parameters(normal pressure, friction coefficient etc). Accordingly, the joint properties can be predicted from other physical parameters; direct testing for the force-deformation characteristics may not be necessary.

§2.11 DEVELOPMENT OF A NEW MICROSLIP ELEMENT

§2.11.1 New Approach for Modelling the Micro-microslip Mechanism

For both Burdekin's and Shoukry's elements, the single asperity is the basic element; either a bilinear or a spherical contact element is assumed for each asperity. These assumptions are clearly idealised. In practice, according to the plastic deformation in the normal direction when a normal load is applied, when an asperity is subjected to significant relative motion with respect to the size of the asperity, plastic deformation of the asperity is bound to occur. Because of the simplified assumption made on the basic element, it will be seen later that both Burdekin's model and Shoukry's model have difficulty fitting the experimental results accurately. It is believed that these idealised

assumptions are mainly responsible for the discrepancies between the experiment and theory.

A new element will be introduced below. In the following analysis, a small area of the interface is considered as the basic element. Each tiny area can comprise several asperities or contain only a part of an asperity.

To simplify the problem, the whole interface of a joint is divided into a series of tiny areas and each tiny area is modelled by a bilinear element. All the bilinear elements have the same stiffness. These assumed bilinear elements may not necessarily represent the real area at the interface.

The assumptions made in this section are more realistic than those made by Burdekin *et al* [48] and Shoukry [49]. This is because the bilinear element does not represent one single asperity. If one asperity is twice as stiff as another asperity, then the first asperity is modelled by two bilinear elements and the second by one. Because the properties of plastic deformation of metals can be modelled by a bilinear assembly system [78], even if an asperity acts plastically in the tangential direction, provided each asperity can be modelled by a bilinear assembly system, the assumption that a tiny area can be modelled by a bilinear element is still valid.

First, stiffness-area (S-area) is defined as a proportion of the total initial stiffness contributed from an interface area; if two small areas at an interface have the same initial stiffness, these two areas are considered to have the same S-area. The total stiffness area (S-area) of the interface is unity.

If the joint has a displacement u at the interface, slip may occur over some of the stiffness area; the slipped stiffness area (S-S-area) is represented by a variable h. Clearly, h is a function of the motion u. Assume the relationship between the motion u and the S-S-area to be a function u=u(h) (or h=h(u)).

When $u \leq u(0)$, there is no slip over any S-area of the interface, hence the whole interface acts as a single spring with a stiffness k. When $u \geq u(1)$, slip occurs over the whole surface, i.e.macro-slip starts. Once macro-slip has started, Coulomb's dry friction law is held.

When the displacement is between u(0) and u(1), slip can only occur at some parts of the interface. Therefore, for the new model, there can be three different displacement ranges; elastic deformation, microslip and macroslip, a schematic diagram for these three displacement ranges is shown in figure 2.13.

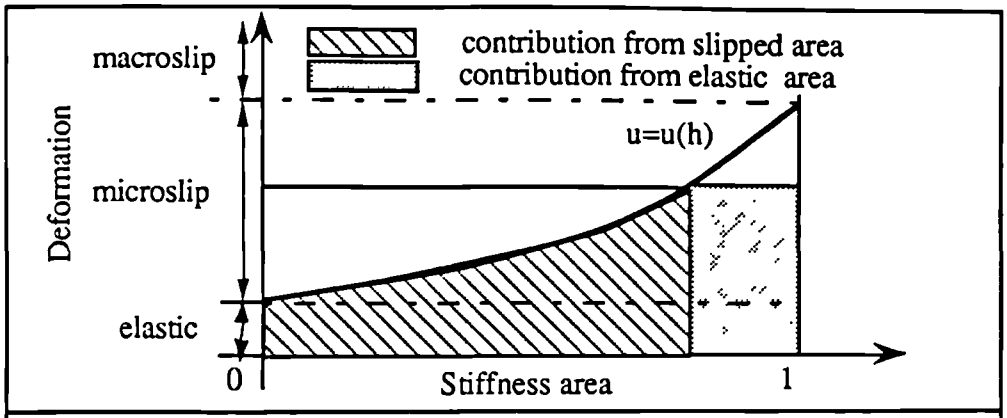

Figure 2.13Schematic diagram from contribution of different areas

Employing the relation u=u(h), one can convert the problem in the displacement domain $[0, \infty]$ to the h-domain [0,1].

Because any tiny area can be modelled by a bilinear element, the force-deformation relation will be linear until slip starts. Accordingly, the total interface is divided into two parts: the elastic part and the slipped part. For the slipped part, the force at any tiny area is their friction limit f(h)=ku(h)dh, and the contribution in the slipped S-area to the tangential force is an integration over an h range [0,h], i.e.

$$T_s=\int_0^h f(h)dh =k\int_0^h u(h)dh \tag{2.49}$$

For the elastic part, the force-deformation relation is linear, hence the contribution from the area must be

$$T_e=ku(h)(1-h) \tag{2.50}$$

The total tangential force is the sum of contributions from the slipped area and the elastic area, hence

$$T=T_s+T_e=k\{\int_0^h u(h)dh +(1-h)u(h)\} \tag{2.51}$$

$\int_0^h u(h)dh$ and (1-h)u(h) are represented by the two shaded areas in figure 2.13.

Equation(2.51) is the implicit formula for the force-deformation relation of the new microslip element.

Differentiating both sides of equation (2.51) with respect to u leads to

$$\frac{dT}{du} = k\,(1-h) \tag{2.52}$$

$$\text{hence } h = 1 - \frac{\frac{dT}{du}}{k} \tag{2.53}$$

Equation(2.52) shows that the slipped S-area can be detected from the local stiffness in a force-deformation curve. The local stiffness is only contributed from the non-slipped S-area.

When u is greater than u(1), slip occurs all over the interface (macroslip), and the tangential force cannot increase any further with displacement, therefore, the limit of the tangential force is $k\int_0^1 u(h)dh$ which is equal to the product of the normal force and the friction coefficient (i.e. $N\mu$).

To summarise; the force-deformation relationship over the loading is:

$$\begin{cases} T = k\int_0^1 u(h)dh & u(1) \le u \\ T = k\left(\int_0^h u(h)dh + (1-h)u\right) & u(0) < u < u(1) \\ T = ku & u \le u(0) \end{cases} \tag{2.54}$$

The three formulae in equation(2.54) represent the force-deformation relationship in elastic deformation, micro-slip and macro-slip range of displacement. Once the relation u=u(h) is known, the relationship between the force and the deformation of the initial loading can be found from equation(2.51), and unloading and reloading curves can be obtained from Masing's rule.

§2.11.2 Generality of the New Model

So far, no assumption about asperity distribution has been made, therefore, equation(2.51) is a generalised formula which can represent any micro-slip mechanism that obeys Masing's rule.

To prove the generality of the new model, one only needs prove that there is a function u=u(h) for any Masing type model, so that the force-deformation relation of a joint model can be represented by equation (2.51) exactly.

Since $\frac{dT}{du}$ is a function of u, equation (2.53) is exactly the function h=h(u). Since h=h(u) is a one-to-one function, its inverse function u=u(h) uniquely exists. Since equation (2.53) is directly deduced from equation(2.51), the generality of the model is proved.

To illustrate the generality of the model, consider Shoukry's model

$$T=a(1-e^{-bu}) \tag{2.55}$$

$$\frac{dT}{du}=abe^{-bu} \tag{2.56}$$

Substituting equation(2.56) into equation(2.52) yields

$$u(h) =-\frac{1}{b}\ln\frac{k(1-h)}{ab} \tag{2.57}$$

If equation (2.57) is substituted into equation(2.54), equation(2.55) is obtained. Therefore, equation(2.57) is the relation between the displacement and the slipped stiffness area for Shoukry's model.

§2.12 TWO APPROACHES TO OBTAIN THE JOINT PARAMETERS: PREDICTION AND IDENTIFICATION

For Burdekin's element, the joint parameters are not available until the loading relation in the tangential direction is obtained from an experiment; the parameters of a joint can then be found from the loading curve. This approach may be referred to as **identification.**

For Shoukry's element, the joint parameters can actually be obtained by other experimental means (not to measure the tangential loading relation experimentally). This approach is referred to as **prediction.**

From the design point of view, the prediction approach is much more desirable than identification, because some of design parameters (normal pressure, friction coefficient, parameters for roughness of the surface etc) can be used directly to predict the force-deformation relation of a joint. Indeed, if this can be done accurately, the friction joint will not be a problem in structural analysis and the damping capacity of the friction joint can be optimised for the reduction of the response of the structure.

Unfortunately, the prediction approach is often not a realistic one because of the complexity of the joint. The joint properties are believed to be determined by normal pressure and surface condition, there is also evidence [31][33] that the properties of a joint depend on the contact duration time and contamination of the interface, and indeed, many other unknown factors. However, the design parameters for the surface condition is usually represented by the roughness, the flatness and the hardness. Clearly, these design parameters can be too approximate to represent the effects of the surface conditions on the interface. Actually, even if it is known how the basic parameters affect the joint properties (which must be formidably complicated if it is possible at all), the parameters will be extremely difficult to obtain. As a result, only some of these

parameters can be used to quantify the joint. However, the joint properties are too difficult to be predicted by a few design parameters accurately. Therefore, although the prediction approach is attractive, it is not a feasible approach, at least in the foreseeable future.

For the identification approach, however, the basic parameters are not used to determine the properties of the joint, instead, some intermediate parameters can be used. The final purpose of these intermediate parameters is to represent the loading relation of a joint accurately. Pure mathematical curve fitting has be proposed [35], usually, polynomials are used to fit the experimental results. However, these mathematical expressions are usually not very satisfactory. Alternatively, one can develop some mathematical formulae with parameters having physical significance. One example is Rogers's formula [30].

In the last section, a new micro-microslip model is proposed. The model is generalized so that it can represent any Masing type joint. More importantly, the joint is represented by a function u=u(h) in an h-domain[0,1]. The function u=u(h) is physically meaningful; it represents the total slipped s-area corresponding to the motion u. Therefore, it must be a smooth and continuous increasing function. Consequently,it may be easier to find a mathematical expression u=u(h) than to find a loading relation T=f(u) directly to yield a satisfactory fit to the experimental results. Once u=u(h) is assumed, the relation T=f(u) can be found from equation(2.51)

§2.13 NUMERICAL METHOD FOR IDENTIFICATION OF MODEL PARAMETERS FROM EXPERIMENTAL LOADING CURVE

An assumed function u=u(h) can only be an approximation and also because of the measurement errors in experimental data, an analytical model usually can not fit experimental data exactly, therefore, one must aim to minimize the difference between the analytical and experimental data. The most commonly used method is to minimize the sum of the square difference, i.e.

$$\Delta E = \sum_{i=1}^{n} \{T_e - T_a\}^2 \rightarrow \text{minimum} \qquad (2.58a)$$

or in a non-dimensional form (which is used in the following analysis)

$$\Delta E = \sum_{i=1}^{n} \{\frac{T_{e(i)} - T_{a(i)}}{\max(T_{e(i)})}\}^2 \rightarrow \text{minimum} \qquad (2.58b)$$

where subscripts $_e$ and $_a$ represent experimental and theoretical data respectively.

Unless T_a is an polynomial in u, the minimisation can not be obtained directly and iterative methods have to be used. Usually the number of parameters for a joint model is small (less than 5 in the following analysis), the Pattern Search algorithm proposed by Hook and Jeeves [84] is used for the identification of the joint parameters. The Pattern

Search method is one of the simplest search methods in finding a minimum for a given objective function.

The method comprises two kinds of moves: exploratory and pattern. A significant advantage of this method is that the derivative of the objective function is not required. The method is briefly described as follows:

If an initial estimation is $\{a^{(i)}\}=\{a_1....,a_n\}^T$ at point A_0, we first search in the direction $\{1,0,0,...,0\}^T$ with a step-length Δ_1 from A_0 to a point A_1 so that $\Delta E(A_1)<\Delta E(A_0)$, then search in the second direction $\{0,1,0,...,0\}^T$ with a step-length Δ_2 to another point A_2 so that $\Delta E(A_1)<\Delta E(A_2)$, repeat searching in a different direction until the last search ends at point A_n with $\Delta E(A_n)<\Delta E(A_{n-1})$ (these searches are called exploratory). After exploratory, we search from A_n in the direction $\{A_n-A_0\}$ until a minimum A_{00} in this direction is found (which is called pattern search). The process is repeated with a new estimate $A_0=A_{00}$. When $A_n-A_0=0$, the step length has to be reduced, convergence is assumed and the process is terminated when the step size falls below a pre-selected value.

The pattern search method may not be very efficient in terms of computing times, however, the method is very simple and easy to program (even with a very complicated objective function). The method is most appropriate in those cases with only a few variables.

§2.14 IDENTIFICATION OF PARAMETERS FOR A TRANSLATIONAL MICROSLIP MODEL USING EXPERIMENTAL DATA

The experimental data for identification purpose were obtained by Masuku *et al* [29] on a bolted joint. Three materials were tested; mild steel, brass and cast iron. In their experiment, a tangential load was applied through a rigid base, hence a uniform shear stress distribution was applied at the interface and different areas at the interface were subjected to the same displacement, which is an ideal case to verify microslip elements.

The original Masuku's data are shown in figure 2.1, the deformation measured consists of two parts, one is the deformation at the interface, the other is contributed to by other deformation of components (which is elastic). The second part deformation is estimated approximately from another specimen made from the same material and has the same geometric shape as the jointed specimen (but without interface). The second part deformation is irrelevant to properties of the joint interface, therefore, it is subtracted from the total deformation in the identification process.

Basically, the identification process is a kind of curve fitting process. To achieve accurate results, the measured data must have high accuracy and also cover a sufficiently wide

range. Usually, the higher the error levels, the wider the data range required. Accordingly, to determine parameters for microslip models accurately, the following two basic requirements on measured data must be satisfied:

1) displacement at interfaces must be a significant part in the whole displacement so as to ensure the accuracy of the measured deformation at the interface.

2)microslip must occur over a sufficiently large area so that enough information is available to determine the model variables.

Based on the above two requirements, two brass interface loading curves (normal load 250kg and 300kg) and two mild steel loading curves (normal load 50kg and 100kg) are selected in the following analysis.

Three microslip elements (micro-microslip models) are investigated, i.e.

1) Generalised micro-microslip model

$$\begin{cases} T = k\int_0^1 u(h)\,dh & u(1)<u \\ T = k\left(\int_0^h u(h)dh + (1-h)u(h)\right) & u(0)<u\le u(1) \\ T = ku(h) & u\le u(0) \end{cases} \tag{2.54}$$

where u=u(h,a,b,..)

2)Shoukry's model

$$T=a\,(1-e^{-bu}) \tag{2.45}$$

3) Burdekin's model

$$\begin{cases} T = bu^2+au & u< -\frac{a}{2b} \\ T = -\frac{a^2}{4b} & u\ge -\frac{a}{2b} \end{cases} \tag{2.44}$$

In the above three models, k, a and b are joint parameters determined from experimental data.

To determine the theoretical expression of u=u(h) for new generalized micro-microslip model, the slopes of the loading curves are estimated. From equation (2.53), a set of (u,h) data are obtained and plotted on a graph.

The following estimation function is used according to the shape of the u-h curve:

$$u=ae^{(bh)} \tag{2.59}$$

More complicated formulae are also tested such as i)$u=bh^c+a$ or ii)$u=ae^{(bh)}+c$, which have three variables, However, it is found that the assumed formula $u=ae^{(bh)}$ gives very satisfactory results fitting the experimental data, hence three variables are not necessary. In addition, it is found that if the function has more than two variables, it tends to be extremely difficult to determine (a,b,c) uniquely; two different sets of (a,b,c) may both fit a loading curve with the same order of accuracy. Fixed order polynomials, such as $u=bh^2+a$ and $u=bh^3+a$ are also tested, and it is found that the results using these formulae are poorer than the expression $u=ae^{(bh)}$. For the above reasons, equation (2.59) is used.

Substituting equation(2.59) into equation(2.54) leads to a loading relation for the generalized microslip model:

$$\begin{cases} T=\dfrac{ka(e^b-1)}{b} & u>ae^b \\ T=\dfrac{k\{u-a+u(b-\log_e u+\log_e a)\}}{b} & a<u\le ae^b \\ T=ku & u\le a \end{cases} \tag{2.60}$$

Physically, parameter 'a' represents a limit that slip can start at the interface, and parameter b represents the levels of difference between asperities at the interface, the greater the difference between bilinear elements, the greater the parameter b.

It can also be noted that a special case for the new micro-microslip model is b=0, the new micro-microslip model becomes a bilinear element, with

$$\begin{cases} T=ka & u>a \\ T=ku & u\le a \end{cases} \tag{2.61}$$

The maximum friction force when gross slip starts can also be predicted. From equations(2.60)(2.45) and (2.44), it can be found that the maximum friction force for different models are:

i) New micro-slip model $T_{max}=\dfrac{ka(e^b-1)}{b}$ (2.62)

ii) Shoukry's model $T_{max}=a$ (2.63)

iii) Burdekin's model $T_{max}=-\dfrac{a^2}{4b}$ (2.64)

Tables 2.1, 2.2 and 2.3 show some identified variables for different models.

	a (10^{-8}m)	b	k (10^{7}kg/m)	K (10^{12}N/m/m^2)	T_{max} (kg)	μ	ΔE (10^{-4})
50kg mild steel	3.43	2.79	5.82	2.26	10.95	0.219	0.390
100kg mild steel	2.18	3.90	8.51	3.54	23.00	0.230	0.301
250kg brass	3.19	3.59	4.20	1.78	13.19	0.053	0.127
300kg brass	1.33	3.75	9.12	3.80	13.55	0.045	0.519
300kg brass	0.53	4.97	10.5	4.37	15.82*	0.053*	0.863

Table 2.1 Parameters for new micro-slip model

	a (kg)	b (10^{6}m)	k (10^{7}kg/m)	K (10^{12}N/m/m^2)	T_{max} (kg)	μ	ΔE (10^{-4})
50kg mild steel	11.67	4.50	6.43	2.67	11.67	0.233	0.385
100kg mild steel	16.87	5.28	8.91	3.70	16.87	0.169	0.590
250kg brass	12.54	2.87	4.21	1.76	12.54	0.050	0.636
300kg brass	12.58	7.14	8.98	3.73	12.58	0.042	0.180
300kg* brass	15.05*	5.39	8.11	3.37	15.05*	0.050*	6.20

Table 2.2 Parameters for Shoukry's model

	a (10^{7}N/m)	b (10^{13}N/m^2)	k=a (10^{7}N/m)	K (10^{12}N/m/m^2)	T_{max} (Kg)	μ	ΔE (10^{-4})
50kg mild steel	5.60	-8.09	5.60	2.32	9.742	0.195	4.2
100kg mild steel	8.55	-15.86	8.55	3.56	11.54	0.115	1.1
250kg brass	3.75	-3.68	3.75	1.58	9.79	0.040	3.5
300kg brass	8.06	-16.41	8.06	3.35	9.90	0.033	5.5

NB: * pre-set values

Table 2.3 Parameters for Burdekin's model

Figure 2.14 shows some regenerated loading curves of a mild steel interface and of a brass interface together with experimental data.

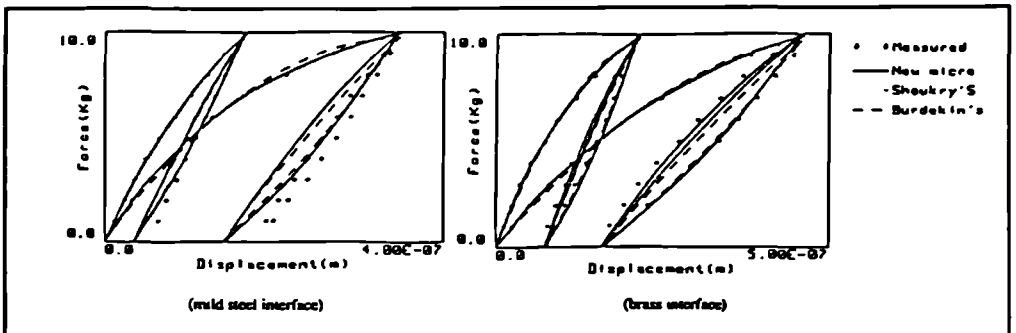

Figure 2.14 Comparison between theoretical and experimental results on a translational joint

In all the cases, the new microslip model gives the best fitting results while Burdekin's model gives the worst (This can be noted by comparing both the values of the objective function ΔE in tables 2.1-2.3 and from figures 2.14 and 2.15. Burdekin's model is clearly unsatisfactory to fit experimental data quantitatively compared with the other two models, the predicted maximum friction forces are even smaller than the force actually

applied in the micro-slip range, therefore, the model may not be as useful as the other two models in quantitative analysis. Shoukry's model leads to very satisfactory results in the displacement range measured, however, the predicted friction coefficients under different pressures vary significantly (about 27% for mild steel interfaces and 16% for brass interfaces), which indicates the limit of this model in the large displacement range. This limit is expected because the model is based on elastic spherical contact, and this assumption is not valid for large deformation.

The new microslip model not only gives very satisfactory results in the measured displacement range, but also gives a satisfactory prediction of friction coefficient in the case of mild steel interface (about 5% variation of friction coefficient). The predicted friction coefficients for the brass interface are not so consistent (with a variation of about 15%). However, for the case of the brass interface, when the clamping force is 300kg, the displacement at the interface is about a half the elastic deformation and also the change of slope of loading curve (which indicates the scale of microslip) is insignificant; in other words, the two basic requirements are not satisfied, hence poor results are expected.

If a friction limit of 300kg is pre-set for the brass interface before identification (hence parameters a, b, k are no longer independent) according to the friction coefficient identified in the case of 250kg clamping force, a new set of variables are found (which is shown in the last row of the table 2.1 and table 2.2). The regenerated loading curves from the new micro-microslip model and Shoukry's model with the pre-set friction coefficient are shown in figure 2.15 together with experimental data and the regenerated loading curves without pre-set condition. It can be seen that the new micro-microslip model still yields good agreement with experimental data ($\Delta E=8.63\times10^{-5}$) but results from Shoukry's model have deteriorated ($\Delta E=6.20\times10^{-4}$).

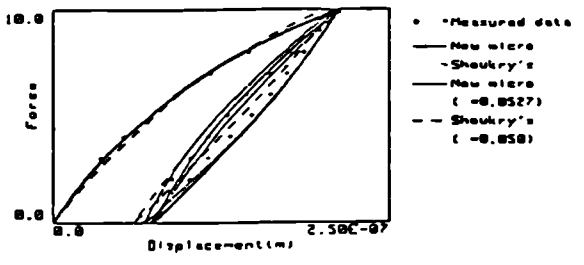

Figure 2.15 Comparison between theoretical and experimental results on a translational joint (brass interface, 300kg normal clamping force)

From figure 2.14 and figure 2.15, it can also be noted that unloading and reloading curves from the new micro-microslip model yields good agreement with experimental data, which indicates that Masing's rule is appropriate for the unloading and reloading process, the discrepancy between experimental data and regenerated data is insignificant.

§2.15 NEW ROTARY JOINT MODEL BASED ON A MICROSLIP ELEMENT

§2.15.1 Formulae Derivation

In the last few sections, a new generalized micro-microslip model (microslip element) has been proposed and verified by the experimental data. In this section, several micro-microslip models are applied to a joint where deformation levels at different area of interfaces are different, this being a rotary joint.

A rotary joint consists of two cylinders as shown in figure 2.16. A pure torque is applied to the top cylinder and this causes a rotational displacement. The difference between a rotary joint and a translational joint [59] is that displacements at different parts of a rotary joint interface are different, they are proportional to the distance to the centre of the cylinder (i.e. the radius), therefore, if the cylinder has an uniform surface condition and pressure distribution over the interface, the part with large radius will slip first. Both the micro-microslip and the macro-microslip have effects on the overall behaviour of the joint.

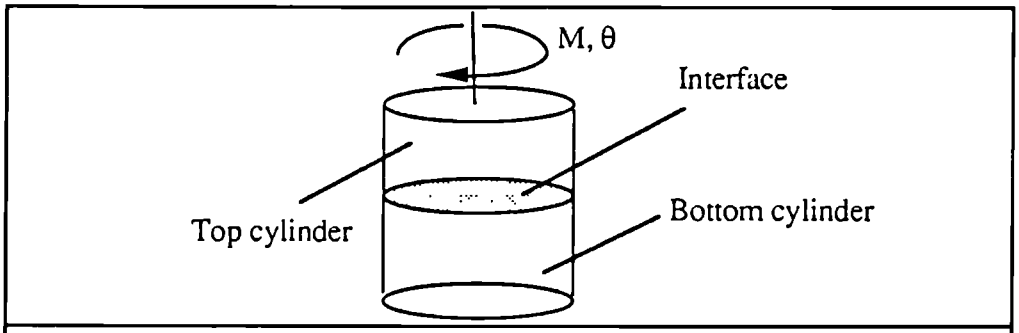

Figure 2.16 A diagram for the rotary joint

The equilibrium condition must be satisfied, hence:

$$M=\int_{r1}^{r2} 2\pi r^2 \tau(r,\theta)dr \qquad (2.65)$$

where r_1 and r_2 are the inside and outside radii respectively

θ is the angular displacement

$\tau(r,\theta)$ is the shear stress area at radius r

If the whole interface has the same surface condition and is subjected to a uniform pressure distribution, the shear stress $\tau(r,\theta)$ at the interface will be a function of the deformation $r\theta$, i.e.

$$\tau(r,\theta)=\tau(r\theta)=\tau(u(r)) \qquad (2.66)$$

Substituting formulae for Shoukry's(equation(2.45)), Burdekin's(equation(2.44)) and the new generalised micro-microslip model (equation(2.60)) into equation(2.65) yields

For Shoukry's model

$$\tau(r,\theta) = a\,(1-e^{-b(r\theta)}) \tag{2.67}$$

$$M=2\pi a\left\{\frac{r^3}{3}+\frac{r^2e^{-br\theta}}{b\theta}+\frac{2re^{-br\theta}}{(b\theta)^2}+\frac{2e^{-br\theta}}{(b\theta)^3}\right\}\Big|_{r_1}^{r_2} \tag{2.68}$$

For Burdekin's model

$$\begin{cases} \tau(r,\theta)=b(r\theta)^2+ar\theta & r< -\dfrac{a}{2\theta b} \\ \tau(r,\theta)= -\dfrac{a^2}{4b} & r \geq -\dfrac{a}{2\theta b} \end{cases} \tag{2.69}$$

$$M=\int_{r1}^{r0}2\pi r^2\{b(r\theta)^2+ar\theta\}dr+\int_{r0}^{r2}2\pi r^2\left\{-\frac{a^2}{4b}\right\}dr$$

$$=\frac{2\pi b\theta^2(r_0^5-r_1^5)}{5}+\frac{\pi a\theta(r_0^4-r_1^4)}{2}-\frac{\pi a^2(r_2^3-r_0^3)}{12b} \tag{2.70}$$

where $r_0=\min\{r_2,\max(r_1,-\frac{a}{2\theta b})\}$

For the new micro-microslip model

$$\begin{cases} \tau(r,\theta)=\dfrac{ka(e^b-1)}{b} & r \geq \dfrac{a\,e^b}{\theta} \\ \tau(r,\theta)=\dfrac{k\{r\theta-a+r\theta(b-\log_e(r\theta)+\log_e a)\}}{b} & \dfrac{a}{\theta}\leq r< \dfrac{ae^b}{\theta} \\ \tau(r,\theta)=kr\theta & r<\dfrac{a}{\theta} \end{cases} \tag{2.71}$$

$$M=\frac{\pi k\theta r^4}{2}\Big|_{r_1}^{r_a}+\{\pi k\theta r^4[\frac{5}{8b}+\frac{1}{2}+\frac{1}{2b}\log_e(\frac{a}{r\theta})]-\frac{2\pi kar^3}{3b}\}\Big|_{r_a}^{r_b}+\frac{2\pi ka(e^b-1)r^3}{3b}\Big|_{r_b}^{r_2} \tag{2.72}$$

where $r_a=\min(r_2,\max(r_1,\frac{a}{\theta}))$ and $r_b=\min(r_2,\max(r_1,\frac{ae^b}{\theta}))$ (2.73)

The first term of equation(2.72) is a contribution from the **micro-elastic** band to the total friction torque while the second and the third terms correspond to contributions from the **micro-microslip** band and **micro-macroslip** band respectively.

If b=0, the rotary joint based on the bilinear element is achieved. The micro-microslip band vanishes. Taking the limit of b=0 for equation(2.73), the loading relation is:

$$M=\frac{\pi k\theta r^4}{2}\Big|_{r1}^{r_a}+\frac{2\pi kar^3}{3}\Big|_{r_a}^{r2} \tag{2.74}$$

$$\text{where } r_a=\min(r_2,\max(r_1,\frac{a}{\theta})) \tag{2.75}$$

The friction torque reaches its limit when micro-macroslip start at inside radius r_1, then the limit for friction torque is

$$\text{Max}(M)=\int_{r1}^{r2}2\pi r^2\tau_{max}dr=\frac{2\pi\tau_{max}r^3}{3}\Big|_{r1}^{r2} \tag{2.76}$$

where τ_{max} is the maximum shear stress of microslip element and can be found from equations(2.62)(2.63)(2.64).

§2.15.2 Identification of Rotary Joint Parameters Using Experimental Data

An ideal source of experimental data is provided by Burdekin *et al* [32]. The tangential displacementsof a stack of circular cast iron joint rings with inside and outside diameter of 0.051m and 0.076m respectively were measured. The thickness of each ring was 0.0127m. The material used was cast iron; two kinds of interfaces were tested, these were ground to ground(G/G) interfaces and ground to hand-scraped(G/H) interfaces. The deformation due to other elastic components is subtracted by using the data from an elastic solid cylinder with the same geometric shape as the cylinder with joints. Similar curve-fitting techniques to §2.8 (pattern search method) are used to identify model parameters.

Tables 2.4-2.7 show some identified model parameters for different micro-slip models, and figure 2.17 and figure 2.18 show regenerated loading curves with experimental data under different normal load for G/G and G/H machined surfaces. The results are very similar to the case of translational joint in §2.14. Again, the new micro-microslip model fits the experimental data best. Shoukry's model gives reasonable results, while Burdekin's model is clearly less appropriate. The rotary model based on the bilinear model is not adequate either, the micro-slip range of displacement (i.e. between elastic deformation and macro-slip) is much smaller than measured data, this indicates that micro-microslip are mainly responsible for overall microslip behaviour of the joint, the micro-slip due to macro-microslip only plays an insignificant role. Therefore, the bilinear element assumption, which is mainly to represent the effects of macro-microslip, is not representative.

	a (10^{-8} m)	b	k (10^{11}N/m/m^2)	T_{max} (10^5N/m^2)	μ	ΔE (10^{-4})
G/G $P_n=1.5\times10^6$N/m^2	1.04	4.856	9.49	2.59	0.172	0.908
G/G $P_n=2.0\times10^6$N/m^2	1.61	4.292	11.34	3.08	0.154	0.318
G/G $P_n=3.0\times10^6$N/m^2	1.75	4.267	15.41	4.44	1.48	8.210
G/G $P_n=4.0\times10^6$N/m^2	1.81	4.401	19.16	6.39	0.159	0.727
G/G $P_n=6.0\times10^6$N/m^2	2.06	4.200	28.00	8.87	0.147	1.480
G/H $P_n=2.0\times10^6$N/m^2	0.77	4.329	22.20	2.95	0.148	2.67
G/H $P_n=4.0\times10^6$N/m^2	0.32	5.587	44.50	6.57	0.164	0.21
G/H $P_n=9.0\times10^6$N/m^2	1.90	2.901	63.67	7.19	0.800	0.15
G/H $P_n=9.0\times10^6$N/m^2	0.368	5.616	77.00	13.82*	0.153*	2.54

NB: * preset values

Table 2.4 New micro-slip rotary model

	a (10^5N/m^2)	b (10^6m)	k (10^{11}N/m/m^2)	T_{max} (10^5N/m^2)	μ	ΔE (10^{-4})
G/G $P_n=1.5\times10^6$N/m^2	2.65	2.70	7.14	2.65	0.177	4.26
G/G $P_n=2.0\times10^6$N/m^2	3.15	3.03	9.53	3.15	0.158	8.67
G/G $P_n=3.0\times10^6$N/m^2	4.52	2.88	13.00	4.51	0.150	9.65
G/G $P_n=4.0\times10^6$N/m^2	6.52	2.41	15.68	6.51	0.163	4.05
G/G $P_n=6.0\times10^6$N/m^2	8.50	2.69	22.80	8.50	0.142	5.93
G/H $P_n=2.0\times10^6$N/m^2	2.90	6.53	18.97	2.90	0.145	5.24
G/H $P_n=4.0\times10^6$N/m^2	5.94	5.37	31.80	5.94	0.149	3.56
G/H $P_n=9.0\times10^6$N/m^2	7.27	9.60	69.97	7.27	0.081	0.45
G/H $P_n=9.0\times10^6$N/m^2	13.82*	4.07	56.24	13.82*	0.153*	18.58

NB: * preset values

Table 2.5 Rotary model using Shoukry's element

	a (10^{11}N/m/m^2)	b (10^{17}N/m^2/m^2)	k (10^{11}N/m/m^2)	T_{max} (10^5N/m^2)	μ	ΔE (10^{-4})
G/G $P_n=1.5\times10^6$N/m^2	5.83	3.54	5.82	2.34	0.160	20.91
G/G $P_n=2.0\times10^6$N/m^2	7.74	5.13	7.73	2.92	0.146	27.16
G/G $P_n=3.0\times10^6$N/m^2	10.98	7.58	10.96	3.97	0.132	15.45
G/G $P_n=4.0\times10^6$N/m^2	12.67	6.90	12.65	5.82	0.146	16.77
G/G $P_n=6.0\times10^6$N/m^2	21.24	15.98	21.21	7.06	0.118	13.15
G/H $P_n=2.0\times10^6$N/m^2	16.00	25.38	16.00	2.52	0.126	15.42
G/H $P_n=4.0\times10^6$N/m^2	27.88	39.72	27.88	4.89	0.122	9.33
G/H $P_n=9.0\times10^6$N/m^2	65.55	202.60	65.55	5.30	0.059	1.06

Table 2.6 Rotary model using Burdekin's element

	a (10^{-7}m)	b	k (10^{11}N/m/m^2)	T_{max} (10^5N/m^2)	μ	ΔE (10^{-4})
G/G P_n=1.5×10^6N/m^2	4.77	0	4.84	2.30	0.153	56.7
G/G P_n=2.0×10^6N/m^2	4.74	0	6.03	2.87	0.142	76.6
G/G P_n=3.0×10^6N/m^2	4.16	0	8.94	3.72	0.124	52.8
G/G P_n=4.0×10^6N/m^2	5.28	0	10.45	5.51	0.137	51.2
G/G P_n=6.0×10^6N/m^2	3.86	0	16.93	6.54	0.108	47.9
G/H P_n=2.0×10^6N/m^2	1.77	0	13.07	2.32	0.116	57.8
G/H P_n=4.0×10^6N/m^2	2.08	0	22.09	4.59	0.114	41.7
G/H P_n=9.0×10^6N/m^2	8.90	0	52.96	4.72	0.052	20.3

Table 2.7 Rotary model using bilinear element

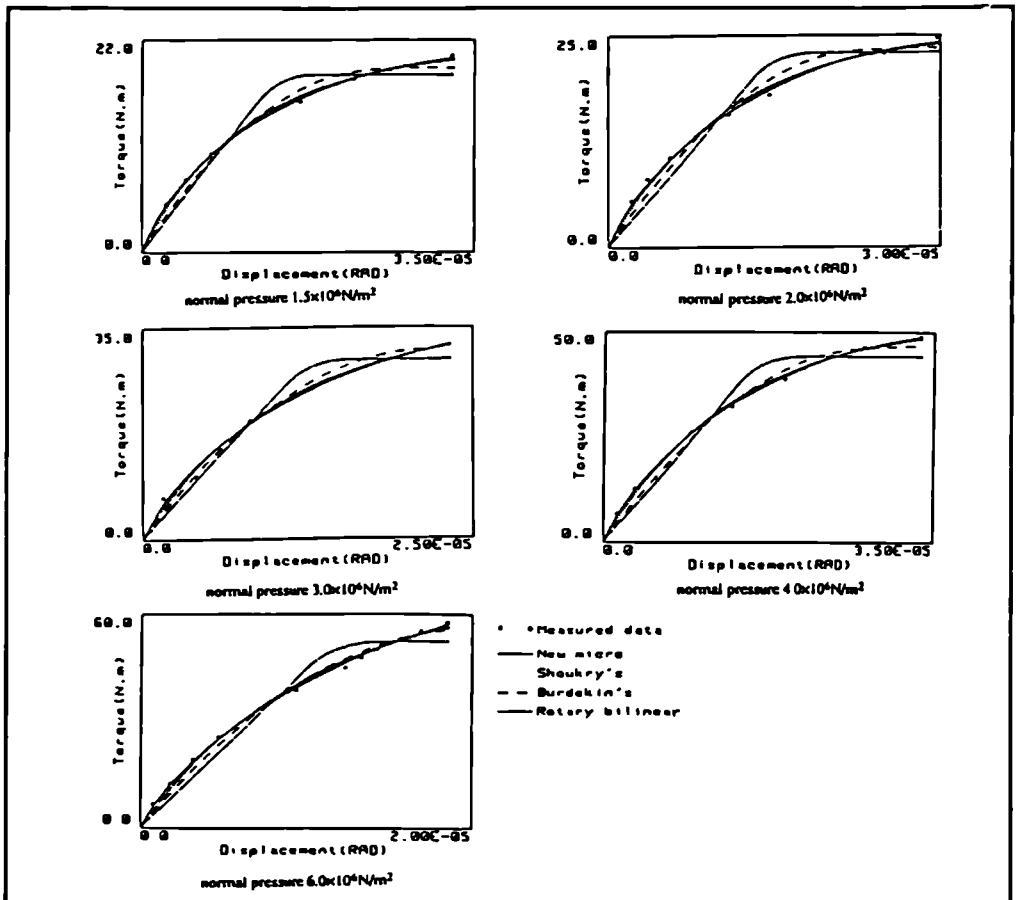

Figure 2.17 Comparison between theoretical and experimental results on a rotary joint with G/G cast iron interface

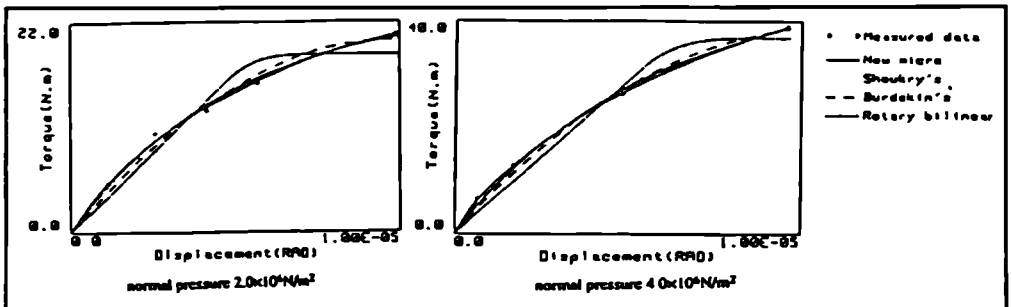

Figure 2.18 Comparison between theoretical and experimental results on a rotary joint with G/H cast iron interface

For all the microslip models, the friction coefficient identified for G/H surfaces under $9\times10^6 N/m^2$ clamping force are obviously underestimated (compared with that identified in the cases under a clamping force $2\times10^6 N/m^2$ and $4\times10^6 N/m^2$). Actually, it can be seen that the change of slope of loading curve is very small under a $9\times10^6 N/m^2$ clamping force. In other words, microslip only exists over a small S-area of the interface. Hence the prediction can be inaccurate. If a friction coefficient is pre-set according to that identified under a smaller clamping force (an intermediate value 0.153 was chosen), a new set of variables can be identified for different models. The new set of identified variables are shown in the last rows of table 2.4 and table 2.5 for the models based on the new micro-slip model and Shoukry's model, their regenerated loading curves are shown in figure 2.19. The results from Burdekin's model and the rotary bilinear model match experimental data poorly and are not listed. Similar results for the brass interface under 300kg normal force are found; the results from Shoukry's element based model deteriorate much more significantly than from the new microslip element based model when a friction coefficient is pre-set. This, again, shows that the new microslip model is more representative and flexible to fit the experimental data.

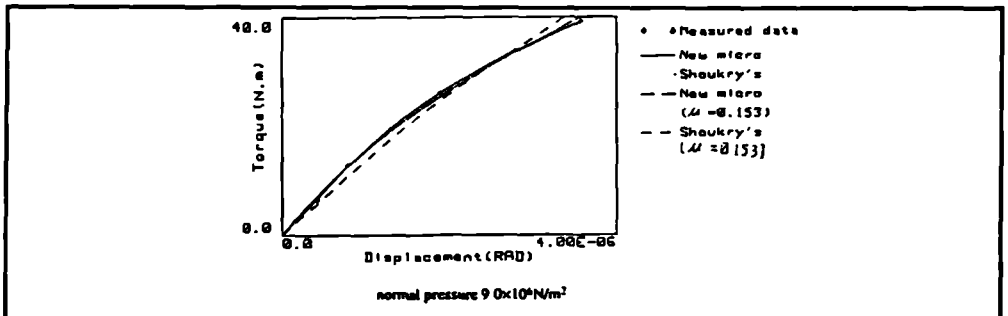

Figure 2.19 Comparison between theoretical and experimental results on a rotary joint with G/H cast iron interface (pre-set friction coefficient)

§2.16 FINITE ELEMENT JOINT MODEL

§2.16.1 Theory

In this section, the second problem mentioned in §2.8.3 is investigated.

It is shown in §2.8.1 that the formulation of the model becomes very complicated when the bilinear element is used to replace the dry friction element; the formula will become much more complicated when a micro-microslip element is used to replace the bilinear element. However, despite the complexity of the formulae, the joint models discussed in the foregoing sections are actually still idealized, in other words, the assumptions of uniform pressure, uniform surface condition and simple geometric configurations are made.

In practice, the real engineering configuration of structures and joints are usually much more complicated. Consequently, it is extremely difficult, if not impossible, to obtain an analytical model directly from the classic stress analysis approach. As a result, the joint models formulated from classic stress analysis methods are usually only useful in modelling some simple joints in a laboratory and act as an tool for understanding the microslip phenomenon. However, it is often not practical to apply these methods to real engineering joints.

Apart from the difficulties in theoretical analysis, neglect of inertia force of the joint can also make the above analysis erroneous at high frequencies, even for some simple joints. In these cases, the finite element method should be used to find the deformation of the joint under an external load.

The finite element algorithm for calculating the deformation under a prescribed load is discussed in detail in many books (e.g. [2]). The basic strategy is as follows:

For any physical system, the equilibrium equation can be written

$$\{F(u)\}=\{P\} \tag{2.77}$$

where $\{F(u)\}$ is the node point force vector corresponding to the deformation $\{u\}$, and $\{P\}$ is an external force vector applied to the node point.

If the system is linear, a stiffness matrix [K] can be found to relate the deformation vector and node point force vector as

$$F(u)=[K]\{u\} \tag{2.78}$$

Therefore, the deformation of the system subjected to load $\{P\}$ is

$$\{x\}=[K]^{-1}\{P\} \tag{2.79}$$

For a nonlinear system, however, an iteration process has to be used to find a deformation vector $\{u\}$ to satisfy equation(2.77). The most commonly used method for static analysis is the Newton-Raphson method:

If an estimation for the deformation is $\{u^{(i-1)}\}=\{u_1^{(i-1)},u_2^{(i-1)},....,u_n^{(i-1)}\}^T$ and the corresponding node point force vector is $\{F^{(i-1)}\}=\{F_1^{(i-1)},F_2^{(i-1)},....,F_n^{(i-1)}\}^T$, the unbalanced excitation force $\Delta P^{(i-1)}$ will be

$$\Delta P^{(i-1)}=P-F^{(i-1)} \tag{2.80}$$

This unbalanced force will cause further deformation. A linear approximation can be used to predict this further deformation as

$$[K^{(i-1)}]\{\Delta u^{(i)}\}=\{\Delta P^{(i-1)}\} \tag{2.81}$$

where $\{\Delta u^{(i)}\}=\{u^{(i)}\}-\{u^{(i-1)}\}$ (2.82)

is a modification on the estimation

$$\text{and } [K^{(i-1)}]=\frac{\partial F}{\partial u}\Big|_{u^{(i-1)}}=\begin{bmatrix} \frac{\partial F_1}{\partial u_1^{(i-1)}} & \frac{\partial F_1}{\partial u_2^{(i-1)}} & \cdots & \frac{\partial F_1}{\partial u_n^{(i-1)}} \\ \frac{\partial F_2}{\partial u_1^{(i-1)}} & \frac{\partial F_2}{\partial u_2^{(i-1)}} & & \frac{\partial F_2}{\partial u_n^{(i-1)}} \\ \cdot & \cdot & \cdot & \cdot \\ \frac{\partial F_n}{\partial u_1^{(i-1)}} & \frac{\partial F_n}{\partial u_2^{(i-1)}} & \cdots & \frac{\partial F_n}{\partial u_n^{(i-1)}} \end{bmatrix} \tag{2.83}$$

is the local stiffness matrix at $\{u^{(i-1)}\}$

From equation(2.81), a better estimation can often be found from

$$\{u^{(i)}\}=\{u^{(i-1)}\}+[K^{(i-1)}]^{-1}\Delta P^{(i-1)} \tag{2.84}$$

The local stiffness matrix $[K^{(i-1)}]$ is often referred to as the Jacobian in the general Newton-Raphson method. A schematic diagram for the Newton-Raphson method is shown in figure 2.20

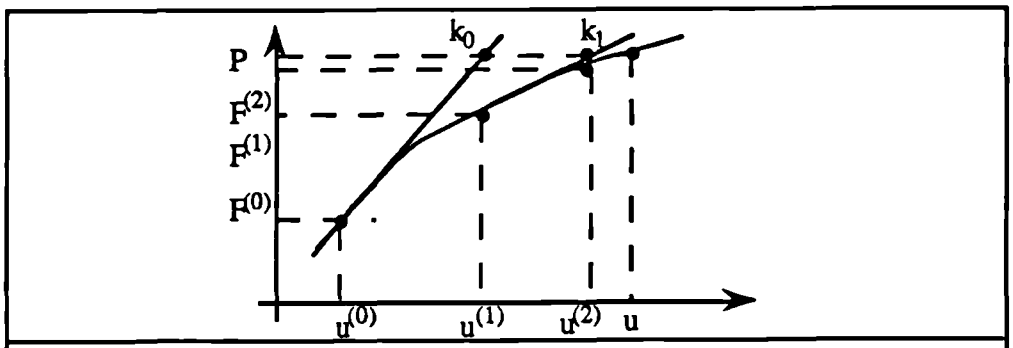

Figure 2.20 Schematic diagram for the Newton-Raphson method

The iteration process is repeated until convergence is achieved. Strictly speaking, for the Newton-Raphson method, the Jacobian should be updated in each iteration, however, calculation of $[K^{(i-1)}]^{-1}$ at each iteration can be prohibitively expensive when the size of the system is significant. Fortunately, the updating of the Jacobian at each iteration is often not required. Actually, depending on the nature of the nonlinearity, the $[K^{(i-1)}]$ matrix may only need to be updated every few iterations [2]. By doing so, the computation cost can be significantly reduced. A schematic diagram to use initial local stiffness $[K^{(0)}]$ in the iteration process is shown in figure 2.21.

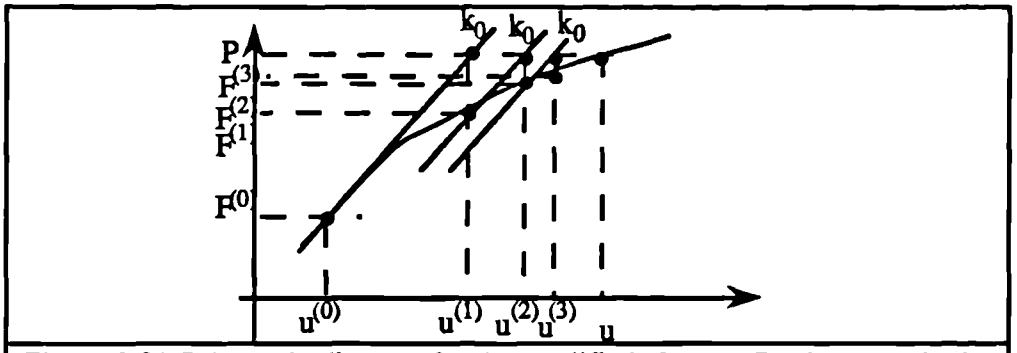

Figure 2.21 Schematic diagram for the modified Newton-Raphson method

For a nonlinear system, the final deformation can be path dependent, (i.e. multi-value nonlinearity), in other words, the final deformation is not only determined by the final load applied, but also by how the load is applied. An example is the deformation of a joint in the tangential direction; even if the final load magnitudes are the same, the deformations during the initial loading and unloading are certainly different. Because of the nature of the nonlinear problem, it is essential to calculate the deformation in a step by step approach to simulate the loading history [2].

Even if a nonlinear system is independent of the loading history (i.e single value nonlinearity), the step by step method should still be applied. This is because the Newton-Raphson method is a first order approximation method and requires a good estimation to ensure convergence. If the initial estimation is too far from the solution, the algorithm can diverge, i.e

$$\|\{P\}-\{F^{(i-1)}\}\| < \|\{P\}-\{F^{(i)}\}\| \qquad (2.85)$$

The linear approximation will be accurate only if the estimation is sufficiently close to the true solution. Therefore, in order to achieve convergence, the basic strategy of the step by step method is to find an estimation close enough to the real solution. Unfortunately, a good estimation to the final solution is often very difficult, and sometimes impossible to obtain. Therefore, an incremental approach (step by step) should be employed.

When the load is zero, the deformation is zero, hence the exact result is known. If a sufficiently small load increment is then applied, the structure will deform, but in most cases, the deformation is not far from the zero deformation. Therefore, the equilibrium position corresponding to a small load can be found using the Newton-Raphson method with zero deformation as an initial estimation. This deformation state will be a good estimation for the system subjected to a further load increment. Repeating the process, the final deformation of the system subjected to a prescribed load can be found. Therefore, the convergence can usually be achieved by using a step-by-step incremental approach.

If the external load is cyclic, both inertia force and damping force can be significant. If this is the case, the inertia and damping force must be included in the equilibrium

equation. For most structural problems, the mass of a structure is constant, and if the nonlinear force is also independent of the excitation frequency, then the equilibrium equation can be expressed as:

$$[M]\{\ddot{x}\}+[C]\{\dot{x}\}+\{F(x)\}=\{P\} \qquad (2.86)$$

The general method for solving equation(2.86) will be discussed in chapter 3. In this chapter, only the problem with negligible inertia and damping force are to be investigated.

§2.16.2 Numerical Case Studies

In this section, results from three case studies are presented. In the first case, a simple geometric translational model is studied. Bilinear contact is assumed to model the properties at small interface areas. The results using the FE method are then compared with the results from Menq's analytical model to demonstrate that the FE method is appropriate; in the second case, a more complicated translational model is studied, the newly developed microslip element is used to model the contact at the interface and different beam and joint parameters are assumed to simulate different pressure and surface conditions over the whole interface. It is extremely difficult to obtain an analytical solution, however, it is shown that there is no additional difficulty by using the FE Method. The case three demonstrates the significance of micro-microslip under some circumstances.

§2.16.2.1 Case One

The system studied is a uniform cross-section bar as shown in figure 2.22. Since dry friction elements can be considered to be a special case of the bilinear element with the very large initial stiffness (theoretically infinite), the friction force at the interface node point is assumed to be bilinear.

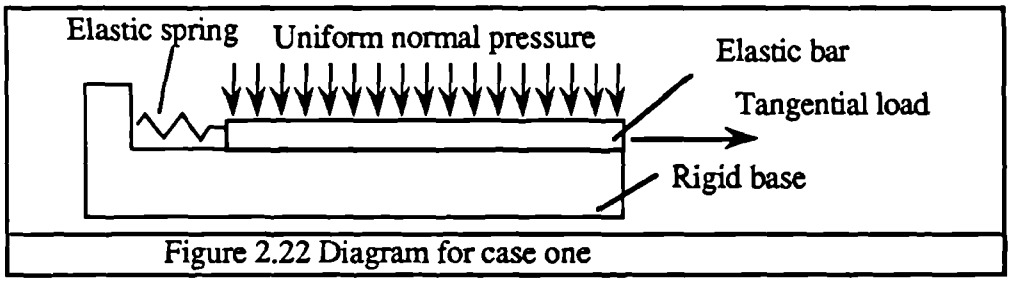

Figure 2.22 Diagram for case one

The distributed friction shear stress over an element is replaced by two concentrated loads at two node points with their magnitudes equal to half of the total shear friction force over the interface.

Figure 2.23 shows the loading curve of the finite element model under static load with 5, and 20 elements. It can be noted that the results from 5 and 20 elements models match

analytical results (Menq's model) very well. Clearly, the finite element method can be accurate with appropriate meshes.

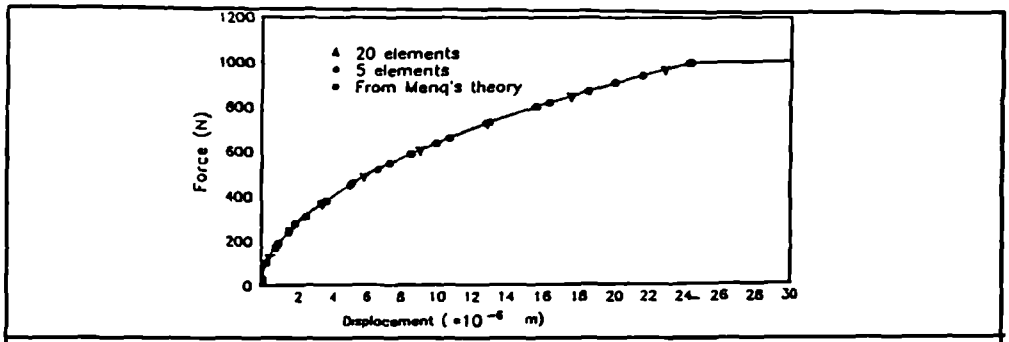

Figure 2.23 Loading curves of case one

§2.16.2.2 Case Two

The system for the second case study is shown in figure 2.24. The system has non-uniform cross-section and non-uniform interface conditions.

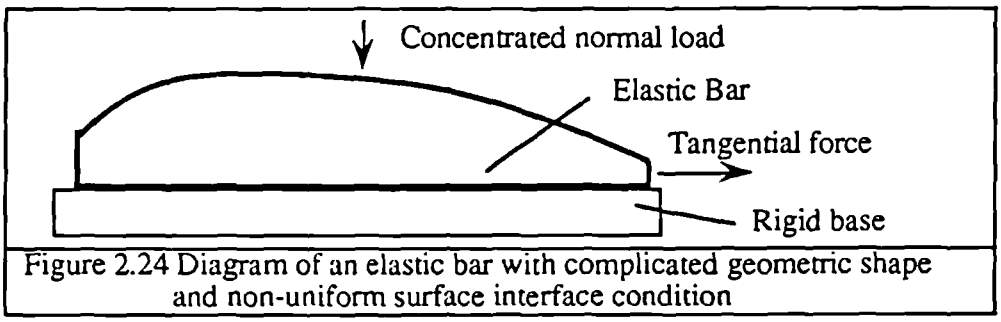

Figure 2.24 Diagram of an elastic bar with complicated geometric shape and non-uniform surface interface condition

The system is modelled by twenty 1D-bar elements and twenty-one new micro-microslip elements. The parameters for these beam elements are shown in table 2.8. If more accurate results are required, smaller meshes should be used. However, to illustrate the FE method, the above simplification is appropriate.

The results of the loading curve is shown in figure 2.25. There is no additional difficulty in the FE analysis for the system with complicated geometry, friction limit and contact elements.

	Data for Beam Element				Data for Interface Element		
No. of element	L (m)	W (m)	H (m)	E (10^{11}N/m^2)	a (10^{-8}m)	b	K (10^{12}N/m/m^2)
1	0.01	0.01	0.005	2.06	5	3	1
2	0.01	0.01	0.006	2.06	5	3	2
3	0.01	0.01	0.007	2.06	5	3	3
4	0.01	0.01	0.008	2.06	5	3	4
5	0.01	0.01	0.010	2.06	5	3	5
6	0.01	0.01	0.011	2.06	5	3	6
7	0.01	0.01	0.012	2.06	5	3	7
8	0.01	0.01	0.013	2.06	5	3	8
9	0.01	0.01	0.014	2.06	5	3	9
10	0.01	0.01	0.015	2.06	5	3	10
11	0.01	0.01	0.017	2.06	5	3	10
12	0.01	0.01	0.018	2.06	5	3	10
13	0.01	0.01	0.019	2.06	5	3	10
14	0.01	0.01	0.020	2.06	5	3	8
15	0.01	0.01	0.020	2.06	5	3	6
16	0.02	0.01	0.020	2.06	5	3	4
17	0.02	0.01	0.018	2.06	5	3	3
18	0.02	0.01	0.014	2.06	5	3	2
19	0.02	0.01	0.010	2.06	5	3	2
20	0.02	0.01	0.008	2.06	5	3	1
21					5	3	1

NB: L=length, W=Width, H=Height, E=Young's Modulus

Table 2.8 The joint component and interface data for Case Two

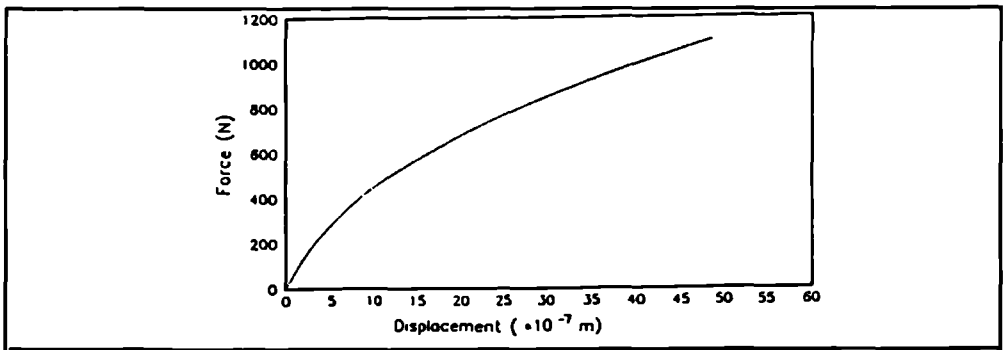

Figure 2.25 Loading curves of case two

§2.16.2.3 Case Three

The purpose of this study is to illustrate similarity and difference of the joint models generated from bilinear elements and micro-microslip elements. Three contact elements are used, one is the new microslip element with a=5×10^{-8}m, b=3 and k=2×10^{12}N/m/m^2, the other two are bilinear elements with the same friction limit as the microslip element, one bilinear element has the same initial stiffness as the microslip element, the other has the same limit for macroslip to occur. The relations between these elements are shown schematically in figure 2.26.

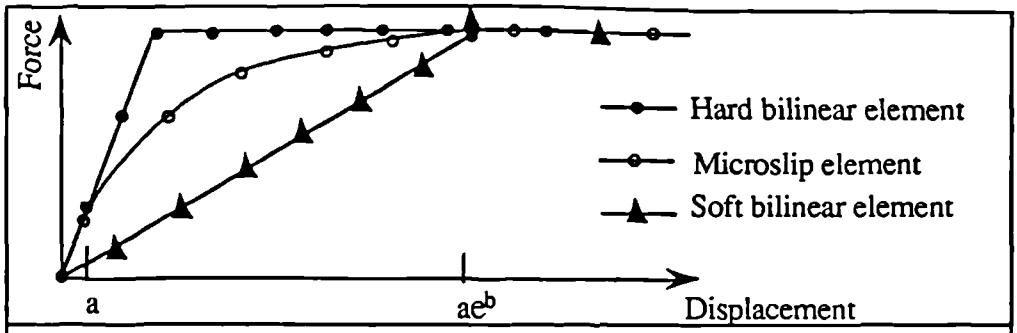

Figure 2.26 Relations between three surface contact elements

Two small cases are studied, for both cases, the joint components are elastic bars with all the properties as the same as those in case One except for the length. In the first case (Case A), the length of the bar is 1m, and in the second case (Case B), the bar is only 0.1m in length.

Surface conditions (interface parameters) are the same. The only difference between case A and case B is that the length of the bar in case B is one-tenth of that in case A, hence the bar in case B is 10 times stiffer than the bar in Case A.

Figure 2.27 and figure 2.28 show the loading curves for case A and case B. It is noted that when the joint component is flexible (case A), the differences of the results from different models are small; however, the difference is much more significant when the joint component is stiff.

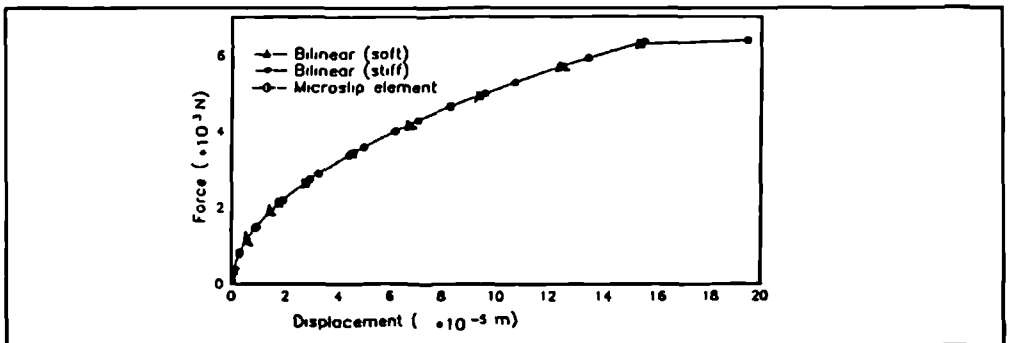

Figure 2.27 Loading curves of case A

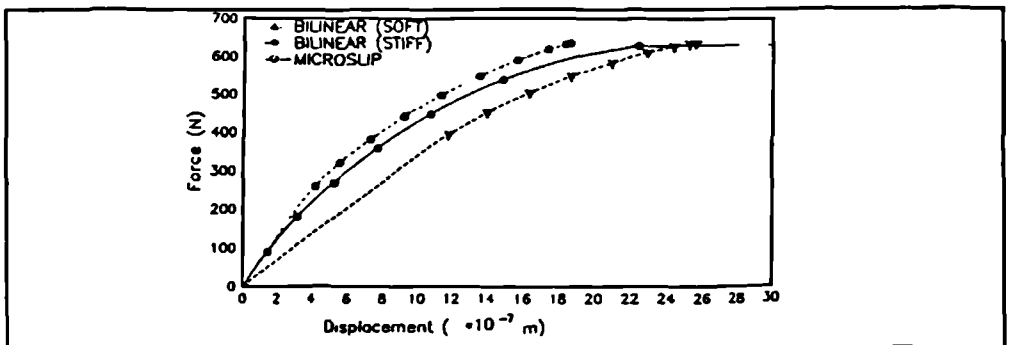

Figure 2.28 Loading curves of case B

The above results demonstrate the effects of the macro-microslip and the micro-microslip. When the joint component is flexible, microslip is dominated by the effects of macro-microslip; when the joint component is stiff, the effects of the asperities become significant.

§2.17 CONCLUSIONS

In this chapter, the relationship between the load and the deformation of friction joints slipping in the tangential direction are studied. It is shown that when the joint component is elastic, slip can initiate at some parts of the interface and extend towards the rest of the area as the load increases. Energy is dissipated due to slip and a hysteresis loop is formed when the joint is subjected to a cyclic load.

A review of the available microslip models is presented. It is summarised that the available models are either based on the dry friction element or the bilinear element. The problem with these two types of basic element is discussed.

Masing's rule, which is useful in predicting unloading and reloading behaviour of the tangential joint, is presented and proved. This rule can be applied to any system which consists of elastic elements and dry friction elements. For Masing type nonlinearity, the properties are fully defined by the force-deformation relation of the initial loading. The analysis process can be significantly simplified with the help of Masing's rule, and properties of the joint, such as unloading, reloading and energy dissipation per cycle, can be found directly from the initial loading relation. When a Masing type joint is subjected to a cyclic load, the energy dissipated per cycle is independent of the absolute value of the load or deformation, but is a function of the peak to peak value of the load (and also the deformation).

The microslip mechanism is discussed, it is shown that microslip can be caused by non-uniform deformation and non-uniform pressure distribution over the interface (macro-microslip), microslip can also be caused by the difference between the asperities on the interface(micro-microslip).

When the joint component is flexible, the effects of macro-microslip is dominant, therefore, the models derived from dry friction and bilinear friction element will usually yield good agreement with experimental results. However, when the joint component is rigid and has small interfaces, micro-microslip plays the most important role, in this case, micro-microslip element must be used to model the joint.

Two approaches may be used to obtain joint parameters. One is the prediction approach, which predicts the joint properties from basic parameters; the other is the identification approach which identifies some intermediate parameters for the joint model. The

prediction approach is more desirable; however, within the foreseeable future, the prediction approach is unlikely to be employed to obtain accurate results. It is suggested that the identification approach should be used if an accurate joint model is required.

A new micro-slip model (element) is proposed for a friction joint, the model is generalized and is able to represent any Masing type joint. The new model uses the concept of stiffness area, which turns the loading problem in a deformation domain $[0,\infty]$ into an h-domain [0,1].

A function $u=ae^{bh}$ is proposed for the new joint model and thus the derived model is able to represent measured loading relations quantitatively for both translational and rotary joints. The model is more flexible than models developed by Shoukry and Burdekin, the regenerated loading curves are closer to the measured data.

Shoukry's model is found to be useful in a small displacement range while Burdekin's model may only be useful in qualitative analysis.

If the joint is too complicated to be studied analytically, the finite element method should be used for obtaining the loading property of the friction joint. For a nonlinear problem, because the final solution may depend on the loading history, the Newton-Raphson iterative algorithm and step by step procedure should be used. The numerical results from the FE method are also presented and compared with the results from an analytical model. It is shown that FE method can yield very accurate results when proper meshes are chosen.

CHAPTER 3

PREDICTION OF THE RESPONSE OF A STRUCTURE WITH NONLINEAR JOINTS ATTACHED

§3.1 INTRODUCTION

In the last chapter, various friction joint models have been discussed. These models are characterised by the relationship between the deformation at the joint and the external load. This relationship is not usually linear and a hysteresis loop is formed if a cyclic load is applied.

In this and the subsequent chapters, the problem considered is the calculation of the response of a structure containing nonlinear joints when the structure is subjected to a well-defined excitation (in contrast to random excitation). Time domain integration methods are investigated in this chapter; other approximate methods are discussed in Chapter 4.

For a linear system, time-domain integration methods can be categorised into two groups:

1) Decoupling and Duhamel integration method [81].

2) Step-by-step Time-domain Integration method (STI)[2, 85-89].

The Duhamel integration method is relatively simple and has effectively only one version; for STI methods, there are many different algorithms. The most basic method for solving differential equations is the Runge-Kutta method [85]. However, the Runge-Kutta method tends to be computationally inefficient for solving second-order problems because the size of the problem is effectively doubled. As a consequence, some other specific methods have since been developed, namely, the indirect integration method [86], the central difference method [2], the Houbolt method [87], the Wilson-θ method [88] and the Newmark-β method [89]. For each of these methods, there can be several modified versions. The step-by-step integration methods are believed to be the only practically applicable methods for calculating the transient response of a general nonlinear system.

§3.2 THEORETICAL BACKGROUND

§3.2.1 General Introduction

All the STI methods utilise a numerical step-by-step procedure; the response at a time t is obtained from the response information prior to the time t and the external force at and/or prior to the time t. Almost all the STI methods are constructed on the basis of the following two strategies [2]:

1) Instead of satisfying the equilibrium condition at any time t, it is aimed to satisfy the equilibrium condition only at discrete time points with an interval Δ apart.

2) The assumption of variations of displacement, velocity and acceleration within each time interval must be made.

The key point for an STI method is the computation efficiency. Theoretically, provided the time interval Δ is small enough, accurate results can usually be obtained by using any of the STI methods. When Δ increases, the accuracy of the numerical results from all the methods deteriorates, but at a different rate.

For some of the methods, if Δ exceeds a certain limit (usually a fraction of the period of the highest natural frequency of the system), the numerical process becomes unstable and the numerical response of a physically stable system becomes unbounded, these methods are called **conditionally stable methods**; for other methods, the numerical results are always bounded (although not necessarily accurate), no matter how great Δ is. These methods are called **unconditionally stable methods**. Greater Δ can often be used for unconditionally stable methods.

The methods can also be **direct** or **indirect** depending on whether an iteration process is required at each time step.

In general, the unconditionally stable and direct methods are more desirable in terms of the computation efficiency. However, due to other factors such as the accuracy of the results, the conditionally stable and indirect methods have also found their applications.

Mathematically, it may be more appropriate to group STI methods according to the time point at which the equilibrium condition is applied. Methods which use the equilibrium condition **prior to** the current time point are called **explicit** methods; methods which use the equilibrium condition **at** the current time point are called **implicit** methods.

Explicit methods have a significant advantage in dealing with displacement dependent nonlinear problems, because iteration is usually not required; for implicit methods,

however, an iteration process is inevitable although some of these can be direct methods for the analysis of a linear system.

Two of the most commonly used methods for linear systems, namely the Newmark-β method and the central difference method, are discussed in this chapter. To overcome the shortcomings of these two methods in nonlinear analysis, two unconditionally stable algorithms are introduced.

§3.2.2 The Central Difference Method

The central difference method uses finite difference in place of the derivatives, i.e. assume

$$\{\ddot{x}_1\}=\frac{1}{\Delta^2}\{x_2-2x_1+x_0\} \tag{3.1}$$

$$\text{and } \{\dot{x}_1\}=\frac{1}{2\Delta}\{x_2-x_0\} \tag{3.2}$$

where $\{x_2\}$, $\{x_1\}$ and $\{x_0\}$ are the displacement vectors at t (current time), t-Δ and t-2Δ respectively.

Substituting equations (3.1) and (3.2) into equilibrium equation (3.3) at time t_1

$$[M]\{\ddot{x}_1\}+[C]\{\dot{x}_1\}+[K]\{x_1\}=\{P_1\} \tag{3.3}$$

leads to

$$[\frac{1}{\Delta^2}M+\frac{1}{2\Delta}C]\{x_2\}=\{P_1\}-[K-\frac{2}{\Delta^2}M]\{x_1\}-[\frac{1}{\Delta^2}M-\frac{1}{2\Delta}C]\{x_0\} \tag{3.4}$$

Equation(3.4) requires both information at time t_1 and at $t_0=t_1-\Delta$. Therefore a special procedure is required to start the first step. A commonly used procedure is to use the Taylor Series expansion

$$\{x_0\}=\{x_1-\Delta\,\dot{x}_1+\frac{\Delta^2}{2}\ddot{x}_1\} \tag{3.5}$$

The initial condition is often defined by the displacement $\{x_1\}$ and the velocity $\{\dot{x}_1\}$, while the acceleration $\{\ddot{x}_1\}$is not directly given. However, the acceleration can be calculated from the equilibrium equation (3.3).

The main advantage of the central difference method is that it is an explicit method, for both linear and (displacement dependent) nonlinear analysis, the iteration process is not required.

The major shortcoming of the central difference method is that it is only conditionally stable; if Δ is greater than the limit $\frac{T_n}{\pi}$, the numerical procedure becomes unstable (where T_n is the period of the highest natural frequency of the structure).

§3.2.3 Newmark-β method

Newmark [89] proposed an STI method in 1959. Because a parameter β is used, his method is often referred to as the Newmark-β method. Several different expressions have been proposed, the expression proposed by Hitchins [86] is presented here due to its simplicity.

The Newmark-β method uses the following assumption:

$$\{\dot{x}_2\}=(1+\gamma)\frac{\Delta}{2}\{\ddot{x}_1\}+(1-\gamma)\frac{\Delta}{2}\{\ddot{x}_2\}+\{\dot{x}_1\}, \text{ and} \tag{3.6}$$

$$\{x_2\}=(2+\beta)\frac{\Delta^2}{6}\{\ddot{x}_1\}+(1-\beta)\frac{\Delta^2}{6}\{\ddot{x}_2\}+\Delta\{\dot{x}_1\}+\{x_1\} \tag{3.7}$$

Parameters β and γ are introduced for the purpose of stabilizing the integration process.

Substituting equations (3.6) and (3.7) into the equilibrium equation at t_2

$$[M]\{\ddot{x}_2\}+[C]\{\dot{x}_2\}+[K]\{x_2\}=\{P_2\} \tag{3.8}$$

yields:

$$[M+(1-\gamma)\frac{\Delta}{2}C+(1-\beta)\frac{\Delta^2}{6}K]\{\ddot{x}_2\}=\{P_2\}-[C]\{(1-\gamma)\frac{\Delta}{2}\ddot{x}_1+\dot{x}_1\}-[K]\{(2+\beta)\frac{\Delta^2}{6}\ddot{x}_1+\Delta\dot{x}_1+x_1\} \tag{3.9}$$

The Newmark-β method is unconditionally stable for a linear system when parameters γ and β are chosen properly. The most commonly used values are

$$\gamma=0, \tag{3.10a}$$

and $\beta=-0.5$, (3.10b)

which ensures that the algorithm is unconditionally stable,

§3.2.4 Stability Analysis

For all the STI methods, the response at time t_2 is obtained from the response prior to time t_2 and the external load at and/or prior to the time t_2.

It is always possible to relate the current state response with the response at the last time point as:

$$\{X\}_2=[B]\{X\}_1+\{L\}_1 \tag{3.11}$$

where $\{X\}_2$ and $\{X\}_1$ are vectors storing the response quantities at t_2 and t_1, and $\{L\}_1$ is the load vector at time t_1. Applying equation(3.11) recursively yields:

$$\{X\}_{1+n}=[B]^n\{X\}_1+[B]^{n-1}\{L\}_1+[A]^{n-2}\{L\}_2+....+[B]\{L\}_{n-1}+\{L\}_n \tag{3.12}$$

Should an algorithm be stable with time interval Δ, the magnitudes of the elements in the matrix $[B]^n$ must not increase continuously with n. Otherwise, the effects of small errors in the response at former steps are magnified continuously in the solution later and the solution becomes unbounded. The matrix [B] is called a **character** matrix.

Using spectral decomposition for matrix [B] yields:

$$[B]=[P][J][P]^{-1} \tag{3.13}$$

where [J] is a diagonal matrix containing the eigenvalues of the matrix [B].

From equation (3.13)

$$[B]^n=[P][J]^n[P]^{-1} \tag{3.14}$$

If the magnitude of the highest eigenvalue $|\lambda_h|$ of the matrix [B] is greater than 1, the magnitude of elements in matrix $[J]^n$, and hence the magnitude of elements in the matrix $[B]^n$, will increase with n. As a result, the algorithm is unstable. The criteria for an algorithm to be stable is that the magnitude of the highest eigenvalue of the matrix [B] must be smaller than 1.

The analysis of stability can be very expensive if all the eigenvalues need to be calculated, since the size of the [B] matrix is usually twice or three times the spatial matrix (i.e. a mass or a stiffness matrix) (see §3.3.3.3) .

If damping of a system is proportional, however, the equilibrium equation(3.8) can be decoupled into N SDOF equations. When these N SDOF equations are integrated with the same Δ, the final results must be exactly the same as that from integrating on the original system. Since N SDOF equations are identical in their forms, only one SDOF equation needs to be studied [2], hence the computation cost becomes negligible. If damping is not proportional, then strictly speaking, the analysis cannot be simplified as a problem with N-SDOF systems. However, it is stated in [90] that since the magnitude of the damping force is usually much smaller than inertia or restoring force, the damping of the system usually does not change the overall stability characteristics of an integration scheme.

When a system is nonlinear, it is not usually possible to have an analytical solution for the stability analysis. However, at each time interval, a nonlinear system can be considered as a linear system [2], thus, the basic requirement for applying an algorithm on a nonlinear system is that the algorithm should be stable for all the approximated linear systems. Further discussion on the stability of an STI method on a nonlinear system is presented in §3.3.3.3.

§3.3 STI METHODS FOR NONLINEAR ANALYSIS

The algorithms discussed in the last few sections are for the analysis of a linear system. However, these STI methods can also be applied to the analysis of a nonlinear system. The basic idea for nonlinear analysis is the same as that for linear analysis, the aim is to achieve the equilibrium condition at discrete time points $t_1, t_2, \ldots t_n$ etc.

The equilibrium condition for a nonlinear system can be expressed as:

$$[M]\{\ddot{x}\}+\{F(x, \dot{x})\}=\{P\} \tag{3.15}$$

If the nonlinear part of the internal force F is independent of the velocity, then the equation(3.15) becomes

$$[M]\{\ddot{x}\}+[C]\{\dot{x}\}+\{F(x)\}=\{P\} \tag{3.16}$$

$$\text{or } [M]\{\ddot{x}\}+[C]\{\dot{x}\}+[K]\{x\}+\{F_n(x)\}=\{P\} \tag{3.17}$$

Clearly, the system with friction joints attached is characterised by equation (3.17). Therefore, in this chapter, only the nonlinear problems which can be represented by equation(3.17) are investigated.

§3.3.1 Direct Extension of Linear STI Methods for Nonlinear Analysis

For the problem such as analysing a system containing friction joints, the following two points can be noted:

1) the joints are only located in parts of the structure; except for the joint part, the property of the structure is linear, i.e. nonlinear part is localised; and

2) the force-deformation relation of the joint is displacement dependent

Because the nonlinearity is localised, the nonlinear force of a joint can be treated as an external force and the equilibrium condition can be expressed as

$$[M]\{\ddot{x}\}+[C]\{\dot{x}\}+[K]\{x\}=\{P\}-\{F_n(x)\} \tag{3.18}$$

For the central difference method, substituting equations (3.1) and (3.2) into equation (3.18) yields

$$[\frac{1}{\Delta^2}M+\frac{1}{2\Delta}C]\{x_2\}=\{P_1\}-\{F_n(x_1)\}-[K-\frac{2}{\Delta^2}M]\{x_1\}-[\frac{1}{\Delta^2}M-\frac{1}{2\Delta}C]\{x_0\} \qquad (3.19)$$

For the Newmark-β method, substituting equations(3.6) and (3.7) into equation (3.18) and setting $\gamma=0$ and $\beta=-0.5$ yields

$$[M+\frac{\Delta}{2}C+\frac{\Delta^2}{4}K]\{\ddot{x}_2\}=\{P_2\}-\{F_n(x_2)\}-[C]\{\frac{\Delta}{2}\ddot{x}_1+\dot{x}_1\}-[K]\{\frac{\Delta^2}{4}\ddot{x}_1+\Delta\dot{x}_1+x_1\} \qquad (3.20)$$

Both sides of equation (3.20) contain terms at t_2, therefore, it must be solved iteratively, an iterative form for equation(3.20) can be presented as

$$[M+\frac{\Delta}{2}C+\frac{\Delta^2}{4}K]\{\ddot{x}_2\}^{(k)}=\{P_2\}-\{F_n(x_2)\}^{(k-1)}-[C]\{\frac{\Delta}{2}\ddot{x}_1+\dot{x}_1\}-[K]\{\frac{\Delta^2}{4}\ddot{x}_1+\Delta\dot{x}_1+x_1\} \qquad (3.21)$$

Direct use of the linear STI methods for nonlinear analysis has the advantage that the computer code for the linear analysis only needs a small modification. However, the shortcomings are also significant. For the central difference method, the time interval is severely limited by the highest natural frequency of the structure. For the Newmark-β method, the algorithm becomes indirect, and experience appears to indicate that the iterative process of equation(3.21) ;often slow and may not converge unless Δ is small enough. Thus, other algorithms are required.

§3.3.2 Algorithm One --An Extension of the Static Analysis

§3.3.2.1 Formulation

The algorithm presented in this section is an extension of the algorithm for the static nonlinear problem (see §2.16) with an inclusion of the effects of the inertia and damping forces. Bathe [2] presented a formula for the system without damping, a modification is made here to include the damping force.

The iteration equation at time t_2 is

$$[M]\{\ddot{x}_2\}^{(k)}+[C]\{\dot{x}_2\}^{(k)}+[K_1]\{\delta x_2\}^{(k)}=\{P_2\}-\{F(x_2)\}^{(k-1)}, \text{ and} \qquad (3.22)$$

$$\{x_2\}^{(k)}=\{x_2\}^{(k-1)}+\{\delta x_2\}^{(k)} \qquad (3.23)$$

where $[K_1]=\frac{\{dF(x)\}}{\{dx\}}|_{\{x\}=\{x_1\}}$ is the local stiffness matrix at deformation $\{x_1\}$(see §2.16 for more details), and $\{F(x)\}=[K]\{x\}+\{F_n(x)\}$ is the total restoring force.

Substituting equations(3.23) and (3.10) into equations(3.6) and (3.7) and rearranging yields

$$\{\dot{x}_2\}^{(k)}=\frac{2}{\Delta}\{x_2^{(k)}-x_1\}-\{\dot{x}_1\}=\frac{2}{\Delta}\{x_2^{(k-1)}+\delta x_2^{(k)}-x_1\}-\{\dot{x}_1\}, \text{ and} \tag{3.24}$$

$$\{\ddot{x}_2\}=\frac{2}{\Delta}\{\dot{x}_2-\dot{x}_1\}-\{\ddot{x}_1\}=\frac{4}{\Delta^2}\{x_2^{(k-1)}+\delta x_2^{(k)}-x_1\}-\frac{4}{\Delta}\{\dot{x}_1\}-\{\ddot{x}_1\} \tag{3.25}$$

Substituting equations(3.24) and (3.25) into equation (3.22) leads to the final iterative equation:

$$[\hat{K}_1]\{\delta x_2\}^{(k)}=\{P_2\}$$
$$-\{F(x_2)\}^{(k-1)}-[M](\frac{4}{\Delta^2}\{x_2^{(k-1)}-x_1\}-\frac{4}{\Delta}\{\dot{x}_1\}-\{\ddot{x}_1\})-[C](\frac{2}{\Delta}\{x_2^{(k-1)}-x_1\}-\{\dot{x}_1\}) \tag{3.26}$$

$$\text{where } [\hat{K}_1]=\frac{4}{\Delta^2}[M]+\frac{2}{\Delta}[C]+[K_1] \tag{3.27}$$

This method is referred to as **Algorithm One** to distinguish it from other versions of the Newmark-β method.

For a nonlinear system, $[K_1]$ changes at each step. Accordingly, $[K_1]$ should be updated and a matrix inversion of $[\hat{K}_1]$ is required at each step too. This tends to make the computation very expensive. However, if the nonlinearity is not very severe, it is possible to update $[K_1]$ for every few steps (see §2.16). Indeed, if a global stiffness matrix $[K_{1g}]$ is used to replace $[K_1]$ at different steps, the inversion only needs to be calculated once. If the property of quick convergence is retained, the computation cost can be reduced significantly.

In computer code, $[\hat{K}_1]$ is only updated if iteration does not converge after N cycles (where N is a positive number. Experience indicates that convergence, if the process is converging, can usually be achieved in under 20 iterations. In order to leave a margin for convergence, N is set to be 30 in the computer code).

The speed of convergence is usually related to the property of the nonlinear force. If the change of $[K_1]$ at each time interval is insignificant, the convergence will be very fast, otherwise, convergence can be very slow, and sometimes may not converge at all. From equation(3.27), it is noted that the matrix $[K_1]$ will be dominated by the mass effect when Δ is very small, as a result, convergence can usually be achieved by using very small Δ.

§3.3.2.2 Convergence Criteria

It is very important to apply the iterative process as Bathe [2] stated:

"The iteration can actually be of the utmost importance since any error admitted in the incremental solution at a particular time directly affects in a path-dependent manner the solution at any subsequent time".

If improper convergence criterion are used, the solution can be inaccurate, and sometimes, the procedure may even be unstable.

Two convergence criterion have been proposed in [2]. An extension to these convergence criterion by including the damping effects are

$$\frac{\|\{P_2\}-\{F_2\}^{(k-1)}-[M]\{\ddot{x}_2\}^{(k-1)}-[C]\{\dot{x}_2\}^{(k-1)}\|}{\|\{P_\tau-F_{\tau-\Delta}\}-[M]\{\ddot{x}_{\tau-\Delta}\}-[C]\{\dot{x}_{\tau-\Delta}\}\|_2^{(max)}} \le RTOL \qquad (3.28)$$

$$\text{and } \left|\frac{\{\delta x_2\}^{(k)T}(\{P_2\}-\{F_2\}^{(k-1)}-[M]\{\ddot{x}_2\}^{(k-1)}-[C]\{\dot{x}_2\}^{(k-1)})}{\{\delta x_2\}^{(1)T}(\{P_2\}-\{F_1\}-[M]\{\ddot{x}_1\}-[C]\{\dot{x}_1\})}\right| \le ETOL \qquad (3.29)$$

where τ is the time point at which $\|\{P_\tau-F_{\tau-\Delta}\}-[M]\{\ddot{x}_{\tau-\Delta}\}-[C]\{\dot{x}_{\tau-\Delta}\}\|_2$ is the maximum, and RTOL and ETOL are the force and the energy convergence criterion respectively.

The convergence is reached when both equation(3.28) and (3.29) are satisfied.

The above criteria work well for the system in which the inertia force is insignificant. However, when the inertia force is significant, the restoring force and the inertia force can be balanced by each other, hence

$$\|\{P_2\}-\{F_2\}^{(k-1)}-[M]\{\ddot{x}_2\}^{(k-1)}-[C]\{\dot{x}_2\}^{(k-1)}\|$$

$$\text{and } \|\{P_\tau-F_{\tau-\Delta}\}-[M]\{\ddot{x}_{\tau-\Delta}\}-[C]\{\dot{x}_{\tau-\Delta}\}\|^{(max)}$$

are of the same order, the appropriate values of convergence criterion are different at different frequencies. In addition, it can be noted that

$$\|\{P_\tau-F_{\tau-\Delta}\}-[M]\{\ddot{x}_{\tau-\Delta}\}-[C]\{\dot{x}_{\tau-\Delta}\}\|_2^{(max)}$$

$$\text{and } |\{\delta x_2\}^{(1)T}(\{P_2\}-\{F_1\}-[M]\{\ddot{x}_1\}-[C]\{\dot{x}_1\})|$$

are closely related to the time interval Δ. Therefore, the proper values of the convergence criterion also depend on the time interval Δ; an RTOL or ETOL can be too tight (small quantity) to achieve for integration with a small Δ, while too loose to yield accurate

results with a large Δ. Without prior knowledge of the response, it is extremely difficult to select proper values with the above criteria.

In this chapter, the following two criteria are used:

$$\frac{\|\{P_2\}-\{F_2\}^{(k-1)}-[M]\{\ddot{x}_2\}^{(k-1)}-[C]\{\dot{x}_2\}^{(k-1)}\|}{\|\{F_2\}^{(k-1)}\|+\|[M]\{\ddot{x}_2\}^{(k-1)}\|+\|[C]\{\dot{x}_2\}^{(k-1)}\|_2} \le \text{FTOL, and} \qquad (3.30)$$

$$\frac{\|\{\delta x_2\}\|}{\|\{x_2\}\|} \le \text{XTOL} \qquad (3.31)$$

Convergence is reached when conditions (3.30) and (3.31) are satisfied. FTOL and XTOL should be tight enough to ensure accurate results.

§3.3.3 Algorithm Two--An Extension of the Central Difference Method

§3.3.3.1 Formulation

Algorithm One uses the same assumption on the variation of acceleration and velocity as the Newmark-β method in linear analysis, however, unlike the Newmark-β method, Algorithm One is an indirect method, and an iterative procedure has to be applied.

For the explicit algorithm (i.e. the central difference method), the nonlinear force is determined by the displacement level prior to the current time, hence iteration is not required. However, there is a severe limitation on Δ for the numerical process to be stable.

Based on the same idea of the Newmark-β method, the central difference method can be modified to yield an algorithm which is unconditionally stable for a linear system and is still a direct method for nonlinear analysis. Such a modification is proposed in [90] which approximates the displacement vector $\{x_1\}$ partly by the linear interpolation of displacement vectors $\{x_0\}$ and $\{x_2\}$ as:

$$\{x_1\}=\{ax_2+(1-2a)x_1+ax_0\} \qquad (3.32)$$

Substituting equations(3.32), (3.1) and (3.2) into equation(3.18) leads to:

$$[M]\frac{\{x_2-2x_1+x_0\}}{\Delta^2}+[C]\frac{\{x_2-x_0\}}{2\Delta}+[K]\{ax_2+(1-2a)x_1+ax_0\}=\{P_1\}-\{F_n(x_1)\} \qquad (3.33a)$$

Rearranging equation(3.33a) yields

$$[\frac{1}{\Delta^2}M+\frac{1}{2\Delta}C+aK]\{x_2\}=\{P_1\}-\{F_n(x_1)\}+[\frac{2}{\Delta^2}M-(1-2a)K]\{x_1\}[\frac{-1}{\Delta^2}M+\frac{1}{2\Delta}C-aK]\{x_0\} \qquad (3.33b)$$

If a=0, this becomes the central difference method.

Parameter "a" is introduced for the same purpose as "γ" and "β" in the Newmark-β method to force the algorithm to be unconditionally stable. Therefore, equation(3.33) can be considered as a particular form of the Newmark-β method. This method is referred to as Algorithm Two in this chapter.

In order to provide statically correct solutions for massless degrees of freedom, it is suggested [90] that the load vector {P} should be averaged over three adjacent time steps in the same way that {x} is averaged, The final equation then becomes:

$$[\frac{1}{\Delta^2}M+\frac{1}{2\Delta}C+aK]\{x_2\}$$

$$=\{aP_2+(1-2a)P_1+aP_0\}-\{F_n(x_1)\}+[\frac{2}{\Delta^2}M-(1-2a)K]\{x_1\}+[-\frac{1}{\Delta^2}M+\frac{1}{2\Delta}C-aK]\{x_0\} \quad (3.34)$$

It has been proved [90] that if $a\geq\frac{1}{4}$, the integration scheme is unconditional stable for a linear proportionally damped system (i.e $\{F_n(x_1)\}=\{0\}$). To provide a margin of stability for a more general problem (e.g those in which the damping is non-proportional or in which nonlinear terms occur), $\frac{1}{3}$ is suggested for the value of a.

§3.3.3.2 Start Procedure for Algorithm Two

Algorithm two is an extension of the central difference method, therefore, the start procedure in §3.2.2 can be used directly. However, the procedure can be erroneous when Δ is large. This is because the start procedure is based on a truncated Taylor series. Δ must be sufficiently small for the truncation to be accurate.

For the central difference method, since Δ is restricted by the period of the highest natural frequency* of the system, it is usually sufficiently small to yield an accurate approximation by using the truncated Talyor series. However, for Algorithm Two, Δ is not directly related to the highest natural frequency and Δ can be much greater than the period of the highest natural frequency of the system. As a result, the truncated Taylor series can be erroneous.

---

* If the system is nonlinear, Δ is restricted by the highest natural frequency of an equivalent system with the replacement of nonlinear elements by linear elements which have the maximum local stiffness of the nonlinear elements.

For example, consider the free vibration of an SDOF system with m=1kg, k=1N/m and c=0N/m/s. If the initial conditions are x_1=1m, and $\dot{x}_1$=0m/s, then from equation(3.5)

$$x_0=x_1-\Delta\dot{x}_1+\frac{\Delta^2}{2}\ddot{x}_1$$

$$=(1-\frac{\Delta^2}{2})x_1$$

When $\Delta>2$, $|x_0|>1$; in other words, the magnitude of the vibration is magnified.

An alternative start procedure is to use Algorithm One to calculate the first step.

For the case that the system is excited from its rest position (i.e. $\{x\}=\{0\}$, $\{\dot{x}\}=\{0\}$), it may also be appropriate to set $\{x_0\}=\{0\}$. This simple assumption usually does not cause significant error.

In the following analysis, only the start procedure which uses Algorithm One is used.

§3.3.3.3 Stability Analysis

The technique for stability analysis of a linear system is well-developed as shown in §3.2.4. In contrast, the stability analysis for nonlinear systems is rather under-developed. Indeed, the literature survey on the integration method produced nothing specific for nonlinear stability analysis, the only relevant discussion was found in the MSC/Nastran manual [90] and Bathe's book [8].

Bathe [2] stated "*in nonlinear analysis, for each time step, the nonlinear response calculation may be thought of, in an approximate way, as a linear analysis.*"

This idea is used for the stability analysis on the nonlinear system.

For a linear system, it is usually found that a stiffer system (i.e. a system with a higher resonance frequency) is likely to cause unstable integration for an STI method. On the basis of this point, a hypothesis is made for the following analysis:

An integration algorithm for a nonlinear system is stable if the algorithm is stable for a linear system which is stiffer than the nonlinear system at any time step.

With this hypothesis, the nonlinear stability study can be effectively turned into a linear problem. For the central difference method, the Newmark-β method and Algorithm One, the analyses are the same as the analysis on an ordinary linear system, and the conclusions are the same. However, for Algorithm Two, the stability analysis is slightly different.

The stiffer linear system to be analysed is

$$[M]\{\ddot{x}\}+[C]\{\dot{x}\}+[K]\{x\}=\{P\}-[K_{je}]\{x\} \tag{3.35}$$

where $[K_{je}]$ is a stiffness matrix which is stiffer than the local stiffness associated with he nonlinear force, i.e. the i'th nonlinear element is replaced by a linear spring with the stiffness

$$k_{ie} \geq \frac{dF_i}{dx_i} \tag{3.36}$$

and the integration formula is

$$\left[\frac{1}{\Delta^2}M+\frac{1}{2\Delta}C+aK\right]\{x_2\}$$

$$=\{aP_2+(1-2a)P_1+aP_0\}-[K_{je}]\{x_1\}+\left[\frac{2}{\Delta^2}M-(1-2a)K\right]\{x_1\}+\left[-\frac{1}{\Delta^2}M+\frac{1}{2\Delta}C-aK\right]\{x_0\} \tag{3.37}$$

Rearranging equation (3.37) with $\{P_2\}=\{P_1\}=\{P_0\}$ and combining with the identity $\{x_1\}=\{x_1\}$ yields

$$\begin{bmatrix} \frac{1}{\Delta^2}[M]+\frac{1}{2\Delta}[C]+a[K] & [0] \\ [0] & [I] \end{bmatrix}\begin{Bmatrix} x_2 \\ x_1 \end{Bmatrix}$$

$$=\begin{bmatrix} \frac{2}{\Delta^2}[M]-(1-2a)[K]-[K_{je}] & -\frac{1}{\Delta^2}[M]+\frac{1}{2\Delta}[C]-a[K] \\ [I] & [0] \end{bmatrix}\begin{Bmatrix} x_1 \\ x_0 \end{Bmatrix} \tag{3.38}$$

Therefore, the character matrix is

$$[B]=\begin{bmatrix} \frac{1}{\Delta^2}[M]+\frac{1}{2\Delta}[C]+a[K] & [0] \\ [0] & [I] \end{bmatrix}^{-1}\begin{bmatrix} \frac{2}{\Delta^2}[M]-(1-2a)[K]-[K_j] & -\frac{1}{\Delta^2}[M]+\frac{1}{2\Delta}[C]-a[K] \\ [I] & [0] \end{bmatrix}$$

(3.39)

The highest eigenvalue of the [B] matrix can be greater than 1 even if $a \geq \frac{1}{4}$, and $[K_{je}]$ must be small enough in order to ensure that the highest eigenvalue of the matrix [B] is not greater than 1. To illustrate this, consider an SDOF system

$$\left(\frac{m}{\Delta^2}+\frac{c}{2\Delta}+ak\right)x_2=aP_2+(1-2a)P_1+aP_0-k_{je}x_1+\left(\frac{2m}{\Delta^2}-(1-2a)k\right)x_1+\left(-\frac{m}{\Delta^2}+\frac{c}{2\Delta}-ak\right)x_0\} \tag{3.40}$$

Rearranging equation(3.40) yields

$$m\frac{\{x_2-2x_1+x_0\}}{\Delta^2}+c\frac{\{x_2-x_0\}}{2\Delta}+(k+k_{je})\{\frac{ak}{k+k_{je}}x_2+(1-2\frac{a(k)}{k+k_{je}})x_1+\frac{ak}{k+k_{je}}x_0\}=\{P_1\} \quad (3.41)$$

It is noted that the effective parameter is

$$a_e=\frac{k}{k+k_{je}}a \quad (3.42)$$

When $k_{je}>0$, $a_e<a$

In order to ensure stability, a_e must be greater than $\frac{1}{4}$.

A remedy to improve the stability of the integration algorithm is suggested in [90], which is to add to both sides of equation(3.35) another stiffness term:

$$[M]\{\ddot{x}\}+[C]\{\dot{x}\}+[K+K_r]\{x\}=\{P\}-[K_{je}-K_r]\{x\} \quad (3.43)$$

Element in matrix $[K_r]$ should be so chosen that the matrix $[K_{je}-K_r]$ corresponds to a structure with negative stiffness.

For an SDOF system, it can be proved in a similar way to equation (3.40) that the effective parameter is:

$$a_e=\frac{k+k_r}{k+k_{je}}a \quad (3.44)$$

When $k_r>k_{je}$, $a_e>a$

Since equation(3.43) cannot be decoupled into a set of independent linear equations, no mathematical proof can be given (at least to the author's knowledge, no proof has been published). However, it will be seen later that the numerical studies carried out in this chapter seem to agree with this explanation on the effective parameter "a_e".

Based on the above discussion, the nonlinear force in a friction joint should be divided into elastic and nonlinear parts as

$$F_n=K_rx+F_{n0} \quad (3.45)$$

$$\text{where } \frac{dF_{n0}}{dx}\le 0 \quad (3.46)$$

In other words, the local stiffness of the nonlinear force should be zero or negative, the equilibrium equation of the nonlinear system becomes

$$[M]\{\ddot{x}\}+[C]\{\dot{x}\}+[K+K_r]\{x\}=\{P\}-(\{F_n(x)\}-[K_r]\{x\}) \quad (3.47)$$

For all the tangential joint models discussed in chapter 2, maximum stiffness is at the beginning of the initial loading. The stiffness of the joint at the beginning of the initial loading can be used as the elastic part of the force in the joint, i.e.

$$[K_r]=\frac{d\{F_n(x)\}}{d\{x\}}\Big|_{t=0} \tag{3.48}$$

§3.4 REDUCTION OF THE SIZE OF THE PROBLEM: CONDENSATION

When a real engineering structure is modelled using FEM, it is common to end up with a system possessing a large number of DOFs. Usually, the model is only representative for the low frequency dynamic behaviour of a real structure, the high frequency property of the model is inevitably determined by the numerical modelling process and has little physical justification. However, these incorrect or inaccurate properties play significant roles in the numerical integration process.

If the frequency of interest is lower than the highest natural frequency of the model (which is true for almost all cases), the time interval Δ for a conditionally stable method is limited by the highest natural frequency of the model rather than the frequency of interest; for a unconditionally stable method, although the stability limit on Δ does not exist, Δ has to be small enough to yield accurate results. Even with a small Δ, the numerical integration on a large DOF model can still be formidably expensive.

Since the highest natural frequency and the properties of the model at high frequency are determined purely by the modelling process, and the frequency range of interest is usually much lower, there is an incentive to develop a coordinate transformation, which will condense the number of DOFs, and hence reduce the highest natural frequency of the model, yet still retain the properties of the original model in the frequency range of interest. By doing so, the cost of the computation can be reduced.

The basic idea is as follows:

For an N-DOF linear model, the equilibrium equation of motion is

$$[M]\{\ddot{x}\}+[C]\{\dot{x}\}+[K]\{x\}=\{P\} \tag{3.49}$$

Applying a linear transformation

$$\{x\}=[T]\{q\} \tag{3.50}$$

where $\{q\}$ is the new (or generalized) displacement vector and $[T]$ is an $N\times N$ non-singular matrix.

to equation(3.49) and pre-multiplying it by $[T]^T$ leads to the equation of motion with respect to the new displacement vector {q}:

$$[\tilde{M}]\{\ddot{q}\}+[\tilde{C}]\{\dot{q}\}+[[\tilde{K}]\{q\}=\{\tilde{P}\}-\{\tilde{F}_n(q)\} \quad (3.51)$$

where $[\tilde{M}]=[T]^T[M][T]$, $[\tilde{C}]=[T]^T[C][T]$, $[\tilde{K}]=[T]^T[K][T]$, $\{\tilde{P}\}=[T]^T\{P\}$

and $\{\tilde{F}_n\}=[T]^T\{F_n\}$

The property of the model is unchanged after the linear transformation if the transformation matrix[T]is not singular, and the original response can be found from equation(3.50)

If a transformation exists so that the response of the system at any time can be approximately expressed as:

$$\{x\}=[T_1,T_2]\{q_1^T,0\}^T=[T_1]_{N\times M}\{q_1\}_{M\times 1} \quad (3.52)$$

where M<N,

then the size of the problem can be reduced by substituting equation(3.52) into equation(3.49) and pre-multiplying it by $[T_1]^T$:

$$[\tilde{M}_1]\{\ddot{q}_1\}+[\tilde{C}_1]\{\dot{q}_1\}+[\tilde{K}_1]\{q_1\}=\{\tilde{P}_1\}+\{\tilde{F}_{1n}(q_1)\} \quad (3.53)$$

where $[\tilde{M}_1]=[T_1]^T[M][T_1]$, $[\tilde{C}_1]=[T_1]^T[C][T_1]$, $[\tilde{K}_1]=[T_1]^T[K][T_1]$, $\{\tilde{P}_1\}=[T_1]^T\{P\}$ and $\{\tilde{F}_{1n}\}=[T_1]^T\{F_n\}$

The new mass, stiffness and damping matrices have a reduced size of M×M.

The transformation in equation(3.52) can only be an approximation, the accuracy of the condensation depends on the accuracy of the transformation in equation(3.52).

Various condensation procedures have been proposed for linear systems and summarised by Hitchins [86], among which the Guyan reduction [91] is the most commonly used. In order to achieve the desired accuracy, a sufficient number of DOF has to be retained. In many cases, the number of the retained DOF can still be too large (hence the computation cost can be too high) for the numerical integration methods to apply. Therefore, further reduction is required.

In the remaining part of this section, this further reduction is discussed.

A subspace condensation method has been investigated by Yao [92]. The basic strategy is to integrate the full system for a certain period of time and then extract a subspace from the vibration shapes of the structure at different time points. This approach can be expensive to apply due to the integration on the full size system.

For the nonlinear problem caused by nonlinear joints, however, a simpler approach can be adopted. Instead of finding the subspace by integrating the full size system, it aims to find a subspace from a linear system.

For a linear system, it is known that the vibration of a structure can be well represented by some mode shapes of the system, i.e, the transformation is

$$[T]=[\phi]_{N\times M} \tag{3.54}$$

Clearly, the most important task is to find a linear system, i.e. to determine the matrix $[K_m]$ in

$$[M]\{\ddot{x}\}+[K_m]\{x\}=\{0\} \tag{3.55}$$

with mode shapes $[\phi]$ which form a representative subspace for the nonlinear system.

In this chapter, two types of $[K_m]$ matrices are tested; for the first case, the sum of the linear stiffness matrix and the initial stiffness matrix of the joints (i.e.$[K]+[K_{j0}]$) is used as the $[K_m]$ matrix; for the second case, the linear stiffness matrix (without joints) [K] is used as the $[K_m]$ matrix. The first condensation is referred to as the lock-mode condensation, and the second is referred to as the free-mode condensation.

The first $[K_m]$ is introduced in an attempt to preserve the properties of the original nonlinear system (i.e. the natural frequency and the mode shape). If the joint is linear, the condensed system has exactly the same natural frequencies and mode shapes of the original system.

The second $[K_m]$ is based on the fact that the nonlinear force at the joint can be considered as the external force, and the properties of the remaining system are characterised by the matrices [M] and [K], hence the mode shape of the remaining system should form a representative subspace for the vibration of the nonlinear system. It should be noted that when the joint is linear, the condensed system does not have the same natural frequency as the original system.

The numerical results and further discussions on these two condensation approaches are presented in §3.6.7.

§3.5 CALCULATION OF NONLINEAR FORCE FROM THE RESPONSE AT THE JOINT

As discussed in chapter 2, the nonlinear element can be categorised into two groups; for the first group, the nonlinear force is completely determined by the current state of the response (displacement and velocity), i.e. the force is a single value function of the current response. The integration scheme discussed in the foregoing sections can be applied directly to this type of nonlinearity. For the second group of elements, the nonlinear force is not only determined by the current response state, but also depends on the loading path (i.e. loading history). A special procedure has to be used to calculate the force from the information of both the current response and the loading history. The friction joint in the tangential direction belongs to the second group.The friction joints are substantially velocity independent.

Two algorithms for calculating the force of a Masing type nonlinear joint from its response are proposed in the next two sections.

§3.5.1 Algorithm A:

In Chapter 2, it has been proved that any Masing type nonlinear element can be represented by a new microslip model.

Define a shear stress distribution relation for the microslip model in the h-domain as s=s(x,h). Physically, this means the shear stress at h with respect to a displacement x. The force in the nonlinear element is an integration of s(x,h) with respect to h in [0,1], i.e.

$$F=\int_0^1 s(x,h)dh \tag{3.56}$$

The interface is divided into two regions, one is the elastic region in which the shear stress is proportional to the displacement, the other is the slipped region in which the shear stress is equal to the shear limit, i.e.

$$\begin{cases} s_i(x_i,h)=kx(h) & h > h_i \\ s_i(x_i,h)=kx_i & h \le h_i \end{cases} \tag{3.57}$$

If the nonlinear element is subjected to a further displacement dx, the slip region will change. The new stress distribution can be calculated in two steps.

i) the new stress distribution due to the additional elastic deformation dx is calculated as:

$$s_i'(x_i,h)=s_{i-1}(x_{i-1},h)+k\,dx \tag{3.58}$$

ii) the calculated $s'_i(x_i,h)$ is compared with its shear limit .

Since s(x,h) must be bound in a range [kx(h),-kx(h)], i.e.

$kx(h) \geq s_i(x_i,h) \geq -kx(h)$

The new stress must be

$$\begin{cases} s_i(x_i,h)=kx(h) & s_i'(x_i,h) > k\,x(h) \\ s_i(x_i,h)=s_i'(x_i,h) & -kx(h) \leq s_i'(x_i,h) \leq kx(h) \\ s_i(x_i,h)=-kx(h) & s_i'(x_i,h) < -kx(h) \end{cases} \qquad (3.59)$$

With the new stress distribution, the nonlinear force can be calculated from equation(3.56).

To start the procedure, if $x_0=0$, $s_0(0,h)=0$; if $x_0 \neq 0$, assume $x_{0-1}=0$, $s_{0-1}(0,h)=0$ and $dx=x_0$.

Only the stress distribution at one response state needs to be stored for this algorithm, and this stress distribution should be updated at each time step. Because the integration of equation(3.56) is actually achieved by using finite summation in the h domain, a sufficient number of points has to be used to ensure accuracy.

§3.5.2 Algorithm B:

§3.5.2.1 Corner Points and Effective Corner Points

This algorithm is also based on Masing's rule and is superior to Algorithm A in many aspects. Figure 3.1 shows a loading curve of a nonlinear element.

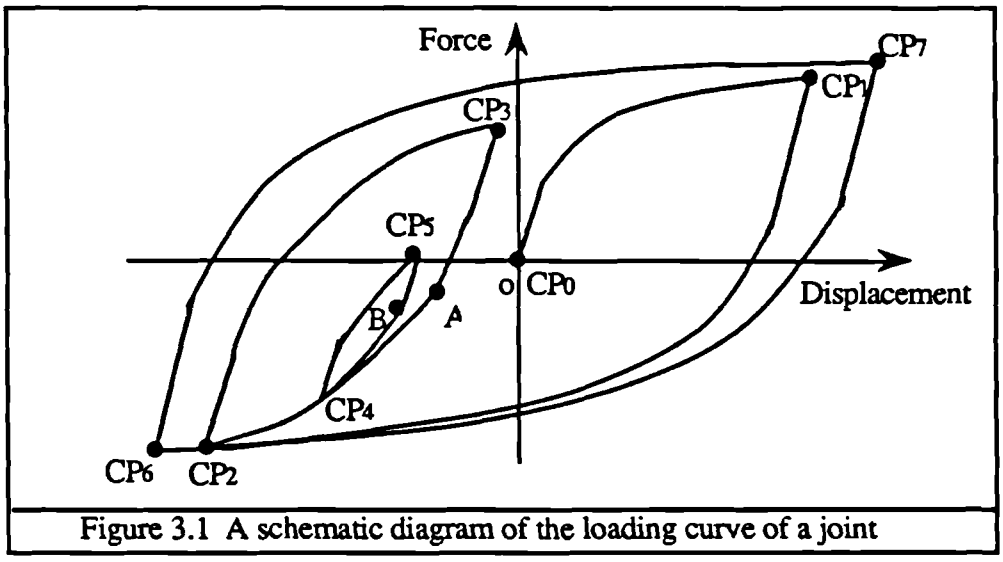

Figure 3.1 A schematic diagram of the loading curve of a joint

Some observations can be made: if the initial loading is F=f(x), the force corresponding to a displacement can be determined from the current displacement, and the force and

displacement at a certain point at which loading changes direction (these points are referred to as **corner points (cp)**, e.g. points CP_1 and CP_2).

If the levels of the displacement and force at the corner points are recorded, the force corresponding to any displacement is determined by the initial loading relation F=f(x) and the information at one corner point (which is referred to as the **effective corner point (ecp)**), that is:

if the effective corner point (ecp) is o, then

$$F=f(x)=sign(dx)\times f(|x|) \tag{3.60}$$

for all other cases

$$F=f_{ecp}+2sign(dx)\times f(|\frac{x-x_{ecp}}{2}|) \tag{3.61}$$

where f_{ecp} and x_{ecp} are the force and displacement at the effective corner point.

The effective corner point is o if and only if the magnitude of the displacement exceeds the magnitude of the maximum displacement in the foregoing loading.

For all other cases, an effective corner point is determined by the local loading loop(e.g. the effective corner point for point A is point CP_3, and the effective corner point B is CP_5).

Clearly, the major task is to determine the effective corner point, which can be achieved as follows:

If the effective corner point is CP_i for displacement x-dx, if loading changes direction, then the new effective corner point is at (x-dx, F(x-dx)); otherwise, if the displacement does not exceed the displacement level at CP_{i-1}, i.e.

$xdx<x(CP_{i-1})\ dx$

then the effective corner point is CP_i, or the displacement exceeds the local loop (and enter another local loop), the new effective corner point becomes CP_{i-2}. If the displacement increment is large enough, the loading may exceed the local loop to which CP_{i-2} belongs, then the effective corner point will be one in CP_{i-4}, CP_{i-6}....$CPi-_{2k}$(where k=1,2..) depending on the magnitude of the displacement increment.

§3.5.2.2 Computer Program

A computer code was written to implement both Algorithm A and Algorithm B. The code for Algorithm A is simple and will not be explained further.The flowchart for Algorithm B is shown in figure 3.2.

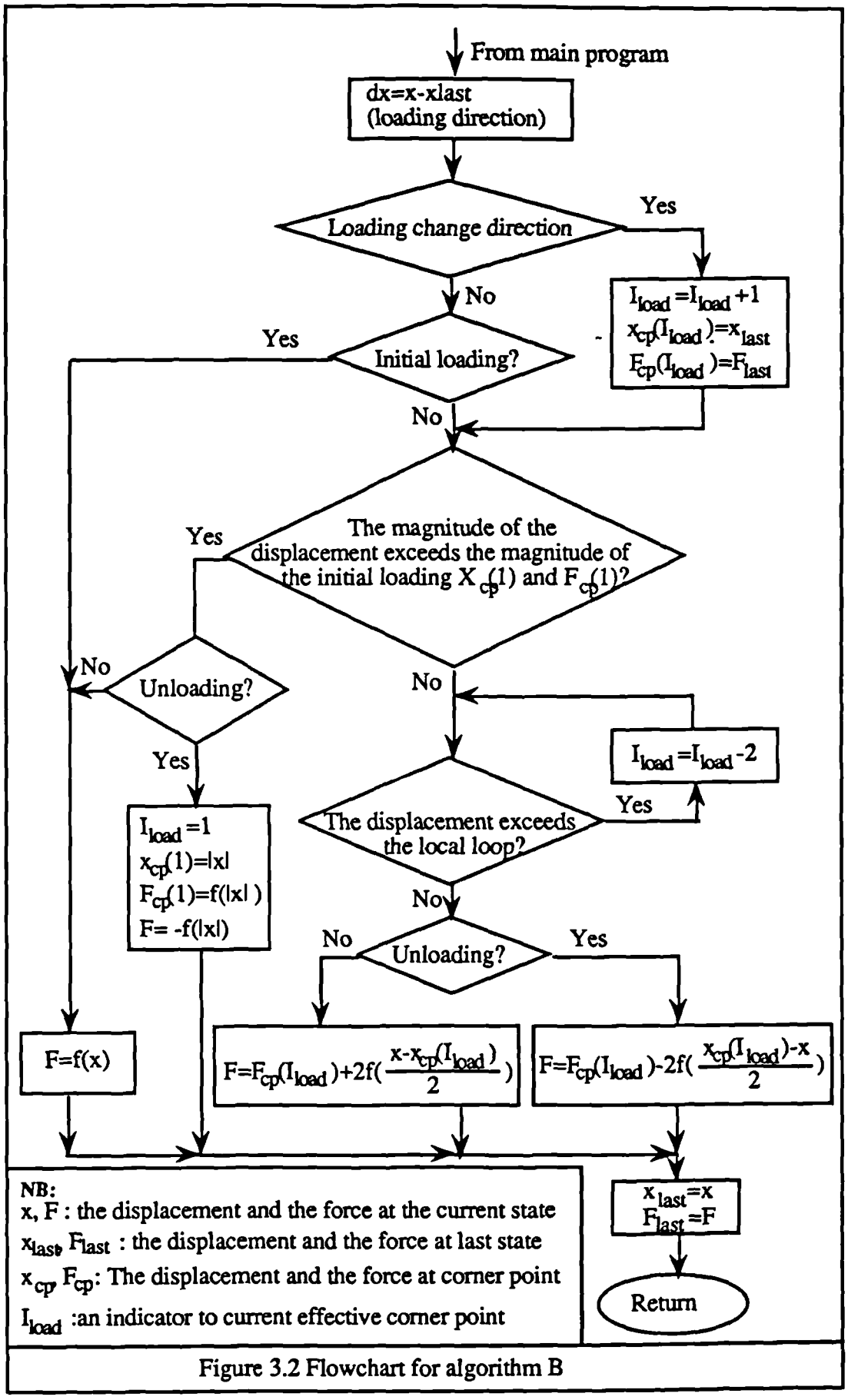

Figure 3.2 Flowchart for algorithm B

The information of the corner points (i.e. displacement and force) are stored in two arrays $\{x_{max}\}$ and force$\{F_{max}\}$. The effective corner point is indicated by an integer I_{load}. The displacement and force at the last time point are represented by two variables X_{last} and F_{last} respectively.

A special case that is worth mentioning is when the magnitude of the displacement in the negative direction exceeds the maximum displacement; there can be two options for numbering the effective corner point. One is to set $I_{load}=0$, the other is to set $I_{load}=1$ and update $X_{max}(1)$ and $F_{max}(1)$ simultaneously. The latter is used in the code because by doing this, one can detect the loading direction (i.e initial loading, unloading and reloading) from the value I_{load}. For any corner point indicator I_{load}, $I_{load}=0$ always corresponds to an initial loading in the positive direction, any other even I_{load} corresponds to a local minimum of the loading, and odd I_{load} corresponds to a local maximum of the loading. In other words, an even I_{load} represents a local reloading and an odd I_{load} corresponds to a local unloading.

It can also be noted from equation(3.60) and equation(3.61) that , the local stiffness for initial loading is

$$k_I=\frac{dF}{dx}=\frac{df(x)}{dx} \tag{3.62}$$

for all the other cases

$$k_I=\frac{dF}{dx}=\frac{df(y)}{dy}\Big|_{y=(x-xecp)/2} \tag{3.63}$$

§3.5.3 Comments on the Two Algorithms

Algorithm B is computationally more effective and accurate than Algorithm A (theoretically, Algorithm B is exact, while Algorithm A is only an approximation due to the finite summation in the place of the integral), therefore, it is selected for study in this chapter. However, there are some cases in which the Algorithm A may be more useful.

One example is when a very lightly damped structure is subjected to an impact; in this case, after reaching its maximum deformation, the magnitude of the vibration decays each cycle. If the Algorithm B is used, I_{load} increases in rate to more than 2 per cycle, very large arrays have to be allocated, for Algorithm A, however, the memory required is unchanged.

Another case when Algorithm A should be used is when the clamping force is also subjected to a variation, Algorithm B is not applicable, while for Algorithm A, all the process is the same except that the shear stress limit at the interface changes at each step.

Figure 3.3 shows three loading loops using Algorithm A and Algorithm B for a new microslip element (with $a=5\times10^{-8}$m, b=3 and $k=10^{6}$N/m). Two loops using Algorithm A have the interval in the h-domain 0.1(N=10) and 0.01(N=100) respectively. It can be seen that the difference between loops from Algorithm B and Algorithm A with $\Delta h=0.01$ is hardly distinguishable.

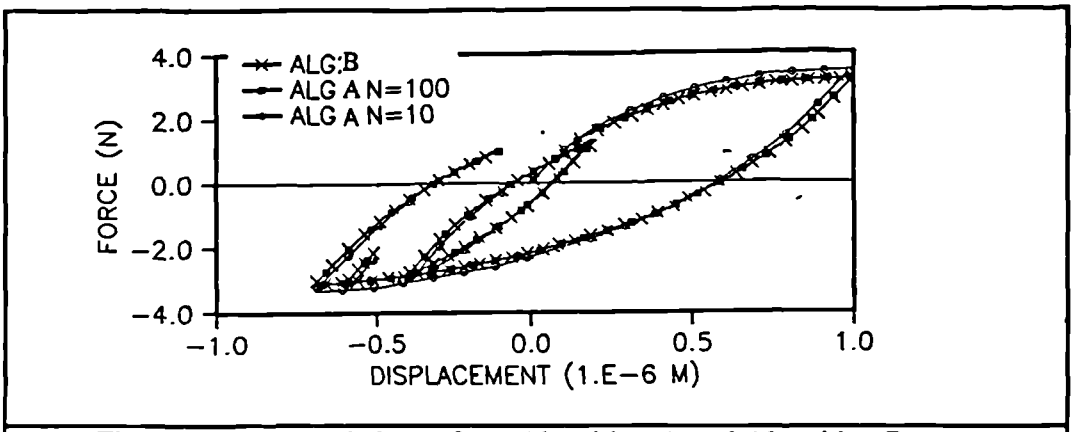

Figure 3.3 Hysteresis loops from Algorithm A and Algorithm B

§3.6 CASE STUDIES

Numerical studies have been carried out in order to evaluate the STI methods discussed in the foregoing sections. Three aspects are of particular interest for evaluation of a method:

1) stability

2) accuracy

3) efficiency (computation time required to implement the job)

The central difference method is only conditionally stable, and it will not be investigated further. The Newmark-β method and Algorithm One use the same assumption on the variation of the response between the neighbouring time points (i.e. equations (3.6) and (3.7)), hence they yield the same accuracy. The only difference between these two methods is that different iteration formulae are used. Experience shows that in almost all the cases, Algorithm One needs less iterations than the Newmark-β method (equation(3.26)), and Algorithm One converges in the case when the Newmark-β method diverges; therefore, the Newmark-β method will not be investigated further either. The two methods investigated are Algorithm One and Algorithm Two.

§3.6.1 Description of the System Studied

The system used for studying the STI methods is an 18 DOF finite element model consisting of two beams as shown in figure 3.4. The odd number coordinates correspond

to the translational DOFs in the vertical direction and the even number coordinates correspond to the rotational DOFs.

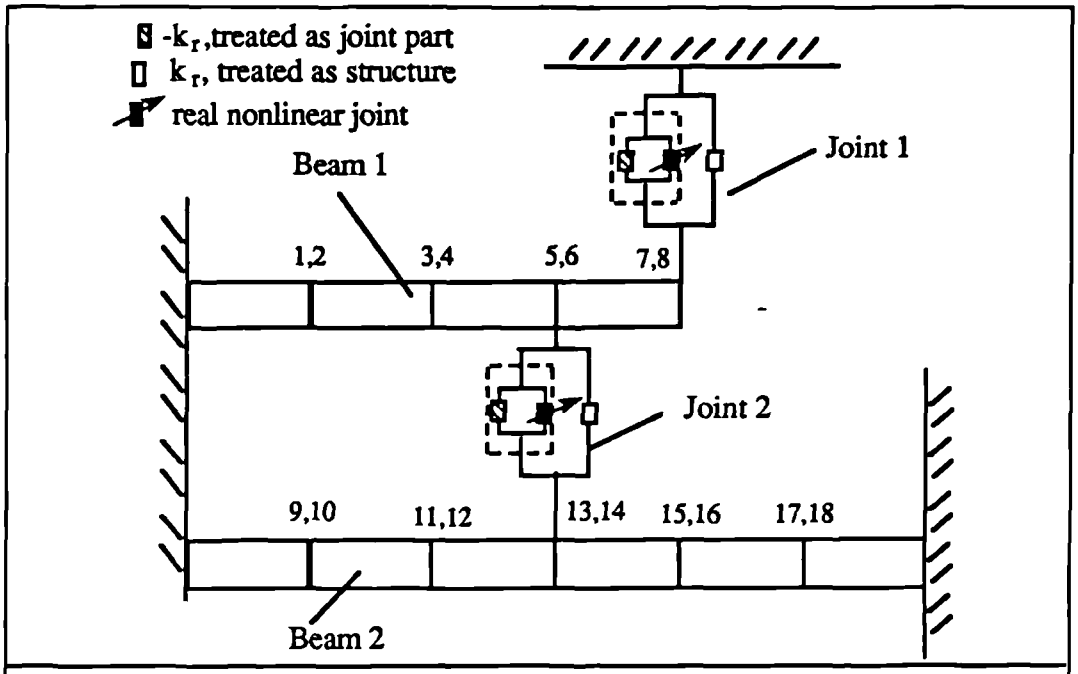

E=2.07E11N/m ρ =7574kg/m w=0.05m L=0.2m
For beam1: h_1 =0.012m For beam 2: h_2 =0.015m

Figure 3.4 The diagram of the beam system

Proportional viscous damping (i.e. $[C]=\alpha[K]$, where α is a positive number) is frequently used, however, such a system tends to have unreasonably high damping at high frequencies. To overcome this problem, the following scheme is used to introduce damping:

Let $[\phi]$ be the eigenvector matrix of the problem

$$[K]\{\phi\}=\lambda[M]\{\phi\} \tag{3.63}$$

and

$$[\hat{k}]=[\phi]^T[K][\phi] \tag{3.64}$$

$$[\hat{m}]=[\phi]^T[M][\phi] \tag{3.65}$$

The damping matrix [C] is constructed as

$$[C]=2\zeta[\phi]^{-T}[\hat{\sqrt{mk}}][\phi]^{-1} \tag{3.66}$$

where ζ is the damping ratio.

The system with this damping matrix has the same level of damping at every resonance. In the following case studies, ζ is set to be 0.01.

There are two joints in the system; one connects coordinates 5 and 13, the other connects coordinate 7 to a rigid base. The system is similar to some real structures such as a bladed turbine disc; for a bladed turbine disc, the first and the second joints can be used to represent the contact at the root of a blade and at the platform between the blades respectively.

For simplicity, the two joints have the same properties. Two types of nonlinear elements are used to simulate the friction joints. The first is the bilinear element with the initial loading relation

$$\begin{cases} F = ka & kx > ka \\ F = kx & kx \le ka \end{cases} \tag{2.61}$$

The second is the new microslip element developed in Chapter 2 with the initial loading relation

$$\begin{cases} F = \dfrac{ka(e^b-1)}{b} & x > ae^b \\ F = \dfrac{k\{x-a+x(b-\log_e x+\log_e a)\}}{b} & a < x \le ae^b \\ F = kx & x \le a \end{cases} \tag{2.60}$$

It should be noted that although only two joint models are used, the computer code is capable of dealing with any Masing type nonlinear joint. The parameters of the nonlinear joints for case studies are shown in table 3.1.

Joint Type	a (m)	b	k (N/m)	T_{max}(m)	Note
A	∞	0	10^6	∞	linear
B	4×10^{-7}	0	10^6	0.4	bilinear
C	4×10^{-9}	0	10^8	0.4	bilinear
D	4×10^{-11}	0	10^{10}	0.4	bilinear
E	6.36×10^{-8}	3	10^6	0.4	microslip

Table 3.1 Parameters for different joints

Two pseudo linear stiffness elements are introduced for each joint, the stiffness of these two elements is the same in magnitude but opposite in sign. The overall effects of these two elements on the structure are zero. $[K_r]$ is treated as part of the system stiffness, while the force $[-K_r]\{x\}$ is treated as an external force.

For clarity, in some cases, the results of an integration are presented by only two values; one is the maximum magnitude in the integration which is referred to as the magnitude of the transient response, the other is the magnitude of the steady-state response. In other cases, the results are presented in the time domain.

If the former method is used, the accurate results are at the points with small time interval Δ or tight convergence criteria TOL.

The excitation is $p=\sin(100\pi t)$, applied at coordinate 5 unless specified.

§3.6.2 Results for Systems with Different Type of Joints

Figures 3.5-3.9 show the displacement at point 5, relative displacement at joint 2, friction force at joint 2 and the hysteresis loop of joint 2 for systems with different types of joints. Sufficient time step Δ is used to ensure the accuracy of the numerical results. The results from **Algorithm One** are plotted using a **solid line** and those from **Algorithm Two** using a **dashed line**. Because the results from the two algorithms are very close, they are hardly distinguishable.

In all the cases studied, the numerical results indicate that all the steady-state responses of systems containing different joints are periodic. It is also noted that the waveform of the displacement is distorted (i.e. not sinusoidal) except for the system with A type joints. The response on the structure (e.g. coordinate 5) is closer to a sinusoidal form than the relative displacement at the joint (e.g. joint 2). The waveform of the relative displacement can have more than one positive(or negative) peak at each cycle of the excitation, which forms a subloop in the loading curves.

If the initial stiffness is significant (i.e. joint type C and D), the calculated friction force at certain periods of a cycle changes violently, these periods correspond to the time when the joint is in the elastic range (i.e. the interfaces 'stick' together). However, although the friction force at these periods changes violently, both the response at point 5 and the relative displacement at joint 2 are very smooth.

Since the friction force calculated from Algorithm One and Algorithm Two are very close, the calculated friction force and displacement are believed to be accurate. The results indicate that the friction force at the joint varies violently at certain time in a cycle. Compared with the results with B and C type joints, it can be noted that the variation of the friction force becomes more significant as the magnitude of the initial stiffness of the joints increases. When initial stiffness of the joint is significant, the joint in the elastic range can be considered to be 'stuck' together. The above results show that the joint can be in a series of stick-slip motions if its initial stiffness is significant.

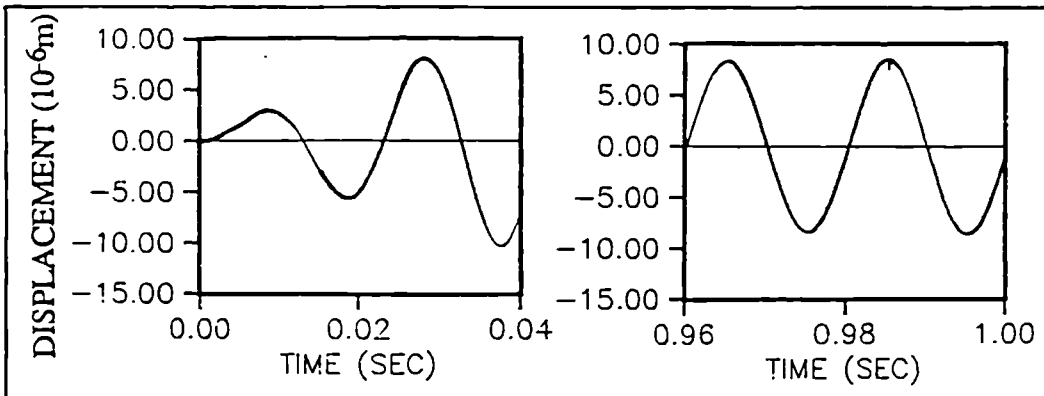

(a) Displacement at coordinate 5

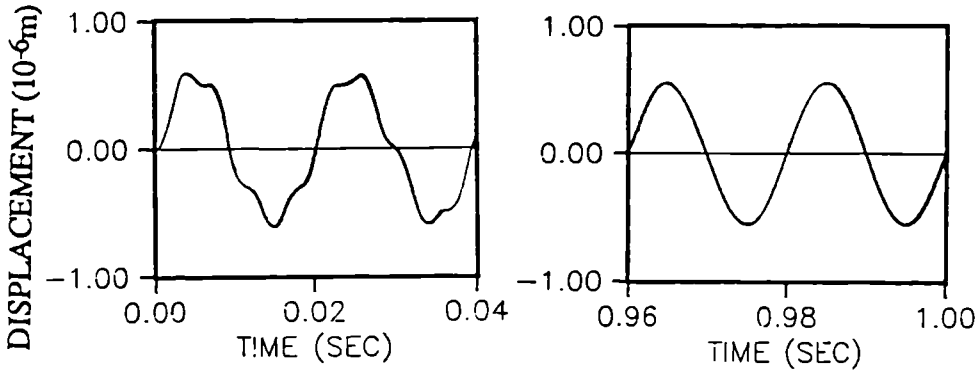

(b) Displacement at joint 2

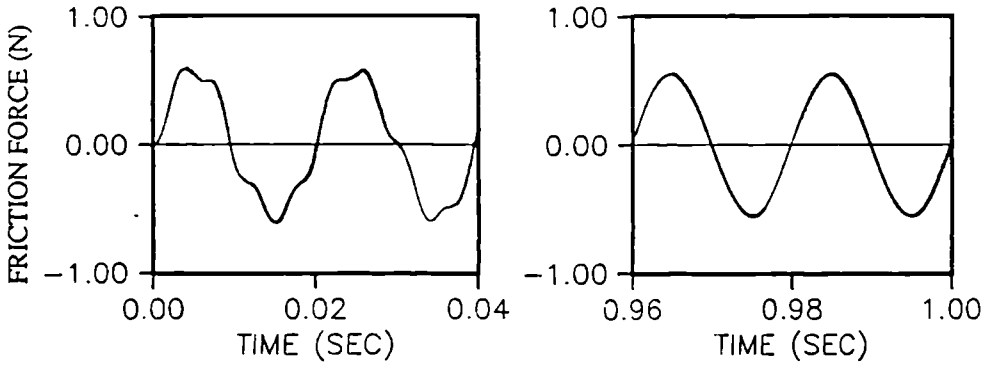

(c) Friction force at joint 2

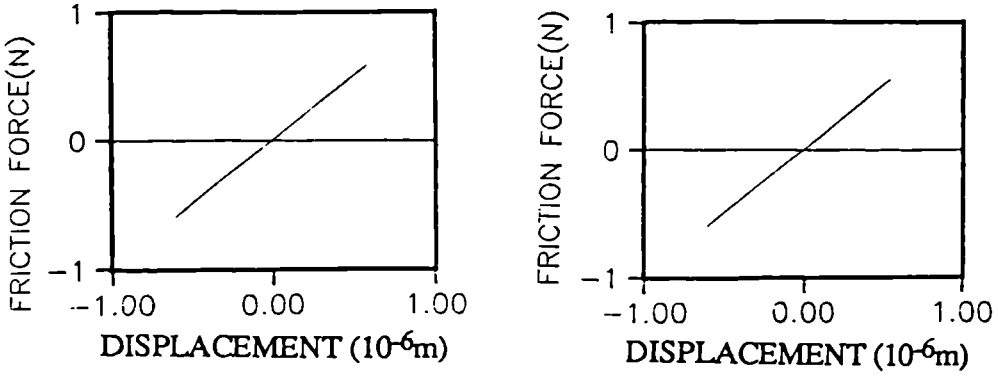

Transient Steady-state

(d) Hysteresis at joint 2

Figure 3.5 Numerical results for the system containing A type joints

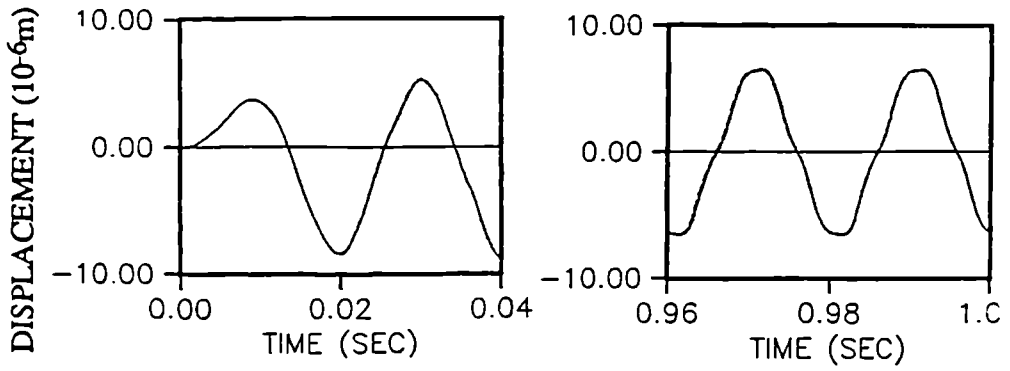

(a) Displacement at coordinate 5

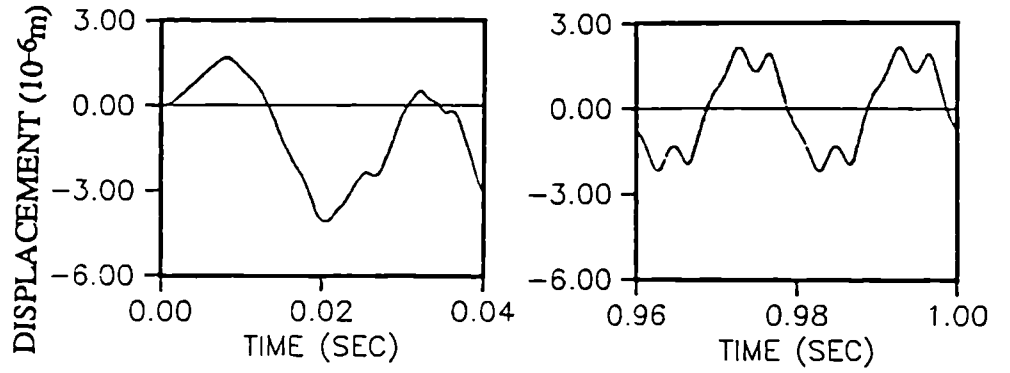

(b) Displacement at joint 2

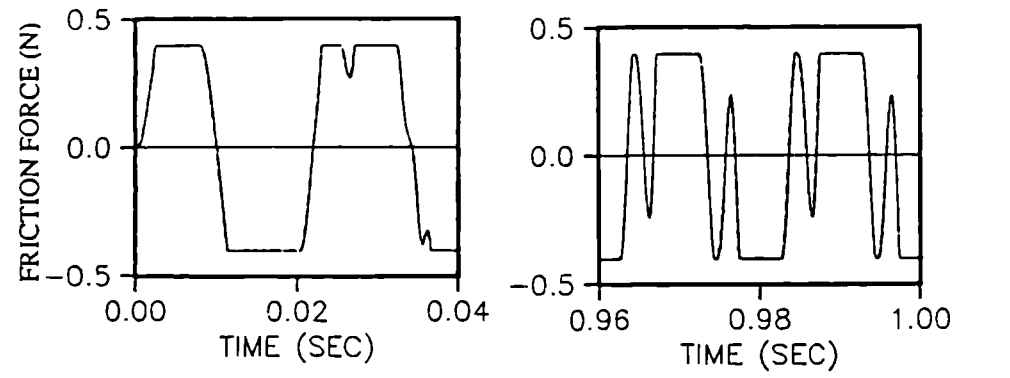

(c) Friction force at joint 2

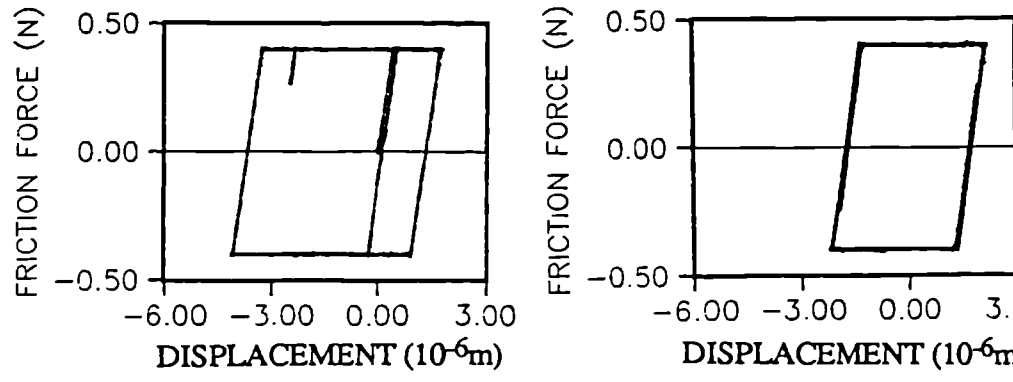

(d) Hysteresis at joint 2

Figure 3.6 Numerical results for the system containing B type joints

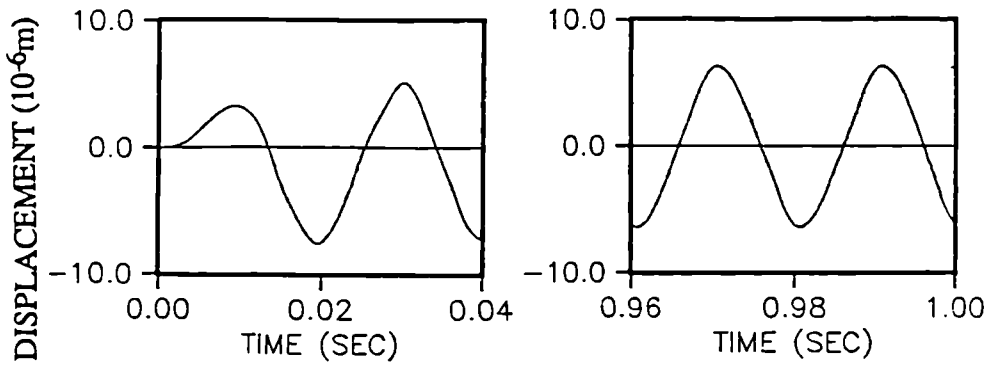

(a) Displacement at coordinate 5

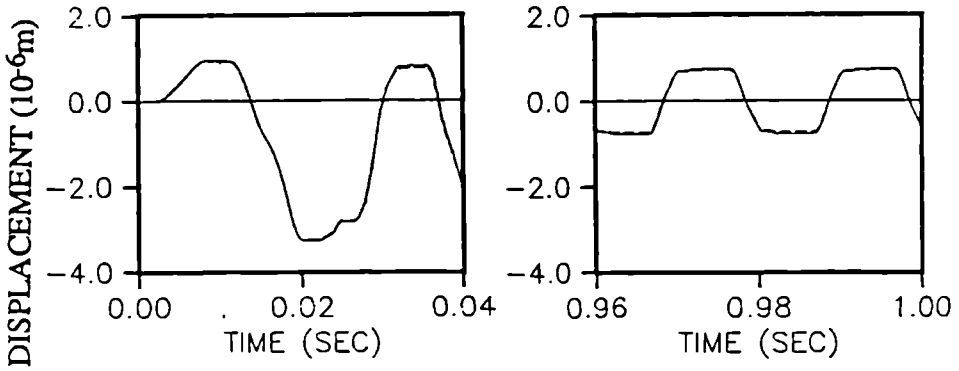

(b) Displacement at joint 2

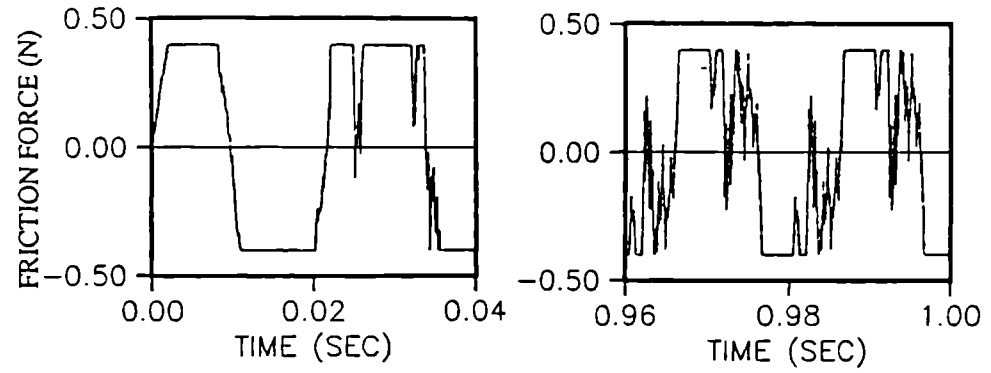

(c) Friction force at joint 2

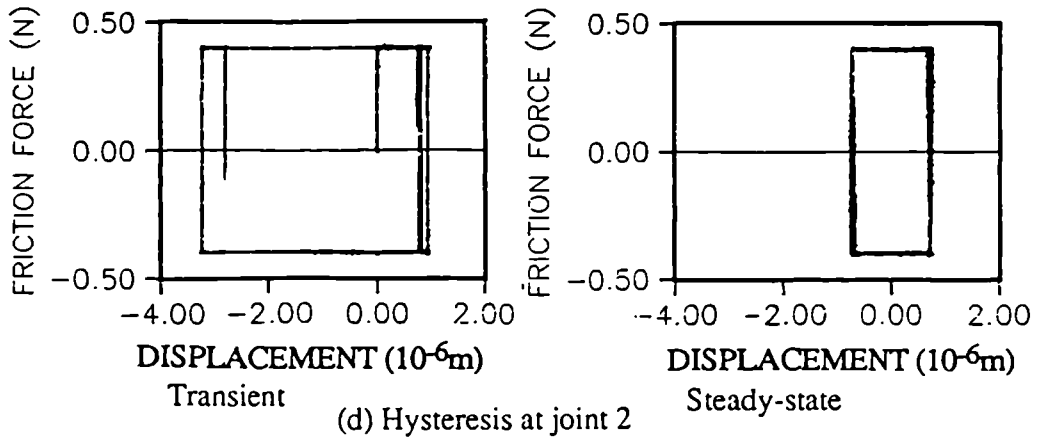

(d) Hysteresis at joint 2

Figure 3.7 Numerical results for the system containing C type joints

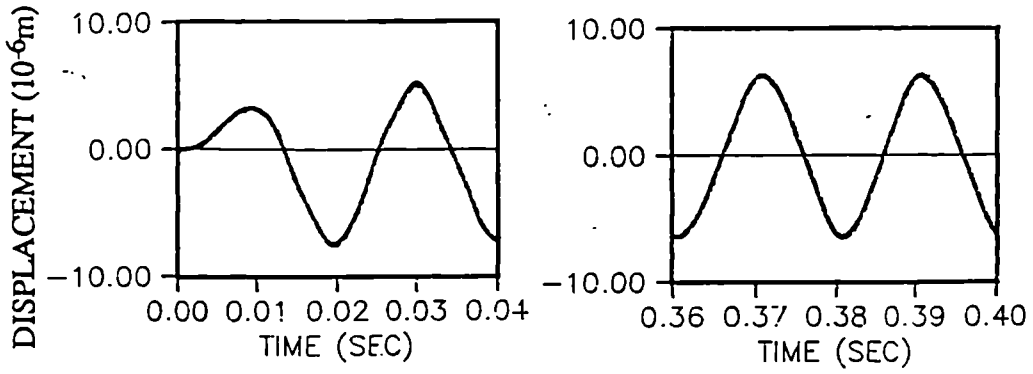

(a) Displacement at coordinate 5

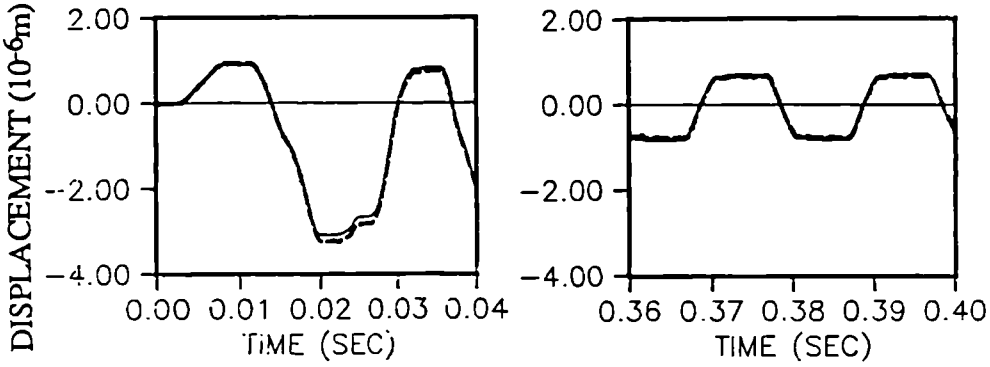

(b) Displacement at joint 2

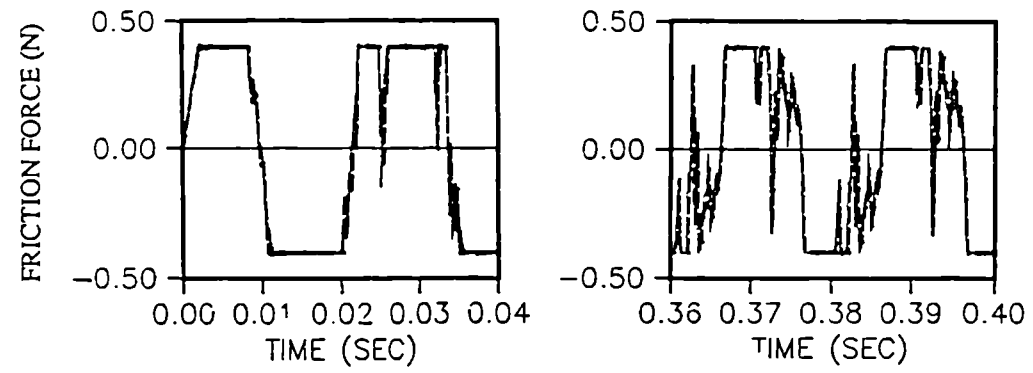

(c) Friction force at joint 2

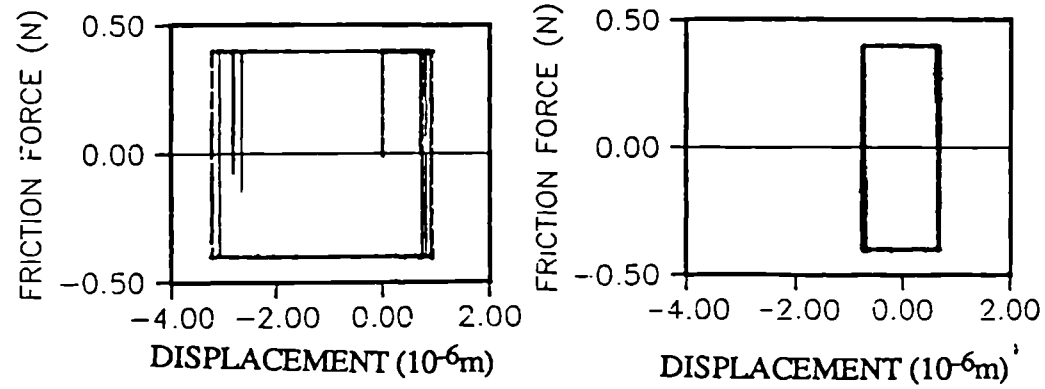

Transient Steady-state

(d) Hysteresis at joint 2

Figure 3.8 Numerical results for the system containing D type joints

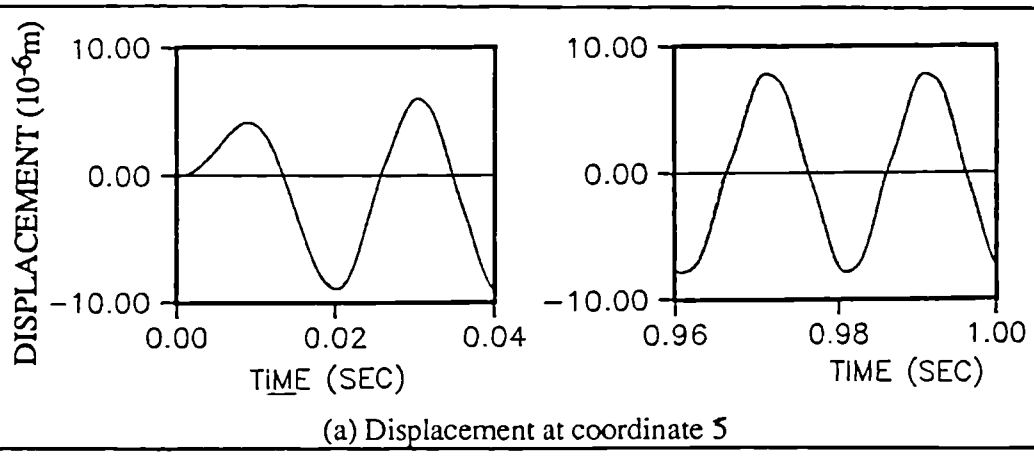

(a) Displacement at coordinate 5

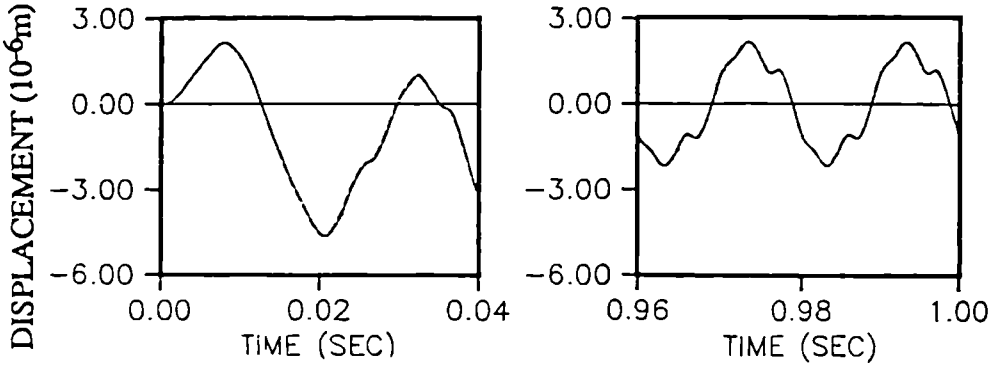

(b) Displacement at joint 2

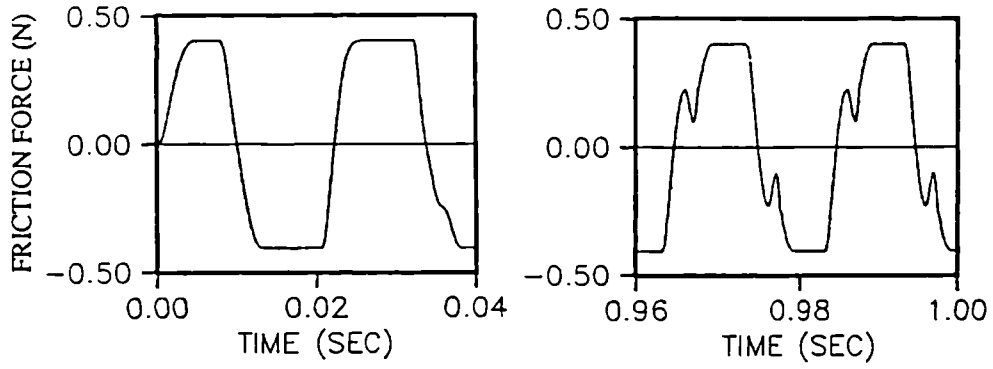

(c) Friction force at joint 2

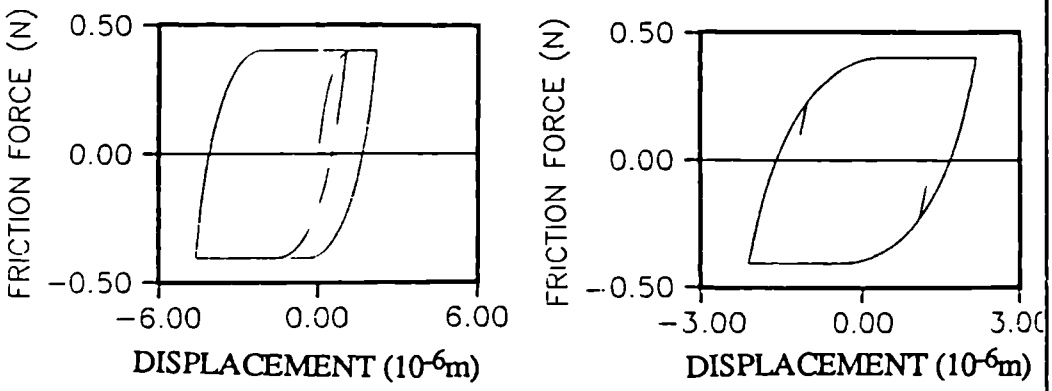

Transient Steady-state

(d) Hysteresis at joint 2

Figure 3.9 Numerical results for the system containing E type joints

In the remaining part of the case studies, attention is paid to the factors which affect the efficiency and accuracy of the integration results. For simplicity, bilinear joint models are used, but the conclusions drawn in the next few sections are also applicable to the system with different joint models.

§3.6.3 Investigation on Algorithm One

Since Algorithm One is iterative, it is believed that convergence criteria is the most important factor.

Figures 3.10 and 3.11 show the magnitudes of the integration results against the magnitude of the convergence criteria TOL (the displacement convergence criteria and the force convergence criteria are set to be the same, i.e. $X_{tol}=F_{tol}=TOL$).

It can be noted that although the excitations are the same, the values of TOL to achieve convergence are significantly affected by the time interval Δ and the property of the joint (mainly the initial stiffness k_i). Loose criteria can be used for small Δ and k_i. If TOL is too loose, the integration may be erroneous; if TOL is too tight, the computation cost can be very expensive, and sometimes the iterations may fail to achieve the convergence at a certain step and hence the whole process may fail (eg. convergence can not be achieved for $TOL<10^{-9}$ with a time step of 10^{-4}sec)

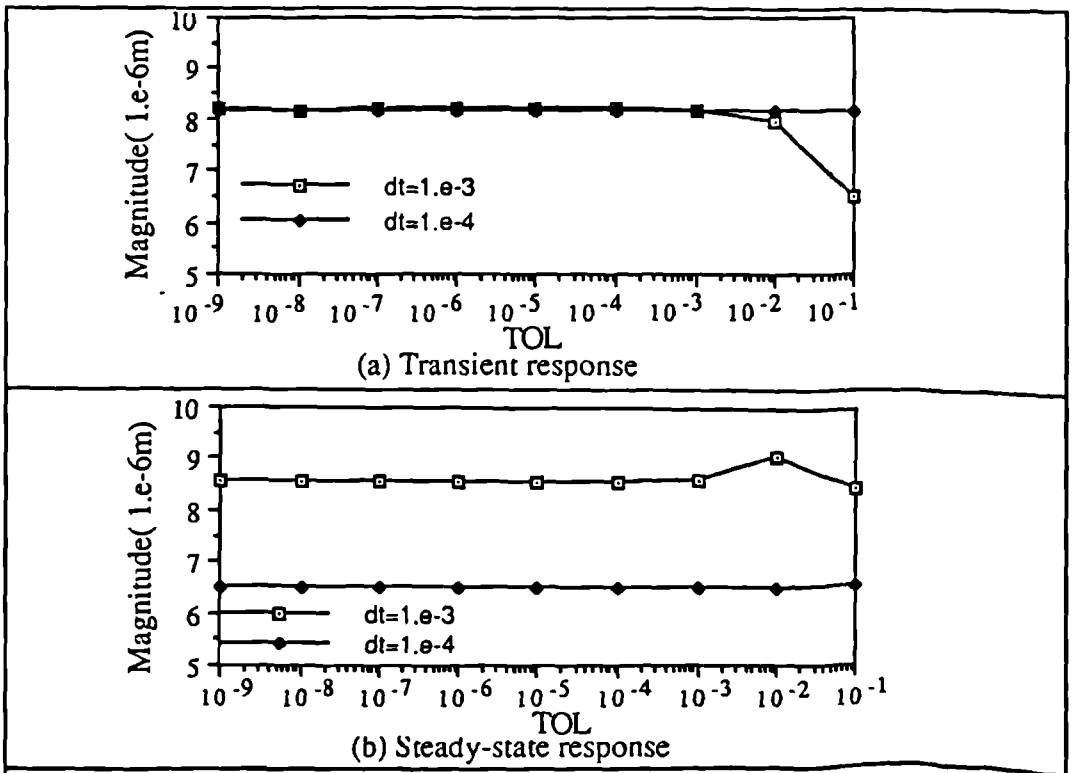

Figure 3.10 Effects of convergence criteria on system containing B type joints

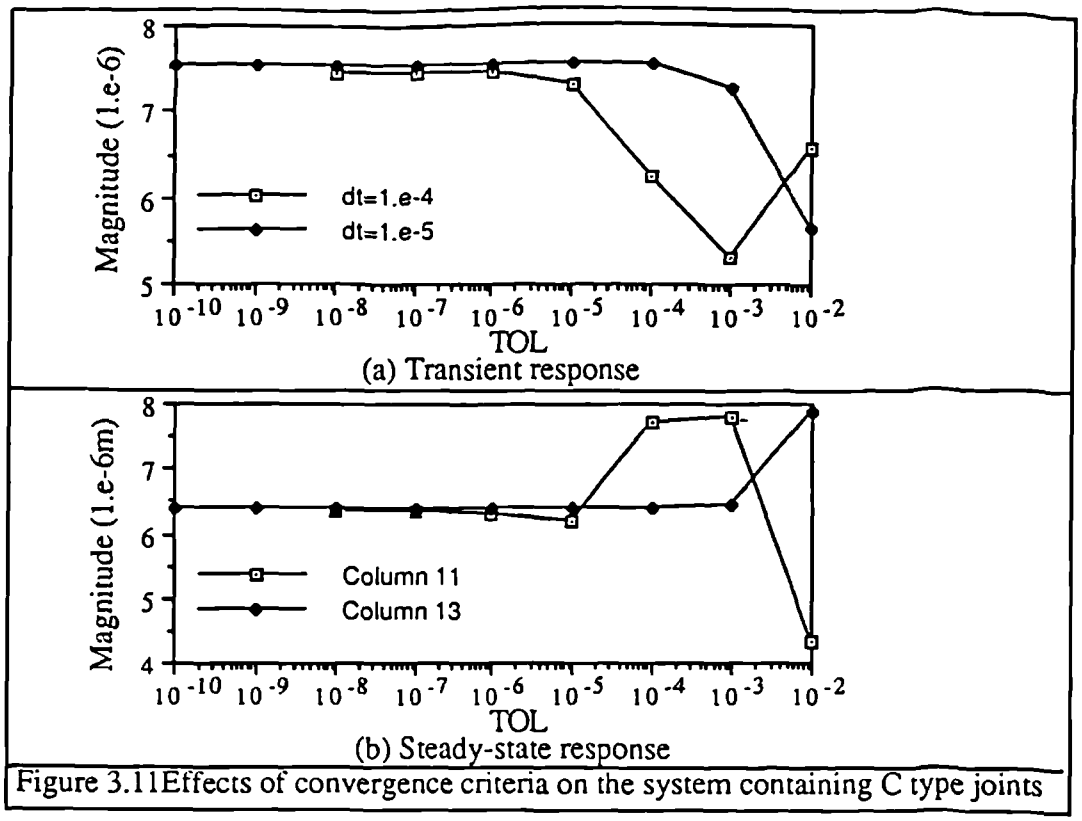

Figure 3.11Effects of convergence criteria on the system containing C type joints

Numerical results show that TOL=10^{-6} is a proper value for Algorithm One.

The initial stiffness of the joint has a significant effect on the efficiency of the integration. Figure 3.12 shows the computation cost (in terms of the average iteration number at each step) against the magnitude of the convergence criterion.

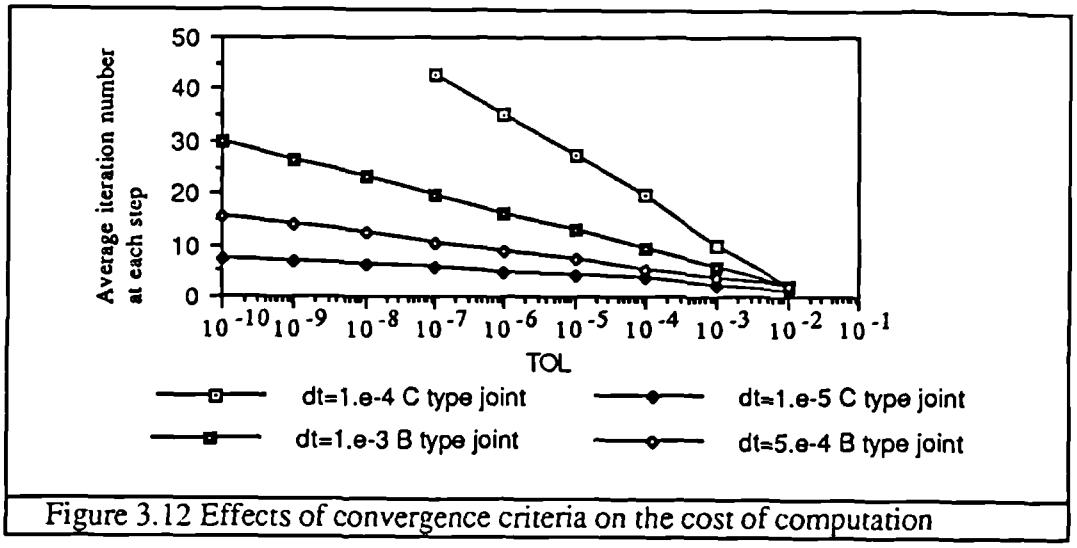

Figure 3.12 Effects of convergence criteria on the cost of computation

The relationship between the number of iterations and the convergence tolerance (logarithmic scale) is approximately linear. The slope is largely affected by the time interval Δ and the joint property (initial stiffness). Convergence is more difficult to achieve for a system with higher k_j. Indeed, if Δ is not smaller than 0.001sec, no

convergence can be achieved for the system with $k_i=10^8$N/m but convergence can be easily achieved for the system with $k_i=10^6$N/m.

The effects of initial stiffness of the joint will be further discussed in §3.6.5.

§3.6.4 Investigation on Algorithm Two

§3.6.4.1 Stability.

The stability analysis of Algorithm One is effectively the same as that of the Newmark-β method, and it has been proved [2] unconditionally stable for a linear system. Since the Newmark-β method has been studied in detail [2], the results of the stability analysis on Algorithm One will not be presented.

For an ordinary linear system, Algorithm Two is always unconditionally stable [90], i.e. the highest eigenvalue of the character matrix is unity. In the following part of this section, the effects of $[K_r]$ on the stability of Algorithm Two is studied.

The two joints for this study are A type joints (see table.3.1). The matrix $[K_r]$ consists of two identical springs with stiffness k_r. Figure 3.13 shows the highest eigenvalue of the character matrix of Algorithm Two. It is noted that k_r must be greater than a certain value for a particular Δ. The greater the Δ, the greater the k_r required to ensure stability. However, providing that k_r is greater than the stiffness of an A type joint (i.e.k_r >10^6N/m), the algorithm is unconditionally stable.

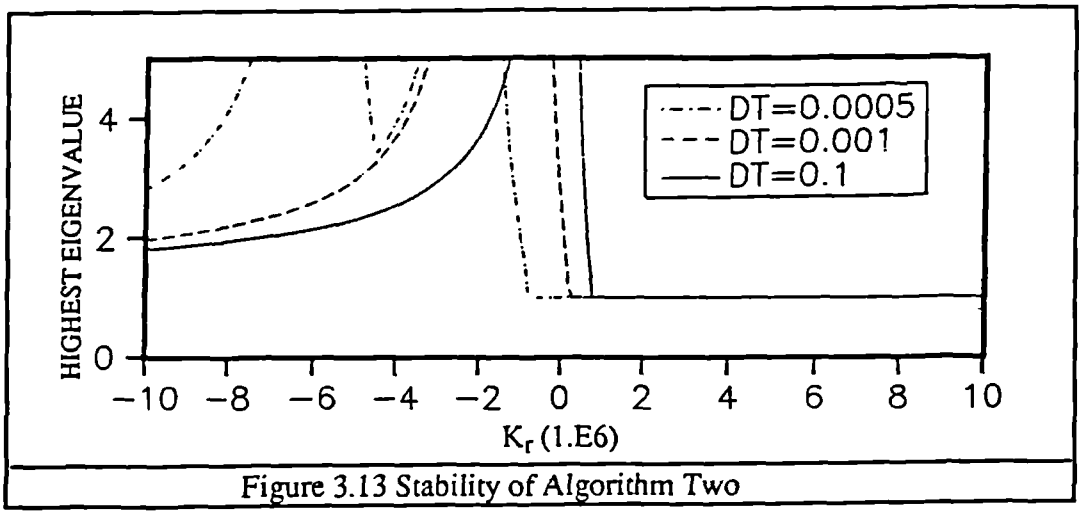

Figure 3.13 Stability of Algorithm Two

To examine the assumption made in §3.3.3.3, numerical integration is carried out on the system with B type joints. Figure 3.14 shows the results of the system with k_r=0N/m and $k_r=10^6$N/m under excitation P=sin(20πt) at coordinate 5 and with a Δ=0.001sec. A feature of figure 3.14 is that all the results are well-bounded. However, the results with k_r=0N/m are inaccurate, and actually these results are not related to the excitation directly.

This is shown more clearly in figure 3.15 in which the excitation force is P=0.01sin(20πt) at coordinate 5.

Inaccurate and well-bounded results for the system with K_r=0N/m are believed to be caused by unstable integration at some time steps and stable integration at the others. When the displacement is small, the stiffness is too high for the integration to be stable. Therefore, the displacement level tends to increase. When the displacement increases, the stiffness at the joint drops, accordingly, the integration tends to be stable. The ultimate result of these two factors is that the numerical results are well bounded, but have no physical significance. This situation can be referred to as a special type of instability. Since the results are well bounded, detection of this type of instability can be very difficult, particularly for a transient response; for example, it is almost impossible to recognize the instability from the results in figure 3.14.

For the integration with $k_r=10^6$N/m, the results are accurate (compared with integration results using very small Δ) and no bounded instability has been observed.

The above results clearly agree with the stability analysis in §3.3.3.3.

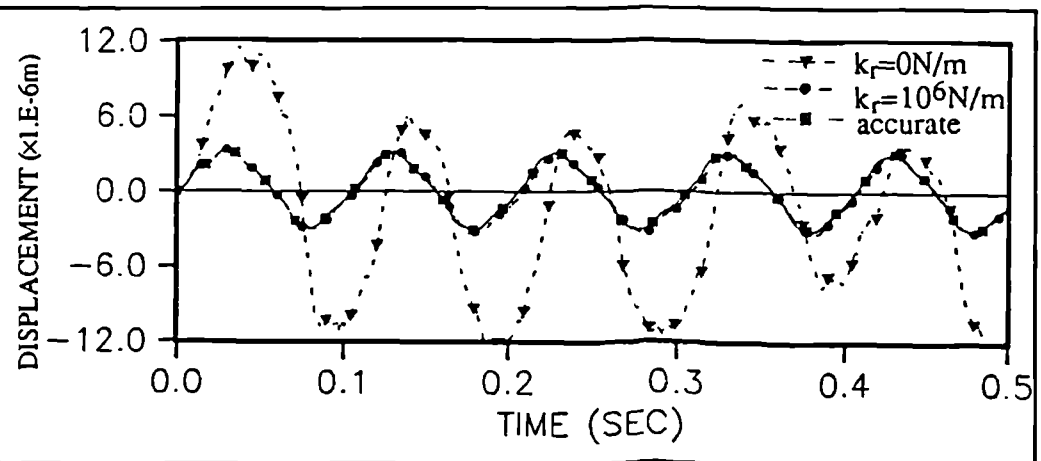

Figure 3.14 Results for the system containing B type joints (P=sin(20 πt))

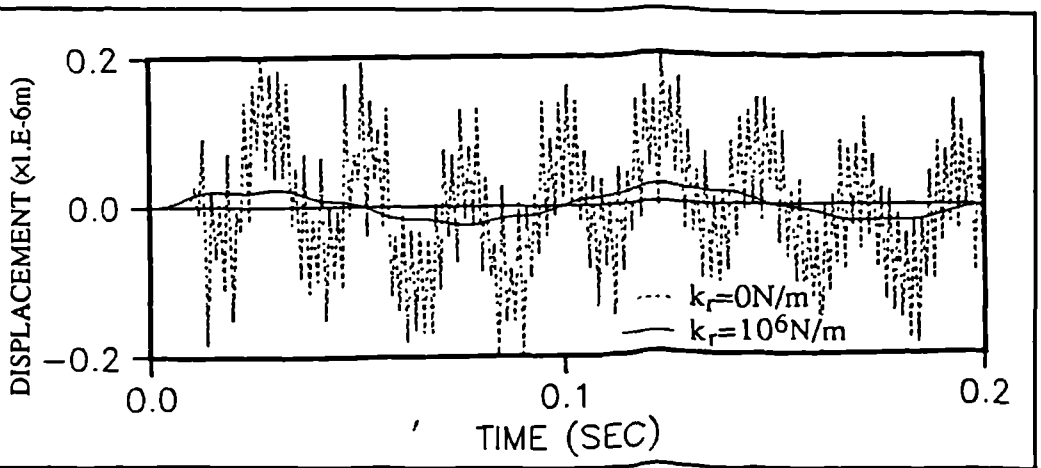

Figure 3.15 Results for the system containing B type joints (P=0.01 sin(20 πt))

§3.6.4.2 Effects of k_r on Accuracy of Algorithm Two.

As shown in the last section, the stability of Algorithm Two depends on the magnitude of k_r. In order to ensure a stable integration, k_r must be great enough so that the force in a joint has a negative slope. In §3.3.3.3, it has been shown that the magnitude of k_r affects the effective parameter 'a_e', hence it has effects on the accuracy of the integration results too. In this section, the effects of k_r on the accuracy of the integration are studied.

Figure 3.16 shows the integration results against the magnitude of k_r for a system with B type joints. When $k_r=10^6$N/m, accurate results are obtained for both cases with $\Delta=10^{-4}$(s) and $\Delta=10^{-5}$(s). However, the integration results become less accurate when the magnitude of k_r increases. A greater k_r (10^8N/m) is allowed for the integration with $\Delta=10^{-5}$, in other words, small Δ has to be used in order to achieve the desired accuracy when the magnitude of k_r is significant.

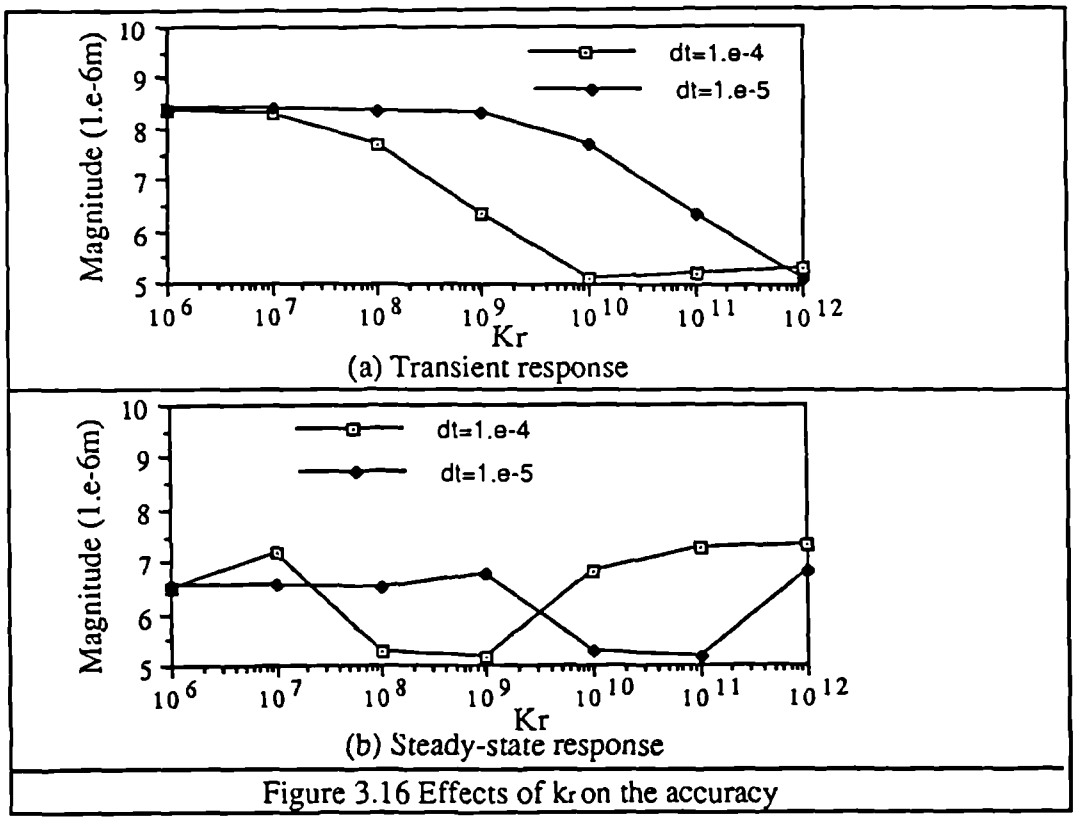

Figure 3.16 Effects of k_r on the accuracy

The effects of k_r on the accuracy of the integration can have a significant impact on the application of Algorithm Two on a system containing joints with very high initial stiffness (e.g. dry friction type nonlinearity). In order to ensure stability, the magnitude of k_r must be set the same as the initial stiffness, while very large k_r means that Δ must be very small to yield accurate results, hence the cost of the integration can be very expensive. This problem will be discussed further in the next section.

§3.6.5 Considerations on Initial Stiffness of the Friction Joint

It has been demonstrated that the initial stiffness of the joint can have significant effects on the efficiency of both Algorithm One and Algorithm Two. For Algorithm One, the initial stiffness determines the maximum Δ for the iteration to converge, and for Algorithm Two, although there is no limit on convergence, a proper Δ for a desired accuracy is largely affected by the initial stiffness. For both algorithms, Δ has to be sufficiently small if the initial stiffness of a joint is significant. This means the cost of computation can be very high.

However, very high initial stiffness may not be necessary in the integration. It is understandable that the change of stiffness of a very rigid joint has little effect on the overall behaviour of the structure. Therefore, the initial stiffness of a joint can sometimes be reduced to a much lower level without affecting the physical system significantly. For the system with lower initial stiffness, a greater Δ can be used, hence, the computation cost can be reduced.

Figure 3.17 shows the magnitudes of the integration results for the system with different initial joint stiffness using Algorithm Two. The friction limit is the same (0.4N). It is noted that the responses for the systems with initial joint stiffness greater than 10^8N/m are very close. This can also been noted from figure 3.7 and figure 3.8.

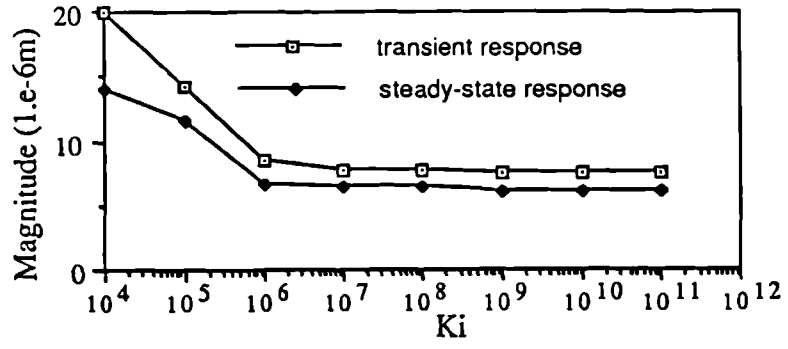

Figure 3.17 Effects of joint initial stiffness on the response of the structure

For the joint with initial stiffness 10^{10}N/m, no convergence for Algorithm One is achieved by using any Δ greater than 2×10^{-6} sec; for Algorithm Two, the results are inaccurate for the integration with $\Delta>10^{-5}$N/m. However, if joints with initial stiffness 10^8N/m are used, reasonably accurate results are achieved with $\Delta=5\times10^{-5}$sec. The results from Algorithm Two are shown in figure 3.18.

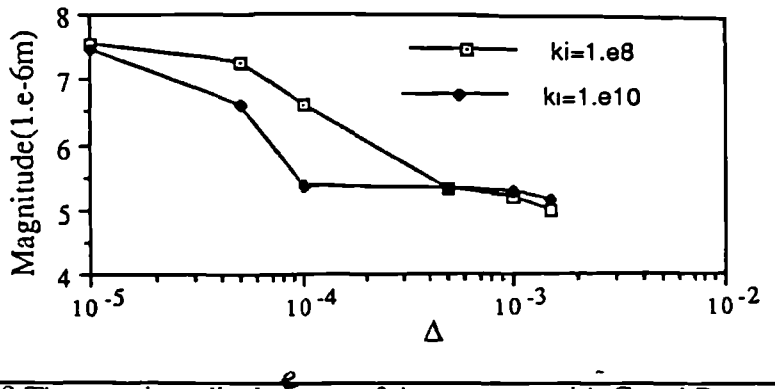

Figure 3.18 The transient displacment of the systems with C and D type joints

It can be noted that even if the real joint has an initial stiffness 10^{10}N/m, if $\Delta=5\times10^{-5}$sec is used, the integration results on a system with joint initial stiffness 10^{8}N/m is closer to the response of the system than the integration results on the original system ($k_i=10^{10}$N/m) directly.

The proper initial stiffness for a friction joint may be estimated by calculating the response of the system with a linear joint (with the stiffness as the initial stiffness of the friction joint) in the place of the friction joint. The stiffness of the linear joint is reduced gradually and the response of the system with these joints calculated. A proper initial stiffness for the friction joint should be such that the ratio of the response between the system with initial stiffness of the real joints and the system with reduced joint stiffness is close to one. Because the response of the system containing friction joints has higher frequency components (harmonics), the reduced stiffness must also be representative at the highest frequency of interest.

Figure 3.19 shows the ratio of the magnitude of the steady-state responses (at coordinate 5) between the reduced stiffness and real initial stiffness (10^{11}N/m) at some frequencies.

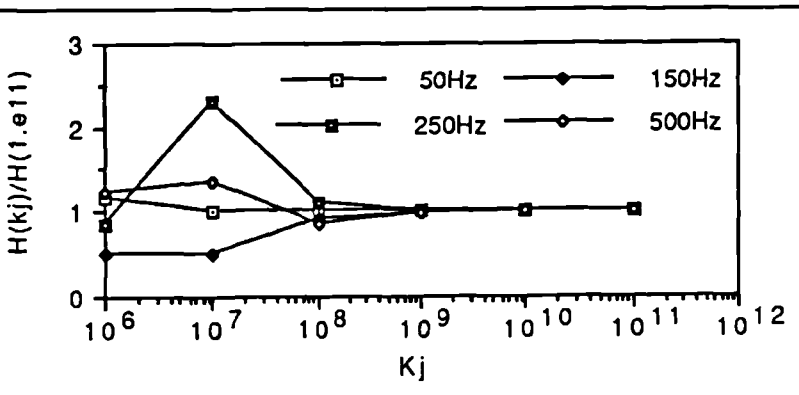

Figure 3.19 Effects of joint stiffness on the response

It can be noted that a reduced stiffness $k_i=10^{8}$N/m gives a good approximation to the system with $k_i=10^{11}$N/m for a frequency range up to 500Hz, which suggests that

$k_i=10^8$N/m can be used for the initial stiffness of the friction joint. Clearly, it can be noted from figure 3.18 that the above conclusion is correct.

§3.6.6 Comparison Between Algorithm One and Algorithm Two

It may not be appropriate to conclude one algorithm is always superior to another. In this section, the advantages and disadvantages of the both algorithms are analysed.

Figure 3.20 and figure 3.21 show the results from the system with B type joints and the system with D type joints.

It can be noted that if initial stiffness is not significant (i.e. $k_i=10^6$N/m), the accuracies of these two algorithms are similar, however, the cost of Algorithm One, because of the iteration process, is higher, which seems to indicate that Algorithm Two should be used.

If initial stiffness is significant (i.e. $k_i=10^8$N/m), accurate results are more difficult to achieve. It is noted with the same time step Δ, the results from Algorithm One are more accurate than those from Algorithm Two. It can also be noted that once convergence is achieved for Algorithm One, the results tend to be accurate, while the results from Algorithm Two can be erroneous when Δ is not small enough. This seems to indicate that Algorithm One is more reliable than Algorithm Two. However, the cost of Algorithm One is much higher with the same time step Δ as shown in figure 3.21c. If the same computation time are used, much smaller Δ can be used for Algorithm Two and even more accurate results can be achieved.

The main disadvantage of Algorithm One is the cost to achieve convergence at each time step and the main disadvantage of Algorithm Two is the errors introduced by using equation(3.32). The computation efficiency can be significantly improved if these two problems are solved.

The comparison between the two algorithms seems in favour of Algorithm Two in terms of efficiency; however, Algorithm One is more reliable.

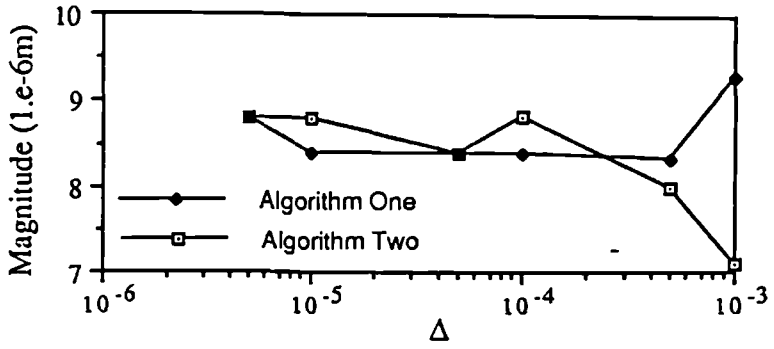

(a) Transient response

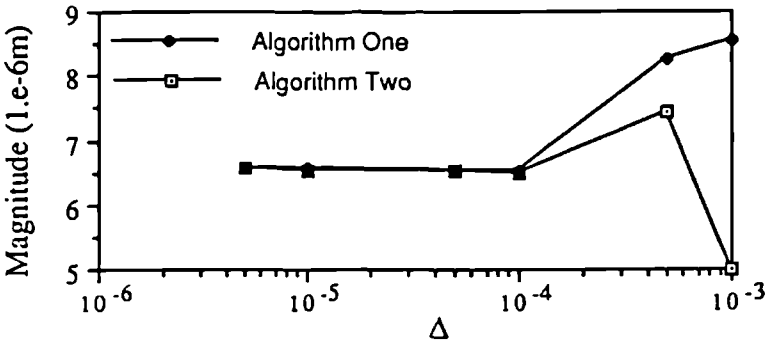

(b) Steady-state response

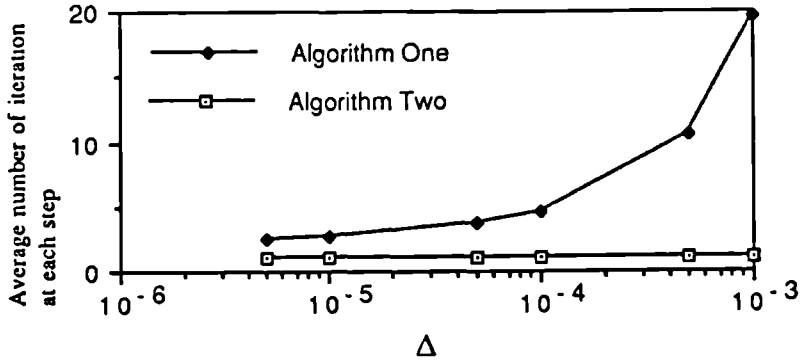

(c) Cost of integration

Figure 3.20 The accuracy of the results for the system containing B type joints using Algorithm One and Algorithm Two

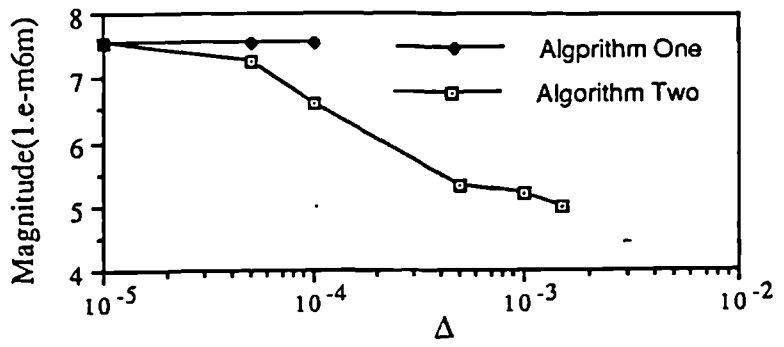

(a) Transient response

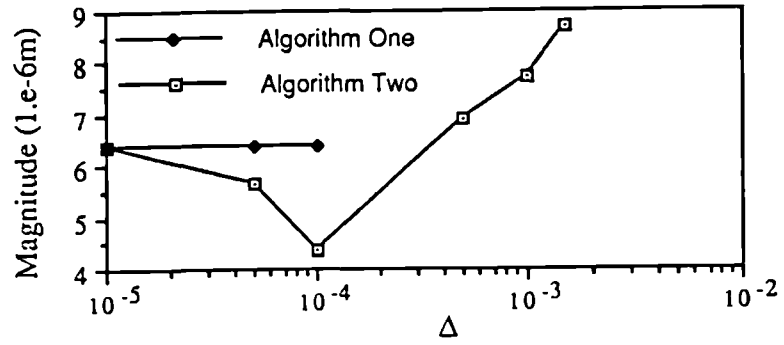

(b) Steady-state response

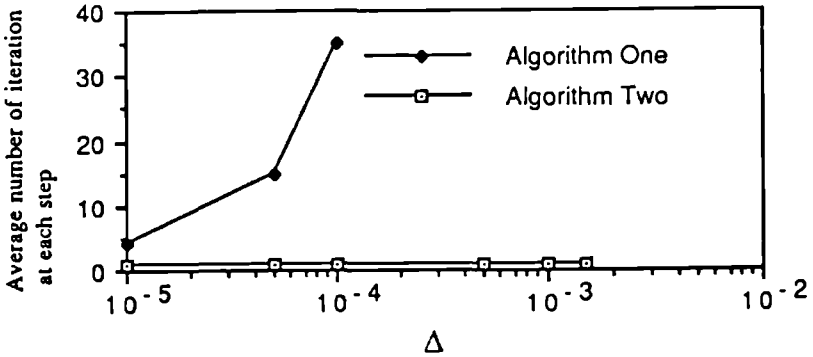

(c) Cost of integration

Figure 3.21 The accuracy of the results for the system containing D type joints using Algorithm One and Algorithm Two

§3.6.7 Condensation

In this section, the effects of condensation are studied. Sufficiently small Δ is used to ensure accuracy of the numerical integration.

Figure 3.22 shows the numerical results against number of modes for the system with A type joints. It can be noted that very accurate results are achieved with 8 lock-modes, while 10 free-modes are required to yield similar accuracy. This indicates that lock-modes form a better subspace for the deformation shape of the linear structure, while free-modes can also be representative with a few additional modes.

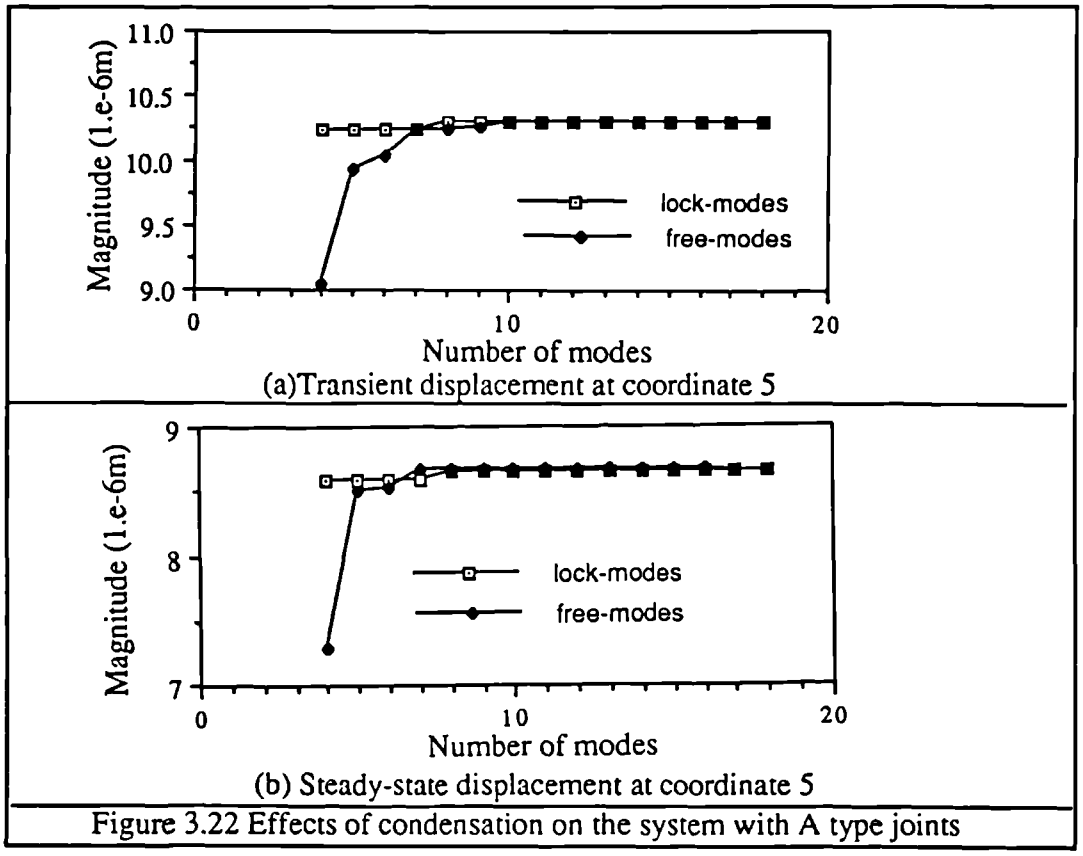

Figure 3.22 Effects of condensation on the system with A type joints

It is of more interest to study the effects of condensation on a nonlinear structure. Figure 3.23 shows the results for the system with B type joints. It can be noted that 10 free-modes are required to form a representative subspace, however, at least 14 lock-modes should be included to yield the same accuracy as using 10 free-modes.

Clearly, the above results indicate that the free-modes are more appropriate for the condensation of a nonlinear system. The lock-modes are not so suitable to form the subspace of the vibration shape. The reason for the poor results of the lock-mode condensation is that the spatial model of the system is changing all the time, while the lock-modes are only representative for spatial systems with the joint stiffness close to the initial stiffness. Usually, the deformation of each lock-mode at a joint is very small, however, when slip occurs at the joint, the local stiffness at the joint drops to zero and the

real deformation at the joint can be much greater than what the linear combination of lock-modes can represent. Consequently, poor results are obtained. The free-modes correspond to the system without joints, and the combination of free-modes allows sufficient deformation at the joint, hence the deformation at the joint is preserved accurately. Accordingly, the overall behaviour of the system is also accurately preserved.

The lock-mode condensation can be even less accurate if the joint has higher initial stiffness. It is found (but not presented in this thesis) that at least 17 lock-modes are required to yield a reasonable accuracy for the original system, while only 10 free-modes are required to achieve the same level of accuracy.

Figure 3.24 hows the time domain response of the system with B type joints. The results using 10 free-modes to 18 free-modes (i.e. no condensation) are hardly distinguishable.

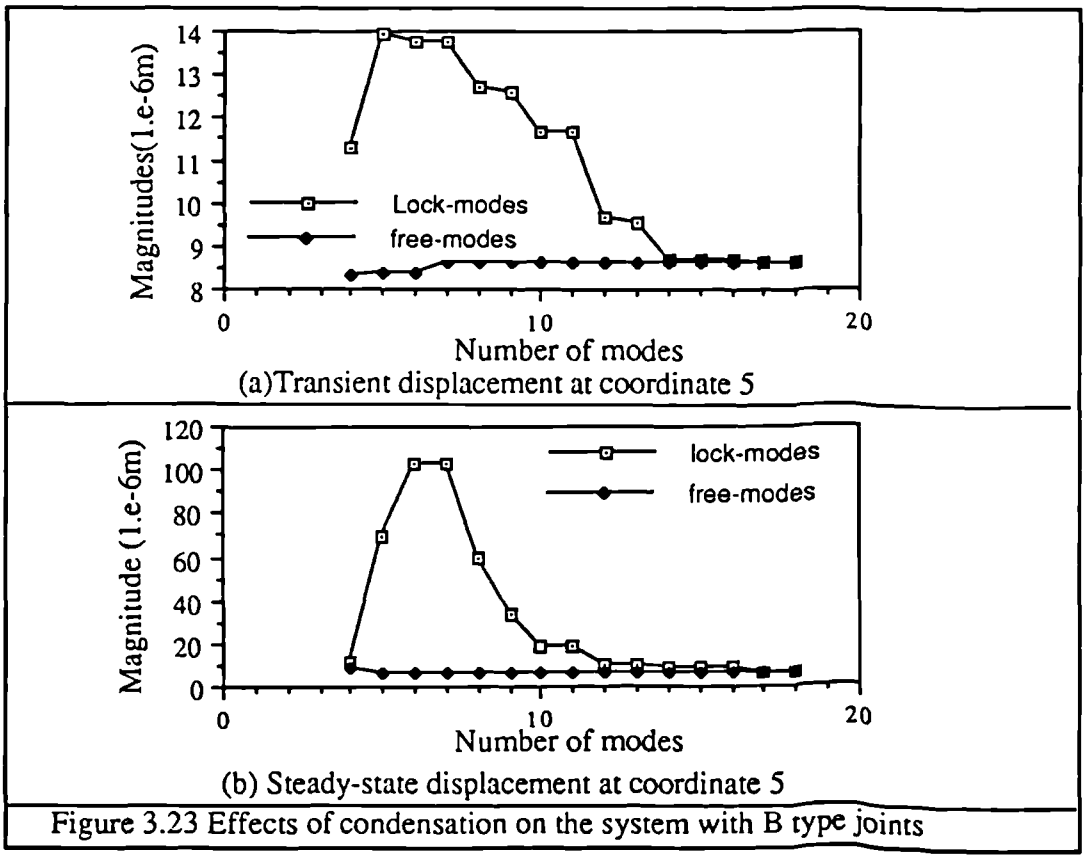

Figure 3.23 Effects of condensation on the system with B type joints

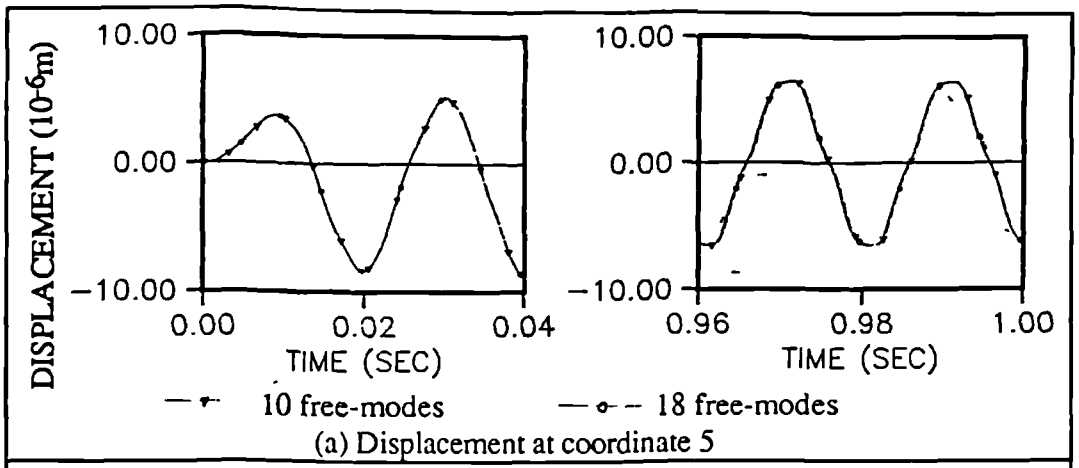

(a) Displacement at coordinate 5

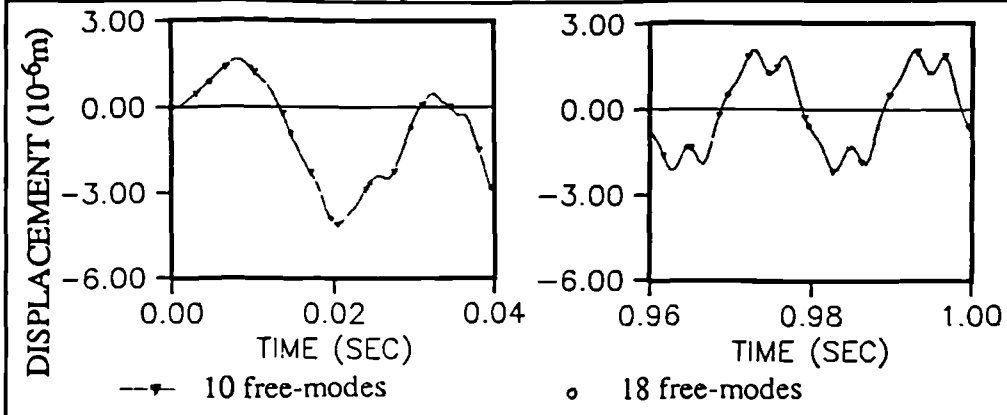

(b) Displacement at joint 2

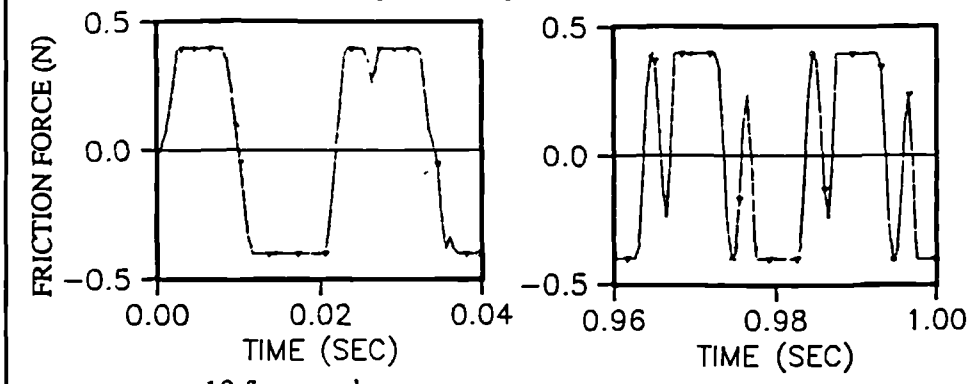

(c) Friction force at joint 2

Figure 2.24 Results of the system with B type joints in time domain using 10 and 18 free-modes

§3.7 CONCLUSIONS

The step-by-step time-domain integration methods for prediction of the response of a system containing nonlinear joints have been studied in this chapter. Two of the STI methods are investigated in detail.

Two algorithms to calculate the force of any Masing type nonlinear element from the response are proposed. Algorithm A is more comprehensive, while Algorithm B is exact and computationally more efficient. The computer codes are verified by numerical case studies.

For the two STI methods studied, Algorithm One is an indirect method and Algorithm Two is a direct method. The numerical case studies indicate that Algorithm Two is more efficient than Algorithm One. However, the results from Algorithm Two can be inaccurate, while the results from Algorithm One are usually reasonably accurate provided proper convergence criterion are used.

For Algorithm Two, in order to ensure the integration being stable, the component of the force in a joint which is treated as the external force must have a zero or negative slope. This can be achieved by adding to both sides of the equilibrium equation a pseudo stiffness matrix consisting of the initial stiffness of the joints. However, this pseudo stiffness matrix can affect the accuracy of the integration results. When the pseudo stiffness matrix is significant, the time interval Δ has to be very small to achieve sufficient accuracy.

It has also been shown that the instability of the numerical process on the system containing a friction joint can be well-bounded. The numerical results may appear to be reasonable, although they are completely different from the real response.

For both algorithms, the initial stiffness of the joint must not be too high. It has been shown that a relatively soft initial stiffness can often be used without significantly affecting the physical system. A greater time step Δ can be used to achieve the desired accuracy for this modified system.

If the initial stiffness of the joint is significant, the friction force at the joint may change violently at some periods in a cycle. These periods correspond to the stages when the joint is in the elastic region, and can be considered as 'stuck'. Therefore, a joint may subjected to many stick-slip motions in each cycle. The waveform of the response at the joint is much smoother than that of the friction force.

The system studied can often be condensed and the computation cost can be reduced. Two condensation methods have been investigated for the system containing nonlinear

joints. It is found that the mode-shapes of the system with no joint attached forms a good subspace for the vibration shape of the nonlinear structure. These mode shapes are suggested for the condensation.

CHAPTER 4

APPROXIMATE METHODS FOR THE CALCULATION OF THE STEADY-STATE RESPONSE OF A NONLINEAR STRUCTURE

§4.1 INTRODUCTION

In chapter 3, STI methods for the prediction of the response of a structure containing nonlinear friction joints have been investigated. In general, provided the time interval Δ is small enough, accurate results can be achieved. For this reason, the results obtained from these methods are often referred to as 'exact results'.

However, these STI methods have severe shortcomings; for a conditionally stable STI method, the time interval Δ has to be smaller than a certain limit to ensure the stability of the numerical process; for an unconditionally stable STI method, although the problem of numerical instability can be avoided, the time interval Δ still has to be sufficiently small in order to achieve a desired accuracy. When the steady-state response is required, the numerical integration has to be carried out over a long period, which can be very expensive. To make things worse, the computation cost increases dramatically with an increase in size of the theoretical model.

Although the use of condensation can reduce the computation expense effectively, the cost of the integration can still be high enough to prevent STI methods from being applied to a wide range of engineering structures. After all, it is normal to have over a hundred resonances lying within the frequency range of interest for a real engineering structure. Apart from the cost in integration, formulation of a mathematical model (a finite element model) can also be a significant cost.

An even more significant problem for STI methods is that a finite element model may not be as reliable as it is expected to be. A survey 'DYNAS'[92] conducted for the estimation of the reliability of the finite element method reveals the existence of a huge difference between the results from different research institutes.

On the other hand, once a structure (or its component) has been made, measurement can often be carried out and some properties (eg. FRF) of the structure can be measured directly. After years of improvement in both measurement equipment and measurement techniques, it is generally accepted that the measured data are usually more accurate than the data predicted from an analytical model.

Based on this argument, it is more appropriate to use the measured data and the properties of the friction joints to predict the response of a structure.

In this chapter, the problem of the prediction of periodic steady-state response of a structure containing nonlinear joints is investigated. The ability to solve this problem will certainly find wide applications in mechanical systems where the source of the excitation arises from rotation. The purpose of this study is to develop new methods which can solve the problem both accurately and cheaply.

§4.2 REVIEW OF APPROXIMATE METHODS

Except for the STI methods, most of the methods for prediction of the response of a structure are based upon some pre-assumptions on the response of the structure. Accordingly, they are often referred to as approximate methods. The accuracy of a specific method largely depends on the accuracy of these pre-assumptions. The most commonly used approximate methods in predicting the steady-state response of a nonlinear structure are perturbation methods (e.g. [93]) and methods based on the balance of the harmonic components.[94][95][65]

For the perturbation methods, the desired quantities are developed in powers of some small parameters, and the original nonlinear equation is turned into a series of linear equations. These methods are usually only applicable to a system with weak nonlinearity and with only a few DOFs. The applications of the perturbation methods to real engineering structures are severely limited. For this reason, no further investigation on the perturbation methods is presented in this chapter.

Approximate methods based on the balance of the harmonics can be sub-divided into three groups; the Harmonic Balance method (HB)[95], the Incremental Harmonic Balance method(IHB)[95] and the Higher order Harmonic Balance method [65](HHB). A brief review of these methods is given below.

§4.2.1 The Harmonic Balance Method

The HB method is for calculating the response of a nonlinear system subjected to a sinusoidal excitation. It is the most widely used technique in the analysis of the response of systems containing friction joints.[5-17, 52-62]

When a nonlinear system is subjected to a sinusoidal excitation, the response of the system is not exactly sinusoidal. However, in most cases, the response is usually periodic and has a period the same as the period of the excitation. The exception to this, i.e. a non-periodic response under a periodic excitation, is often referred to as chaotic vibration and is beyond the scale of this research.

When the response of a system is periodic, it can always be resolved into a Fourier series. If the Fourier series is dominated by its fundamental terms, it may be reasonable to assume that the response of the system can be represented by the fundamental terms of the Fourier series. With a periodic response, the friction force in the joint must also be periodic, and similarly to the response, the friction force can also be approximated by the fundamental terms of its Fourier series. The solution of the response should be such that all the fundamental harmonic forces are balanced by each other. To illustrate the concept of the HB method, consider a nonlinear SDOF system subjected to a sinusoidal excitation.

$$m\ddot{x}+c\dot{x}+kx+F(x,\dot{x})=P_1e^{i\omega t}, \tag{4.1}$$

Assume

$$x=a_1\cos\omega t-b_1\sin\omega t=X_1e^{i\omega t} \tag{4.2}$$

where $X_1=a_1+ib_1$

then

$$F(x,\dot{x})=F((a_1+ib_1)e^{i\omega t},i\omega(a_1+ib_1)e^{i\omega t}) \tag{4.3}$$

is a periodic function and can be resolved into a Fourier series as:

$$F(t)=\sum_{n=0}^{\infty}F_ne^{i\omega t} \tag{4.4}$$

where $F_0=\frac{A_0}{2}$, $F_n=A_n+iB_n$ $(n=1,\ldots,\infty)$

$$A_n=\frac{2}{T}\int_{-\frac{T}{2}}^{\frac{T}{2}}F(t)\cos(n\omega t)dt \tag{4.5}$$

$$B_n=-\frac{2}{T}\int_{-\frac{T}{2}}^{\frac{T}{2}}F(t)\sin(n\omega t)dt \tag{4.6}$$

$$T=\frac{2\pi}{\omega} \tag{4.7}$$

Approximating the friction force by its fundamental term (n=1) and substituting it together with the assumed response (equation(4.2)) into equation(4.1) yields:

$$-\omega^2 mX_1+i\omega cX_1+kX_1+F_1=P_1 \qquad (4.8)$$

Equation(4.8) is used to obtain X_1

Equation (4.8) can be written in a different way as

$$X_1=\frac{1}{-\omega^2 m+k+i\omega c}(P_1-F_1) \qquad (4.9)$$

It can be noted that $\frac{1}{-\omega^2 m+k+i\omega c}$ is the receptance of the linear system without joint , and it can often be measured directly by experimental means. Therefore, for the HB method, a spatial model (i.e. mass, stiffness and damping) is not necessary, only the FRF data are required.

The use of FRF data has significant advantages over the use of spatial data for the localized nonlinear problem. Not only due to its simplicity (the FRF data can be measured directly), but also because the FRF data are usually more accurate if they are measured directly from a real structure.

An even more attractive advantage of using FRF data is that only the coordinates where nonlinear elements are attached need to be considered. This reduces the size of the problem significantly. To illustrate this, consider an N-DOF system with a nonlinear joint attached to its i'th coordinate and subjected to a sinusoidal excitation at the j'th coordinate. The equilibrium equation in its receptance form with respect to coordinate x_i can be written as

$$X_1=H_{ij}(\omega)P_1-H_{ii}(\omega)F_1 \qquad (4.10)$$

Only two real unknowns (a_1,b_1) in equation (4.10) are to be found for the N-DOF system.

For a general system, the equilibrium equation with m joint coordinates and k excitation coordinates is:

$$\{X_1\}=[H_{ij}(\omega)]\{P_1\}-[H_{ii}(\omega)]\{F_1\} \qquad (4.11)$$

where $[H_{ij}(\omega)]$ is an m×k matrix and $[H_{ii}(\omega)]$ is an m×m matrix. $\{F_1\}$ is a vector containing the fundamental terms of the friction force at the joint coordinates.

This equilibrium equation can be used to find $\{X_1\}$ and $\{F_1\}$.

Once $\{F_1\}$ and $\{X_1\}$ have been found, the response at any other coordinate can be calculated from the FRF data (of the system without joints) and the excitation force $\{P_1\}$ and friction force $\{F_1\}$ without any difficulty.

The HB method is one of the most commonly used approximate methods in the analyses of nonlinear systems containing friction joints. The advantages and shortcomings are summarised as follows:

Advantages

1)Using FRF data, the size of the problem is independent of the actual size of the physical system, but only depends on the number of joint coordinates; and

2) it is capable of dealing with various types of nonlinearity.

Shortcomings

1) it is only applicable when the excitation is sinusoidal or close to sinusoidal;

2) the accuracy of the results cannot be evaluated; and

3) a set of nonlinear equations have to be solved, which can be extremely difficult. In most applications [5-17, 52-62], the assembly contains only one friction joint.

§4.2.2 Incremental Harmonic Balance Method

The Incremental Harmonic Balance method(IHB) was first proposed by Lau *et al* [95] in 1981. The method has been applied to various nonlinear systems(e.g.[96][97]). An extension on the IHB method has been made so that it can be used for a dry-friction damped system [63][64].

The basic principle of the method is as follows:

For a nonlinear system

$$[M]\{\ddot{x}\}+[C]\{\dot{x}\}+\{F(x,\dot{x})\}=\{P\} \tag{4.12}$$

If the solution for equation(4.12) under an excitation of

$$\{P(t)\}=\{\sum_{n=0}^{N} P_n e^{in\omega t}\} \tag{4.13}$$

can be approximated as:

$$\{x(t)\}=\{\sum_{n=0}^{N} X_n e^{in\omega t}\} \tag{4.14}$$

and the nonlinear force as:

$$\{F(t)\}=\{\sum_{n=0}^{N} F_n e^{in\omega t}\} \tag{4.15}$$

then the nonlinear force and the response under the excitation

$$\{P+\Delta P\}=\{\sum_{n=0}^{N} (P_n+\Delta P_n)e^{in(\omega+\Delta\omega)t}\} \tag{4.16}$$

can be presented as:

$$\{F+\Delta F\}=\{\sum_{n=0}^{N} (F_n+\Delta F_n)e^{in(\omega+\Delta\omega)t}\}, \text{ and} \tag{4.17}$$

$$\{x+\Delta x\}=\{\sum_{n=0}^{N} (X_n+\Delta X_n)e^{in(\omega+\Delta\omega)t}\} \tag{4.18}$$

Substituting equation(4.17) and (4.18) into equation(4.12), neglecting the higher order incremental terms (e.g. ΔX_n^2) and setting the coefficients of the different harmonics on the right and left hand sides of the resultant equation to be the same yields:

$$[A]\{y\}=\{R\}+[Q]\{\Delta\omega\}+[T]\{\Delta P\} \tag{4.19}$$

where

$$\{y\}=\{\text{real}\{\Delta X_1\}^T,\text{imag}\{\Delta X_1\}^T,.....,\text{real}\{\Delta X_n\}^T, \text{imag}\{\Delta X_n\}^T\}^T \tag{4.20}$$

contains the variation of the harmonic coefficients of the displacement at joint coordinates, and [A], [Q] and [T] are coefficient matrices and {R} is a coefficient vector. {Δω} and {ΔP} are the magnitude and frequency perturbations of the excitation.

Hence the solution is

$$\{y\}=[A]^{-1}(\{R\}+[Q]\{\Delta\omega\}+[T]\{\Delta P\}) \tag{4.21}$$

Since higher order incremental terms are neglected, the solution from (4.21) is usually not exact. However, an iteration procedure can be used to yield sufficiently accurate results, i.e.

$$\|\{R\}+[Q]\{\Delta\omega\}+[T]\{\Delta P\}\|<\varepsilon \tag{4.22}$$

where ε is a small positive number.

The advantages and shortcomings of the IHB method are as follows:

Advantages

1) The desired accuracy of the solution can usually be achieved by including a large number of harmonic terms.

2) Equation(4.19) is linear and can be easily solved.

3)The method is capable of handling strong nonlinearity.

4) Because the information at the neighbouring state is used, the method is very efficient for studying the variation of the response with change of excitation.

Shortcomings

1) The method is mainly for the single value type nonlinearity of which the harmonic coefficientsof the nonlinear force (i.e.ΔF_n) can be represented explicitly in terms of the polynomial of the harmonic coefficients of the response (i.e.ΔX_n). (Although the method has been extended to deal with dry friction type nonlinearity [63][64], the process becomes very complicated.)

2) Although the principle is general, each dynamic system requires its own formulation and the effort in formulation increases dramatically when the size of the system increases.

§4.2.3 Higher-order Harmonic Balance Method(HHB)

The IHB method is actually a kind of higher-order harmonic balance method. However, the HHB method presented here refers to an extension of the HB method.

One of the main advantages of the HB method is that the size of the problem dealt with is independent of the actual size of the system; the main advantage of the IHB method is that a sufficiently accurate solution can be achieved by including a large number of harmonic terms.

To retain the advantages and overcome the disadvantages of the HB and the IHB methods, the HB method has been extended. Probably the most attractive method is the Alternating Frequency/Time domain method(AFT) proposed by Cameron and Griffin[65], which can be presented as follows:

For an M-DOF system

$$[M]\{\ddot{x}\}+[C]\{\dot{x}\}+[K]\{x\}+\{F(x,\dot{x})\}=\{P\} \qquad (4.23)$$

Recall the assumption in §4.2.2

$$\{x(t)\}=\{\sum_{n=0}^{N} X_n e^{in\omega t}\} \tag{4.14}$$

and

$$\{F(x,\dot{x}_i\}=\{\sum_{n=0}^{N} F_n e^{in\omega t}\} \tag{4.15}$$

where $\{X_n\}=\{a_n+ib_n\}$ and $\{F_n\}=\{A_n+iB_n\}$ (n=1,...,N) are the harmonic coefficients of the displacement and friction force respectively.

Substituting equations(4.14) and (4.15) into equation(4.23) yields a set of equations with M×N complex unknowns (2×M×N real unknowns). The coefficients for all the harmonics must be balanced, hence the resultant equations can be resolved into 2×M×N equations, and the response ($\{a_1\},\{a_2\},..\{a_N\},\{b_1\},\{b_2\},..\{b_N\}$) can be determined uniquely.

When the nonlinearity is localized such as the case of a system containing friction joints, the FRF data can be used in the AFT method in exactly the same way as that in the HB method, thus the number of unknowns can be significantly reduced. (Surprisingly, this was not noted by Cameron and Griffin in their paper [65].) The FRF based HHB method can be expressed as follows:

Consider N frequency components, the equilibrium equation for a system with i joint coordinates and j excitation coordinates is

$$\begin{cases} \{X_1\}=[H_{ij}(\omega_1)]\{P_1\}-[H_{ii}(\omega_1)]\{F_1\} \\ \{X_2\}=[H_{ij}(\omega_2)]\{P_2\}-[H_{ii}(\omega_2)]\{F_2\} \\ \qquad\qquad \cdots\cdots \\ \qquad\qquad \cdots\cdot \\ \{X_N\}=[H_{ij}(\omega_N)]\{P_N\}-[H_{ii}(\omega_N)]\{F_N\} \end{cases} \tag{4.24}$$

where $\{X_k\}$ and $\{F_k\}$ (k=1,2,...N) are the harmonics of the Fourier series of the response and nonlinear force at frequency ω_k respectively.

It can be noted that the HB method is a special case of the HHB method with one frequency component.

The HHB method has many advantages as follows:

1) the method can be used to deal with general type of nonlinearity;

2) when sufficient harmonics are included, desired accuracy can be achieved; and

3) the method is particularly suitable for the localised nonlinear problem. By using the FRF data, the unknown numbers can be significantly reduced.

The main disadvantage of the HHB method is that the equations to be solved are nonlinear and the solution is difficult to obtain.

It is believed that the difficulty in solving the nonlinear equation is the main obstacle for the applications of the HHB. Indeed, because of the difficulty in solving the nonlinear equations, Cameron's AFT method [65] appears to be the only publication of the HHB method.

In this chapter, effort is devoted to developing a new scheme to solve equation(4.24) for the HB and HHB methods.

§4.3 THE HB METHOD FOR A SYSTEM CONTAINING ONE JOINT

The main difficulty in the application of the HB and HHB methods is that the equations to be solved are nonlinear. This problem becomes even more significant when the harmonic coefficients of the nonlinear force cannot be obtained analytically from the coefficients of the harmonics of the displacement, i.e. the coefficients of the nonlinear force is an implicit function of the coefficients of the displacement (which is the case for most of the friction joint models).

In this section, a method to find the HB solution for a system containing one nonlinear joint is proposed, the solution can be found efficiently. The general scheme for the solution will be discussed in the next few sections

For a system containing one joint, two variables have to be determined, i.e. the real and imaginary parts a_1, b_1 of X_1 from equation,

$$X_1=H_{ij}P_1-H_{ii}F_1 \qquad (4.25)$$

where F_1 is a function of a_1 and b_1. This is a two-dimensional problem (i.e. with two unknowns). However, based on a physical observation, this two-dimensional problem can be turned into a one-dimensional case and finding a solution in a single dimension is much simpler and faster than that in two dimensions.

Instead of considering the excitation being $|P_1|e^{i\omega t}$, the excitation can be considered as

$$P_1=P_r+iP_i \tag{4.26}$$

so that

$$b_1=0. \tag{4.27}$$

This does not change the properties of the system except for a shift of the signal in the time record.

Substituting equation(4.26) and equation(4.27) into equation (4.25) leads to:

$$a_1=H_{ij}P_1-H_{ii}F_1 \tag{4.28}$$

Rearranging equation(4.28) yields

$$P_1=\frac{a_1+H_{ii}F_1}{H_{ij}} \tag{4.29}$$

Now, define a function

$$f(a_1)=|P_1|-|\frac{a_1+H_{ii}F_1}{H_{ij}}| \tag{4.30}$$

The solution a_1 of equation(4.28) must be a root of $f(a_1)$

Since there is one variable a_1 in equation(4.30) the problem becomes one-dimensional.

Solving a one-dimensional problem is trivial. The algorithm such as the Newton-Raphson method can be used. However, a simpler scheme based on a physical observation may be more effective.

The observation is that a greater response a_1 almost always corresponds to a greater excitation P_1, and vice versa. Accordingly, the following searching scheme is adopted.

1) make an initial guess on $a_1^{(i)}$, i=0.

2) calculate $f(a_1^{(i)})$; if $f(a_1^{(i)})>0$, a_1 is under-estimated; if $f(a_1^{(i)})<0$ a_1 is over-estimated.

3) if $f(a_1^{(i)})\times f(a_1^{(i-1)})<0$, go to step 6)

4) i=i+1, $a_1^{(i+1)}=a_1^{(i)}+\Delta a$, where Δa is a modification on the new estimation from step 2

5) repeat step 2)-4) until 3) is satisfied.

6) The root of $f(a_1)$ must lie within the range of $[a_1^{(i-1)},a_1^{(i)}]$, a one-dimensional searching method such as Golden-Section search method is used to find the root.

Once a_1 is known, P_r and P_i can be found from equation (4.29).

If $P_r\cos(\omega t)-P_i\sin(\omega t)=|P_1|\cos(\omega t+\phi)$, then the response corresponding to the excitation $P\cos(\omega t)$ is $x=a_1\cos(\omega t-\phi)$, and the coefficient for the friction force F can be found accordingly.

A similar method can be applied to a system with a nonlinear element connecting two coordinates of the structure.

Assume the system is excited by a sinusoidal excitation at coordinate j and a nonlinear element is connected to coordinates i and k. The equilibrium equations at coordinates i and k are

$$X_1(i)=H_{ij}P_1-H_{ii}F_1-H_{ik}(-F_1) \tag{4.31}$$

$$X_1(k)=H_{kj}P_1-H_{kk}(-F_1)-H_{ki}(F_1) \tag{4.32}$$

Subtracting equation(4.31) by (4.32) yields

$$X_1(i)-X_1(k)=(H_{ij}-H_{kj})P_1-(H_{ii}-H_{ik}-H_{ki}+H_{kk})F_1 \tag{4.33}$$

Assume $X_1(i)-X_1(k)=a_1$, F_1 can be found by using the same approach discussed above, and $X_1(i)$ and $X_1(k)$ can be found from equations (4.31) and (4.32) respectively.

§4.4 INVESTIGATION ON THE HB METHOD--GENERAL SYSTEM

The HB method is a special case of the HHB method, therefore, all the algorithms applicable to the HHB method can also be applied to the HB method. However, the HB method can sometimes be solved using other special methods. A special method is discussed in the next few sections

§4.4.1 Direct Iteration Scheme for the HB method

Write the general equilibrium equation as:

$$\{X_1\}=[H_{ij}(\omega)]\{P_1\}-[H_{ii}(\omega)]\{F_1\} \tag{4.34}$$

The direct iteration method is expressed as [65].

$$\{X_1^{(n+1)}\}=[H_{ij}(\omega)]\{P_1\}-[H_{ii}(\omega)]\{F_1^{(n)}\} \tag{4.35}$$

where superscripts $^{(n)}$ and $^{(n+1)}$ denote the current and new estimations.

This algorithm is simple, and in some cases, the convergence is achieved very rapidly. However, there are even more cases that the algorithm will diverge.

§4.4.2 Convergence Analysis on Direct Iteration Method

In order to understand which factors affect the convergence of the direct iteration method, a linear system is considered. The linear force $\{F(x_i)\}$ can always be decomposed as

$$\{F_1\}=[K_1^*]\{X_1\}=([K_1]+i[D_1])\{X_1\} \tag{4.36}$$

hence equation(4.34) becomes

$$\{X_1\}=[H_{ij}(\omega)]\{P_1\}-[H_{ii}(\omega)][K_1^*]\{X_1\} \tag{4.37}$$

For simplicity, let

$[A]=[H_{ij}(\omega)]$ and $[B]=[H_{ii}(\omega)][K_1^*]$

Then iterative equation becomes

$$\{X_1^{(1)}\}=[A]\{P_1\}-[B]\{X_1^{(0)}\} \tag{4.38}$$

$$\{X_1^{(2)}\}=[A]\{P_1\}-[B]\{X_1^{(1)}\}$$

$$=([A]-[B][A])\{P_1\}+(-[B])^2\{X_1^{(0)}\} \tag{4.39}$$

This gives a recurrence relationship so that the response at end of the n'th iteration is

$$\{X_1^{(n)}\}=([A]-[B]([A]-[B]([A].....))))\{P_1\}+(-[B])^n\{X_1^{(0)}\} \tag{4.40}$$

The convergence of the direct method can now be investigated by considering the behaviour of $[B]^n$ when n becomes large. The iteration process will converge if and only if the magnitudes of elements in matrix $[B]^n$ decrease as n increases. From the stability analysis in Chapter 3. it is understood that the magnitudes of elements in the matrix $[B]^n$ are related to the magnitude of the highest eigenvalue of the matrix [B]. For the direct method to converge, the magnitude of the highest eigenvalue of the matrix $[B]=[H_{ii}(\omega)][K_1^*]$ must be smaller than 1. This usually means that magnitudes of the elements in the matrix [B] should be sufficiently small. Since the matrix $[H_{ii}(\omega)]$ is fixed, the elements in the matrix $[K_1^*]$ should be sufficiently small, i.e. the stiffness should be sufficiently low.

For a nonlinear joint, the $[K_1^*]$ matrix changes from one iteration to the other. Therefore, the above analysis does not hold directly. However, the principle of the analysis is still valid. When the estimate of the solution is sufficiently close to the true solution, the corresponding matrix $[K_1^{*(n)}]$ should also be close to the $[K_1^*]$ matrix of the exact solution.

In this case, the nonlinear system can be approximated by a linear system. If the magnitude of the highest eigenvalue of the matrix $[B^{*(n)}]=[H_{ii}(\omega)][K_1^{*(n)}]$ is smaller than

1, the iteration will converge, otherwise, even if the exact solution is used as an initial estimation, the iteration process will still diverge due to computation errors.

§4.4.3 Equivalent Stiffness and Damping

In the last section, it has been shown that the magnitudes of the elements in the matrix $[K_1^*]$ must be sufficiently small to achieve convergence for the direct iteration method. In order to enhance the convergence of the direct iteration method, the concept of equivalent stiffness and damping is introduced in this section as follows:

If the frequency component of the deformation of the nonlinear element at frequency ω is

$$x(t)=X_1\cos(\omega t) \tag{4.41}$$

then the fundamental harmonics of the nonlinear force can be written as

$$F_1=K_eX_1+iD_eX_1 \tag{4.42}$$

where

$$K_e=\frac{2}{TX_1}\int_{-\frac{T}{2}}^{\frac{T}{2}} F(t)\cos(\omega t)dt \tag{4.43}$$

$$D_e=-\frac{2}{TX_1}\int_{-\frac{T}{2}}^{\frac{T}{2}} F(t)\sin(\omega t)dt \tag{4.44}$$

$$T=\frac{2\pi}{\omega} \tag{4.45}$$

K_e and D_e in equation (4.42) are defined as the **equivalent stiffness** and **equivalent damping** respectively

For a Masing type nonlinear element, the equivalent stiffness and damping can be calculated directly from the initial loading relation (APPENDIX B)

The equivalent damping is closely related to the energy dissipation of a nonlinear element. The damping of a structure is usually defined as a mechanism of energy dissipation. For a linear hysteretic damping D, the energy dissipated each cycle is

$$E=\oint F_d\,dx$$

$$=\int_0^{2\pi} -DX_1\sin(\omega t)\,dX_1\cos(\omega t)$$

$$=\pi DX_1^2 \tag{4.46}$$

hence

$$D=\frac{E}{\pi X_1^2} \tag{4.47}$$

In many engineering applications, the energy dissipated by the friction force is often approximated by a linear hysteretic damper which satisfies equation(4.47).

From equation(4.44), the equivalent damping is

$$D_e=\frac{1}{\pi X_1^2}\int_{-\frac{T}{2}}^{\frac{T}{2}} F(X_1\cos(\omega t))\, dX_1\cos(\omega t) \tag{4.48}$$

The integral of the equation(4.48) is the energy dissipated in one cycle, hence

$$D_e=\frac{E}{\pi X_1^2} \tag{4.49}$$

Comparing equations(4.47) and (4.49), it is noted that if the response is sinusoidal, the energy dissipated by the nonlinear element is the same as the energy dissipated by a linear hysteretic damper with the coefficient of the equivalent damping.

§4.4.4 Improved Direct Iteration Method-New Development

Recall equation(4.37) in §4.4.2

$$\{X_1\}=[H_{ij}(\omega)]\{P_1\}-[H_{ii}(\omega)][K_1^*]\{X_1\} \tag{4.37}$$

Equation (4.37) can be rearranged as

$$\{X_1\}=([I]+[H_{ii}(\omega)][K_1^*])^{-1}[H_{ij}(\omega)]\{P_1\} \tag{4.50}$$

Equation (4.50) is a direct scheme and no iteration is required.

Similar extension can be made for a nonlinear system using the concept of equivalent stiffness and damping to yield a new iterative scheme:

$$\{X_1^{(n+1)}\}=([I]+[H_{ii}(\omega)][K_1^{*(n)}])^{-1}[H_{ij}(\omega)]\{P_1\} \tag{4.51}$$

where $[K_1^{*(n)}]=[K_e^{(n)}]+i[D_e^{(n)}]$ is the complex equivalent stiffness matrix at $\{X_1^{(n)}\}$.

Direct use of equation(4.51) may diverge too. Therefore, a monitoring algorithm is used as follows:

$$\text{Define } f(X_1^{(n+1)})=\|\{X_1^{(n+1)}\}-([I]+[H_{ii}(\omega)][K_1^{*(n)}])^{-1}[H_{ij}(\omega)]\{P_1\}\| \tag{4.52}$$

If $f(X_1^{(n+1)})<f(X_1^{(n)})$, the iteration is converging, hence set $X_1^{(n)}=X_1^{(n+1)}$, and a new iteration is carried out; if $f(X_1^{(n+1)})>f(X_1^{(n)})$, the iteration process of equation(4.51) diverges. In this case, a searching direction is calculated as:

$$\{\Delta X\}=\{X_1^{(n+1)}\}-\{X_1^{(n)}\} \tag{4.53}$$

A one-dimensional searching process is carried out to find a minimum of f(X) in the direction $\{\Delta X\}$ from $\{X_1^{(n)}\}$. i.e. to find a parameter α so that

$$f(X_1^{(n)}+\alpha\Delta X)<f(X_1^{(n)}+\beta\Delta X).$$

for any parameter $\beta\neq\alpha$

The iterative process is repeated using the new estimation $X_1^{(n)}+\alpha\Delta X$.

The solution is found if

$$\|f(X_1^{(n)})\|<\varepsilon\|X_1^{(n)}\| \tag{4.54}$$

where ε is a small positive number.

§4.5 EXTENSION OF THE DIRECT ITERATION APPROACH TO THE HHB METHODS

The principle of the algorithm discussed for the HB method can also be used for the HHB method. However, some modifications have to be made.

In §4.4.3 , the concept of equivalent stiffness and damping is introduced. It is natural to extend this concept directly in the HHB method. Unfortunately, this is not appropriate, because the frequency component of the friction force is not caused exclusively by the corresponding frequency component of the displacement. To illustrate this, consider a nonlinear element with a pure sinusoidal deformation $X_1\cos(\omega t)$. The n'th ($n\neq1$) frequency component of the force is

$$F_n=A_n\cos(n\omega t)-B_n\sin(n\omega t) \tag{4.55}$$

Since the corresponding frequency component of the displacement is zero, an infinite equivalent stiffness (and also the equivalent damping) is obtained. This is clearly not appropriate.

The concept of the equivalent stiffness and damping is based on the definition

$$K^*=\frac{F}{x} \tag{4.56}$$

A more appropriate definition for the equivalent stiffness and damping is to use the derivatives, i.e.

$$K^*=\frac{dF}{dx} \tag{4.57}$$

For a linear system, equation(4.56) and equation(4.57) are exactly the same. However, for a nonlinear system, equation (4.56) represents the global property of the stiffness, while equation(4.57) represents the local property of the stiffness. In this chapter, the **local equivalent stiffness** and damping are defined as follows:

If the n'th harmonic displacement component is $X_n=a_n$ and its corresponding harmonics of the force is $F_n=A_n+iB_n$, the n'th local equivalent stiffness and damping are

$$K_n=\frac{\partial A_n}{\partial a_n} \text{ and } D_n=\frac{\partial B_n}{\partial a_n} \tag{4.58}$$

The complex local equivalent stiffness is

$$K_n^*=K_n+iD_n \tag{4.59}$$

The local equivalent stiffness and damping can be used for both the HB and the HHB methods in a similar way to the equivalent stiffness and damping for the HB method. The iterative formula is

$$\{X_k^{(n+1)}\}=([I]+[H_{ii}(\omega_k)][K_k^{*(n)}])^{-1}([H_{ij}(\omega_k)]\{P_k\}-[H_{ii}(\omega_k)](\{F_k^{(n)}\}-[K_k^{*(n)}]\{X_k^{(n)}\})) \tag{4.60}$$

§4.6 NEWTON-RAPHSON METHOD

Experience shows that for the HB method, equivalent stiffness and damping (or local stiffness and damping) scheme (ESD) usually leads to convergence. However, for the HHB method, convergence is more difficult to achieve. In some cases, the local stiffness and damping scheme(LESD) may fail to achieve convergence.

Use of local equivalent stiffness and damping is equivalent to assuming that the change of the harmonics of the nonlinear force is caused by the change of the corresponding harmonics of the deformation of the nonlinear element. In most cases, this is not true. In some cases, if the change of harmonics of the nonlinear force is caused mainly by the change of other harmonic components of the displacement, then the LESD scheme is likely to fail. In order to include the effects of other harmonics of the displacement on that of the nonlinear force, the Newton-Raphson method is suggested.

Define a set of nonlinear equations as:

$$\begin{cases} \{g_1(y)\}=\text{Real}(\{X_1\}-[H_{ij}(\omega_1)]\{P_1\}-[H_{ii}(\omega_1)]\{F_1\}) \\ \{g_2(y)\}=\text{Imag}(\{X_1\}-[H_{ij}(\omega_1)]\{P_1\}-[H_{ii}(\omega_1)]\{F_1\}) \\ \qquad\qquad \cdots\cdots \\ \{g_{2n-1}(y)\}=\text{Real}(\{X_n\}-[H_{ij}(\omega_n)]\{P_n\}-[H_{ii}(\omega_n)]\{F_n\}) \\ \{g_{2n}(y)\}=\text{Imag}(\{X_n\}-[H_{ij}(\omega_n)]\{P_n\}-[H_{ii}(\omega_n)]\{F_n\}) \end{cases} \tag{4.61}$$

where

$$\{y\}=\{\text{Real}(\{X_1\})^T, \text{Imag}(\{X_1\})^T,\cdots\cdots \text{Real}(\{X_n\})^T, \text{Imag}(\{X_n\})^T\}^T \tag{4.62}$$

is the solution for the HHB approach.

and write

$$\{g\}=\{\{g_1\}^T,\ldots\ldots,\{g_{2n}\}^T\}^T \tag{4.63}$$

The solution $\{y\}$ for the HHB method must be such that

$$\{g(y)\}=\{0\} \tag{4.64}$$

The iterative equation using the Newton-Raphson method is

$$\{y^{(i+1)}\}=\{y^{(i)}\}-[J]^{-1}\{g(y^{(i)})\} \tag{4.65}$$

where $[J]=\dfrac{\partial\{g(y^{(i)})\}}{\partial\{y^{(i)}\}}$ is the Jacobian

As discussed in Chapter 2, the analytical partial derivatives in the Jacobian are not available, hence the finite difference has to be used in place of partial derivatives in the Jacobian.

The Newton-Raphson algorithm is a linear approximation, therefore, it may diverge as well as converge depending on both the accuracy of the estimation and properties of the nonlinear equations. If divergence occurs, i.e. $\|g(\{y^{(i+1)}\})\|>\|g(\{y^{(i)}\})\|$, one-dimensional function minimisation technique is used to determine the value of γ in equation(4.66):

$$\{y_m^{(i+1)}\}=\{y^{(i)}\}-\gamma[J(y^{(i)})]^{-1}\{g(y^{(i)})\} \tag{4.66}$$

so that $\|g(\{y_m^{(i+1)}\})\|$ is a minimum in the direction $\{\Delta y_i\}= -[J(y^{(i)})]^{-1}\{g(y^{(i)})\}$ from $\{y^{(i)}\}$.

$\{y_m^{(i+1)}\}$ is then used as a new estimation for the next iteration.

Most of the computation time is spent on calculation of the Jacobian. In order to save computation cost, the Jacobian is only updated when

$$\|g(\{y^{(i+1)}\})\| > 0.9\|g(\{y^{(i)}\})\|. \qquad (4.67)$$

§4.7 PERTURBATION APPROACH

§4.7.1 Basic Strategy

In solving a set of nonlinear equations using an iterative method, the initial estimation of the solution must be of sufficient accuracy. Cameron *et al* [65] suggested that when the Newton-Raphson method fails, more robust algorithms should be used. However, this does not solve the problem completely; even the most robust algorithm may still fail to converge to the solution if the initial estimation is too far away from the solution.

The key to the wide application of the HB and HHB methods is believed to be the determination of a good initial estimation for the iteration process.

Unfortunately, in many applications, little knowledge is known about the solution.

In Chapter 2, it is shown that the deformation of a system should be calculated in a step-by-step way; for the IHB method, incremental parameters are used to calculate the response at a neighbouring state. This incremental (or perturbation) approach can be utilised to obtain an accurate initial estimate for the HB or HHB method.

For a linear system, solution can be found by using equation(4.50), i.e. the solution for a linear system is always available.

If the system is subjected to a small perturbation, providing the solution changes continuously with the perturbation, the solution of the new system is usually very close to the solution of the original system. Therefore, if the solution of the original system is used as the initial estimate for the solution of the new system, the solution of the new system can usually be found provided the perturbation is sufficiently small. Since the solution for any linear system is known, a step-by-step perturbation approach can be used to convert a linear system to the nonlinear system as follows:

Two parameters α_p and α_j are introduced to implement the perturbation.

$$\text{Define } \{P'\}=\{\alpha_p P\} \qquad (4.68)$$

$$\text{and} \quad \{F'\}=\{\alpha_j F\} \qquad (4.69)$$

$\{P'\}$ and $\{F'\}$ are used in place of $\{P\}$ and $\{F\}$ during the iteration process.

It can be noted that if α_j=0, the nonlinear force has no effect on the system, hence the system is linear and a solution can be found; if α_p is sufficiently small so that the response of the system is small, the dynamic characteristics of the most nonlinear joints are effectively linear, hence the whole system is substantially linear, then it is possible to find a solution corresponding to a small α_p. The α_p and α_j are called the **excitation increment** and **joint increment** respectively. The perturbations using excitation increment and joint excitation increment are called excitation incremental perturbation and joint incremental perturbation respectively.

After a solution for a linear (α_j=0 and α_p=1) or a quasi-linear(α_j=1 and α_p is small) system is found, a perturbation of $\alpha_j=\alpha_j+\Delta\alpha_j$ and/or $\alpha_p=\alpha_p+\Delta\alpha_p$ is made to yield a new system, using the iteration scheme discussed in the foregoing sections, the solution corresponding to the newly perturbed system can be found. The process of perturbation and iteration is repeated until $\alpha_j=\alpha_p$=1 is reached, then the solution for the nonlinear system is found.

A system containing friction joints is close to a linear system under the following two cases:

1) the excitation is very small, or

2) the excitation is very large

In the first case, the excitation incremental perturbation is more effective, and in the second one, the joint incremental perturbation is more efficient. Depending on the excitation level, appropriate incremental approach should be used.

§4.7.2 Initial Estimation for the Newly Perturbed System

In the last section, the latest solution is used as the initial estimation for the newly perturbed system, i.e.

$$\{^{(n+1)}y^{(1)}\}=\{^{(n)}y\} \tag{4.70}$$

where the left-superscripts $^{(n+1)}$, $^{(n)}$ represent the number of perturbations

This estimation on the newly perturbed system is referred to as the direct estimation.

For most of the systems, the change of solution due to the change of the perturbation is continuous. When perturbations have been applied several times, the variation of the solution with the change of the excitation or joint increment contains useful information for the solution of the new system, and they can often be used to find a more accurate solution. In the following part of this section, linear and quadratic estimations are proposed.

A linear approximation for the solution is proposed as follows:

let $\alpha=\alpha_j+\alpha_p$ (4.71)

If the solution with α_{n-1} is $\{^{(n-1)}y\}$ and the solution with α_n is $\{^{(n)}y\}$, then the linear prediction for the system with α_{n+1} is

$$\{^{(n+1)}y^{(1)}\}=\{^{(n)}y\}+\frac{\alpha_{n+1}-\alpha_n}{\alpha_n-\alpha_{n-1}}(\{^{(n)}y\}-\{^{(n-1)}y\}) \quad (4.72)$$

The quadratic approximation is as follows:

If the latest three solutions corresponding to α_{n-2}, α_{n-1} and α_n are $\{^{(n-2)}y\}$, $\{^{(n-1)}y\}$ and $\{^{(n)}y\}$, then for any element y(k), (k=1, ...,2n) in {y}, a set of parameters A(k),B(k) and C(k) for a second order polynomial can be defined uniquely so that

$$^{(n-2)}y(k)=A(k)\alpha_{n-2}^2+B(k)\alpha_{n-2}+C(k) \quad (4.73a)$$

$$^{(n-1)}y(k)=A(k)\alpha_{n-1}^2+B(k)\alpha_{n-1}+C(k) \quad (4.73b)$$

$$^{(n)}y(k)=A(k)\alpha_n^2+B(k)\alpha_n+C(k) \quad (4.73c)$$

Then the new estimate from the quadratic approximation is

$$^{(n+1)}y(k)^{(1)}=A(k)\alpha_{n+1}^2+B(k)\alpha_{n+1}+C(k) \quad (4.74)$$

Figure 4.1 shows the predictions from equations (4.70),(4.72) and (4.74) schematically for a one-dimensional case.

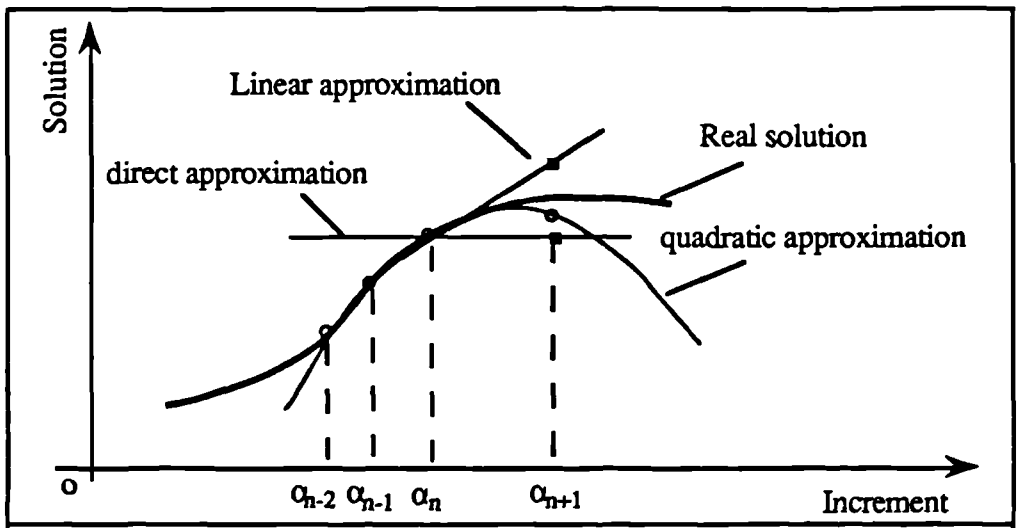

Figure 4.1 A schematic diagram for the initial estimation

In most cases, the quadratic approximation yields the best approximation and the linear approximation the second best. However, there can be some exceptions. In the computer

code, all three approximations are calculated and these estimations are used to calculate the value of the objective function $\|g(\{y\})\|$. The approximation which yields a minimum value of the objective function is used as the initial estimate for the newly perturbed system.

Higher order approximation (e.g. cubic approximation) may also be used with exactly the same principle as the quadratic approximation. However, experience indicates that the estimate to the newly perturbed system using a higher order approximation is usually not more accurate than using the quadratic approximation. Indeed, because a higher order approximation tends to be dominated by information several steps away from the current perturbed system, the accuracy of the higher order approximation is usually lower than the quadratic approximation.

Experience appears to indicate that much greater joint or excitation increment can be used if linear and quadratic approximations are employed.

§4.7.3 Other Perturbation Approaches

The response of a system subjected to a periodic force is often dominated by only a few frequency components, and sometimes by only one frequency component (i.e. the fundamental harmonic). Therefore, the responses of these frequency components are a good approximation to the real response which contains more frequency components.

An order-by-order perturbation approach can be used to improve the accuracy of the solution by including more frequency components as follows:

First, some of the most important frequency components are taken, and the solution from these frequency components is used to find the solution with an inclusion of an additional frequency component (an additional order). When the convergence is achieved, the latest solution is used as the initial estimate for the solution with another frequency component included. The process can be repeated until sufficient accuracy is achieved.

Using the order-by-order approach, the initial solution may contain only a few (sometimes only one) frequency components, thus, the computation cost can be saved during the incremental perturbation process. However, it should be emphasised that the most important frequency components must be included first, otherwise the order-by-order approach may converge to a local minimum.

Usually, the importance of frequency components decreases with the order in the Fourier series. The importance of the frequency can also be estimated using the following method:

If the Fourier Series of the force corresponding to the current estimate of the response is

$$\{F(t)\}=\frac{\{A_0\}}{2}+\sum_{n=1}^{\infty}\{A_n\}\cos(n\omega t)-\{B_n\}\sin(n\omega t) \qquad (4.75)$$

The n'th response caused by the corresponding nonlinear and excitation harmonic forces is

$$\{X_n\}=[H_{ij}(n\omega)]\{P_n\}-[H_{ii}(n\omega)]\{F_n\} \qquad (4.76)$$

The importance of the frequency can be estimated according to the Euclidean norm of the response, i.e. if $\|\{X_{n1}\}\|>\|\{X_{n2}\}\|$, the frequency component of $n_1\omega$ is more important than the frequency component of $n_2\omega$, and it should be included first.

Except for the order-by-order approach, the perturbation principle can also be applied to investigate the effects of the variation of a parameter (e.g. excitation frequency, a joint model parameter) on the overall behaviour of the structure.

§4.8 Consideration on Computation Efficiency

§4.8.1 Calculation of the Coefficients of Fourier Series

For both the HB method and the HHB method, most of the computation cost arises from obtaining the coefficients of the harmonics of the nonlinear force from the harmonics of the response. This is to integrate equations(4.5) and (4.6). In most cases, the analytical solution of equations(4.5) and (4.6) is not available, hence a numerical integration scheme has to be used.

To implement the numerical integration, equations(4.5) and (4.6) are approximated by a summation as

$$F_k=\frac{2}{N_0}\sum_{j=0}^{N_0-1}F(j)\ \mathrm{EXP}(-i\ \frac{2\pi jk}{N_0}) \qquad (4.77)$$

or

$$A_k = \frac{2}{N_0} \sum_{j=0}^{N_0-1} F(j) \cos\left(\frac{2\pi jk}{N_0}\right) \qquad (4.78a)$$

$$B_k = -\frac{2}{N_0} \sum_{j=0}^{N_0-1} F(j) \sin\left(\frac{2\pi jk}{N_0}\right) \qquad (4.78b)$$

Because discrete series of F(j) is used in equations(4.77) and (4.78), equations (4.77) and (4.78) are often referred to as the Discrete Fourier Transform(DFT). If all the coefficients in equations(4.77) and (4.78) are required, $2N^2$ multiplications are required. This can be very expensive if N is very large.

Fortunately, a remarkably efficient algorithm was developed in 1942 and has found wide applications since 1960 [98]. The algorithm reduced the number of multiplications required for the DFT from $2N^2$ to $2N\log_2 N$. This algorithm is, of course, the Fast Fourier Transform (FFT).

For the HHB method, only a few frequency components (say m) are required. Therefore, one only needs to calculate m harmonics. In this case, the direct solution from equation (4.77) requires 2Nm multiplications; if FFT is used, $2N\log_2 N$ multiplication is required. If DFT only needs to be calculated once, then even if $2Nm<2N\log_2 N$, the computation cost of the direct solution can still be higher than FFT, because more values of the exponential function are calculated for the direct solution, however, if DFT needs to be calculated many times (which is the case for the HHB method), the values of $EXP(-i\frac{2\pi jk}{N_0})$ only need to be calculated once and stored in the computer memory, these stored values can be used in the subsequent calculation of the DFT. Therefore, the computation cost is mainly spent on the multiplication operations. In this case, if $2Nm<2N\log_2 N$, the direct solution for the DFT is computationally more efficient.

Another technique to improve the computation efficiency is to use a relatively small value of N_0 during the incremental perturbation process. When α_p and α_j reach unity, N_0 is doubled and a new solution is calculated. When the new solution is found, N_0 is doubled again and the process repeated until N_0 reaches a pre-set value.

§4.8.2 Switch Principle in the Computer Code

In the foregoing sections, the ESD scheme, the LESD scheme and the Newton-Raphson method have been proposed.

The ESD scheme is much cheaper to implement than the other two methods, the LESD scheme requires about half of the computation of the Newton-Raphson method. However, the Newton-Raphson method converges at the time that the ESD or LESD scheme fails and usually it needs less iterations to converge when all the methods converge. In order to use these methods effectively, the following switch principle is adopted.

First, the ESD method (for HB) or LESD method (for HHB) is used in the incremental perturbation process and if $\|g(\{y^{(i+1)}\})\|<\varepsilon\|g(\{y^{(i)}\})\|$, the iteration process is repeated. (where ε is a positive number to evaluate the efficiency of the iteration, for the HB method $\varepsilon=0.9$, and for the HHB method, $\varepsilon=0.5$). Experience shows that once the ESD or the LESD method fails to converge or converges very slowly, it is likely to be unsuccessful in the following incremental perturbation. Accordingly, if $\|g(\{y^{(i+1)}\})\|>\varepsilon\|g(\{y^{(i)}\})\|$, the Newton-Raphson method is used for the remaining process.

§4.9 NUMERICAL CASE STUDIES

The system for investigation of the HB and HHB methods are exactly the same as the system in chapter 3 for the study of the STI methods (see figure 3.4). Unless specified, the excitation force is $P=\sin(100\pi t)$, applied at coordinate 5.

§4.9.1 Results

In the following sections, most of the numerical results obtained from the HB and HHB methods are presented in time-domain in **dashed lines**. The 'exact' results (obtained by using the STI method with sufficiently small time interval Δ) are also presented (**in solid lines**) for comparison. The response at coordinate 5, the relative displacement at joint 2 and the friction force at joint 2 are presented. The friction force is calculated from the relative displacement at joint 2 and contains much higher frequency components than the response.

§4.9.1.1 Results Using the Harmonic Balance Method

Figures 4.2-4.4 show the results of systems containing B, C and E type joints (see table 3.1). It is noted that all the results have reasonable accuracy. The calculated magnitude of the response at coordinate 5 may contain 10-20% error. Because only the fundamental harmonic term is considered, the distortion of the waveform of the response (particularly at joint 2) cannot be accurately presented.

The above results indicate that the HB method may be useful for qualitative study and quantitative study with low accuracy demand. However, the HB method is not appropriate for the investigation with high accuracy demand.

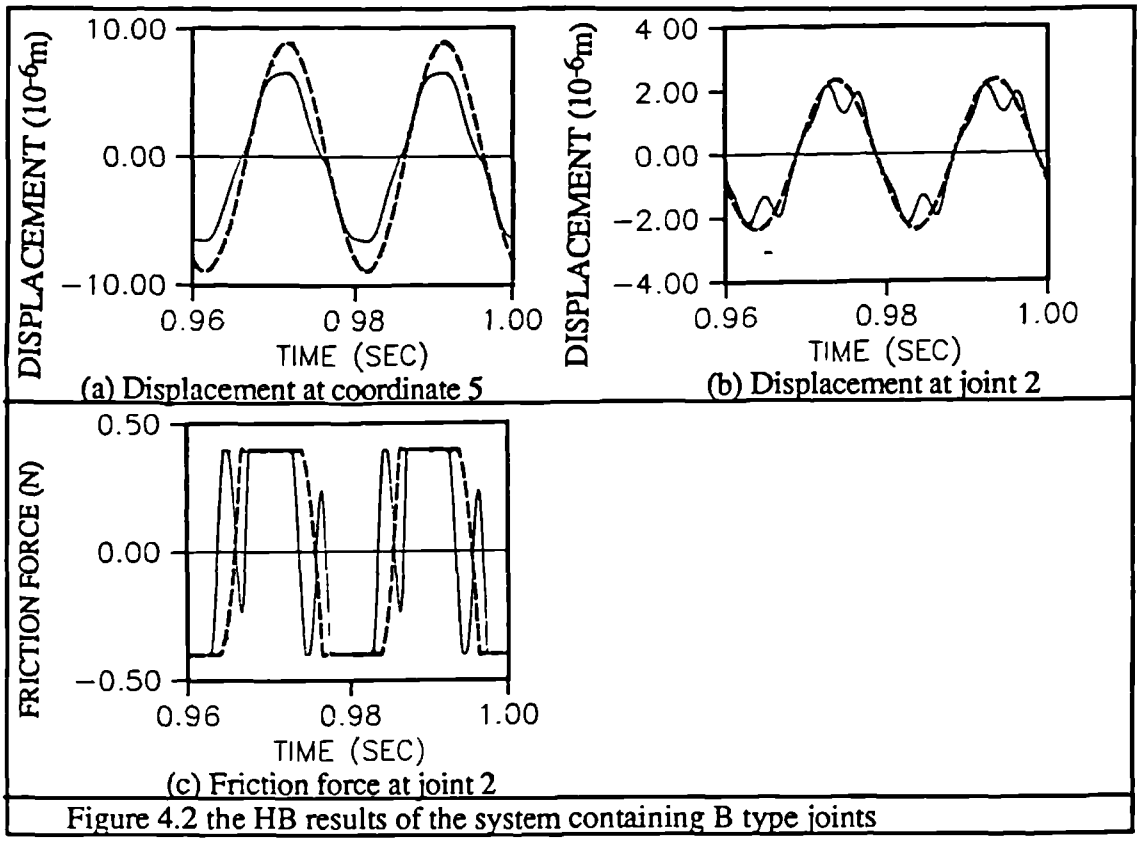

(a) Displacement at coordinate 5 (b) Displacement at joint 2

(c) Friction force at joint 2

Figure 4.2 the HB results of the system containing B type joints

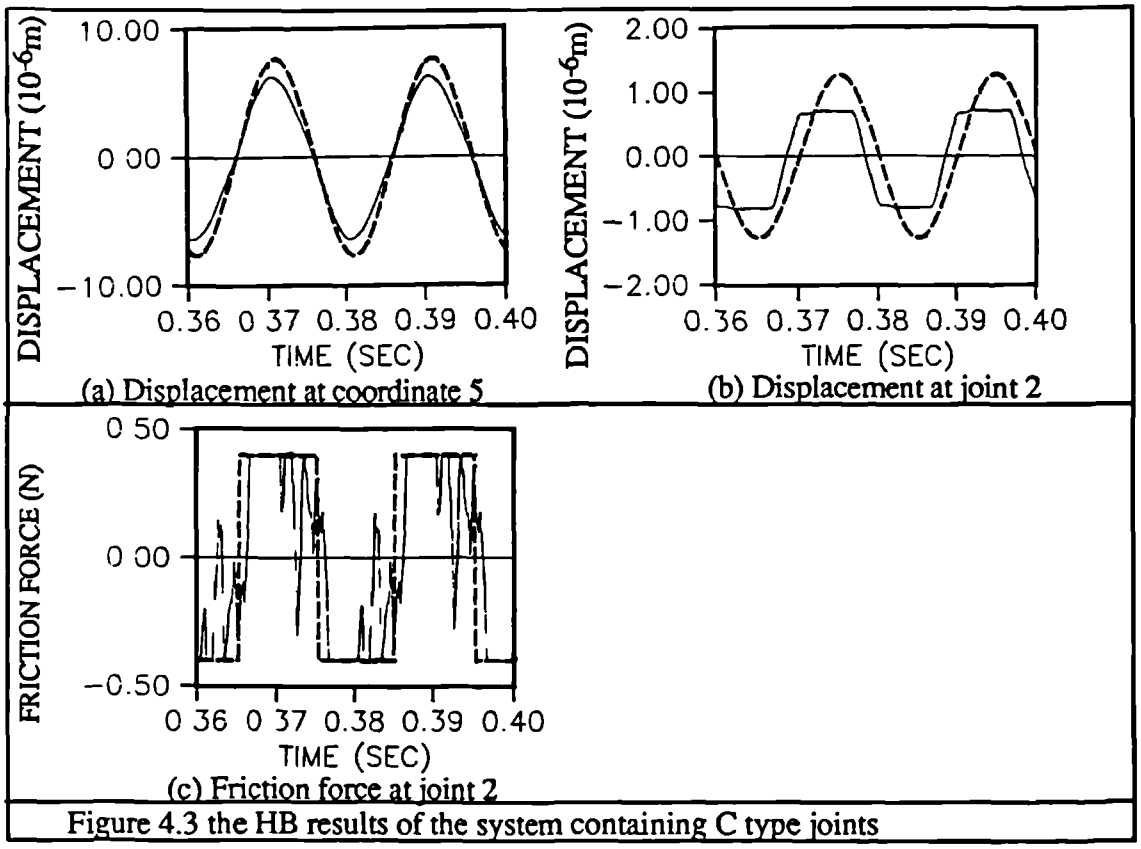

(a) Displacement at coordinate 5 (b) Displacement at joint 2

(c) Friction force at joint 2

Figure 4.3 the HB results of the system containing C type joints

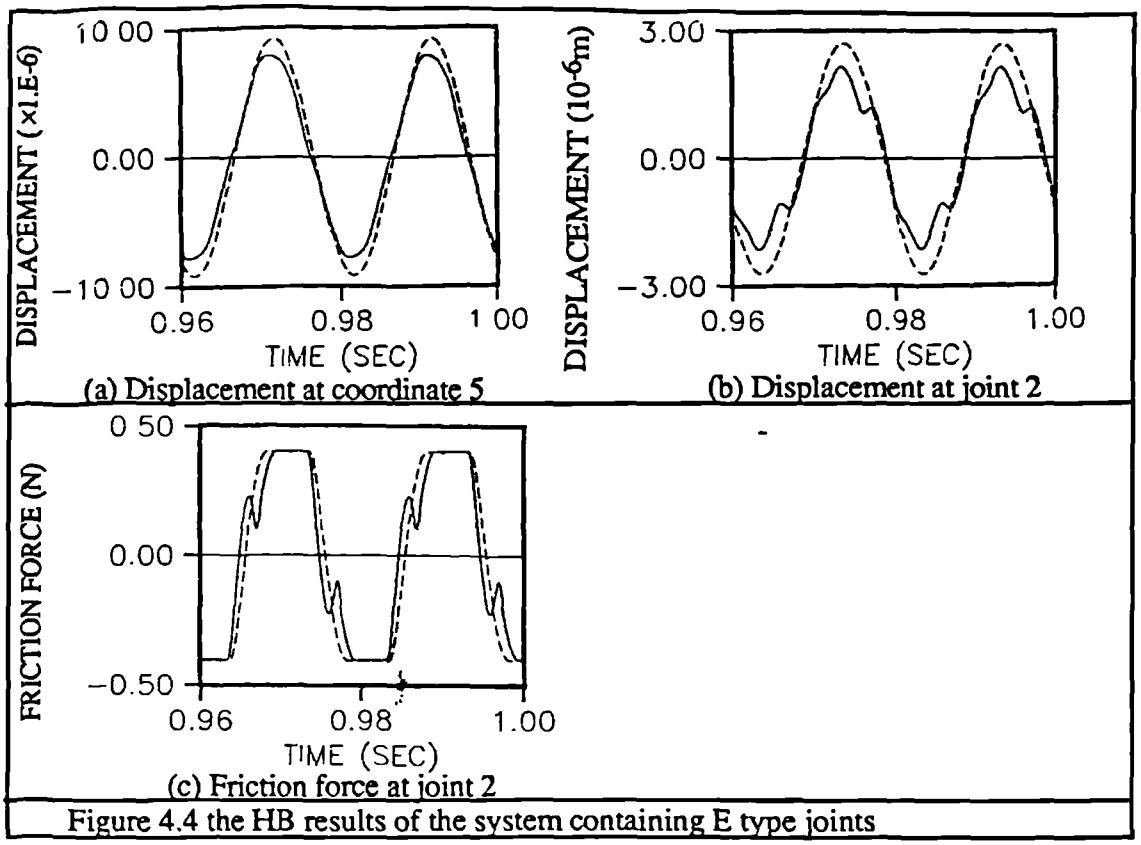

(a) Displacement at coordinate 5

(b) Displacement at joint 2

(c) Friction force at joint 2

Figure 4.4 the HB results of the system containing E type joints

§4.9.1.2 Results Using the HHB Method

Figures 4.5-4.8 show the results obtained by using the HHB method.

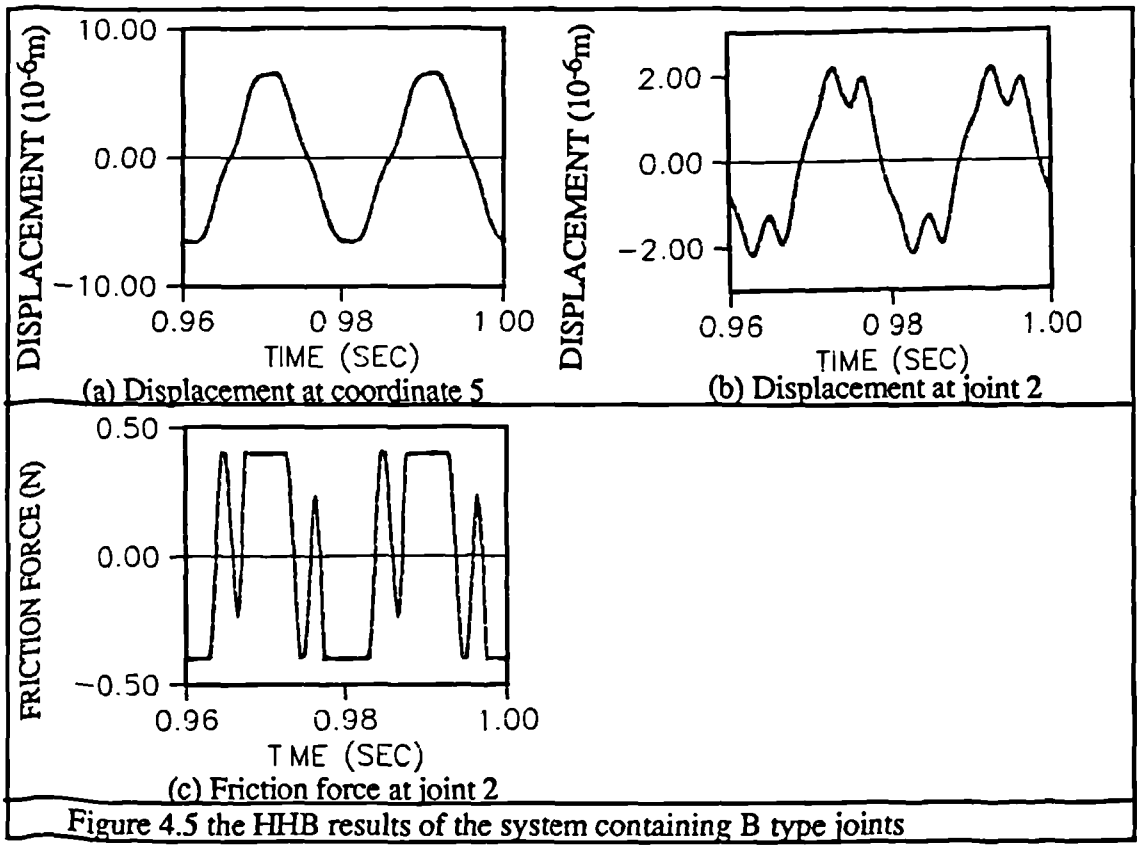

(a) Displacement at coordinate 5

(b) Displacement at joint 2

(c) Friction force at joint 2

Figure 4.5 the HHB results of the system containing B type joints

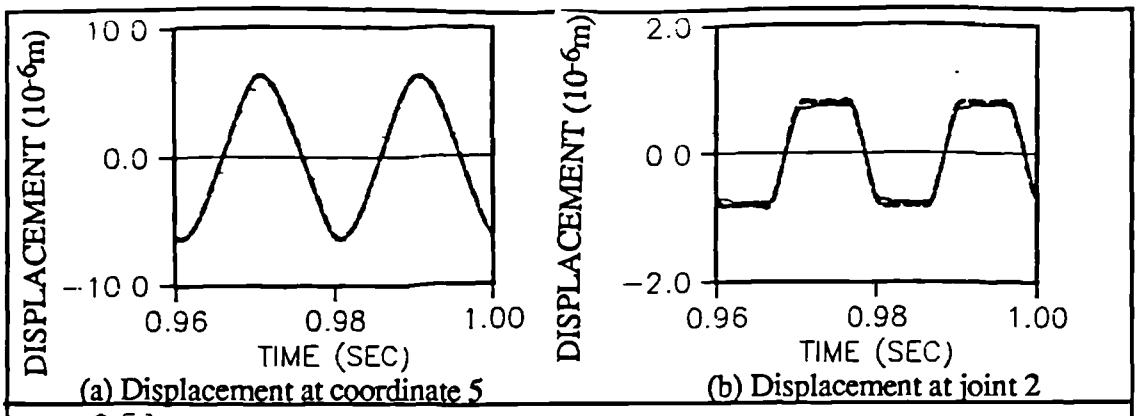

(a) Displacement at coordinate 5 (b) Displacement at joint 2

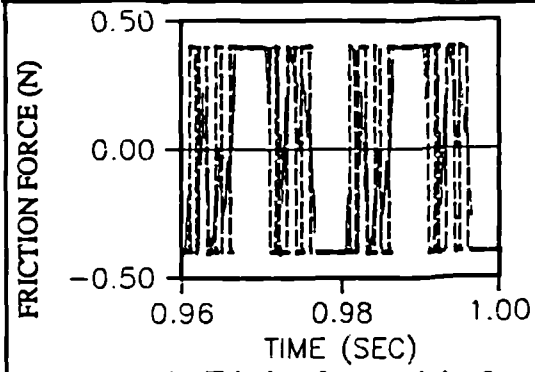

(c) Friction force at joint 2

Figure 4.6 the HHB results of the system containing C type joints

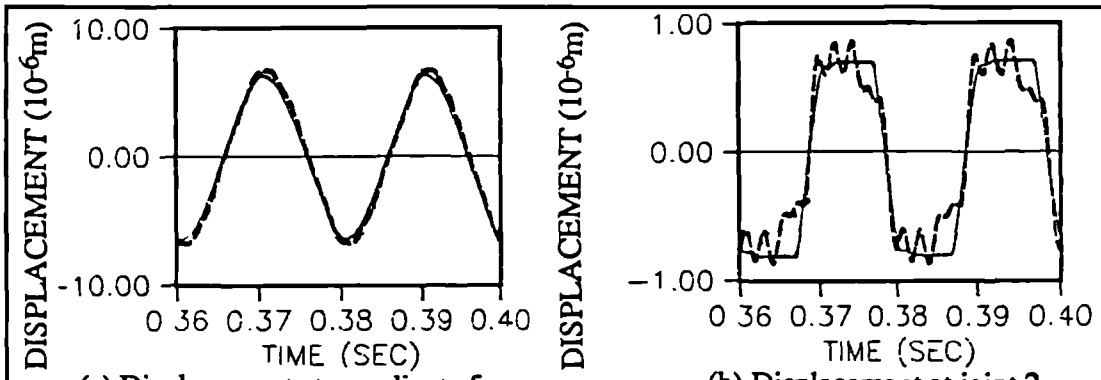

(a) Displacement at coordinate 5 (b) Displacement at joint 2

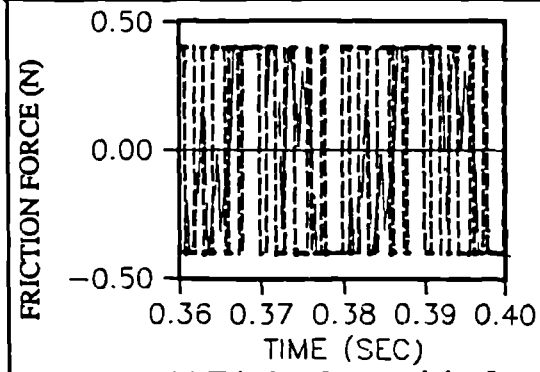

(c) Friction force at joint 2

Figure 4.7 the HHB results of the system containing D type joints

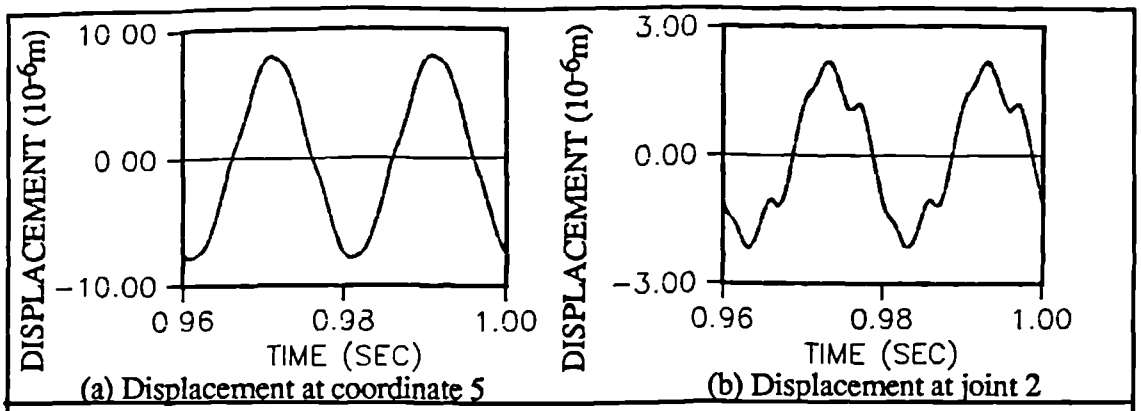

(a) Displacement at coordinate 5

(b) Displacement at joint 2

(c) Friction force at joint 2

Figure 4.8 the HHB results of the system containing C type joints

Because the excitation only contains odd order harmonics and the friction force is an odd function of the displacement, the even order harmonic components of the response must be zero and can be ignored. Five odd order harmonics (N=1,3,5,7,9) are considered for the HHB method and 512 points are used in DFT.

It can be noted that the results from the HHB method are much more accurate than those from the HB method. For the systems with B and E type joints, the results from the HHB method and from the STI method (i.e. the accurate results) are hardly distinguishable. For the systems with C and D type joints, the accuracy is slightly poorer, but the accuracy of the magnitude of the predicted response at coordinate 5 using the HHB method is still over 95%, although the difference between the friction force from the STI method and the HHB method is significant.

The slightly poorer accuracy of the results is believed to be caused by stick-slip motion at the joints. As can be noted from figure 4.6b-c and figure 4.7b-c that due to high initial stiffness of the joint, a small error in response (which may be a result of neglecting the harmonic components with N>9) causes a significant change in the friction force. Accordingly, the accuracy of the results is reduced. However, an accuracy of 95% is often well-within the demand for general engineering applications.

If a system is in a state without (significant) stick-slip motion, higher accuracy can be achieved for the results from the HHB method even if the initial stiffness of the joint is significant. Figure 4.9 shows that the results for the system with D type joints, the excitation force is p=100 sin(100πt). Under such a high level of excitation, stick-slip motion can not occur. It can be noted that very accurate results are obtained.

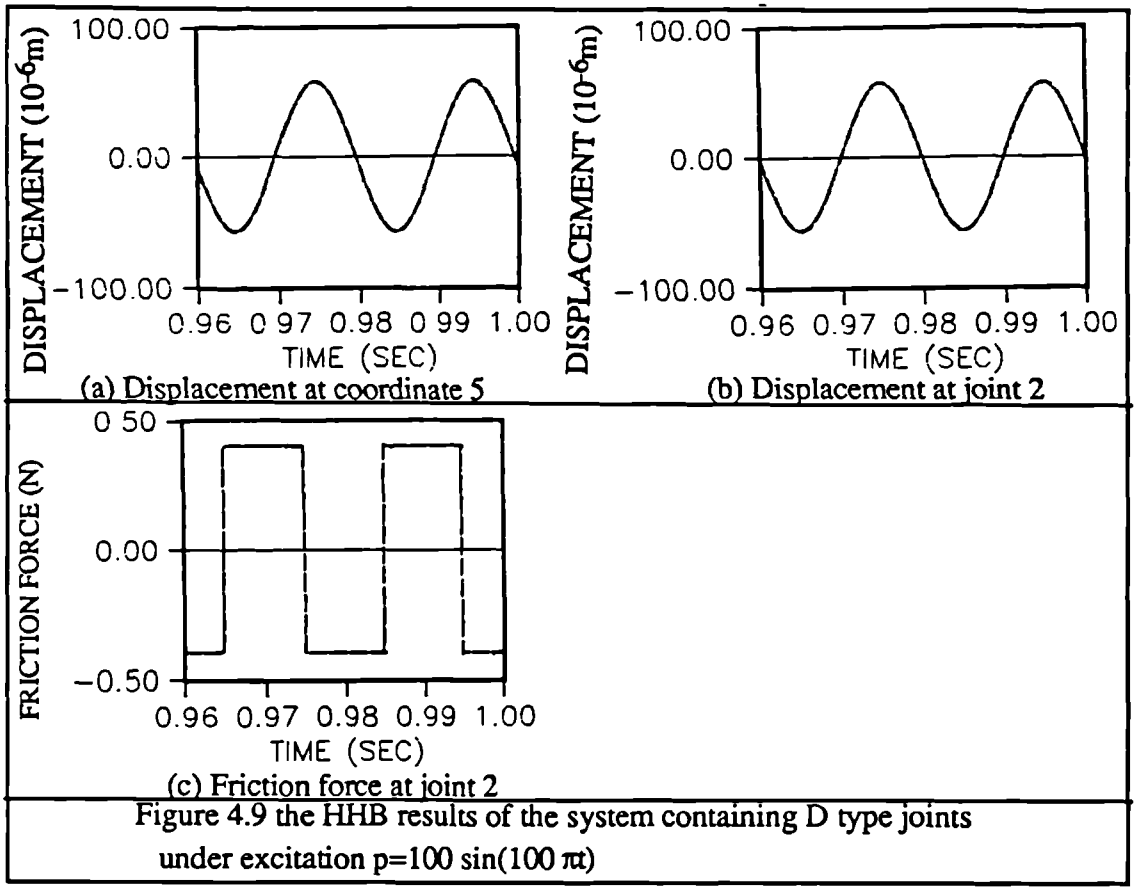

(a) Displacement at coordinate 5

(b) Displacement at joint 2

(c) Friction force at joint 2

Figure 4.9 the HHB results of the system containing D type joints under excitation p=100 sin(100 πt)

Even if the joint is in a series of stick-slip motion, it is believed that provided a sufficient number of harmonics is considered for the HHB and a sufficient number of points is used in DFT, higher accuracy can be achieved, but at the price of increased computation cost.

Another advantage of the HHB method over the HB method is when the excitation is not sinusoidal. In this case, the response contains more than one significant frequency component, and the HB method is not applicable. However, using the HHB method, the response can be calculated with no additional difficulty.

Figure 4.10 shows the system containing B type joints and under an excitation of $P=\sin(100\pi t)+\sin(300\pi t)+\sin(500\pi t)$. The results from the STI method and the HHB method are hardly distinguishable.

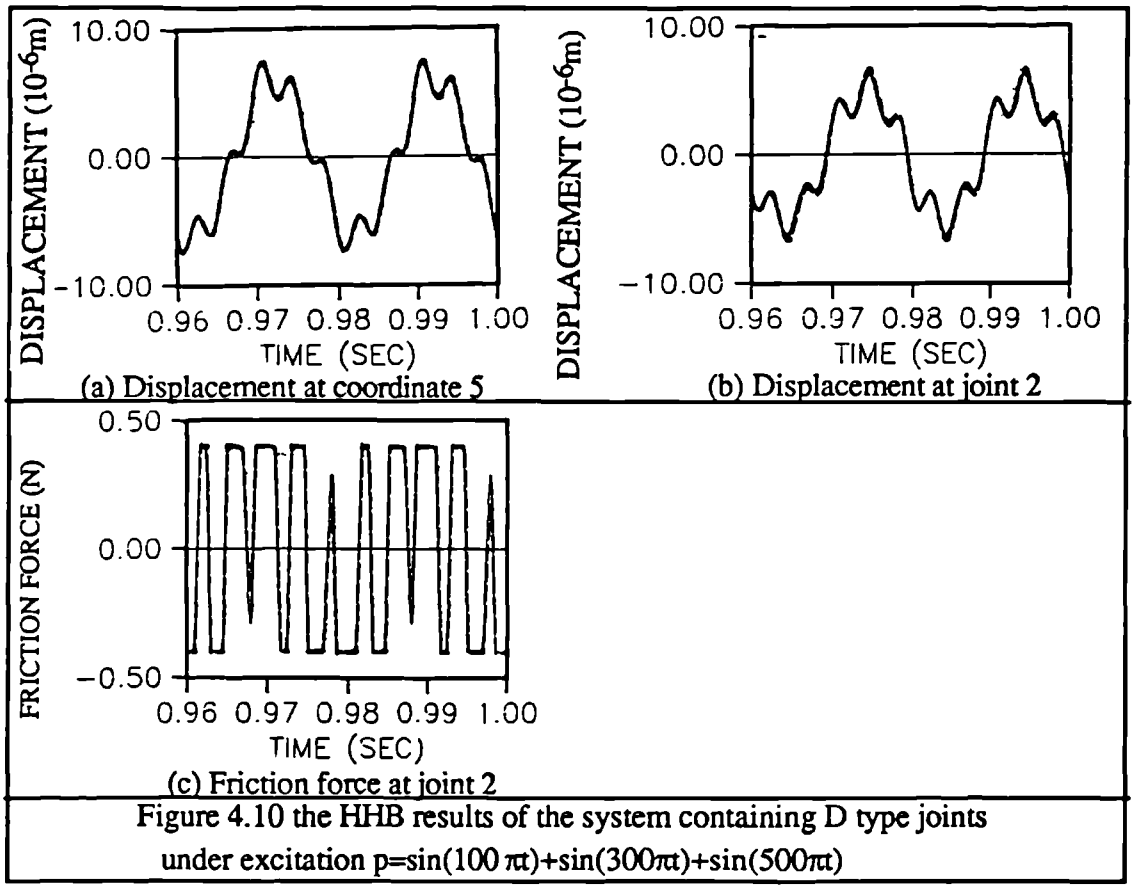

Figure 4.10 the HHB results of the system containing D type joints under excitation $p=\sin(100\pi t)+\sin(300\pi t)+\sin(500\pi t)$

An even more attractive advantage of the HHB method is that the perturbation approach can be used to obtain the response at a neighbouring state. Hence the computation cost can be significantly reduced.

Figure 4.11 and figure 4.12 show the results of the systems with B type joints and the system with E type joints in frequency domain. The STI method can be too expensive to apply for this kind of study, but using the HHB method, calculation of the response at a neighbouring frequency often requires only a few iterations. Therefore, the job was done at a much lower cost than using the STI method.

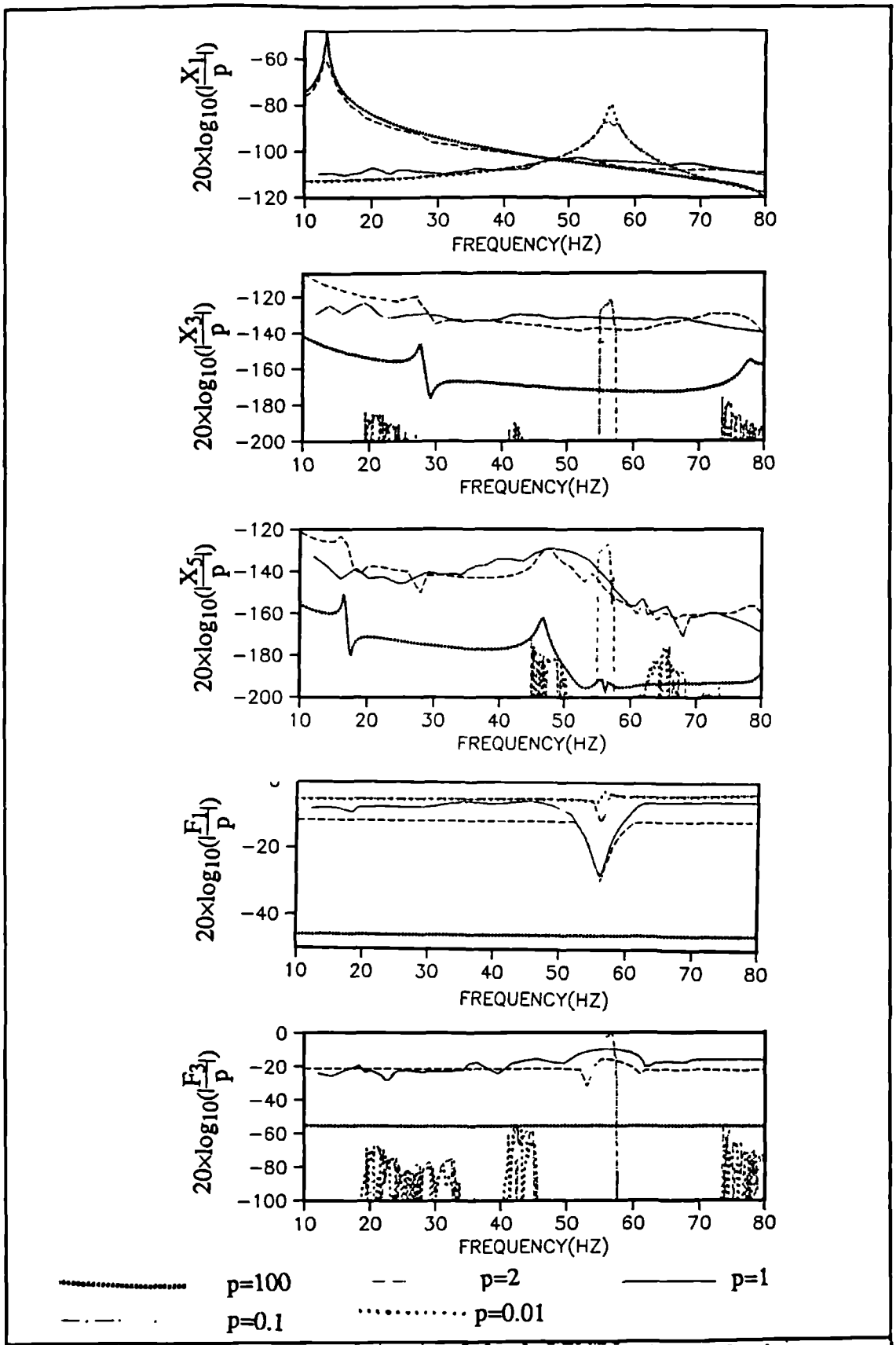

Figure 4.11 The response and friction force in the frequency domain for the system with B type joints

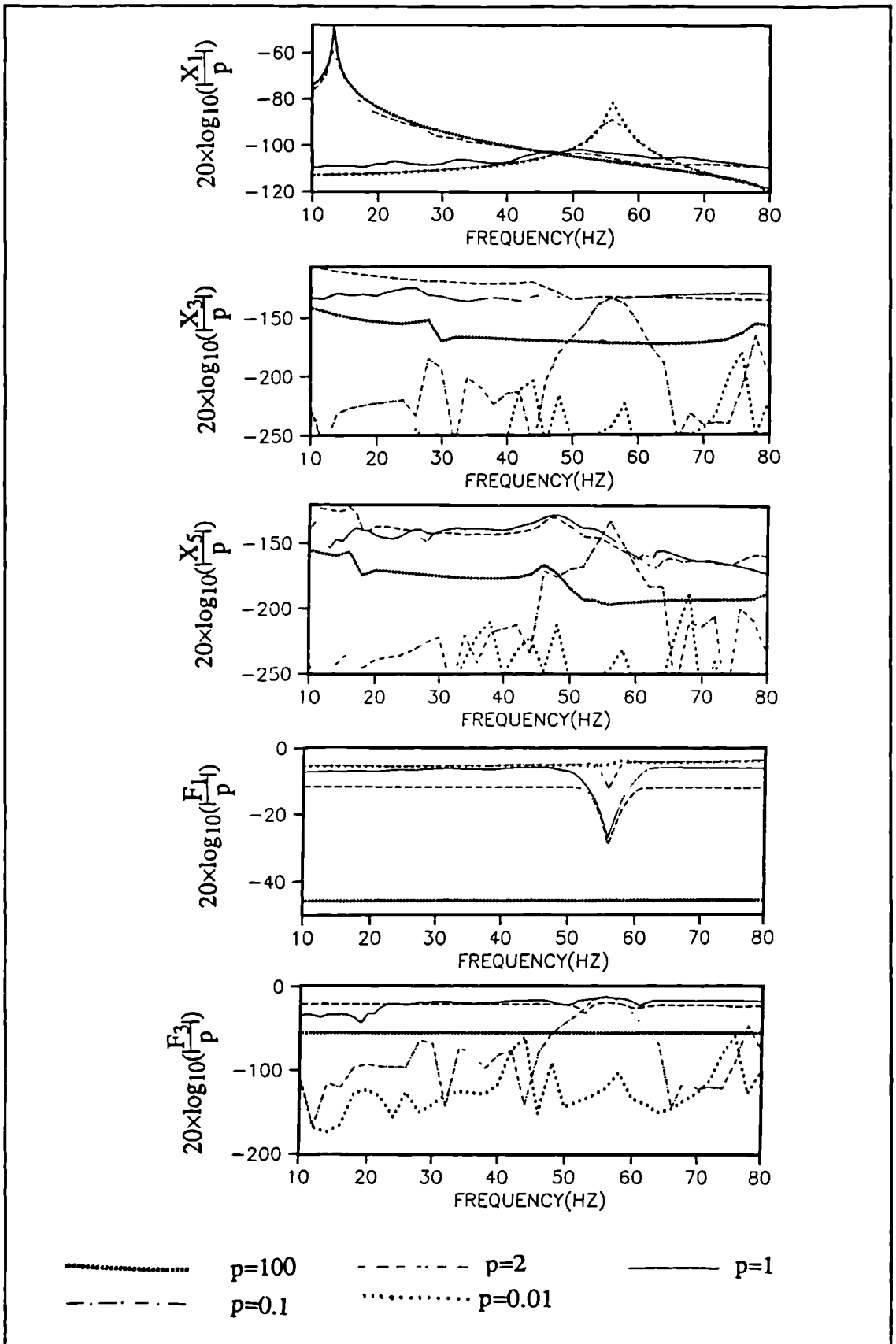

Figure 4.12 The response and friction force in the frequency domain for the system with E type joints

The displacement at coordinate 5 and the friction force at joint 2 are presented. For clarity, both the displacement and the friction force are presented in dB with respect to the magnitude of the excitation, i.e. if the excitation is P=psin(ωt) and the magnitude of the n'th harmonic of the displacement (or friction force) is X_n (or F_n), the response (or the friction force) in dB is $20\times\log_{10}(|\frac{X_n}{p}|)$ (or $20\times\log_{10}(|\frac{F_n}{p}|)$. The magnitudes of the excitations used are p=100, 2, 1, 0.1, 0.01 respectively. Three harmonics of the response and two harmonics of the friction force are presented.

It is noted that in most cases, the response is dominated by the first harmonic component (the fundamental harmonics). The ratio of the response to the excitation varies significantly under different excitation. 20-40dB difference can be observed in figure 4.11a and figure 4.12a between the response under excitation with p=1 and with p=100 (or p=0.01). This clearly indicates that the significance of the friction joint on the reduction of the response of the system.

It is also noted that the higher harmonic terms of the response vary significantly with the level of the excitation and also the frequency of the excitation. When the excitation level is small, the joint behaves approximately linearly, hence the higher-order harmonic components are insignificant, an exception is at a frequency close to the 'lock-resonance' frequency (around 55Hz), the displacement at the joint under some excitation (e.g. p=0.1) increases to such a level that the characteristics of the joints become significantly nonlinear; when the excitation is significant, the friction force becomes insignificant compared with the excitation, hence the higher-order harmonics of the response component is insignificant. In between these two extremes, the higher harmonic components are most significant.

Since the magnitudes of the higher-order harmonic components of the response under small excitation are much smaller than the fundamental terms except for those close to the 'lock-resonance', the results obtained at the frequencies other than those close to the 'lock-resonance' frequency are prone to numerical errors and are inaccurate in their absolute values. However, since the magnitude of these components are insignificant, they do not affect the overall accuracy of the HHB method (i.e. the response signal in the time domain).

§4.9.2 Discussion

It is found that during the computing process, without using the perturbation approach, convergence can only be achieved with a system containing weak nonlinearity (i.e. either the excitation is very high or the excitation is very low) even if the Newton-Raphson method is used. However, if the perturbation approach is used, convergence can be achieved for a much wider group of systems. The ESD and ELSD methods are found to

be effective in dealing with systems with weak nonlinearity, but convergence for systems with strong nonlinearity can only be achieved by using the Newton-Raphson method.

It is also found that computation cost heavily depends on the perturbation approach used (i.e. joint incremental perturbation or excitation incremental perturbation). Although final convergence can usually be achieved by using both the joint and excitation perturbation approaches, the ratio of the computation cost between two perturbation methods may well be over 100 times. The joint incremental approach should be used for high excitation cases (e.g p=2 and p=100), while the excitation incremental approach should be used for low excitation cases (i.e. p=0.1and p=0.01). For the case with p=1, the computation cost using these two perturbation approaches is similar.

The cost of the HHB is much lower than the STI method for a system with weak nonlinearity (i.e. p=100, 2, 0.1, 0.01). For a system with strong nonlinearity (p=1 and with a D type joint), the computation cost of the HHB method for a calculation of the response under an excitation can be up to 5 times more expensive than that of the STI method. However, much more information is obtained from using the HHB method than from using the STI method since the response corresponding to each perturbed system is available. If the variation of the response against one variable (e.g. against the change of frequency) is required, the cost of the STI method increases linearly with the number of states to be calculated, while for the HHB method, calculation of the response at a neighbouring state often needs a few more iterations only, hence the cost of the calculation of the response at a neighbouring state using the HHB method is much cheaper. What is more, because the cost of the HHB method depends only on the number of coordinates where the nonlinear joints are attached, the ratio of the computation cost between the HHB and the STI method should drop significantly with an increase of the size of the theoretical model.

If the response at several states are required and the calculation of the response at a single state using the STI method is cheaper, then the response at the first state can be calculated using the STI method. The response signal in the time domain can then be resolved into frequency domain components using the Fourier series, and these frequency components can be used for the calculation of the response at a neighbouring state using the HHB method and perturbation approach. Consequently, the overall cost of computation can be reduced.

In addition, if very accurate results are required, the results from the HHB method can be used as the initial condition for the STI method.Hence the steady-state response can be achieved in a much shorter time. Accordingly, the cost of the STI method for calculating the steady-state response can be significantly reduced.

§4.10 CONCLUSIONS

In this chapter, approximate methods based on the balance of the harmonics of the response signal are investigated, and their advantages and disadvantages are discussed. It is believed that in order to extend the applications of the approximate methods to quantitative engineering problems, two problems needs to be solved; 1) the accuracy, and 2) the efficiency.

It has been shown that use of FRF data for the HB method is very attractive in reduction of the computation cost since the size of the problem is independent of the complexity of the physical system. It is also shown that accuracy can be increased by taking more harmonics into account in the IHB and AFT methods. Based on the discussion of the approximate methods it is concluded that the FRF based HHB method is very attractive for calculation of the steady-state response of a system containing localised nonlinear elements.

Because the solution of the FRF based HHB method can only be obtained by solving a set of nonlinear equations, it is believed that the development of a new scheme for solving these nonlinear equations is of the utmost importance for the HHB method.

The direct iteration scheme is investigated, and based on the concept of local or global equivalent stiffness and damping, the new direct iterative scheme is proposed. The Newton-Raphson algorithm is proposed for the HB and HHB methods when the direct iterative scheme fails.

It is believed that the determination of a good estimate for the solution is the key to solve the nonlinear equations. The new perturbation method has been developed. Theoretically, provided the change of solution with the perturbation is continuous, the solution for the HB and HHB methods can always be found.

The change of the solution with the perturbation contains useful information for the solution of the newly perturbed system. Linear and quadratic approximations are proposed for the estimation of the new system. It is found that the step of the perturbation can be significantly increased with the help of the linear and quadratic approximations, hence the computation cost is significantly reduced. Two perturbation schemes have been suggested; the excitation incremental perturbation is suggested for the system subjected to a small excitation and the joint incremental perturbation is suggested for the system subjected to a large excitation.

The HB method is a special case of the HHB method, however, if the system only contains one nonlinear joint, the HB solution can be found more efficiently with a newly

developed algorithm. The key point is to turn a two dimensional problem into a one dimensional one.

Numerical case studies have been carried out. It is found that solutions from the HB method usually have reasonable accuracy. However, if higher accuracy is required, the HHB method has to be used. The other case when the HHB method should be used is when the excitation contains several significant harmonic components.

It is also illustrated that using the perturbation approach, the effects of the friction joint on the response of the system can be studied at a significantly reduced cost.

The FRF based HHB method developed in this chapter is accurate and cost effective in calculating the steady-state response of engineering structures, particularly when the size of the physical system is significant, and/or responses at several states are required, and/or the nonlinearity of the system is weak.

It is believed that the HHB method can be used in place of the STI method or incorporated with the STI method for the calculation of the accurate steady-state response of a nonlinear system at a much reduced cost.

CHAPTER 5

GENERALISED COUPLING TECHNIQUES USING FRF DATA

§5.1 INTRODUCTION

Although systems with friction joints usually demonstrate nonlinear characteristics, there are two extreme cases under which such a system behaves linearly. These two extremes are the 'free-joint' case when the clamping force is zero and the 'locked-joint' case when the clamping force is very large. These two extreme cases set the lower and upper bounds for the natural frequencies (or to be more appropriate, the frequencies at which the responses are the maximum) of the system with intermediate clamping force applied to the joints. Clearly, the ability to predict the system response with 'locked joint' from the response the 'free-joint' system is desirable.

The dynamic characteristics of an assembled structure (the 'locked joint' system) can be deduced from the properties of the substructures (the 'free-joint' system) by imposing some additional constraints (i.e the conditions of equilibrium and compatibility). The process for predicting the assembly properties from the substructures is called coupling or substructure synthesis.

Generally speaking, the coupling methods can be divided into three groups[99], the first uses the spatial data (i.e. stiffness and mass), the second uses the modal data(e.g.[100-102]), while the third uses the measured response data (FRFs) directly(e.g. [103][104]). A detailed review on all three groups of methods can be found in [99].

First group methods, because stiffness and mass matrices are required, are usually only used in theoretical analysis. These methods can be considered as special cases of the finite element method. For the second group methods, the required modal data can be derived from a theoretical approach (FE), it can also be extracted from the experimental data using the modal analysis techniques. Therefore, for the second group methods, both theoretical and experimental data can be used. However, these methods are usually only for a structure with light damping or with proportional damping; difficulties arise when a

structure has significant non-proportional damping, which, unfortunately, is often the case for the structures with some friction joints.

In contrast to the first and the second group methods, the third group methods use the frequency response data (FRFs) measured directly from experiment, and it can deal with the non-proportionally damped system very well. For most of these methods, the coupling process is simple, it usually only involves the basic matrix operations, no data processing being required.

In this chapter, only the FRF coupling techniques are investigated. A new mathematically and physically generalized FRF coupling method, which possess the advantages of the available methods, is developed. A new algorithm to solve the coupling problem is proposed, which is computationally simple and efficient; the matrix inversion operation is not required. This new algorithm is also found to be very effective in detecting the linear dependency between the joint coordinate pairs.

It is also shown in this chapter that both consistent and inconsistent measurement errors can cause errors in the predication of the assembly response. The consistent errors are sometimes more dangerous because the errors in the predicted response are difficult to detect. Using the new algorithm developed, it is possible to find the lower and upper bounds of the natural frequencies for the assembly.

§5.2 BASIC CONDITIONS FOR FRF COUPLING

For all the FRF coupling methods, the basic conditions in the coupling process are compatibility and equilibrium. The conditions of compatibility and equilibrium are such that if a coordinate on the assembled structure corresponds to n coordinates in the substructure system, then the displacement and force on the assembly and the substructure systems must have the relation

$$x_a=x_1=x_2=...=x_n \tag{5.1}$$

and $$f_a=\sum_{i=1}^{n} f_i \ , \tag{5.2}$$

where subscript a refers to the coordinate on the assembly and subscripts 1,2,...n refer to the coordinates on the substructures.

If for the substructure system

$$\{x_s\}=[H_s]\{f_s\}, \tag{5.3}$$

with compatibility and equilibrium conditions

$$\{x_s\}=[T]\{x_a\} \tag{5.4}$$

and $$\{f_a\}=[T]^T\{f_s\}, \tag{5.5}$$

the purpose of coupling is to find the relation between displacement $\{x_a\}$ and force $\{f_a\}$ of the assembly, i.e. to find the matrix $[H_a]$ in the equation

$$\{x_a\}=[H_a]\{f_a\}. \tag{5.6}$$

§5.3 CONDITIONS FOR THE GENERALIZED COUPLING METHODS

If no optimization such as the least-squares algorithm is involved in the coupling process, the solution for $[H_a]$ in equation(5.6) is unique. Therefore, the final results from different FRF coupling methods should be exactly the same. However, due to computation errors, the results from different coupling methods can be different. Coupling methods can also be different in terms of the formulation, computation speed and occupied computation memory; there can also be some restrictions on the different FRF coupling methods in their applications. The coupling methods may be evaluated by considering:

1) Accuracy: the predicted characteristics of the coupled structure should not be sensitive to computation errors (eg. rounding off errors).

2) Efficiency: which may have two aspects;

i) the amount of computation memory and time required to implement the coupling process should be small, and

ii) the amount of time spent by the user in preparing the computing code and data should be small .

3) Simplicity: all kinds of problem can be solved using the same formulae so that once a computation code is made, it can be used to solve different coupling problems without large modifications.

4) Generality: there should be no severe restriction on the applications of the coupling methods, in other words, there should be no severe restrictions on the substructure receptance matrix$[H_s]$ and the restriction matrix [T].

The generality can have two aspects, one is physical generality, which means that the method can predict the response of an assembled structure generated from

(i) grounding some coordinates of a structure, or

(ii) coupling several coordinates together on one structure, or

(iii) coupling several substructures.

The other aspect is the mathematical generality, which means that application of the method should not be restricted due to numerical properties of the receptance matrix (eg. singularity), provided the substructures can be coupled physically.

Accuracy, efficiency, simplicity and generality are the four criteria used to evaluate a coupling method in this chapter. Simplicity is closely related to the efficiency. Practically, with respect to the problem to be solved and the computation resources available, different weighting should be given to the above four criteria.

The mathematical generality should be considered for all the coupling problems. For the study of a friction joint, in addition to the mathematical generality, the physical generality is of particular importance. It is often necessary to know the properties of the structure when two points on it are clamped together.

§5.4 THE IMPEDANCE COUPLING METHOD

The first coupling method developed is the Impedance Coupling Method. The original impedance coupling method was developed by Imregun *et al* [103] to couple two substructures together. However, the method is actually a physically generalized coupling method (or it can be easily extended to be a physically generalized coupling method). Because the first step in this method is to invert the receptance matrix, this method will be referred as the Generalized Impedance Coupling method(GIC) in the following analysis.

The basic strategy of the GIC method is as follows:

For the substructure system

$$\{x_S\}=[H_S]\{f_S\}, \tag{5.7}$$

multiplying both sides of equation(5.7) by the inverse of the matrix $[H_S]$ yields

$$\{f_S\}=[H_S]^{-1}\{x_S\}=[Z_S]\{x_S\}. \tag{5.8}$$

Substituting equation(5.3) and (5.4) into equation(5.8) leads to

$$\{f_a\}=[T]^T[Z_s][T]\{x_a\},$$

hence

$$[Z_a]=[T]^T[Z_s][T]. \tag{5.9}$$

Therefore

$$[H_a]=[Z_a]^{-1}=([T]^T[H_s]^{-1}[T])^{-1}. \tag{5.10}$$

Once the inverse of the receptance matrix of the substructures is calculated, the rest of the process is the same as assembling a global stiffness matrix from local element stiffness matrices in FE analysis.

If the substructure system has several substructures which are independent of each other, the inversion of the matrix $[H_s]$ can be completed by inverting the substructure receptance matrices separately and then assembling these inverted matrices. By doing this, computation cost can usually be reduced.

The column number in the matrix [T] corresponds to the assembly coordinates and the row number corresponds to the substructure coordinates. For an element in the transformation matrix T(i,j), if the i th coordinate in the substructure corresponds to the j th coordinate of the assembly , then T(i,j)=1, otherwise, T(i,j)=0.

If some of the coordinates are grounded, modifications have to be made. If the substructure coordinates to be grounded are denoted by $\{x_g\}$, and the partitioned displacement vector, the force vector and the dynamic stiffness matrix of the substructure are

$$\{x_s\}=\{x_n,x_g\}^T, \tag{5.11}$$

$$[Z_s]=\begin{bmatrix} Z_{nn} & Z_{ng} \\ Z_{gn} & Z_{gg} \end{bmatrix}, \text{ and} \tag{5.12}$$

$$\{f_s\}=\{f_n,f_g\}^T. \tag{5.13}$$

Since the response at grounded coordinates must be zero,

$$\{x_g\}=0. \tag{5.14}$$

Substituting equation (5.14) into (5.13) yields

$$\{f_n\}=[Z_{nn}]\{x_n\} \tag{5.15}$$

Hence

$$[H_a]=[Z_{nn}]^{-1} \tag{5.16}$$

To be compatible with equation(5.9), equation (5.15) can be expressed as:

$$\{f_n\}=[\,[I]\;[0]\,]\begin{bmatrix} Z_{nn} & Z_{ng} \\ Z_{gn} & Z_{gg} \end{bmatrix}\begin{bmatrix} [I] \\ [0] \end{bmatrix}\{x_n\}=[T]^T[Z_s][T]\,\{x_n\} \tag{5.17}$$

Then equation(5.10) can be used directly.

It can be noted that the GIC method satisfies the criterion of physical generality, and it is also very simple to implement. However the GIC method is usually computationally inefficient: it can be seen that two inversions of the full size matrices are required. In addition, because the full size matrix inversion is required, the numerical error levels can be significant (especially when the full size receptance matrix is rank deficient). In the case when the full size receptance matrix is singular, the GIC method will collapse, in other words, the method is not mathematically generalized.

In summary, the GIC method is a physical generalized method, but not a mathematically generalized one.

§5.5 TWO SUBSTRUCTURE RECEPTANCE COUPLING METHOD

Another coupling method often used is the receptance coupling method proposed by Tsai and Chou[104]. The method is developed to couple two substructures only. Because this method uses the receptance matrix directly, it will be called the Receptance Coupling method (RC method). Write the receptance matrices of substructure **A** and **B** in partitioned forms as

$$[{}_AH] = \begin{bmatrix} {}_AH_{mm} & {}_AH_{mi} \\ {}_AH_{im} & {}_AH_{ii} \end{bmatrix} \tag{5.18}$$

$$[{}_BH] = \begin{bmatrix} {}_BH_{mm} & {}_BH_{mi} \\ {}_BH_{im} & {}_BH_{ii} \end{bmatrix} \tag{5.19}$$

Then the receptance of the assembled structure is proved to be

$$\begin{bmatrix} {}_AH_{nn} & {}_AH_{nj} & {}_{AB}H_{nn} \\ {}_AH_{jn} & H_{jj} & {}_BH_{jn} \\ {}_{AB}H_{nn} & {}_BH_{nj} & {}_BH_{nn} \end{bmatrix} = \begin{bmatrix} {}_AH_{ii} & {}_AH_{im} & 0 \\ {}_AH_{mi} & {}_AH_{mm} & 0 \\ 0 & 0 & {}_BH_{ii} \end{bmatrix} - \begin{bmatrix} {}_AH_{im} \\ {}_AH_{mm} \\ -{}_BH_{im} \end{bmatrix} ({}_AH_{mm}+{}_BH_{mm})^{-1} \begin{bmatrix} {}_AH_{im} \\ {}_AH_{mm} \\ -{}_BH_{im} \end{bmatrix}^T \tag{5.20}$$

where subscripts m and i represent the coordinates to be coupled (master coordinates) and not to be coupled (internal coordinates) on the substructures. Subscripts j and n represent the joint coordinates (corresponding to master coordinates in substructure) and non-joint coordinates (corresponding to internal coordinates in substructure) on the assembly respectively. ${}_AH$, ${}_BH$ and ${}_{AB}H$ represent the receptance sub-matrices corresponding to the coordinates on A, B and between coordinates on substructure A and B respectively

It can be noted that the method requires only one matrix inversion and the size of the matrix to be inverted is determined by the number of the joint coordinates on the assembly, therefore, the RC method is computationally much more efficient and accurate then the GIC method.

Because the matrix to be inverted is actually a summation of two receptance sub-matrices which are much smaller than the whole receptance matrix in size, it is likely to be a well-conditioned matrix. If a substructure receptance matrix is singular, the GIC method will fail, but the coupling may still be completed using the RC method, that is , the RC method is mathematically more general than the GIC method.

However, the RC method can only be applied to couple two (group) substructures. If several substructures are to be coupled, multi-step coupling has to be used[99]. Figure 5.1 shows a diagram for coupling four beams into a frame using two steps.

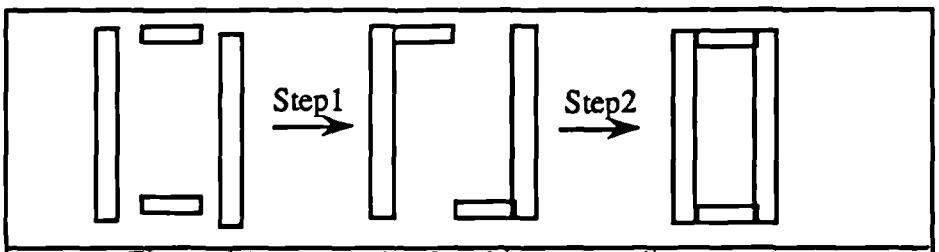

Figure 5.1 A example of multi-step coupling

An even greater shortcoming for the RC method is that the condition of physical generality is not satisfied. The RC method is derived from the case with two (group) substructures, it assumes that before coupling, the two substructures are independent of each other. Consequently, some sub-matrices of the substructure receptance matrix are always zero (This can be noted from equation(5.20)).

If coupling takes place on the same structure, i.e. several coordinates on one structure are clamped together as shown in figure 5.2, no sub-matrix is zero and the RC method is not applicable.

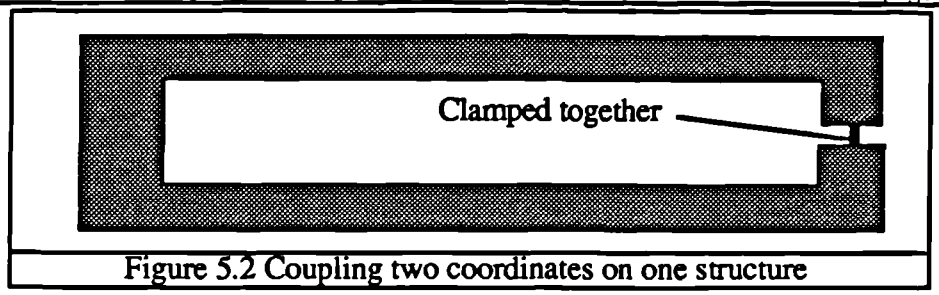

Figure 5.2 Coupling two coordinates on one structure

§5.6 THE GENERALIZED RECEPTANCE COUPLING METHOD -- A NEW DEVELOPMENT

§5.6.1 Derivation of the Basic Formulae of the Generalized Receptance Coupling Method

The GIC and RC methods are two of the most commonly used coupling methods. The GIC method is physically, but not mathematically generalized, while the RC method is efficient and mathematically more generalized than the GIC method, however, it is not physically generalized.

In considering the problem of coupling several coordinates on one substructure together, if the whole receptance matrix of the substructure is singular, both the GIC and RC methods will fail. Clearly, a new coupling method, which has the advantages of both the GIC and RC methods, is required.

In this section, a new coupling method is developed to satisfy both the physical and mathematical generality, it also retains the efficiency of the RC method. This new coupling method will be called the Generalized Receptance Coupling method(GRC).

To be physically general, we treat all the substructures as a substructure system. For this substructure system, the receptance matrix is partitioned in such a way that the relationships between response and excitation are

$$\begin{Bmatrix} x_a \\ x_b \\ x_c \end{Bmatrix} = \begin{bmatrix} H_{aa} & H_{ab} & H_{ac} \\ H_{ba} & H_{bb} & H_{bc} \\ H_{ca} & H_{cb} & H_{cc} \end{bmatrix} \begin{Bmatrix} f_a \\ f_b \\ f_c \end{Bmatrix}, \tag{5.22}$$

For the assembled system, the relationships between response and excitation are

$$\begin{Bmatrix} x_n \\ x_j \end{Bmatrix} = \begin{bmatrix} H_{nn} & H_{nj} \\ H_{jn} & H_{jj} \end{bmatrix} \begin{Bmatrix} f_n \\ f_j \end{Bmatrix} \tag{5.23}$$

where subscripts a and n represent the internal coordinates on the substructure and assembly, and subscripts b, c and j represent the joint coordinates. Substructure joint

coordinates x_b and x_c are so arranged that conditions of equilibrium and compatibility yield:

$$\{f_b\}+\{f_c\}=\{f_j\}, \text{ and} \tag{5.24}$$

$$\{x_b\}=\{x_c\}=\{x_j\}. \tag{5.25}$$

The force and the deformation at the internal coordinates on the substructure and assembly systems must be the same, hence

$$\{f_a\}\equiv\{f_n\}, \text{ and} \tag{5.26}$$

$$\{x_a\}\equiv\{x_n\}. \tag{5.27}$$

From equations (5.22) and (5.25),

$$\{x_b\}=[H_{ba}]\{f_a\}+[H_{bb}]\{f_b\}+[H_{bc}]\{f_c\}=[H_{ca}]\{f_a\}+[H_{cb}]\{f_b\}+[H_{cc}]\{f_c\} \tag{5.28}$$

Substituting equations (5.24)(5.26) into (5.28) yields

$$([H_{bb}]+[H_{cc}]-[H_{cb}]-[H_{bc}])\{f_b\}=\{([H_{ca}]-\{H_{ba}])\{f_n\}+([H_{cc}]-[H_{bc}])\{f_j\}\} \tag{5.29}$$

If matrix $([H_{bb}]+[H_{cc}]-[H_{cb}]-[H_{bc}])$ is non-singular, then

$$\{f_b\}=([H_{bb}]+[H_{cc}]-[H_{cb}]-[H_{bc}])^{-1}\{([H_{ca}]-\{H_{ba}])\{f_n\}+([H_{cc}]-[H_{bc}])\{f_j\}\} \tag{5.30}$$

$$\text{and } \{f_c\}=\{f_j\}-\{f_b\} \tag{5.31}$$

Substituting equations (5.30)(5.31) into (5.22) and comparing with equation (5.23) yields:

$$[H_{nn}]=[H_{aa}]-([H_{ab}]-[H_{ac}])([H_{bb}]+[H_{cc}]-[H_{bc}]-[H_{cb}])^{-1}([H_{ba}]-[H_{ca}]) \tag{5.32}$$

$$[H_{nj}]=[H_{ac}]-([H_{ab}]-[H_{ac}])([H_{bb}]+[H_{cc}]-[H_{bc}]-[H_{cb}])^{-1}([H_{bc}]-[H_{cc}]) \tag{5.33a}$$

$$=[H_{ab}]-([H_{ac}]-[H_{ab}])([H_{bb}]+[H_{cc}]-[H_{bc}]-[H_{cb}])^{-1}([H_{cb}]-[H_{bb}]) \tag{5.33b}$$

$$[H_{jn}]=[H_{nj}]^T \tag{5.34}$$

$$[H_{jj}]=[H_{cc}]-([H_{cb}]-[H_{cc}])([H_{bb}]+[H_{cc}]-[H_{bc}]-[H_{cb}])^{-1}([H_{bc}]-[H_{cc}]) \tag{5.35a}$$

$$=[H_{bb}]-([H_{bc}]-[H_{bb}])([H_{bb}]+[H_{cc}]-[H_{bc}]-[H_{cb}])^{-1}([H_{cb}]-[H_{bb}]) \tag{5.35b}$$

$$=[H_{bc}]-([H_{bb}]-[H_{bc}])([H_{bb}]+[H_{cc}]-[H_{bc}]-[H_{cb}])^{-1}([H_{cc}]-[H_{bc}]) \tag{5.35c}$$

$$=[H_{cb}]-([H_{cc}]-[H_{cb}])([H_{bb}]+[H_{cc}]-[H_{bc}]-[H_{cb}])^{-1}([H_{bb}]-[H_{cb}]) \tag{5.35d}$$

Equations (5.32) to (5.35) can be arranged in a more concise form as

$$\begin{bmatrix} H_{nn} & H_{nj} \\ H_{jn} & H_{jj} \end{bmatrix} = \begin{bmatrix} H_{aa} & H_{ac} \\ H_{ca} & H_{cc} \end{bmatrix} - \begin{bmatrix} (H_{ab}-H_{ac}) \\ (H_{cb}-H_{cc}) \end{bmatrix} [H_{bb}+H_{cc}-H_{bc}-H_{cb}]^{-1} \begin{bmatrix} (H_{ab}-H_{ac}) \\ (H_{cb}-H_{cc}) \end{bmatrix}^T \quad (5.36a)$$

$$= \begin{bmatrix} H_{aa} & H_{ab} \\ H_{ba} & H_{bb} \end{bmatrix} - \begin{bmatrix} (H_{ac}-H_{ab}) \\ (H_{bc}-H_{bb}) \end{bmatrix} [H_{bb}+H_{cc}-H_{bc}-H_{cb}]^{-1} \begin{bmatrix} (H_{ac}-H_{ab}) \\ (H_{bc}-H_{bb}) \end{bmatrix}^T \quad (5.36b)$$

It can be noted that the GRC method is very similar to the RC method in its formulation. Actually, the RC method can be considered as a special case of the GRC method. It is proved (in Appendix C) that for two substructure coupling, equation (5.36) is exactly the same as the formulae of the RC method (equation(5.20)). Therefore, the GRC method retains all the advantages of the RC method, but it is physically much more generalized. The GRC method can also be used to couple some coordinates on one structure or to couple several substructures together in a single step without any difficulty.

The GRC method is physically more general than the RC method, however, to satisfy all the generality conditions, some special considerations have to be made.

§5.6.2 Coupling with Ground Coordinates

If some coordinates on a structure are grounded, all the responses at these coordinates are zero. Physically, the ground can be considered to be a structure with infinite mass, therefore, to ground a structure at some coordinates is the same as coupling the structure at these coordinates to another structure with infinite mass. The FRFs of the infinite mass structure is zero. Therefore, setting sub-matrices $[H_{ac}]$,$[H_{bc}]$,$[H_{cc}]$, $[H_{cb}]$ and $[H_{ba}]$ in equation (5.36) to zero leads to the following formulae for grounding a structure

$$\begin{bmatrix} H_{nn} & H_{nj} \\ H_{jn} & H_{jj} \end{bmatrix} = \begin{bmatrix} H_{aa} & 0 \\ 0 & 0 \end{bmatrix} - \begin{bmatrix} (H_{ab}) \\ (0) \end{bmatrix} [H_{bb}]^{-1} \begin{bmatrix} (H_{ab}) \\ (0) \end{bmatrix}^T \quad (5.37)$$

or $[H_{nn}]=[H_{aa}]-[H_{ab}][H_{bb}]^{-1}[H_{ba}]$ (5.37a)

$[H_{nj}]=[0]$,$[H_{jn}]=[0]$ and $[H_{jj}]=[0]$ (5.37b)

§5.6.3 Coupling Several Substructure Coordinates Into One Assembly Coordinate

The GRC method satisfies the criterion of accuracy, generality, simplicity and the first condition of efficiency. If every joint coordinate only couples with another joint coordinate (which is referred to as pair coupling (PC)), the coupling process can be implemented in a single step, i.e. the second condition of efficiency is also satisfied.

If several coordinates (more than two) are to be coupled into one coordinate (which is referred as Multi-Coordinate Coupling (MCC)), then coupling can be implemented in several steps. One example for coupling three coordinates together is shown in figure 5.3. However, it is not impossible to complete the coupling in a single step even in the case of MCC.

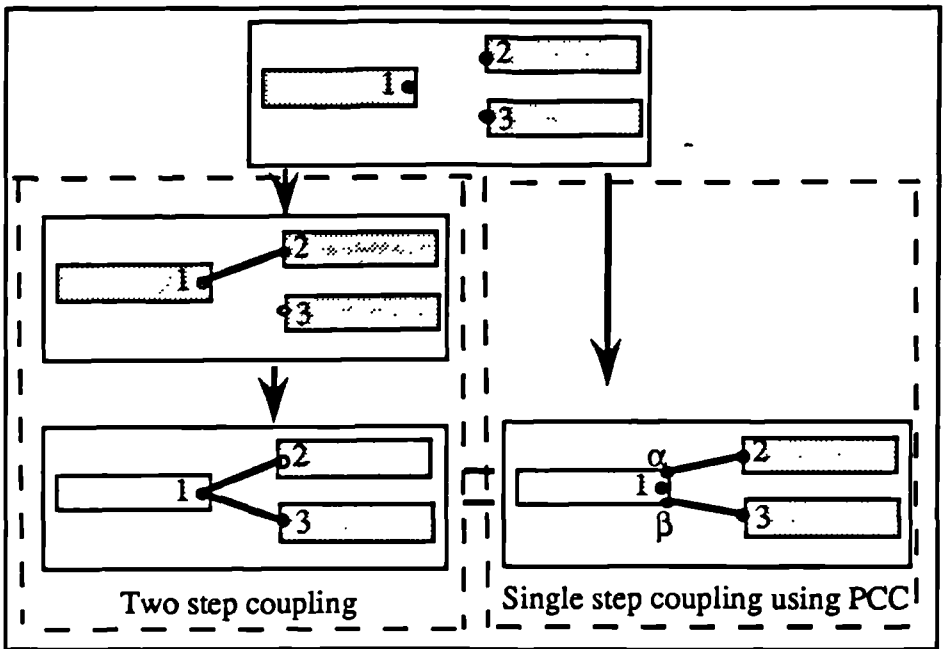

Figure 5.3 Examples using two step coupling and pseudo coordinate single step coupling

To complete the coupling in a single step for the MCC case, we have to employ a new concept of Pseudo Coordinate Coupling (PCC). Suppose we want to couple three coordinates together as shown in figure 5.3. Instead of considering point 1 as a single coordinate, we can consider that there are two coordinates α and β which are located infinitesimal distant about at point 1 (hence they have exactly the same response as point 1). If we couple point 2 with point α, and point 3 with point β, we turn the MCC problem into a PC problem, and the coupling can then be completed in a single step.

Because coordinates α and β are actually the same point, their corresponding rows and columns in the substructure FRF matrix will be exactly the same. However, because the matrix to be inverted is the sum of four matrices, there will be no numerical problems if one of these are rank-deficient. To illustrate this, consider the example in figure 5.3:

$$\{x_b\}=\{x_\alpha,x_\beta\}^T, \tag{5.38}$$

$$\{x_c\}=\{x_2,x_3\}^T, \tag{5.39}$$

$$[H_{bb}]=\begin{bmatrix} H_{\alpha\alpha} & H_{\alpha\beta} \\ H_{\beta\alpha} & H_{\beta\beta} \end{bmatrix}=H_{11}\begin{bmatrix} 1 & 1 \\ 1 & 1 \end{bmatrix}, \tag{5.40}$$

$$[H_{bc}]=\begin{bmatrix} H_{\alpha 2} & H_{\alpha 3} \\ H_{\beta 2} & H_{\beta 3} \end{bmatrix}=\begin{bmatrix} H_{12} & H_{13} \\ H_{12} & H_{13} \end{bmatrix}, \text{ and} \tag{5.41}$$

$$[H_{cc}]=\begin{bmatrix} H_{22} & H_{23} \\ H_{32} & H_{33} \end{bmatrix}. \tag{5.42}$$

The matrix to be inverted is

$$[H_{bb}+H_{cc}-H_{bc}-H_{cb}]=H_{11}\begin{bmatrix} 1 & 1 \\ 1 & 1 \end{bmatrix}+\begin{bmatrix} H_{22} & H_{23} \\ H_{23} & H_{33} \end{bmatrix}\begin{bmatrix} H_{12} & H_{13} \\ H_{12} & H_{13} \end{bmatrix}\begin{bmatrix} H_{12} & H_{12} \\ H_{13} & H_{13} \end{bmatrix}$$

$$=\begin{bmatrix} H_{11}+H_{22}-2H_{12} & H_{11}+H_{23}-H_{12}-H_{13} \\ H_{11}+H_{23}-H_{12}-H_{13} & H_{11}+H_{33}-2H_{13} \end{bmatrix} \tag{5.43}$$

It is clear that although the matrix $[H_{bb}]$ is singular, the matrix $[H_{bb}+H_{cc}-H_{bc}-H_{cb}]$ is not. Therefore, there is no numerical difficulty in inverting $[H_{bb}+H_{cc}-H_{bc}-H_{cb}]$.

From the computing point of view, it is only necessary to invert one matrix for the PCC method, while utilising the multi-step GRC method involves inverting several smaller matrices.

With recent developments in both computer hardware and software, the computation cost and time have decreased dramatically. However, the cost of manpower in programming becomes more and more expensive. Although the computation cost using the PCC method can be slightly higher, the manpower required is much lower, and because there is less intermediate matrix required for the PCC method in computing, the space required can be smaller. Therefore, the PCC method may be more attractive than the usual Multi-step GRC method, especially when the matrix to be inverted is not very large.

§5.6.4 Multi-step Two-coordinate Coupling (MTC)

The PCC method was originally developed for simplicity in programming. However, the coupling can be implemented by coupling two coordinates at one time and repeating the two coordinate coupling process until all the coordinates are coupled together. Because at each step, there are always two coordinates to be coupled together, the multi-step two-coordinates coupling method can be programmed systematically.

From equation(5.36), it can be noted that the assembly from coupling coordinates i and j is

$$[H_a]=[H_s]-\frac{1}{h_{ii}+h_{jj}-2h_{ij}}(\{h_{sj}\}-\{h_{si}\})(\{h_{sj}\}-\{h_{si}\})^T, \tag{5.44}$$

where $\{h_{si}\}$ and $\{h_{sj}\}$ represent the ith and jth columns in the substructure matrix $[H_s]$ and $[H_a]$ is the receptance matrix of the assembly.

It can be noted that the inversion for two coordinate coupling is trivial because the matrix size is one by one. The implementation of equation(5.44) requires n^2+n multiplications, where n is the size of the substructure matrix. However, because the ith and jth columns(rows) of the assembly are exactly the same, one of these coordinate can be deleted, therefore, the actual multiplication required is $(n-i)^2+(n-i)$. Therefore, the total multiplications required to couple *m* pairs of coordinates are

$$N_1= \sum_{i=1}^{m}(n-i)(n+1-i)) \tag{5.45}$$

Inversion of a m×m matrix using Gaussian-elimination algorithm requires approximately $\sum_{i=1}^{m-1}\{2(m-i)(m+1)\}+m^2$ multiplications (Appendix D), hence, the total multiplications required(which is sum of the multiplication for the inversion and the multiplication required to multiply the three matrices) using equation(5.36) is

$$N_2=mn(n-m) + \sum_{i=1}^{m-1}\{2(m-i)(m+1)\}+m^2 \tag{5.46}$$

Figure 5.4 shows the ratio between the number of multiplications required using equation(5.45) and using equation (5.46). It can be noted that in terms of the computation efficiency, the MTC method is more attractive than the GRC method.

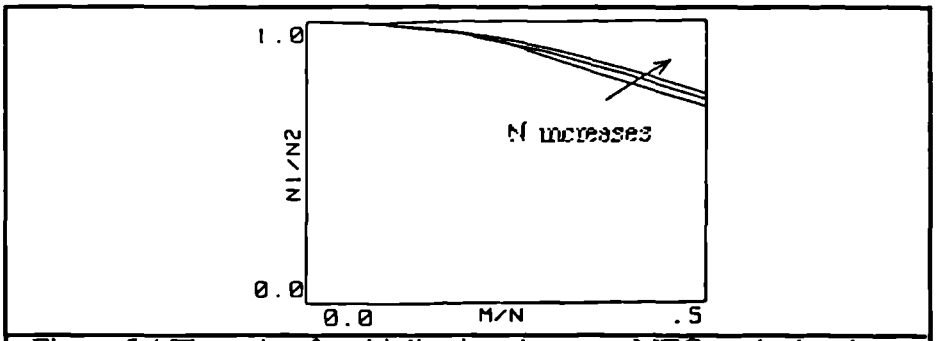

Figure 5.4 The ratio of multiplications between MTC method and GRC method (N=4, 10, 200)

§5.7 REDUCTION OF THE EFFECTS OF NUMERICAL AND MEASUREMENT ERRORS

§5.7.1 The Measurement Errors and the Model Inconsistency

The measured data from experiments usually contain some errors generated at different experimental stages. Mass loading, interaction between shaker and structure, windowing and aliasing are some common sources of measurement errors [105]. Because of these errors, the measured data are shifted from their true values.

The most severe problems caused by measurement errors are model inconsistency. A receptance matrix can be generated from a spatial or a modal model [1] as

$$[H]=(-\omega^2[M]+[K]+i\omega[C]+i[D])^{-1}, \quad (5.47)$$

$$\text{or } [H]=[\Phi][(\omega_r^2-\omega^2)]^{-1}[\Phi]^T. \quad (5.48)$$

When the measured receptance matrix is contaminated by measurement errors, say $[H]_m=[H]+\delta[H]$, it is not possible not find a physically meaningful spatial or modal model which exactly satisfies

$$[H]_m=(-\omega^2[M]_m+[K]_m+i\omega[C]_m+i[D]_m)^{-1} \quad (5.49)$$

$$\text{or } [H]_m=[\Phi]_m[(\omega_r^2-\omega^2)]_m^{-1}[\Phi]_m^T, \quad (5.50)$$

where subscript m represent the measured data.

In other words, the measured receptance matrix does not represent any physically meaningful structure exactly. This phenomenon is called model inconsistency.

In the matrix operations, the effects of the errors is usually most significant in matrix inversion. To illustrate the effects of inconsistent measured data, consider a 3-DOF system with hysteretic damping as shown in figure 5.5.

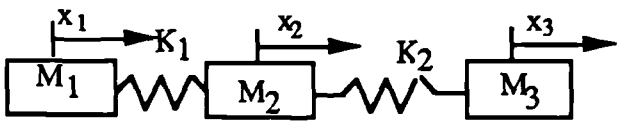

M_1=1kg, M_2=2kg, M_3=0.5kg, K_1=2.E6 N/m, K_2=1.E6 N/m, [D]=0.001[K]

Figure 5.5 Diagram for a 3DOF system

Theoretically,

$$[Z]=[H]^{-1}=-\omega^2[M]+[K]+i[D].$$

Figure 5.6 shows the first elements of real and polluted receptance matrices, and figure 5.7 shows the first element of the dynam. stiffness matrix and the first element from the inversion of the polluted receptance matrix (with 5% random error). (A receptance matrix is said to be polluted by 5% random errors if the real and imaginary parts of each element in the true receptance matrix are multiplied by random numbers ranging from 0.95 to 1.05 respectively). The difference between the polluted and exact receptance data is so small that the polluted data are shifted by 1dB. The difference between the real and predicted impedance matrix is usually greater than 5%, in other words, the effects of errors are magnified

through the matrix inversion. It can also be noted that the worst occurs at the frequencies near resonance.

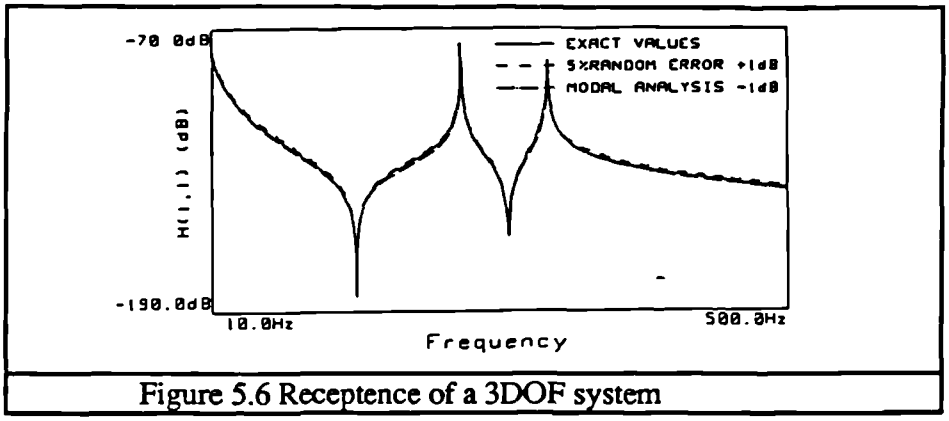

Figure 5.6 Receptence of a 3DOF system

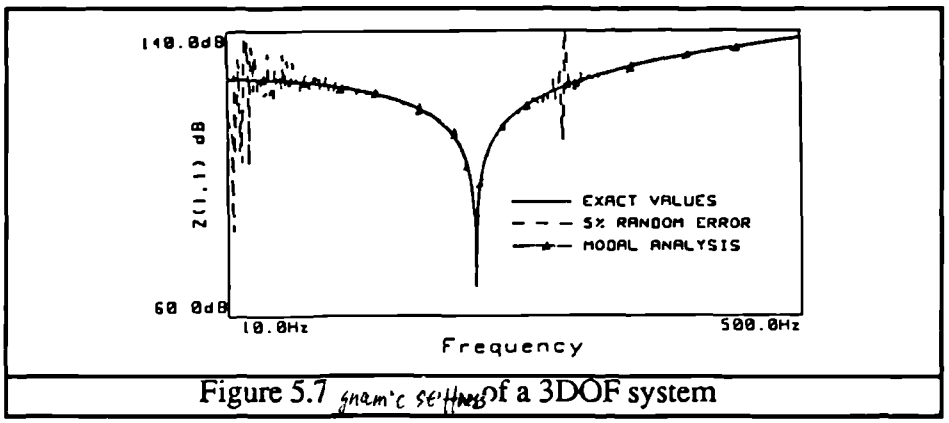

Figure 5.7 Dynamic stiffness of a 3DOF system

At frequencies near resonance, the receptance tends to be dominated by only one mode, which results in the columns and rows in the receptance matrix to be approximately linearly dependent. In other words, if the receptance matrix is ill-conditioned, the inversion of the receptance matrix tends to be erroneous even if the error levels in the receptance matrix is small.

§5.7.2 Reduction of the Effects of Measurement Errors Using Modal Analysis Techniques

One technique to reduce the effects of random errors is to force the receptance data to be consistent. This can usually be achieved by extracting the modal parameters via modal analysis techniques for each measured receptance curve [106] and forcing the modal data from different receptance curves to be consistent. The consistent modal data are then used to regenerate the receptance matrix from equation(5.48). Thus the generated receptance matrix is consistent. Figure 5.6 and figure 5.7 also show that first element of the real and predicted first element in the receptance and impedance matrix for the 3-DOF system used in the last section, after applying modal analysis to the polluted receptance data. The discrepancy is significantly reduced.

It can be noted that there are still some differences between the real and predicted impedance matrix. Using modal analysis, measurement errors can be reduced, but not completely eliminated. The errors retained after modal analysis are called consistent errors in this chapter, which can sometimes have significant effects on the coupling results as will be shown later.

§5.8 APPLICATION OF PSEUDO INVERSE IN COUPLING PROCESS

In the above derivation, it has been assumed that the matrix $[H_{bb}+H_{cc}-H_{bc}-H_{cb}]$ is non-singular. However if the matrix $[H_{bb}+H_{cc}-H_{bc}-H_{cb}]$ happens to be singular, its inverse does not exist. Therefore, equation (5.36) cannot be used directly.

If the matrix $[H_{bb}+H_{cc}-H_{bc}-H_{cb}]$ is ill-conditioned, then the inversion of $[H_{bb}+H_{cc}-H_{bc}-H_{cb}]$ can be very sensitive to numerical and measurement errors.

Urgueira [99] pointed out that singular or ill-conditioned matrices may occur for the following reasons:

1) The receptance matrix is regenerated from a set of modal data which has fewer modes than the size of the receptance matrix to be inverted,

2) The receptance matrix is dominant by one mode at resonance, and

3) Some interface coordinates are situated on a locally rigid region.

The first type of singular problem should never be allowed. The number of modes used to regenerate the receptance matrix effectively means the DOF of the receptance matrix. Generally, coupling two coordinates means imposing a restriction to the system. If the restrictions are independent, imposing one restriction means the system will have a reduction of one in the DOF. Imposing more coupling than the DOF will certainly lead to zero response of the assembly.

In the second case, because of the effects of other modes, the receptance matrix will not be singular. If modal analysis is applied, the effects of the measurement errors are usually not significant.

The worst rank deficient problem is the third. Usually, the modal analysis technique is not effective in eliminating consistent errors. However, the consistent errors can have significant effects on the predicted assembly response if the third type of rank-deficiency occurs.

A common technique for solving the singular or rank-deficient problem is to apply the pseudo inverse using singular value decomposition algorithm(SVD)[99][107]

§5.8.1 Pseudo Inverse and Singular Value Decomposition

If the relationship between a matrix [B] and a matrix [A] satisfies the following four equations, then the matrix [B] is called the pseudo inverse of the matrix [A] and also the matrix [A] is the pseudo inverse of matrix [B]:

$$[A][B][A]=[A], \tag{5.51a}$$
$$[B][A][B]=[B], \tag{5.51b}$$
$$([A][B])^H=[A][B], \text{ and} \tag{5.51c}$$
$$([B][A])^H=[B][A]. \tag{5.51d}$$

It is proved[108] that for any matrix [A], there is an unique matrix which satisfies all four equations. The pseudo inverse [B] of a matrix A is often denoted as A^+.

The pseudo inverse of a matrix can be obtained using the Singular-Value-Decomposition algorithm (SVD) , which may be expressed as follows:

Any matrix $[A]_{n\times m}$ (where $n\geq m$) can be decomposed uniquely into the product of three matrices [U],[Σ] and [V] as

$$[A]=[U][\Sigma][V]^H \tag{5.52}$$

$$\text{where } [\Sigma]=\begin{bmatrix} \sigma_1 & & & 0 \\ & \sigma_2 & & \\ & & \ddots & \\ 0 & & & \sigma_m \\ 0 & 0 & 0 & 0 \\ \vdots & \vdots & \vdots & \vdots \\ 0 & 0 & 0 & 0 \end{bmatrix} \tag{5.53}$$

is a diagonal matrix with all the diagonal element non-negative, i.e

. $\sigma_1\geq\sigma_2\geq\ldots\geq\sigma_i>0=\sigma_{i+1}=\ldots=\sigma_m$

$[U]_{m\times m}$ and $[V]_{n\times n}$ are orthnormal matrices, i.e.

$$[U]^H[U]=[I], \tag{5.54}$$
$$\text{and } [V]^H[V]=[I]). \tag{5.55}$$

The element in the matrix [Σ] is called the singular value of the matrix [A].

Once the SVD of a matrix is known, the pseudo inverse of matrix [A] is available in a very simple form as

$$A^+=[V][\Sigma]^+[U]^H \tag{5.56}$$

$$\text{where } [\Sigma]^{+}=\begin{bmatrix} \frac{1}{\sigma_1} & & & 0 \\ & \ddots & & \\ & & \frac{1}{\sigma_i} & \\ & & & \ddots \\ 0 & & & 0 \end{bmatrix} \tag{5.57}$$

Penrose [109] had proved that for a set of linear equations -

$$[A]\{x\}=\{b\}, \tag{5.58}$$

If the notation $\|x\|=\{x\}^H\{x\}$ is used for the Euclindine norm of $\{x\}$ and the best solution $\{x_0\}$ of equation (5.58) is defined to satisfy following conditions:

for any $\{x\}$, either

$$1)\ \|[A]\{x\}-\{b\}\|>\|[A]\{x_0\}-\{b\}\| \tag{5.59}$$

$$\text{or}\ \ 2)\ \|[A]\{x\}-\{b\}\|=\|[A]\{x_0\}-\{b\}\| \text{ and } \|x\|\geq\|x_0\|, \tag{5.60}$$

then the best solution for equation(5.58) is

$$\{x_0\}=[A]^{+}\{b\}. \tag{5.61}$$

In the case that there are more than one exact solutions, the solution $\{x_0\}=[A]^{+}\{b\}$ have the smallest Euclindine norm.

§5.8.2 Reduction of the Effects of Consistent Errors Using SVD

Although modal analysis can reduce the effects of the measurement error significantly, the process of extracting modal data can be time consuming. In some cases, even after applying modal analysis, the coupled results can still be inaccurate. If the rank-deficiency is caused by some joint coordinates located on the rigid region of the structure, use of modal analysis may not be enough to eliminate the effects of the measurement errors, and because the coupled results using the FRF data generated from modal data are usually very smooth, the erroneous results can be mis-leading.

Otte *et al* [107] have proposed that pseudo inverse can be used to replace the real inverse to eliminate some noise effects.

The basic strategy (applying to the new generalized coupling formulae) is as follows:

Recall equation (5.29)

$$([[H_{bb}]+[H_{cc}]-[H_{cb}]-[H_{bc}])\{f_b\}=\{([H_{ca}]-\{H_{ba}])\{f_n\}+([H_{cc}]-[H_{bc}])\{f_j\}\} \quad (5.29)$$

$$\text{Let } [A]=[H_{bb}]+[H_{cc}]-[H_{cb}]-[H_{bc}]=[U][\Sigma][V]^H \quad (5.62)$$

$$\text{and } \{b\}=\{([H_{ca}]-\{H_{ba}])\{f_n\}+([H_{cc}]-[H_{bc}])\{f_j\}\} \quad (5.63)$$

then

$$\{f_b\}=[V][\Sigma^{-1}][U]^H\{b\}$$

$$= \frac{1}{\sigma_1} \sum_{i=1}^{n} \frac{u_i^T b v_i}{\frac{\sigma_i}{\sigma_1}} \quad (5.64)$$

When [A] is ill-conditioned, $\frac{\sigma_n}{\sigma_1}$ is usually very small and also very sensitive to the noise effects. From equation(5.64), it can be noted that $\{f_b\}$ is significantly affected by the small singular values and thus the measurement errors. In other words, the force $\{f_b\}$ can be unrealistic due to the effects of measurement errors.

For a physical system, the structure tends to be in the minimum energy state, that is, the structure tends to be in a state with minimum strain and stress. If [A] in equation (5.62) is ill-conditioned, it may be a reasonable assumption that the force $\{f_b\}$ is very close to the force in a neighbouring state with

$$[A']=[U][\Sigma'][V]^H \quad (5.65)$$

where $[\Sigma']$ is the same as $[\Sigma]$ in equation(5.58) except that all the singular values less than a faction of the maximum singular value ($\varepsilon\sigma_1$) are set to zero.

For the singular matrix [A'], the solution with minimum norm is

$$\{f_b\}=[V][\Sigma']^+[U]^H\{b\}$$

$$= \frac{1}{\sigma_1} \sum_{i=1}^{m} \frac{u_i^T b v_i}{\frac{\sigma_i}{\sigma_1}} \quad (5.66)$$

where m is the number of singular values retained, i.e.

$$\frac{\sigma_m}{\sigma_1} > \varepsilon \geq \frac{\sigma_{m+1}}{\sigma_1} \quad (5.67)$$

§5.8.3 New Development in Selection of Effective Joint Coordinates

There is a problem in using the SVD algorithm to eliminate the effects of the measurement errors, this is the determination of the threshold ε for the smallest singular value. If the threshold is too small, the effects of errors will be significant. When the threshold is too large, the system properties are significantly altered.

If several pairs of joint coordinates are situated in a relatively rigid region of the structure, when one pair of these coordinates in each direction are coupled, the responses at other pairs of coordinates will be very close (exactly the same if these coordinates situated in an absolutely rigid region). Therefore, it is only necessary to couple one pair of coordinates in one direction.

Urgueira[99] suggested that it is appropriate to eliminate some approximate linearly dependent coordinates. He suggested that the linearly dependent coordinate pairs can be detected using the QR factorisation on the projections of $[U_1][U_1]^H$. However, only a simple case was tested and no mathematical proof was given to guarantee that the algorithm will work for more complicated cases. The process itself can also be time consuming.

Using the MTC method, it is possible to couple two coordinates on the same structure together. Synthesis of substructures is implemented by coupling two joint coordinates at one time and coupling all the joint coordinates using several steps. If the response at two pairs of joint coordinates are linearly dependent or near linearly dependent, then once one pair of coordinates are coupled, the responses at the other coordinate pair will be very similar to each other (exactly the same if they are exactly linearly dependent).

The inversion for two coordinate coupling is

$$([H_{ii}]+[H_{jj}]-[H_{ij}]-[H_{ji}])^{-1}=\frac{1}{h_{ii}+h_{jj}-2h_{ij}} \tag{5.68}$$

If two coordinates are linearly dependent, the response at these two coordinates will be 'similar', hence

$$h_{ii}\approx h_{jj}\approx h_{ij} \tag{5.69}$$

The dependency of two coordinates can be investigated using a parameter

$$\alpha=\frac{|h_{ii}-h_{jj}|+|h_{ii}-h_{ij}|+|h_{ij}-h_{jj}|}{|h_{ii}|+|h_{jj}|+|h_{ij}|} \tag{5.70}$$

The threshold MTC formulae becomes:

$$[H_a]=[H_s] - \beta(\{h_{sj}\}-\{h_{si}\})(\{h_{sj}\}-\{h_{si}\})^T \tag{5.71}$$

$$\text{where } \beta=\begin{cases} \dfrac{1}{h_{ii}+h_{jj}-2h_{ij}} & \alpha > \varepsilon \\ 0 & \alpha \leq \varepsilon \end{cases} \tag{5.72}$$

The linear dependency between the coordinates is automatically checked using the MTC method, no additional checking is required (such as the method suggested by Urgueira[99]). In addition, this method is physically more significant than Urgueira's method.

However, experience indicates that the α value can be very large at the anti-resonance of h_{ii}, h_{jj} or h_{ij}, even if the coordinate pair should be eliminated. If the α value is set to be large enough so that the rigid joint pair are deleted at all the frequencies, some other joint coordinate pairs can be deleted too, which results in an erroneous prediction.

An alternative way is to divide the coupling process into two steps. First, all the coordinate pairs are coupled with α values calculated over the frequency range. These α values are checked over a frequency range to determine if some pairs of the coordinates should be deleted. The coupling process is carried out again with the exclusion of the linear-dependent coordinate pairs.

§5.9 NUMERICAL CASE STUDIES

§5.9.1 Verification of Various Coupling Methods

Case A. A 7DOF System.

The substructure system consists of three substructures as shown in figure 5.8. There are three joints to connect three substructures together, these are the coordinate pairs (2, 5), (3, 6), and (4,7).

If the GIC or GRC are used, only one step is required to couple all three structures together; if the RC method is used, then two steps have to be taken to couple the three structures together, in the first step, two substructures should be coupled, then the coupled structure and the other substructure are coupled together. If the MTC method is used, three steps should be used.

Figure 5.9 shows the results of coupling using different methods. To distinguish the results from different coupling methods, the curves using different methods are shifted by

different constant levels (with even space 15dB). It can be noted that all the methods give correct results.

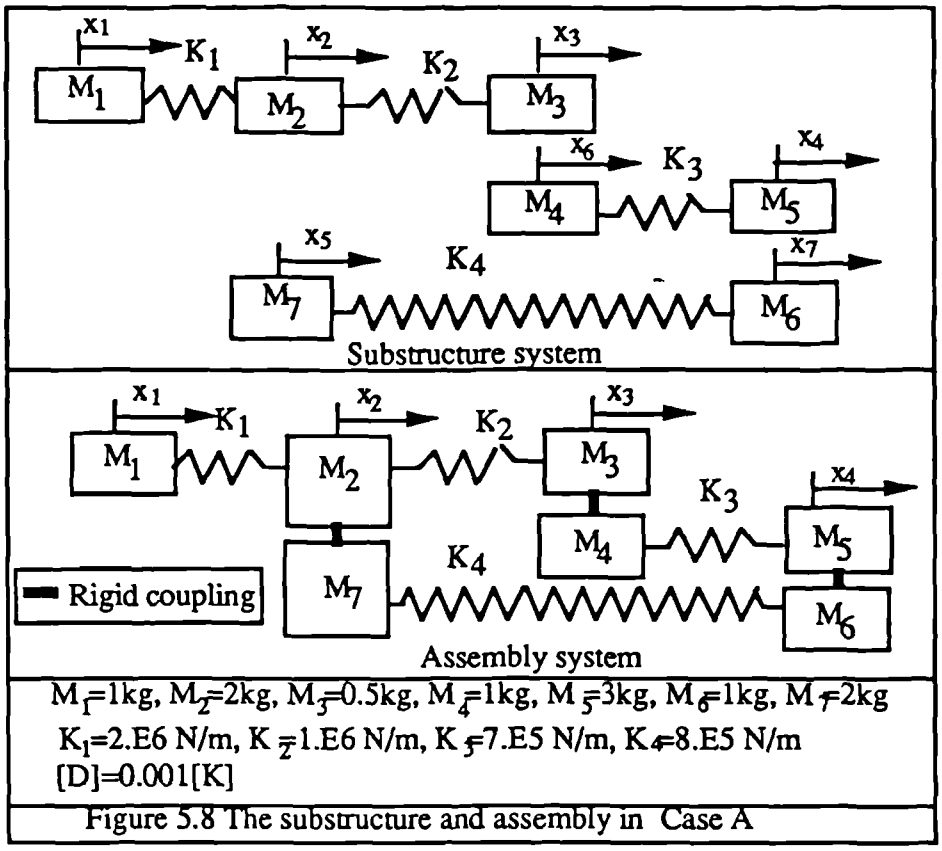

M_1=1kg, M_2=2kg, M_3=0.5kg, M_4=1kg, M_5=3kg, M_6=1kg, M_7=2kg
K_1=2.E6 N/m, K_2=1.E6 N/m, K_3=7.E5 N/m, K_4=8.E5 N/m
[D]=0.001[K]

Figure 5.8 The substructure and assembly in Case A

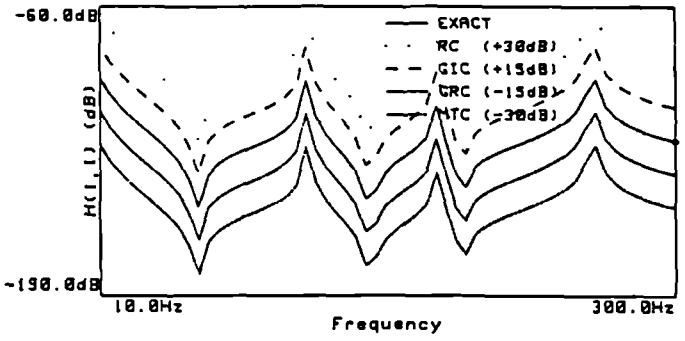

Figure 5.9 The predicted assembly point receptance (at point 1) using different coupling methods for case A (error free)

Case B: An 8DOF system

This case study will show an application of the PCC method. The total DOF is eight with coordinate 1 grounded, and coordinates 3, 4, 5, 6 and 7 coupled together. Therefore, the final assembly is a 3DOF system. The diagram for the substructure and assembly system is shown in figure 5.10.

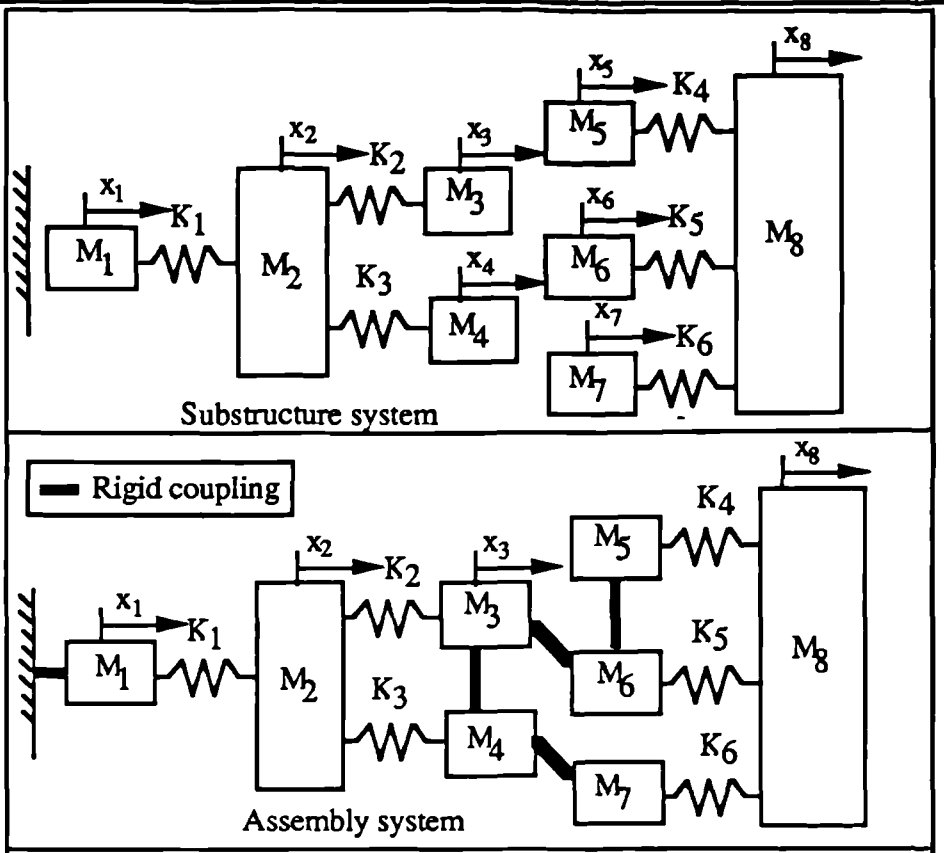

M_1=1kg, M_2=4kg, M_3=2kg, M_4=M_5=1kg, M_6=3kg M_7=2kg, M_8=5kg
K_1=1.E6 N/m, K_2=2.E6 N/m, K_3=4.E6 N/m, K_4=5.E6 N/m
K_5=2.E6 N/m, K_6=1.E6 N/m, [D]=0.001[K]

Figure 5.10 The substructure and assembly in case B

The purpose of this case study is to show the principles of the PCC method. It is clear that the ordinary RC method is not applicable in this case.

If the coupling should be implemented in a single step, the following five coordinate pairs are assumed

$(x_3,x_6),(x_3,x_4),(x_4,x_7),(x_5,x_6)$ and (x_1,x_0)

where coordinate x_0 refers to a coordinate on the ground. Consequently, there are in total ten joint coordinates in which only six coordinates are real. In the coupling process, a 5× 5 matrix is to be inverted.

Figure 5.11 shows the coupled results using different coupling techniques.

From the above two examples, it is clear that all the methods(GIC, RC, GRC, MTC, PCC) are correct if they are applicable. From the computational point of view, GRC, MTC and PCC methods are more efficient.

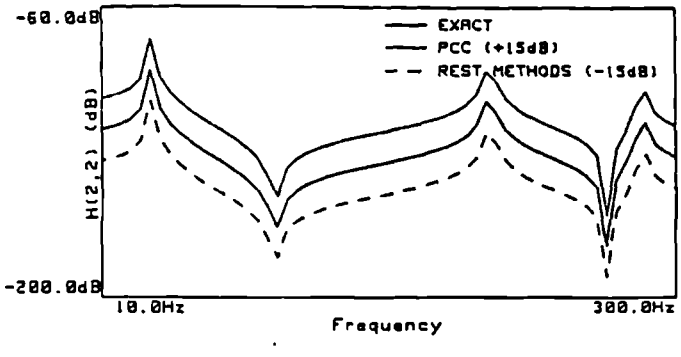

Figure 5.11 The predicted assembly point receptance (at point 2) using different coupling methods for case B (error free)

§5.9.2 The Effects of Random Noise and Elimination of Random Noise Using Modal Analysis Techniques

When the measurement data are polluted by random noise (5%), the coupled results deteriorate. Figure 5.12 and figure 5.13 show the coupled results for case A and case B. In both cases, the results from all of the coupling methods are not exact, however, the results from different coupling methods are the same. This indicates that all the coupling methods give exactly the same results if no numerical errors are involved.

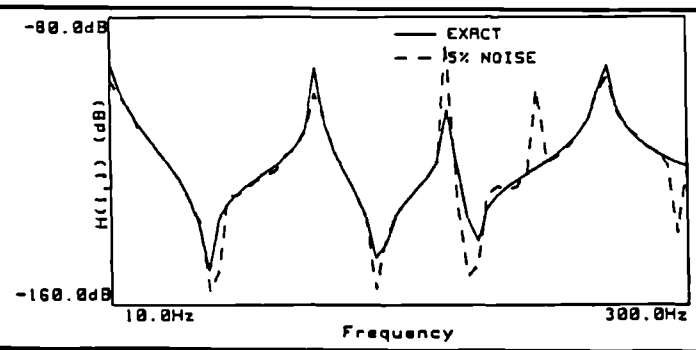

Figure 5.12 Comparison between the predicted and exact assembly point receptance for case A (5% random errors)

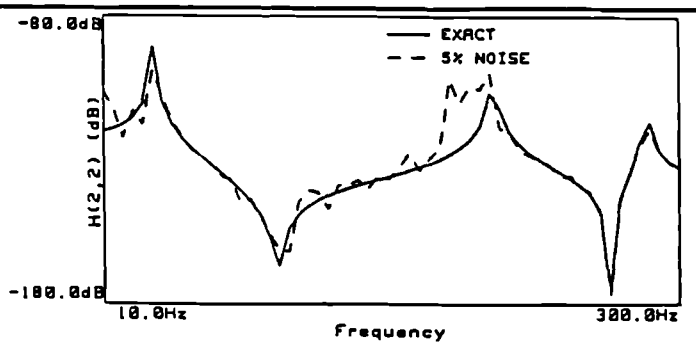

Figure 5.13 Comparison between the predicted and exact assembly point receptance for case B (5% random errors)

Some peaks can be found in the coupled receptance data, which do not represent real resonance frequencies. Further investigation indicates that the frequencies of these peaks

correspond to the natural frequencies of the substructures. The reasons for these peaks are that the substructure matrix at these frequencies tends to be ill-conditioned, consequently, the errors in the measurement data are significantly magnified. In addition, the magnitude of the substructure FRFs are much greater than the magnitude of the assembly at the substructure resonance. From equation(5.36), it can be noted that the assembly FRF matrix is a subtraction between the substructure FRF matrix and a product of three matrices. These two matrices must have similar magnitudes so that the assembly response will be much smaller than the substructure response. Therefore, the results are sensitive to errors even if the errors in the matrix inversion are not magnified.

At frequencies other than the substructure natural frequencies, the errors in the coupled results are much smaller.

If the modal analysis technique is applied, a consistent model can be obtained. The receptance matrix can be regenerated from

$$[H]=[\phi][\,(\omega_r^2 - \omega^2+i\eta_r\omega_r^2)\,]^{-1}[\phi]^T \qquad (5.65)$$

To simulate the data after applying modal analysis, the mode shape matrix $[\phi]$, natural frequencies ω_r (r=1,n) and damping η_r(r=1,n) are polluted by 5%, 1% and 1% random errors, respectively.

Figure 5.14 and figure 5.15 show the coupled results with modal analysis techniques applied to measured substructure data. It can be seen that the results are much smoother, the pseudo resonant peaks having disappeared. This indicates that by eliminating inconsistent errors in the measured data, the effects of measurement errors on the coupled results can be reduced.

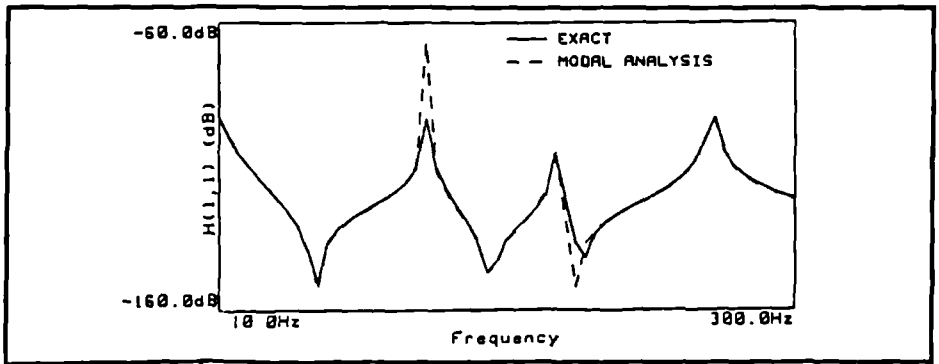

Figure 5.14 Comparison between the predicted and exact assembly point receptance for case A (using modal analysis)

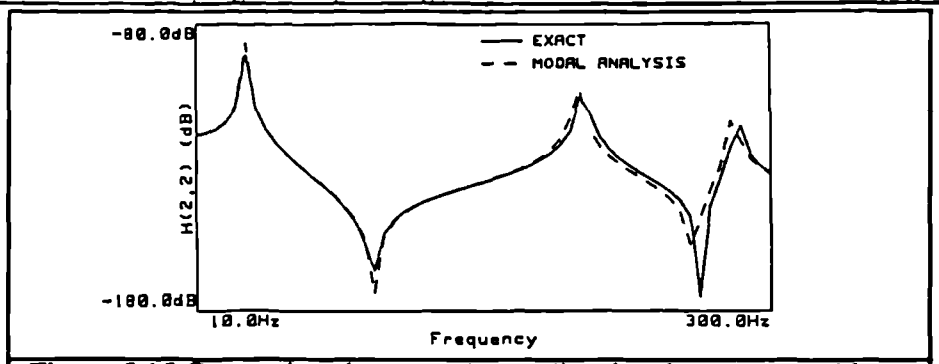

Figure 5.15 Comparison between the predicted and exact assembly point receptance for case B (using modal analysis)

However, the elimination of inconsistent errors does not mean that the coupled results are bound to be accurate. Applying modal analysis cannot eliminate consistent errors, and indeed, consistent errors may be introduced during the application of modal analysis. It is noted that there are some shifts between the predicted and real natural frequencies of the assembly from figure 5.14 and figure 5.15. The effects of these consistent errors will be investigated in the next section.

§5.9.3 Effects of Consistent Measurement Errors and Reduction of the Effects of Measurement Errors Using Threshold SVD and MTC.

Case C: An effective 7-DOF system

Applying modal analysis can eliminate the inconsistent errors, but consistent errors are retained or even introduced during modal analysis. These consistent errors can have significant effects on the coupling. To illustrate this, consider the 11-DOF system shown in figure 5.16. Coordinates 1,2,3,4 and 5 are coupled to coordinates 10,9,8,7 and 6 respectively.

It can be seen that k_1, k_4, k_8 and k_{11} are 1000 times greater than other springs, therefore the responses at the coordinates connected through these springs (eg. coordinates 1 and 2) are approximately the same at low frequencies. Physically, it is known that once coordinates 1 and 11 are coupled, the responses at coordinates 2 and 10 are very close; further, coupling coordinates 2 and 10 together has little effect on the properties of the assembly. Therefore, it is not necessary to couple coordinates 2 and 10. Similarly, it is only necessary to couple one pair of coordinates in the coordinate pairs (4,8) and (5,7).

Figure 5.17 show the predicted receptance from coupling three pairs of coordinates ((1,11), (3,9) and (5,7)), from coupling five pairs of coordinates ((1,11), (2,10), (3,9), (4,8) and (5,7)) . It is noted that the differences between the results are negligible.

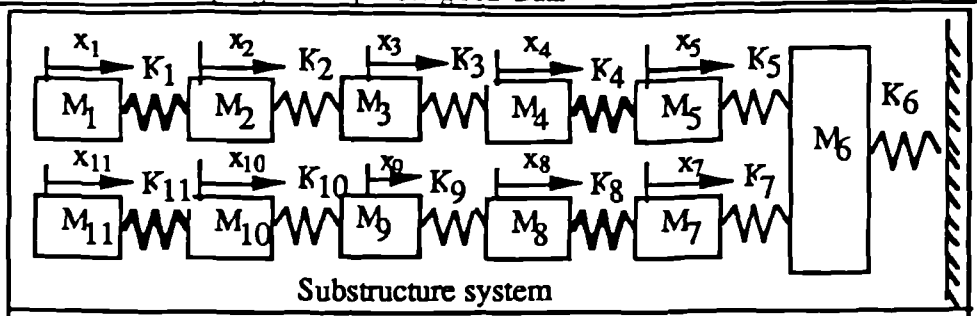

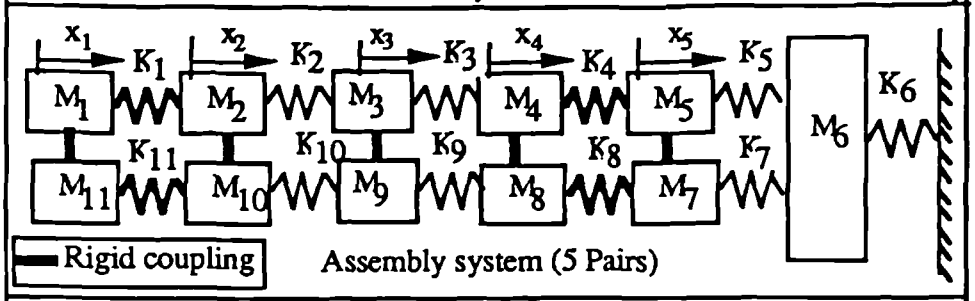

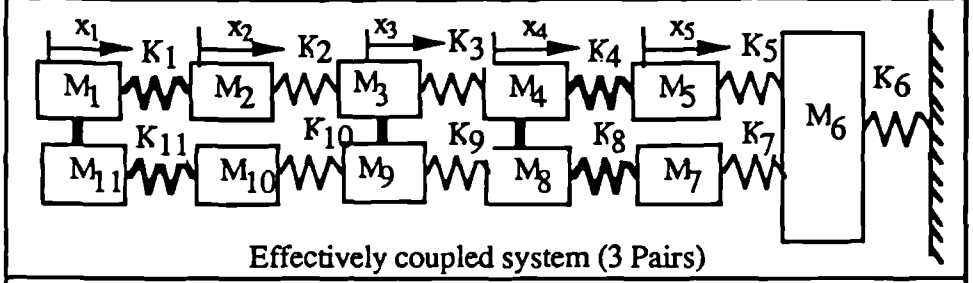

M_1=1kg, M_2=2kg, M_3=3kg, M_4=4kg, M_5=5kg

M_6=M_7=M_8=M_9=M_{10}=M_{11}=1kg

K_2=K_3=K_5=K_6=K_7=K_9=K_{10}=1.E6 N/m

K_1=K_4=K_8=K_{11}=1.E9 N/m

[D]=0.001[K]

Figure 5.16 Diagram for substructure and assembly system of case C

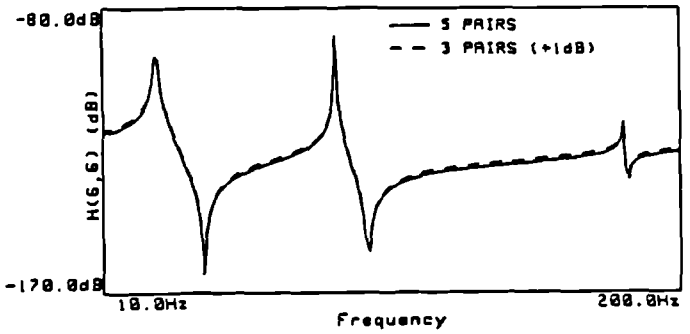

Figure 5.17 The assembly receptance by coupling 5 and 3 pairs coordinates (error free)

If the receptance matrix is polluted by random errors(5%), because the substructure receptance matrix is rank-deficient due to local rigidity of the interfaces, the coupled results are very sensitive to noise. Figure 5.18 and figure 5.19 show the predicted

assembly response using the GRC method. It is noted that the results from coupling three coordinate pairs ((1,11), (3,9) and (4,8)) are much better than those from coupling five coordinate pairs.

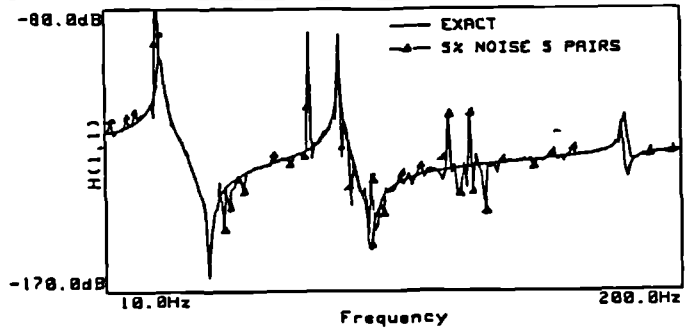

Figure 5.18 The assembly receptance by coupling 5 pair coordinates (5% random errors)

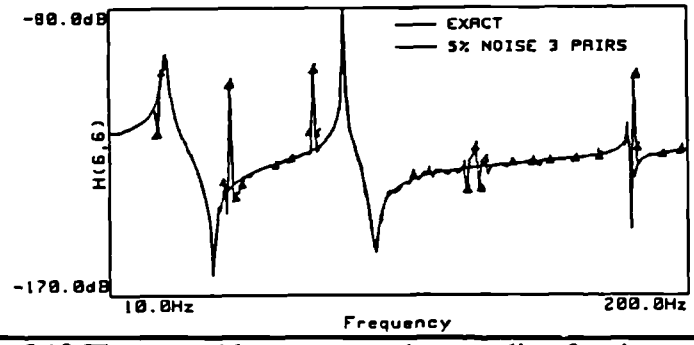

Figure 5.19 The assembly receptance by coupling 3 pair coordinates (5% random errors)

If modal analysis is applied, inconsistent errors can be removed, but the effects of the consistent errors are still significant. Figure 5.20 and figure 5.21 show the predicted assembly data using simulated modal analysis data (with 5%, 1% and 1% errors in mode shape, natural frequency and modal damping) using the GRC method. It is noted that although the predicted results are smooth curves, it is quite different from the real assembly response (especially for the second resonance). The second resonance frequency is significantly shifted for five pair coupling, however, the results from coupling only three pairs ((1,11), (3,9) and (4,8)) yield very high accuracy .

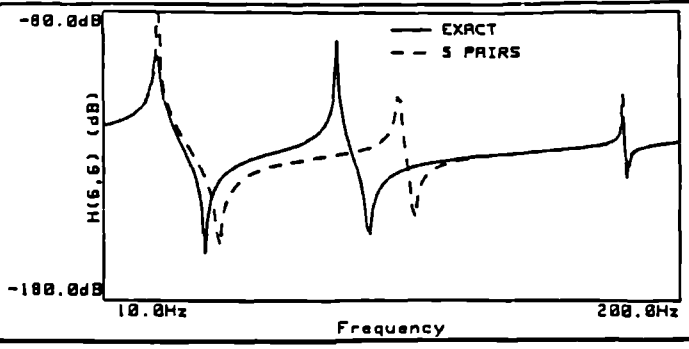

Figure 5.20 The assembly receptance by coupling 5 pair coordinates (after modal analysis)

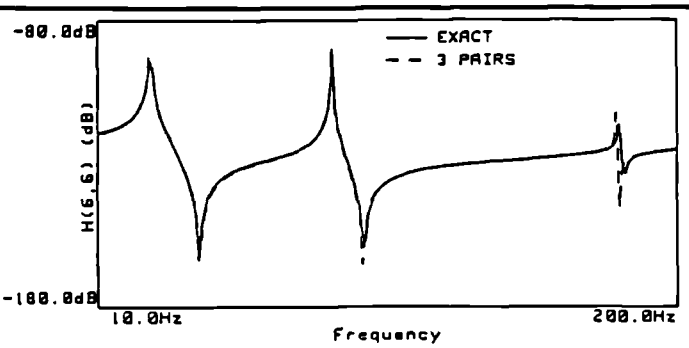

Figure 5.21 The assembly receptance by coupling 3 pair coordinates (after modal analysis)

Figures 5.22, 5.23, 5.24 show the results using the GRC method with the threshold SVD algorithm. If ε=0.01, very good results are found; however, if ε is too large (0.05) or too small (0.001), the results at some frequencies are very poor. Because the proper value of ε depends on the size of matrix to be inverted and the frequency increment, it is usually very difficult to determine the threshold of the SVD. Indeed, if a very fine frequency increment is chosen, it is possible that no threshold is available to yield accurate results at all the frequencies.

To avoid the dependency of the threshold on the size of the coupling, the threshold MTC method is used. Figures 5.25, 5.26 and 5.27 show the results using the threshold MTC method. It is noted when ε=0.3, the accuracy of the results is improved significantly, however, at some frequency points, the results are poor (which coincides with the results of four or five pair coupling).

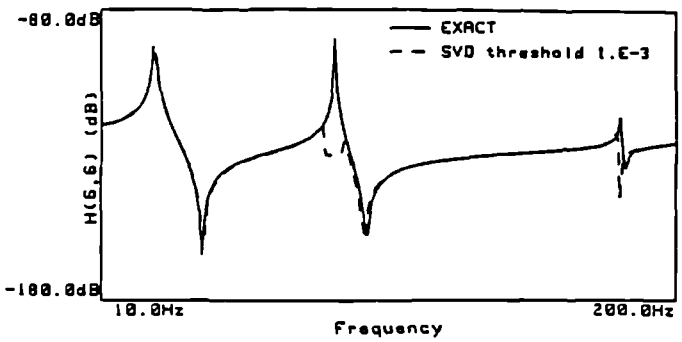

Figure 5.22 The assembly receptance using SVD with threshold 1.E-3

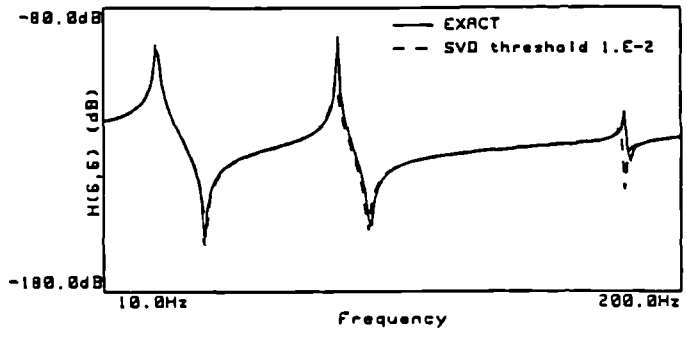

Figure 5.23 The assembly receptance using SVD with threshold 1.E-2

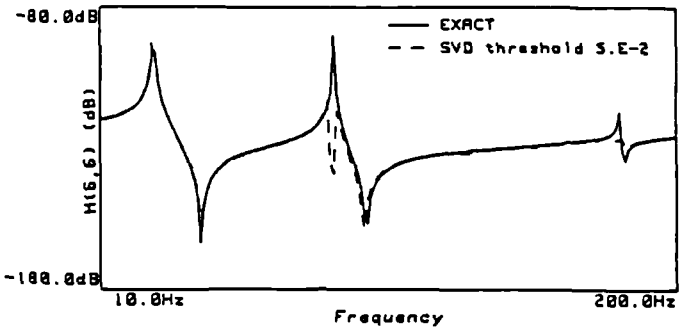

Figure 5.24 The assembly receptance using SVD with threshold 5.E-2

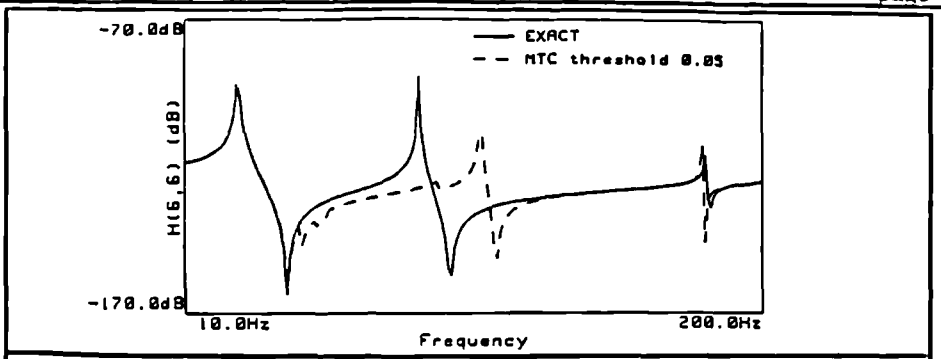

Figure 5.25 The assembly receptance using MTC with threshold 5.E-2

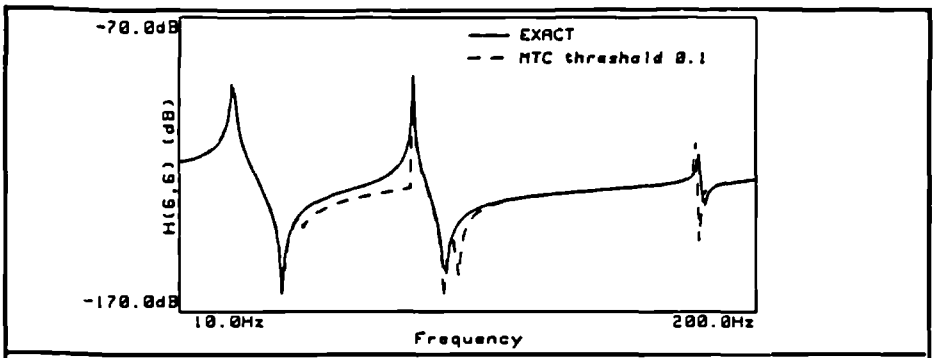

Figure 5.26 The assembly receptance using MTC with threshold 1.E-1

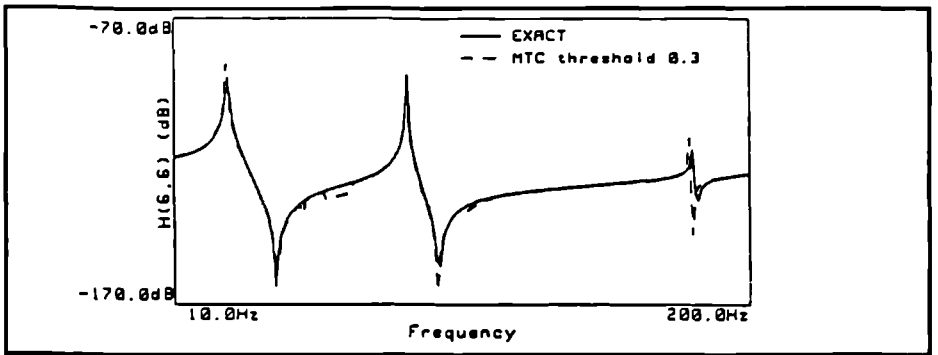

Figure 5.27 The assembly receptance using MTC with threshold 3.E-1

In order to obtain a more accurate assembly response, the problem of linear dependent coordinate pairs can be dealt with systematically. The α values over the frequency range are shown in figure 5.29 for the error-free case, figure 5.31 for the case with consistent errors and figure 5.32 for the case with random errors. From all of the three figures, it can be clearly noted that the overall α values for coordinate pairs (2,10) and (5,7) are smaller than the α values of the other pairs, which indicates that coordinate pairs (2,10) and (5,7) clearly tend to be dependent on other joint coordinate pairs.

The peaks of the α values for the coordinate pairs (2,10) and (5,7) in figure 5.29 and figure 5.31 correspond to the anti-resonance of the these coordinates when they are to be coupled. The point receptance curves at coordinates 2 and 5 just before they are coupled (i.e. the receptance at coordinate 2 after coupling coordinate (1,11) and the receptance at

coordinate 5 after coupling coordinates (1,11), (2,10), (3,9) and (4,8)) for the error free case and the case with consistent errors are shown in figures 5.28 and 5.30.

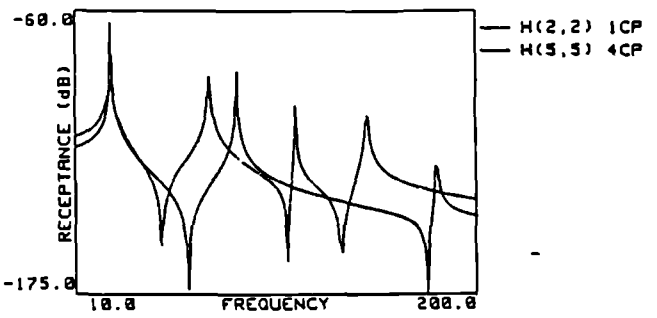

Figure 5.28 The receptance at the coordinates 2 and 5 before they are coupled (error free)

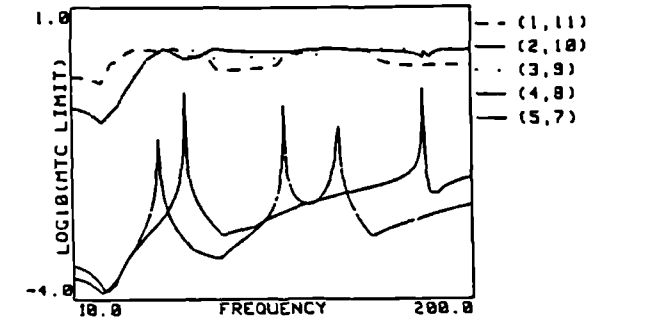

Figure 5.29 The α values for different coordinate pairs using MTC method (error free)

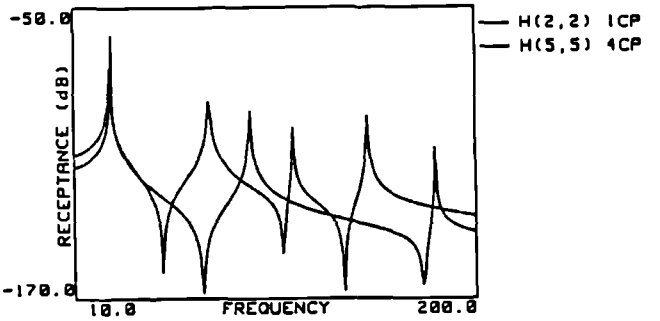

Figure 5.30 The receptance at the coordinates 2 and 5 before they are coupled (modal analysis)

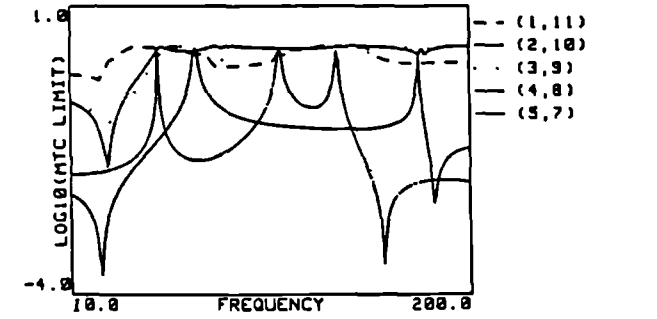

Figure 5.31 The α values for different coordinate pairs using MTC method (modal analysis)

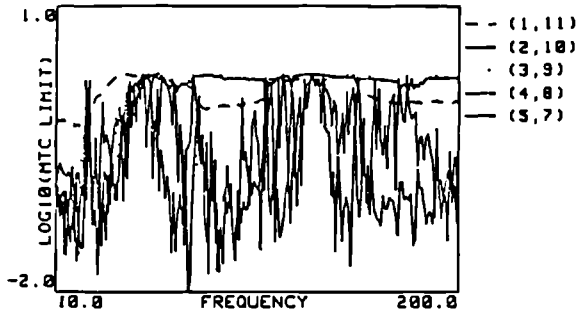

Figure 5.32 The α values for different coordinate pairs using MTC method (5% random errors)

§5.9.4 Discussion of Numerical Results

The numerical results shown above demonstrate the various coupling methods. When numerical errors are insignificant, all the coupling methods yield the same results. Also the newly developed GRC, PPC and MTC methods are verified in the above numerical studies.

The measurement noise may be divided into consistent and inconsistent errors. It is shown in the numerical studies that the inconsistent errors can be eliminated by using modal analysis techniques. However, modal analysis techniques have little effect on reducing consistent errors. The threshold SVD technique is useful in reducing the effects of consistent errors, however, the choice of the proper threshold for the SVD can be difficult.

With the newly developed MTC algorithm, the linearly dependent coordinate pairs can be detected by checking the α values. Then the dependent coordinate pairs can be deleted. However, care should be taken in deleting approximately linearly dependent coordinate pairs. If the one coordinate pair is not severely dependent on the other pairs, deleting this coordinate pair will cause error in the predicted response . However, the predicted assembly responses including and excluding this coordinate pair should yield the upper and lower bounds of the natural frequencies for the real assembly response.

Another point that can be drawn from the numerical case studies is that the predicted resonance frequencies of the assembly can be different from the true values due to the consistent errors in the measured data. In many applications, the effects of joints are often blamed for the discrepancy between the predicted and measured assembly response. From the above studies, one should be aware that the discrepancy can also be the results of the consistent errors

§5.10 CONCLUSIONS

A new generalized coupling method (GRC) method is proposed in this chapter, which is physically more general than the RC method and is computationally more efficient than the GIC method. The GRC method takes the advantages from both the GIC and the RC methods, hence it is superior to the GIC and the RC methods. The RC method can be considered as a special case of the GRC method.

Using the GRC method, the coupling procedure can be implemented in a single step. If several substructure coordinates are to be coupled into one assembly coordinates, then the concept of pseudo coordinates can be used, which leads to the PCC method.

In contrast to implementation of coupling in a single step, the coupling can be implemented by coupling two coordinates at one step and complete the coupling in several steps systematically. This leads to the MTC method. The MTC method is computationally more efficient (it requires less multiplications than the GRC method) and also easier to program.

The modal analysis technique is very effective in eliminating inconsistent errors, but not in eliminating consistent errors.

The SVD algorithm can be effective in eliminating consistent errors, but it is usually not easy to determine a proper threshold for the algorithm. When the threshold is too large or too small, the assembly results are erroneous.

The threshold MTC method is very useful for detecting the dependency between the joint coordinate pairs. But the process to delete the linearly dependent coordinate pair should be used with caution.

CHAPTER 6

IDENTIFICATION OF JOINT PROPERTIES USING FRF DATA

§6.1 INTRODUCTION

In Chapter 2, various friction joint models have been discussed. Because there are too many parameters that can affect the overall behaviour of the joint, it is suggested that the intermediate parameters should be used to represent the joint.

Once a joint is made, most of the parameters (such as the surface conditions and the geometric shape of the joint) are fixed. However, some parameters can still be changed, one of these being the pressure at the interface.

In Chapter 2, it is shown that the joint parameters can be identified from the static loading curves. Theoretically, it is possible to identify the relationship between the variation of the intermediate joint parameters and the change of the pressure from a series of experimental loading curves under different pressures. Once these relations are known, provided the pressure distribution over the interface is also known, the overall characteristics of the joint can be found using the finite element method discussed in Chapter 2.

However, the application of this approach can be rather expensive. In addition, the pre-condition to apply this approach is that the pressure distribution over the joint interface is known. Unfortunately, this pre-condition is not always satisfied. Apart from these difficulties, the interface conditions may change due to some unexpected factors such as fretting corrosion and contamination at the interface. These changes make the intermediate joint parameters invalid. Therefore, the above approach can also be inaccurate.

When a jointed structure is excited by a dynamic load, the relationship between the excitation and the response of the structure contains structural information (including the joint effects). Therefore, it should be possible to identify the joint properties from the relationship between the excitation and the response.

Although the behaviour of a friction joint is usually nonlinear, if the vibration magnitude is small, the friction joint behaves like a linear component. On the other hand, using the principle of the harmonic balance method, even a nonlinear joint can be treated

approximately as a linear component (an experimental case with a nonlinear friction joint is investigated in Chapter 7). Therefore, to identify the nonlinear joint, it is appropriate to start by developing methods for the identification of linear joints. After a full understanding of linear joint identification is obtained, the method may be extended to identify the nonlinear joint, or the new method can be developed to deal with the problem of the nonlinear joint identification based on the understanding in the linear joint identification approach.

In this chapter, linear joint identification methods are studied. A new FRF based method is developed and techniques to improve the accuracy of the identification results are presented.

§6.2 BACKGROUND OF THE JOINT IDENTIFICATION METHODS

From the research carried out, several identification methods have been proposed. As with the coupling methods, they can be divided into two groups according to the type of data used in identification, one uses the measured Frequency Response Function (FRF) data [110][111] directly, the other processes the FRF data first to obtain modal data and then uses modal data for the identification of the joints [104][112][113].

For the methods using modal data, a finite element model is usually required. The basic strategy is to minimise the difference between the measured and the predicted mode shapes and natural frequencies (from the FE model) by adjusting the joint parameters by using the Newton-Raphson iteration algorithm (this technique is also referred to as the inverse sensitivity analysis technique).

For the methods using FRF data, the basic strategy is to minimise the FRFs between the measured assembly response and predicted assembly response.

The first group of methods has some advantages over the second group. Firstly, no data pre-processing is required, hence no processing error is introduced. Secondly, an analytical model is not necessary, therefore, modelling errors do not exist (and there is no FE modelling cost either). In addition, (perhaps most attractively), the methods are principally applicable to non-linear structures: this is discussed in §6.3.

Two sets of data are required for joint identification: one contains the system properties without the joint (the substructure system), the other contains the system properties with joint (the assembly system). These differences between these two systems are due to the effects of the joints.

Usually, the assembly data are experimentally derived, but for the data on substructures, some are obtained from an FE model and the other from measurements. If the data from an FE model are used, the identified joint model will not be "real", but the "best" to

compensate the effects of joint and the modelling errors in the FE model. If experimental data are used, the identified joint model will be "real", but may be polluted by some measurement errors. If real joint properties are required, it may be more appropriate to use the experiment data.

The earliest joint identification method using FRF data was proposed by Tsai and Chou [104] in 1988 and Wang and Liou [112] in 1989. The methods developed are not generalized; the joints are explicitly [112] or implicitly [104] assumed to consist of elastic springs.

In the following sections, two new generalized joint identification methods are developed. It is found that unlike the coupling methods, the accuracy of the identified joint results are closely related to the identification formulae if the FRF data are polluted by measurement errors. A generalized method was found to be superior to the other. Similar identification formulae have been proposed by Lee and Hong [113] very recently (1991).

Most of this chapter is devoted to developing new techniques to reduce the effects of the measurement errors.

§6.3 DEVELOPMENT OF NEW GENERALIZED JOINT IDENTIFICATION METHODS

§6.3.1 General

In the following studies, two systems are used. The first is a system of substructures (all of the joints are considered as an independent joint substructure) and the second is an assembly as shown in figure 6.1.

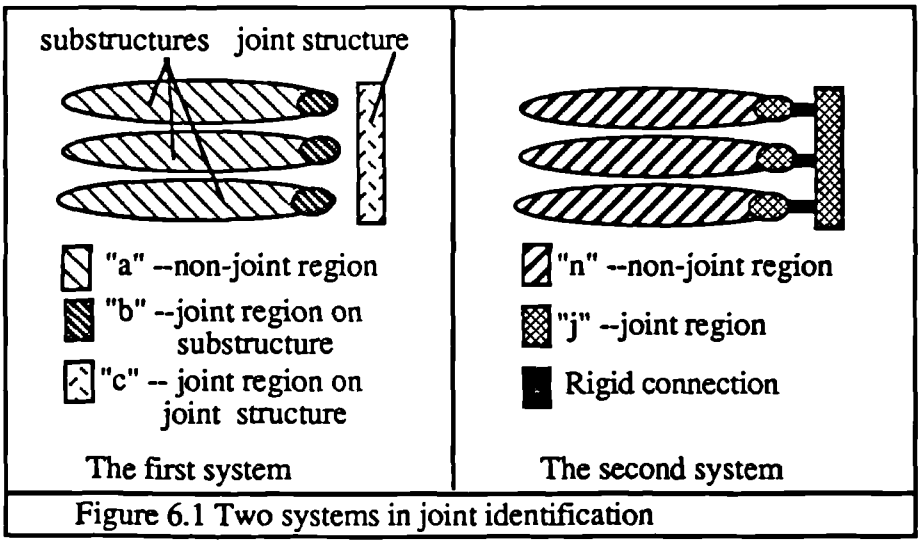

Figure 6.1 Two systems in joint identification

The regions in the second system are divided into non-joint and joint regions which are represented by subscripts n and j respectively. The coordinates in the non-joint region and

joint region are called **"non-joint coordinates"** and **"joint coordinates"** respectively. For the first system, there is a region which corresponds to the non-joint region in the second system, and this is represented by subscript a; the remaining region in the first system can be subdivided into the joint region on real substructures, and on the joint substructure, which are represented by subscripts b and c respectively.

The relationship between the displacement vectors and the force vectors for the assembly and the substructures (excluding joint substructure) are:

$$\begin{Bmatrix} x_n \\ x_j \end{Bmatrix} = \begin{bmatrix} H_{nn} & H_{nj} \\ H_{jn} & H_{jj} \end{bmatrix} \begin{Bmatrix} f_n \\ f_j \end{Bmatrix} \qquad (6.1)$$

and

$$\begin{Bmatrix} x_a \\ x_b \end{Bmatrix} = \begin{bmatrix} H_{aa} & H_{ab} \\ H_{ba} & H_{bb} \end{bmatrix} \begin{Bmatrix} f_a \\ f_b \end{Bmatrix} \qquad (6.2)$$

where H,x and f represent the receptance, displacement and force respectively, and subscripts on H,x,and f represent the regions where H,x and f are related. eg. H_{ab} is the receptance matrix with response at region a and excitation at region b.

For the joint structure, we have

$$[Z_j]\{x_c\}=\{f_c\}, \qquad (6.3)$$

where $[Z_j]$ is the impedance matrix of the joint substructure.

§6.3.2 Development of Method One

The derivation of this generalized identification method is very similar to the derivation of the formulae for the GRC method in Chapter 5. The non-joint coordinates on the substructure and assembly systems are actually the same, hence:

$$\{f_a\}\equiv\{f_n\}, \qquad (6.4)$$

and

$$\{x_a\}\equiv\{x_n\}. \qquad (6.5)$$

The conditions of compatibility and equilibrium must be satisfied at the joint coordinates after assembly of the structure (see figure 6.1), therefore

$$\{f_b\}+\{f_c\}=\{f_j\}, \qquad (6.6)$$

and

$$\{x_j\}=\{x_b\}=\{x_c\}. \qquad (6.7)$$

Rearranging equation (6.6) as

$$\{f_b\}=\{f_j\}-\{f_c\} \tag{6.8}$$

and substituting equation (6.8) into equation (6.2) yields

$$\{x_b\}=[H_{ba}]\{f_a\}+[H_{bb}](\{f_j\}-\{f_c\}) \tag{6.9}$$

Substituting equations (6.4), (6.5), (6.7), (6.8) and (6.9) into equation (6.2) and deleting $\{f_c\}$ and $\{x_b\}$, the following equation is obtained

$$\{f_b\}=[[I]-[Z_j][H_{bb}]]^{-1}(\{f_j\}-[Z_j][H_{ab}]\{f_n\}) \tag{6.10}$$

Substituting equations (6.5)(6.7) and equation (6.10) into equation (6.2), and rearranging leads to

$$\begin{Bmatrix} x_n \\ x_j \end{Bmatrix} = \begin{bmatrix} [H_{aa}]-[H_{ab}]([I]+[Z_j][H_{bb}])^{-1}[Z_j][H_{ba}] & [H_{ab}]([I]+[Z_j][H_{bb}])^{-1} \\ [H_{ba}]-[H_{bb}]([I]+[Z_j][H_{bb}])^{-1}[Z_j][H_{ba}] & [H_{bb}]([I]+[Z_j][H_{bb}])^{-1} \end{bmatrix} \begin{Bmatrix} f_n \\ f_j \end{Bmatrix} \tag{6.11}$$

Comparing equation (6.11) with equation (6.1), it can be noted that

$$\begin{cases} [H_{nn}]=[H_{aa}]-[H_{ab}]([I]+[Z_j][H_{bb}])^{-1}[Z_j][H_{ba}] & (6.12) \\ [H_{nj}]=[H_{ab}]([I]+[Z_j][H_{bb}])^{-1} & (6.13) \\ [H_{jn}]=[H_{ba}]-[H_{bb}]([I]+[Z_j][H_{bb}])^{-1}[Z_j][H_{ba}] & (6.14) \\ [H_{jj}]=[H_{bb}]([I]+[Z_j][H_{bb}])^{-1} & (6.15) \end{cases}$$

Substituting equations (6.13) and (6.15) into equations (6.12) and (6.14) and rearranging equations (6.13) and (6.15), equations (6.12-6.15) become:

$$\begin{cases} [H_{nj}][Z_j][H_{ba}]=[H_{aa}]-[H_{nn}] & (6.16) \\ [H_{nj}][Z_j][H_{bb}]=[H_{ab}]-[H_{nj}] & (6.17) \\ [H_{jj}][Z_j][H_{bb}]=[H_{bb}]-[H_{jj}] & (6.18) \\ [H_{jj}][Z_j][H_{ba}]=[H_{ba}]-[H_{jn}] & (6.19) \end{cases}$$

Equations (6.16-6.19) are four basic formulae to identify the joint impedance matrix $[Z_j]$. The identification formulae are frequency based, i.e. the FRF data at one frequency are enough for the identification. This is a very attractive property. For a nonlinear joint, the properties at different frequencies are different, so that it is not possible to find a linear joint to represent the nonlinear joint over a wide range of frequencies. However, at one

frequency or in a narrow frequency range, the properties of the non-linear joint can be represented by an equivalent linear joint if an appropriate control process is taken in the experiment. This is one of the main reasons why the FRF data identification method is more attractive than modal data identification methods for non-linear joint studies.

§6.3.3 Development of Method Two

It can be noted that the procedure to develop method one in the last section is very similar to the procedure to develop the GRC method in Chapter 5. The method developed in this section is closely related to the other generalized coupling method, the GIC method. Partition the inverse of the substructure (system) receptance matrix in the same way as partitioning the substructure receptance matrix:

$$\begin{bmatrix} H_{aa} & H_{ab} \\ H_{ba} & H_{bb} \end{bmatrix}^{-1} = \begin{bmatrix} Z_{aa} & Z_{ab} \\ Z_{ba} & Z_{bb} \end{bmatrix} \tag{6.20}$$

Because the assembly is the structure generated by coupling the substructure and the joint together,

$$\begin{bmatrix} Z_{aa} & Z_{ab} \\ Z_{ba} & Z_{bb}+Z_j \end{bmatrix} \begin{bmatrix} H_{nn} & H_{nj} \\ H_{jn} & H_{nn} \end{bmatrix} = \begin{bmatrix} I & 0 \\ 0 & I \end{bmatrix}. \tag{6.21}$$

Expanding and rearranging equation(6.21) leads to

$$\begin{cases} [Z_j][H_{jn}] = -[Z_{ba}][H_{nn}] - [Z_{bb}][H_{jn}] & (6.22) \\ [Z_j][H_{jj}] = [I] - [Z_{ba}][H_{nj}] - [Z_{bb}][H_{jj}] & (6.23) \end{cases}$$

§6.3.4 The Availability of the Measurement Data

There are measurement difficulties in obtaining FRF data. Usually, the non-joint coordinates can be chosen for the convenience of the measurement, and therefore, the FRFs between the non-joint coordinates (i.e $[H_{aa}]$ and $[H_{nn}]$) are easy to obtain; however, the substructure FRFs between the non-joint and the joint coordinates (i.e.$[H_{ab}]$) are rather difficult to measure. The substructure FRFs between the joint coordinates (i.e. $[H_{bb}]$), and the assembly FRFs between the non-joint and the joint coordinates (i.e. $[H_{nj}]$) are even more difficult to obtain. The assembly FRFs between the joint coordinates $[H_{jj}]$) are the most difficult to measure.

If the receptance data of the substructure is from an FE model, then $[H_{aa}]$, $[H_{ab}]$ and $[H_{bb}]$ are always available.

To use equations (6.16-6.19) for the joint identification, sub-matrices $[H_{aa}]$, $[H_{nn}]$, $[H_{ab}]$ and $[H_{nj}]$ must be available(so that at least equations (6.16) and (6.17) can be used); to

use equation (6.22-6.23), $[H_{nn}]$, $[H_{nj}]$ and all the substructure receptance matrices must be available (so that equation(6.22) can be used). The minimum data required for method two are more than for method one.

§6.3.5 Comments on the Two New Generalized Methods

A significant advantage of the formulae developed in the last two sections over some of the other identification (or decoupling) methods is that they are not limited to the structure assembled from one joint and two substructures (comparing with [104]). There is also no pre-assumption on the properties of the joint (comparing with [112]). Distinguishing joint and non-joint coordinates gives a clearer view on the data required in the identification (comparing with [113])

Due to the generality of the identification formulae, they can also be applied to correcting the FE model (Model updating) using experimental data[114][115]. In fact, the problems of analytical model updating and joint identification are to find the difference between two systems, (i.e. for identification, one system is the assembly, the other consists of uncoupled substructures; for model updating, one system is the real structure, the other is the analytical model). From this point of view, model updating and joint identification are two phases of the same problem. If the mis-modelled region is known, the coordinates in the mis-modelled region can be treated as joint coordinates and mis-modelling parts can be identified. If the mis-modelled region is unknown, one has to assume that modelling errors exist in all the coordinates. In this case, the non-joint coordinates vanish and only equation (6.19) can be used. It can be proved that equation (6.19) is still valid when there is no non-joint coordinates and equation (6.19) becomes exactly the same as the formula previously developed by Lin *et.al* for analytical model improvement using FRF data [114].

Equations (6.16-6.19) and (6.22)(6.23) are actually a set of linear equations and solving these equations is mathematically simple.

§6.4 ALGORITHM FOR THE IDENTIFICATION OF THE JOINT PROPERTIES

All of the proposed identification equations (i.e.equations(6.16-6.19) or (6.22)(6.23)) have the following form

$$[A]_{M\times N}[Z_J]_{N\times N}[B]_{N\times L}=[C]_{M\times L} \qquad (6.24)$$

where [A], [B] and [C] are coefficient matrices, and M, N and L represent row or column numbers of a matrix. (for equations (6.22) and equation (6.23), [A] is a unit matrix)

If M,L≥ N and matrices [A] and [B] are nonsingular, equation (6.24) becomes determined or over-determined and $[Z_j]$ can be solved uniquely. If the input data (i.e. FRFs) are polluted by measurement errors, such over-determined equations usually have no exact solution. In this case, a least-squares method can be applied to minimize the effects of random errors in the input data. It has been proved [108][109] that the least-squares solution for equation (6.24) is

$$[Z_j]= [A]^+[C][B]^+ \tag{6.25}$$

Apart from the above solution, there is an alternative to obtain the least-squares solution for equation (6.24). Equation (6.24) is the same as a series of (M× L) linear equations

$$[E]_{(M\cdot L)\times(N^2)}\{z\}_{(N^2)\times 1}=\{g\}_{(M\cdot L)\times 1} \tag{6.26}$$

where E((m-1)L+l,(i-1)N+j)=A(m,i)B(j,L)

z((i-1)N+j)=Z_j(i,j)

g((m-1)L)=C(m,L)

(m=1···M, l=1···L, i=1···N, j=1···N)

Equation (6.26) is a set of standard linear algebraic equations whose least-squares solution is

$$\{z\}=[E]^+\{g\} \tag{6.27}$$

The solutions of both equations (6.25) and (6.27) are the least-squares solution of equation (6.24), and hence are exactly the same.

In terms of the computation efficiency, equation (6.25) is more attractive, because calculation of the pseudo inverses of two small matrices ($[A]_{M\times N}$ and $[B]_{N\times L}$) usually requires less computation time than that required for the inversion of a large matrix $[E]_{(M\cdot L)\times(N^2)}$. In addition, the rearrangement of equation (6.26) from (6.24) also takes time. However, equation (6.25) has some severe disadvantages which make equation (6.27) preferable in practical applications:

(i) Due to the effects of measurement errors in the FRF data, the results from different equations (6.16-6.19) or (6.22) (6.23) are usually different. Equation (6.26) can combine equations (6.16-6.19) or (6.22) (6.23) into a set of linear equations and hence give the least-squares solution to all these equations.

(ii): Equation (6.25) uses only a very small part of the available information for identification at one time, the information at different frequencies cannot be used together.

It will be shown later that the information at a single frequency point may not be enough to extract the joint parameters accurately when the measured FRFs are polluted by measurement errors. However, using equation(6.26), it is possible to combine the equations obtained from different frequencies together, hence increasing the total information for the identification.

(iii) Considerable effort should be devoted to collecting measured data. To use equation (6.25), the conditions that M, L≥ N and matrices [A] and [B] are not rank-deficient must be satisfied. If equation (6.26) is used, such conditions are not necessary. From equation (6.26), it can be seen that one row in matrix [A] and one column in matrix [B] together with one element in matrix [C] are the data required for one equation in equation(6.26) as shown in figure 6.2. If M,L≥ N is not satisfied, the equations obtained from (6.26) at each frequency are underdetermined, and the solution is not unique. However if the equations at different frequency points are combined together, or some constraints are imposed in solving equation (6.26), a unique least-squares solution can be obtained.

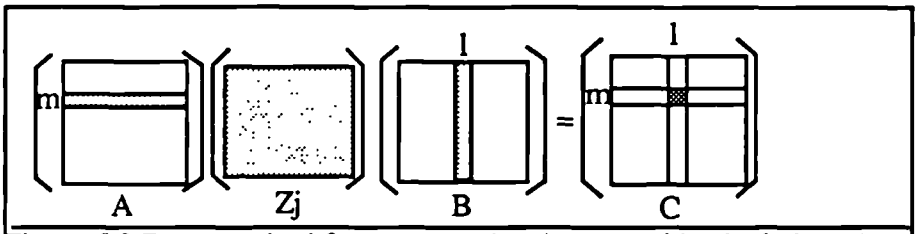

Figure.6.2 Data required for one equation (presented in shaded area)

(iv) There is a danger of losing the physical interpretation of the identified joint model. Experimental data are always contaminated by measurement errors so that the solution can only be an approximation. If equation (6.24) is used, we assume that no relations between the elements in the $[Z_j]$ matrix are known. In practice, some knowledge about the joints is usually available and, in some cases, must be retained in the identified joint results: for example, the symmetry of the $[Z_j]$ matrix is possessed by most of the mechanical joints some of the joint coordinates are obviously uncoupled if they belong to different joints. These properties cannot be retained if equation (6.24) is used. However, if equation (6.26) is used, they can be incorporated into the process for the solution by imposing a restriction matrix: this is discussed below.

§6.5 UTILIZATION OF THE TRANSFORMATION AND RESTRICTION

Because the measured data are contaminated by measurement errors, efforts have to be made to reduce the effects of the measurement errors on the accuracy of the identified joint properties.

The basic strategy to improve the accuracy of the identified results is to impose all the available constraints. In other words, the measured FRFs should be used at one time. A

by-product of using all of the FRF data at one time is that the identified results are consistent over the whole frequency range.

One problem in using all of the measured data at one time is to combine the information obtained at different frequencies. If the joint properties are independent of frequency, the equations obtained from different frequencies can be combined together directly. However, if the joint contains mass, the impedance matrix of the joint will be frequency dependent, then the equations at different frequencies cannot be combined directly. In this case, the frequency dependent unknowns must be first transferred into frequency independent unknowns.

The impedance of the joint can be written in terms of the stiffness, mass and damping matrices as follows.

$$[Z_j(\omega)]=[K]-\omega^2[M]+ i(\omega[C]+[D]) \tag{6.28}$$

where [K], [M], [C] and [D] represent the stiffness, mass, viscous and hysteretic damping matrices respectively

Unlike the impedance matrix, the mass, stiffness and damping matrices are frequency independent. Arranging all the elements in a matrix into a vector (eg. from [K] to {k}) and rewriting equation (6.28) in the vector form yields

$$\{z_i(\omega)\}=\{k\}-\omega^2\{m\}+ i(\omega\{c\}+\{d\})=[T_\omega]\{x\}, \tag{6.29}$$

where

$$[T_\omega]=\left[[I] \;\; -\omega^2[I] \;\; i\omega[I] \;\; i[I]\right], \tag{6.30}$$

and

$$\{x\}=\begin{Bmatrix}\{k\}\\ \{m\}\\ \{c\}\\ \{d\}\end{Bmatrix}. \tag{6.31}$$

Substituting equation (6.31) into equation(6.26)leads to

$$[E(\omega)][T_\omega]\{x\}=\{g(\omega)\} \tag{6.32}$$

Let

$$[\bar{E}'(\omega)]=[E(\omega)][T_\omega] \tag{6.33}$$

Equation (6.32) then becomes

$$[\bar{E}'(\omega)]\{x\}=\{g(\omega)\} \tag{6.34}$$

The vector {x}, which consists of the elements in the mass, stiffness and damping matrices, is frequency-independent, thus, equation (6.34) at different frequencies can be combined directly.

A problem with the transformation matrix $[T_\omega]$ is that the magnitudes of the elements corresponding to stiffness and mass (also viscous damping) elements are different by a factor of ω^2 (and ω for viscous damping), which can lead to numerical difficulties in solving the equation (6.34). This difficulty can be overcome by using a **transformation** matrix $[T_f]$ in the place of the matrix $[T_\omega]$, where

$$[T_f]=\left[[I] \quad -\frac{\omega^2}{\omega_0^2}[I] \quad i\frac{\omega}{\omega_0}[I] \quad i[I]\right] \tag{6.35}$$

ω_0 is a reference angular frequency. In the following analysis, the maximum measured frequency is chosen as the reference frequency. It should be noted that the thus identified joint parameters with transformation matrix $[T_f]$ are

$$\{x\}=\begin{Bmatrix}\{k\}\\ \omega_0^2\{m\}\\ \omega_0\{c\}\\ \{d\}\end{Bmatrix} \tag{6.36}$$

If some relations between the elements in {x} are known, the number of unknowns can be reduced, and in the meantime, the physical properties of the joint retained. If the relationship between the elements in {x} and the independent elements is linear (which is usually the case) and the number of independent elements is k_0, then the elements of {x} can be written in terms of independent variables as follows

$$x_i=\sum_{k=1}^{k_0} t_{ik}y_k \qquad (i=1\cdots 4n^2) \tag{6.37}$$

where y_k is the independent element, t_{ik} is the coefficient, and x_i is the element in {x} matrix.

Equation (6.37) can be written in matrix form as:

$$\{x\}_{(4n2)\times 1}=[T]_{(4n2)\times(k_0)}\{y\}_{(k_0)\times 1} \tag{6.38}$$

where [T] is called the restriction matrix

Substitution of equation(6.38) into equation (6.34) yields:

$$[E']_{(ml)\times(4n2)}[T]_{(4n2)\times(k_0)}\{y\}_{(k_0)\times 1}=\{g\}_{(ml)\times 1}, \qquad (6.39)$$

and let

$$[\bar{E}(\omega)]=[\bar{E}'(\omega)][T]=[E(\omega)][T_f][T]. \qquad (6.40)$$

Equation (6.39) thus becomes

$$[\bar{E}(\omega)]\{y\}=\{g\} \qquad (6.41)$$

In some cases, some of the independent elements are known. If the total number of independent elements is k_0 and the number of independent unknowns is k_{00}, then let

$$\{y\}_{(k_0)\times 1}=\begin{Bmatrix}\{y_1\}_{k_{00}\times 1}\\ \{y_2\}_{(k_0-k_{00})\times 1}\end{Bmatrix} \qquad (6.42)$$

and partition matrix $[\bar{E}]$ accordingly into

$$[\bar{E}]_{(ml)\times(k_0)}=[[E_1]_{(ml)\times k_{00}},[E_2]_{(ml)\times(k_0-k_{00})}] \qquad (6.43)$$

Substitute equations (6.42)(6.43) into equation (6.41) so that:

$$[E_1]\{y_1\}=\{p_1\} \qquad (6.44)$$

where $\{p_1\}=\{g\}-[E_2]\{y_2\}$ (6.45)

$\{y_1\}$ consists of real variables, but $[E_1]$ and $\{p_1\}$ are usually complex, hence equation(6.45) is equivalent to

$$\begin{cases}\text{Real}([E_1])\{y_1\}=\text{Real}(\{p_1\})\\ \text{Imag}([E_1])\{y_1\}=\text{Imag}(\{p_1\})\end{cases} \qquad (6.46)$$

or $[E_0]\{y_1\}=\{p_0\}$ (6.47)

where $[E_0]=\begin{bmatrix}\text{Real}([E_1])\\ \text{Imag}([E_1])\end{bmatrix}$ and $\{p_0\}=\begin{Bmatrix}\text{Real}(\{p_1\})\\ \text{Imag}(\{p_1\})\end{Bmatrix}$ (6.48),(6.49)

Combining equation (6.46) at different frequencies yields

$$\begin{cases} [E_0(\omega_1)]\{y_1\} = \{p_0(\omega_1)\} \\ [E_0(\omega_2)]\{y_1\} = \{p_0(\omega_2)\} \\ \vdots \\ [E_0(\omega_i)]\{y_1\} = \{p_0(\omega_i)\} \\ \vdots \\ [E_0(\omega_n)]\{y_1\} = \{p_0(\omega_n)\} \end{cases} \tag{6.50}$$

or $$[A_1]\{y_1\}=\{b_1\} \tag{6.51}$$

where ω_i (i=1...n) are the frequencies at which the FRFs are measured, and

$$[A_1]=\begin{bmatrix} [E_0(\omega_1)] \\ [E_0(\omega_2)] \\ \vdots \\ [E_0(\omega_i)] \\ \vdots \\ [E_0(\omega_n)] \end{bmatrix} \text{ and } \{b_1\}=\begin{Bmatrix} \{p_0(\omega_1)\} \\ \{p_0(\omega_2)\} \\ \vdots \\ \{p_0(\omega_i)\} \\ \vdots \\ \{p_0(\omega_n)\} \end{Bmatrix} \tag{6.52)(6.53}$$

The least-squares solution for equation(6.51) is

$$\{y_1\}=([A_1]^T[A_1])^{-1}[A_1]^T\{b_1\}$$

$$=[\sum_{i=1}^{n}[E_0(\omega_i)]^T[E_0(\omega_i)]\,]^{-1}\sum_{i=1}^{n}([E_0(\omega_i)]^T\{p_0(\omega_i)\} \tag{6.54}$$

Equation (6.54) uses equations obtained directly at different frequencies. However, it may not improve the results significantly. If the system is lightly damped, the magnitude of the FRFs at resonance frequencies will be much higher than that at other frequencies. Consequently, the magnitude of the element in matrices $[[E_0(\omega_i)]^T[E_0(\omega_i)]\,]$ and $[E_0(\omega_i)]^T\{p_0(\omega_i)\}$ can be significantly different at different frequencies. In other words, although all the measured data are used at the same time, the results are dominated by the data at a few frequency points only.

To improve the results, data at all the frequencies should be considered with the same importance. This can be achieved by using the "normalized least-squares" method(NLSM) which is actually the same as the well-known weighted least-squares method (eg. [116]).

Multiplying both sides of the equations for each frequency by a constant, equation (6.50) becomes:

$$\begin{cases} \alpha_1[E_0(\omega_1)]\{y_1\} = \alpha_1\{p_0(\omega_1)\} \\ \alpha_2[E_1(\omega_2)]\{y_1\} = \alpha_2\{p_0(\omega_2)\} \\ \vdots \\ \alpha_i[E_1(\omega_i)]\{y_1\} = \alpha_i\{p_0(\omega_i)\} \\ \vdots \\ \alpha_n[E_1(\omega_n)]\{y_1\} = \alpha_n\{p_0(\omega_n)\} \end{cases} \tag{6.55}$$

or $[A_2]\{y_1\}=\{b_2\}$ (6.56)

where α_i (i=1...n) are scaling factors and

$$[A_2]=\begin{bmatrix} \alpha_1[E_0(\omega_1)] \\ \alpha_2[E_0(\omega_2)] \\ \vdots \\ \alpha_i[E_0(\omega_i)] \\ \vdots \\ \alpha_n[E_0(\omega_n)] \end{bmatrix} \text{ and } \{b_2\}=\begin{Bmatrix} \alpha_1\{p_0(\omega_1)\} \\ \alpha_2\{p_0(\omega_2)\} \\ \vdots \\ \alpha_i\{p_0(\omega_i)\} \\ \vdots \\ \alpha_n\{p_0(\omega_n)\} \end{Bmatrix} \tag{6.57,6.58}$$

Then the solution is

$$\{y_1\} =([A_2]^T[A_2])^{-1}[A_2]^T\{b_2\}$$

$$=\Big[\sum_{i=1}^{n} \alpha_i^2[E_0(\omega_i)]^T[E_0(\omega_i)]\Big]^{-1}\sum_{i=1}^{n}\left(\alpha_i^2[E_0(\omega_i)]^T\{p_0(\omega_i)\}\right) \tag{6.59}$$

Scaling factors $\alpha_1, \alpha_2 ..., \alpha_n$ should be so chosen that $\alpha_i^2[\bar{E}_0(\omega_i)]^T[\bar{E}_0(\omega_i)]$ at different frequencies have similar magnitudes. To simplify the problem, values of α_i can be chosen to make the maximum element in the matrix $\alpha_i^2[\bar{E}_0(\omega_i)]^T[\bar{E}_0(\omega_i)]$ to be unity.

To distinguish the results obtained from one single frequency and from several frequencies, the results obtained using information at more than one frequency are referred to as the averaged results. The least-squares method which does not use normalization for the equations is later noted as the "direct least-squares method"(DLSM).

§6.6 NUMERICAL ILLUSTRATION

§6.6.1 Description of the System Studied

The system studied is a 14DOF finite element beam structure as shown in figure 6.3 and is referred to as case A.

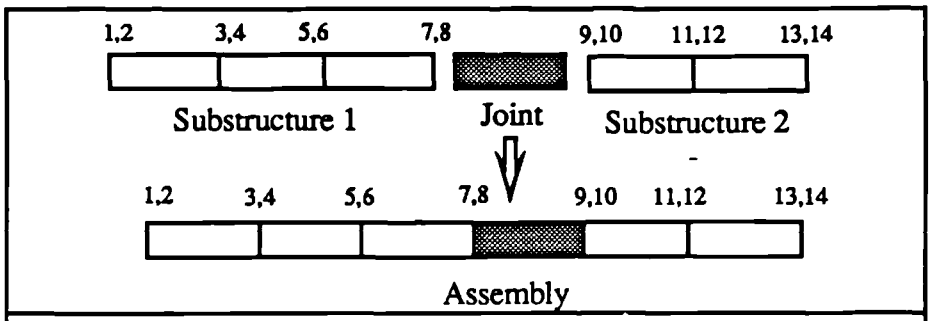

Figure.6.3 The diagram of a 14DOF mc m

The assembly consists of two substructures and one joint. Substructure A consists of three identical beam elements and substructure B has two. The beam element of the substructure has the following physical properties:

length L =0.3 m , thickness h =0.012 m, width w =0.05m,

density ρ=7547 kg/m^3 and Young's modulus E=2.07×10^{11} N/m^2.

The stiffness and mass matrices of a beam element are found as:

$$[K]=\frac{EI}{L^3}\begin{bmatrix} 12 & 6L & -12 & 6L \\ 6L & 4L^2 & -6L & 2L^2 \\ -12 & -6L & 12 & -6L \\ 6L & 2L^2 & -6L & 4L^2 \end{bmatrix}=\begin{bmatrix} 662400 & 99360 & -662400 & 99360 \\ 99360 & 19872 & -99360 & 9936 \\ -662400 & -99360 & 662400 & -99360 \\ 99360 & 9936 & -99360 & 19872 \end{bmatrix}$$

and

$$[M]=\frac{mL}{420}\begin{bmatrix} 156 & 22L & 54 & -13L \\ 22L & 4L^2 & 13L & -3L^2 \\ 54 & 13L & 156 & -22L \\ -13L & -3L^2 & -22L & 4L^2 \end{bmatrix}=\begin{bmatrix} 0.5 & 0.021 & 0.1746 & -0.0126 \\ 0.021 & 0.001 & 0.0126 & -0.00087 \\ 0.1746 & 0.0126 & 0.5 & -0.021 \\ -0.0126 & -0.00087 & -0.021 & 0.001 \end{bmatrix}$$

where m=ρhw and $I=\frac{wh^3}{12}$

The damping of the beam element is assumed to be hysteretic and proportional to the stiffness matrix, i.e.

$$[D]= 0.001[K]$$

The joint element has no mass but has the same stiffness and damping as the beam element, i.e.

$$[M_j]=0\ ,\ [K_j]=[K] \text{ and } [D_j]=[D]$$

The joint element in this case is not realistic since it is the same as a finite element beam. However, as K_j and D_j matrices are fully populated, the joint model is complicated enough to simulate a real joint. In a real case, a joint can sometimes be modelled by lumped parameters (therefore possessing less unknown variables), which is much simpler.

For most, if not all, mechanical joints, the impedance matrices are symmetric, hence the condition of symmetry of the impedance matrix can always be imposed, thereby reducing the number of unknown variables in an n×n impedance matrix from n^2 to $\frac{n(n+1)}{2}$.

Equations (6.16-6.19) and (6.22)(6.23) are verified by two cases at each frequency and over a frequency range. In the first case, all non-joint coordinates are "measured" and in the second case, only five non-joint coordinates (1,3,5,11 and13) are measured. Exact results are found using any of the above equations.

§6.6.2 Joint Identification with Contaminated FRF Data

In practice, measured data are always polluted by random errors. To simulate measurement errors, 5% random noise is added to the FRF data in the following studies. In addition, the use of equations (6.18)(6.19) and equation(6.23) requires the matrix $[H_{jj}]$ which is often very difficult to measure in practice. Therefore, in the following analysis, for method one, equations (6.16) and (6.17) are used and for the method two, equation (6.22) is used.

§6.6.2.1 The Identified Results Using Method One

The input data for ten numerical cases, as listed in table 6.1, are studied. The first case is the reference one and results from the other cases are compared with the results from the first case. The purpose of the different case studies is listed in the last column of table 6.1. Some relations between the elements in the joint stiffness and damping matrices are used for case A9 and case A10. These relations are shown in table 6.2.

	Start frequency	finish frequency	frequency points	Measured coordinates	weighting	restriction	purposes
case A1	400	1000	31	all	Yes	No	Basic case
case A2	400	1000	31	all	No	No	Weighting
case A3		405					Frequency range
case A4	400	450	101	all	Yes	No	
case A5			121				Frequency points
case A6	400	1000	301	all	Yes	No	
case A7				1,3,5,11,13			Measured coordinates
case A8	400	1000	31	1,13	Yes	No	
case A9						T10-4	
case A10	400	1000	31	all	Yes	T10-2	Restriction

Table 6.1. Input data for case A

Restriction T10-4:
Assuming stiffness and damping matrices have the following form

$$[K_j]=\begin{bmatrix} A_k & B_k & -A_k & B_k \\ B_k & C_k & -B_k & D_k \\ -A_k & -B_k & A_k & -B_k \\ B_k & D_k & -B_k & C_k \end{bmatrix} \quad [D_j]=\begin{bmatrix} A_d & B_d & -A_d & B_d \\ B_d & C_d & -B_d & D_d \\ -A_d & -B_d & A_d & -B_d \\ B_d & D_d & -B_d & C_d \end{bmatrix}$$

where A_k, B_k, C_k, D_k, A_d, B_d, C_d and D_d, are independent unknowns.

Restriction T10-2:
Assuming stiffness and damping matrices have the following form

$$[K_j]=\begin{bmatrix} A_k & 99360 & -A_k & 99360 \\ 99360 & C_k & -99360 & 9936 \\ -A_k & -99360 & A_k & -99360 \\ 99360 & 9936 & -99360 & C_k \end{bmatrix} \quad [D_j]=\begin{bmatrix} A_d & 99.360 & -A_d & 99.360 \\ 99.360 & C_d & -99.360 & 9.936 \\ -A_d & -99.360 & A_d & -99.360 \\ 99.360 & 9.936 & -99.360 & C_d \end{bmatrix}$$

where A_k, C_k, A_d and C_d are independent unknowns and figures are exact values for the joint

Table 6.2 Restriction applied on case A9 and case A10

The joint stiffness and damping parameters obtained at each individual frequency are far from satisfactory; figure 6.4 shows the identified first element of the joint stiffness matrix at each frequency, it can be clearly seen that the identified $K_j(1,1)$ varies in the range by more than -500% to +500%. With a variation of this scale, it is not possible to extract any sensible results. This indicates that the information at a single frequency point may not be sufficient for the identification when the FRFs are polluted with measurement errors. Therefore information obtained over the frequency range must be used (i.e. the averaged results).

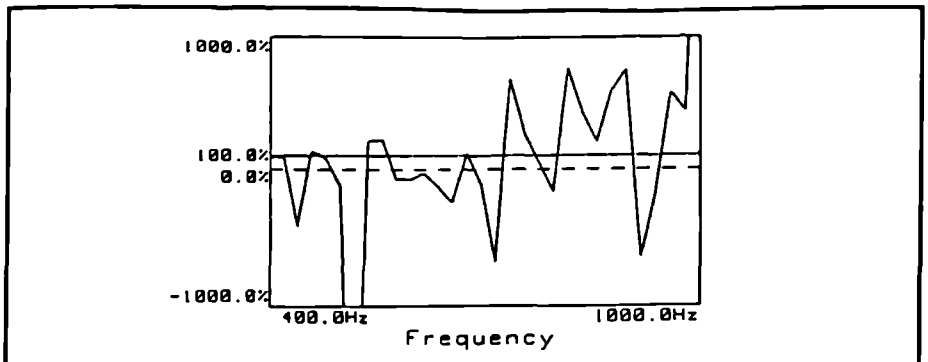

Figure 6.4 Identified $K_j(1,1)$ using FRF at one frequency only

In the following studies, only the results identified over a frequency range will be presented, the identified results are shown as their relative values with respect to the corresponding true values. The perfect result will be 1. Because the identified results (i.e. the stiffness and damping matrices) are symmetrical, only the elements in the upper triangle of the matrix , which has 10 elements for a 4×4 matrix, are shown.

The identified stiffness and damping parameters of the joint are shown in table 6.3.and table 6.4 respectively.

	K(1,1)	K(1,2)	K(1,3)	K(1,4)	K(2,2)	K(2,3)	K(2,4)	K(3,3)	K(3,4)	K(4,4)
Case A1	1.006	0.994	1.040	0.955	0.986	0.962	1.049	0.908	1.056	0.981
Case A2	0.889	1.147	1.518	0.691	0.787	0.639	1.149	0.224	1.475	0.675
Case A3	0.682	0.883	1.168	0.436	-0.163	0.411	-0.675	0.645	0.878	-0.135
Case A4	0.863	0.905	1.160	0.615	0.677	0.874	0.413	0.891	1.101	0.395
Case A5	1.040	0.970	0.992	0.988	1.017	1.004	1.017	1.023	1.019	0.989
Case A6	1.025	0.990	0.993	0.997	0.994	0.996	0.991	1.015	1.010	0.984
Case A7	1.029	0.979	1.033	0.833	1.021	0.969	1.109	0.772	1.208	0.839
Case A8	0.612	1.232	-0.261	1.760	0.801	1.615	0.241	1.494	0.608	1.147
Case A9	0.930	1.011	0.930	1.011	1.031	1.011	1.046	0.930	1.011	1.031
CaseA10	0.986	1.000	0.986	1.000	0.993	1.000	1.000	0.986	1.000	0.993

Table 6.3 Identified relative stiffness using method one

	D(1,1)	D(1,2)	D(1,3)	D(1,4)	D(2,2)	D(2,3)	D(2,4)	D(3,3)	D(3,4)	D(4,4)
Case A1	0.441	1.217	1.244	0.910	0.982	0.903	1.201	1.028	1.059	1.006
Case A2	0.485	0.945	0.188	1.637	1.361	1.532	0.978	3.027	-0.517	1.956
Case A3	0.742	0.470	0.709	0.329	0.189	0.231	-0.053	0.727	0.410	0.300
Case A4	0.801	0.839	0.886	0.640	0.777	0.804	0.619	0.937	0.810	0.584
Case A5	0.758	1.119	1.134	0.890	0.946	0.955	1.040	0.863	1.133	0.887
Case A6	0.890	1.071	1.076	1.003	0.949	0.948	0.991	0.649	1.104	0.983
Case A7	0.778	1.182	1.204	0.489	0.935	0.828	1.249	1.712	1.112	0.598
Case A8	0.452	1.156	3.314	-0.041	1.110	-0.074	1.878	2.128	0.482	1.297
Case A9	0.843	1.028	0.842	1.028	1.027	1.028	1.039	0.843	1.028	1.027
CaseA10	1.032	1.000	1.032	1.000	0.981	1.000	1.000	1.032	1.000	0.981

Table 6.4 Identified relative damping

The only difference between case A1 and case A2 is that the weighting technique is used for case A1; it is very clear that the results from case A1 are much better. Except for a few elements in the damping matrix, errors in the identified results do not exceed 10%, and for most stiffness elements, the error levels are less than 5%. This proves that the normalized least-squares method, which uses the information available more effectively, is more appropriate for identification purpose than the direct least-squares method. For this reason, the normalized least-squares method is used in all other cases.

From the results of case A1, case A3 and case A4, it is clear that although the number of frequency points in the latter two cases are approximately three times the reference case, the identified results are much poorer. This indicates that it is not the total number of equations, but the number of effective equations that is important in identification, and there are more effective equations in a wider frequency range than in a narrow frequency range.

In a prescribed frequency range, using reasonably smaller frequency increments can increase the number of effective equations, and hence improve the accuracy of the identified results, as can be noted from the the results of case A1, case A5 and case A6. However, very small frequency increments (2Hz or smaller in this case) may not be appropriate, because the equations accumulated tend to be proportional.

The same reasoning applies to the measured coordinates. With more coordinates measured, the accuracy of the results is improved (case A1, case A7 and case A8). However, using very closely located coordinates may not be effective in improving the accuracy of identification. It is not possible to show this deduction with the 14 DOF system studied. However, the deduction has been verified from other numerical case studies which are not shown in this thesis due to the limited space available.

The effects of imposing restriction conditions are identified from the results of case A9 and case A10. For case A9, there are eight unknowns (four stiffness elements and four damping elements), and for case A10, there are four unknowns (two stiffness elements and two damping elements). It is clearly shown, as expected, that when there are less unknowns to be identified, the accuracy of the results is improved.

§6.6.2.2 The Identified Results Using Method Two

Case A1 is investigated using method two (as case A11). The identified results are shown in table 6.5. Although the formulae of method two have been verified in §6.6.1, it can be noted that the identified results using method two are more sensitive to the measurement errors than using method one, for example, K(3,4) from method one is 1.056 while it is 0.688 from method two. This is clearly different from the case for coupling. In coupling,

the results of different methods always yield the same results if the effects of numerical errors are negligible.

	K(1,1)	K(1,2)	K(1,3)	K(1,4)	K(2,2)	K(2,3)	K(2,4)	K(3,3)	K(3,4)	K(4,4)
Case A1	1.006	0.994	1.040	0.955	0.986	0.962	1.049	0.908	1.056	0.981
CaseA11	0.921	1.019	0.976	0.971	0.966	0.765	1.209	1.033	0.688	1.238
	D(1,1)	D(1,2)	D(1,3)	D(1,4)	D(2,2)	D(2,3)	D(2,4)	D(3,3)	D(3,4)	D(4,4)
Case A1	0.441	1.217	1.244	0.910	0.982	0.903	1.201	1.028	1.059	1.006
CaseA11	24.240	-9.872	-5.167	0.570	11.290	1.895	9.398	4.738	-3.168	6.187

Table 6.5 The relative values of the identified results from method one and method two

The reason that the results from these two methods have different accuracy is because some kind of optimization was used. In both method one and method two, the concept of the least-squares solution is used to solve a set of linear equations. i.e. to find the least-squares solution for a set of equations with the form

$$[A]\{x\}=\{b\}. \tag{6.60}$$

If the [A] matrix is not an ill-conditioned matrix, the accuracy of the identified results [x] are mainly determined by the error levels in matrix [A] and vector {b}.

For method two, the receptance matrix is first inverted. As discussed in Chapter 5, the measurement errors are usually magnified during the inversion. Therefore, the error levels in $[Z_{aa}]$, $[Z_{ab}]$, $[Z_{ba}]$ and $[Z_{bb}]$ are greater than the error levels in $[H_{aa}]$, $[H_{ab}]$, $[H_{ba}]$ and $[H_{bb}]$. Consequentely, the accuracy of the results from method two is usually poorer than that from method one.

In the following analysis, only method one is considered.

§6.7 THE REFINED WEIGHTING METHOD

§6.7.1 Theory of the Refined Weighting Method

The weighting method proposed in §6.5 is based on the observation that the FRF magnitudes change greatly at different frequencies. To use information at all frequencies effectively, the magnitude of the FRFs at different frequencies should be scaled. However, sometimes the aim of weighting information at each frequency with the same importance cannot be achieved by using the weighting method proposed in §6.5. It is noted that $[E_1(\omega_i)]$ is generated from multiplication of the coefficient matrix $[E(\omega_i)]$ with transformation and restriction matrices $[T_f]$ and $[T]$, and partition of the matrix at a particular stage to distinguish the real unknowns from the independent variables. Consequently, the elements of the resultant matrix $[E_1(\omega_i)]$ do not always reflect the magnitudes of the elements in matrix $[E(\omega_i)]$. In other words, it is not always true that if the FRFs have large magnitudes, the matrix $[E_1(\omega_i)]$ must have large elements or vice versa, especially when the matrix $[E(\omega_i)]$ is an ill-conditioned matrix or the magnitudes of

the elements in the transformation matrix change greatly at different frequencies (Examples of these two cases are the case of a free-free vibrating structure dominated by the rigid body mode at very low frequencies, and the transformation matrices of the mass over a wide frequency range). Therefore, it is more appropriate to impose weighting before any transformation and restriction. i.e. to select scaling factors to make the maximum element (or the maximum of the sum of a row or a column) in the matrix $[E(\omega_i)]$ unity, this weighting method is referred as the Weighting-Before method(WB). The weighting method in §6.5 is referred as the Weighting-After method(WA) in this section.

As well as variations occurring in FRFs at different frequencies, FRFs at different coordinates can also vary, and as a result, the elements of different equations at the same frequency can also be significantly different in magnitude. When equations with small magnitude elements are combined with equations with large ones, the effects of these equations with small elements on the least-squares solution will be overshadowed by the equations with large elements; in other words, the information in these small magnitude equations are wasted. To overcome this problem, independent weighting can be imposed on each equation according to their magnitudes, i.e. to multiply both sides of an equation by a scaling factor so that the maximum coefficient (or the sum of the coefficient squares) in the equation is unity. This weighting method is called the Weighting-Before (transformation)-Single (equation) method (WBS).

Initially, the WBS method looks perfect because all the equations accumulated at all the coordinates and frequencies are considered with the same importance. However, it is questionable if all the equations should be considered with the same importance. The error levels in different equations can be significantly different even if all the FRFs have the same levels of error. This is because the [C] matrix in equation(6.24) is a subtraction between two matrices ($[C]=[C_1]-[C_2]$). If the corresponding elements in these two matrices have similar magnitudes (i.e. $c_1(i,j)$ and $c_2(i,j)$ are close to each other), the resultant [C] matrix (or some elements in the matrix [C]) can have very high error levels. Fortunately, the effects of these erroneous equations on identified joint parameters are often insignificant because the magnitude of $c_1(i,j)-c_2(i,j)$ of these equations is often very small. However, if the WBS method is used, the magnitude of these erroneous equations can be significantly magnified and, accordingly, the effects of these equations on the solution can also be significant.

To overcome the shortcoming of the WBS method, these erroneous equations must be deleted before the identification process. However, in practice, this is almost impossible simply because it is not known how much error there is in the matrix $[C_1]-[C_2]$ (otherwise, it can be corrected).

Fortunately, although we do not know exactly how much error there is in each equation, we do know that if two right hand side elements $c_1(i,j)$ and $c_2(i,j)$ of an equation have similar magnitudes, the equation is prone to have high error levels. Therefore, we can delete the erroneous equations simply by deleting these equations with

$$\frac{|c_1(i,j)-c_2(i,j)|}{\frac{|c_1(i,j)|+|c_2(i,j)|}{2}} \leq \Delta \qquad (6.61)$$

where Δ is a small positive number in the range $2 > \Delta \geq 0$.

When $\Delta=0$, no equation is deleted and when $\Delta=2$, all equations are deleted. When some of the equations are deleted using equation(6.61), we not only delete erroneous ones, but other equations with low error levels as well. Consequentely, some information is rejected. However, this small sacrifice is proved to be worthwhile and can often be compensated for by the reduction of the total error levels and effective use of information in the remaining equations.

The choice of the Δ value should be determined both by error levels in the measured data and by the amount of measured data. If the error levels are high and the measured data are sufficient, a large Δ value may be appropriate; if error levels are low and the total measured data are limited, then a small Δ should be chosen. The requirement on the accuracy of the right hand side element c_1-c_2 should not be set too high, otherwise, too many equations will be deleted.

If the errors in c_1 and c_2 are $c_1\delta_1$ and $c_2\delta_2$, then the error level in c_1-c_2 is $\frac{|c_1\delta_1-c_2\delta_2|}{|c_1-c_2|}$, and the worst possible case is $\delta_1\delta_2 < 0$ (let $\delta_1=-\delta_2>0$), then the error level is $\frac{|c_1+c_2|\delta_1}{|c_1-c_2|}$. If the maximum error level in c_1-c_2 should be less than m, i.e.

$$\frac{|c_1+c_2|\delta_1}{|c_1-c_2|} < m,$$

Then

$$\Delta > \frac{2\delta_1}{m} \qquad (6.62)$$

If the error level in the measured data is 5% and the maximum error level in the equations allowed is 10%, then from equation (6.62), Δ must be greater than 1. If the error in c_1-c_2 must be less than 5%, $\Delta>2$, which actually means all the equations should be deleted, therefore, the requirement is not achievable.

An alternative to the WBS method is to divide the equations obtained at each frequency into several groups and weight these groups separately. Provided the equations are properly grouped, the erroneous equation will not be over magnified. This is because an erroneous equation can only be over magnified if c_1-c_2 is much smaller than the magnitudes of c_1 and c_2, and also the coefficients on the left hand side of the equation must be very small so that they are of the same order as c_1-c_2. When the equation is grouped and weighted, all the equations in the group are weighted by the same factor which is determined by the equation with the largest coefficients.Therefore, over-magnifing erroneous equations is prevented. This weighting method is referred to as the Weight-Before (transformation)-Group (equations) method(WBG).

It can be noted that the WB and WBS methods are actually two special cases of the WBG method; if all equations from equations(6.16-6.19) are treated as one group, the WBG method becomes the WB method; if each equation in equations(6.16-6.19) is considered as single group, the WBG method becomes the WBS method

The following method to group equations for the WBG method is proposed. From the discussion in §6.5, it is known that each equation in (6.16-6.19) is generated from one row of matrix[A] and one column from matrix [B]. If all equations which involve one row of matrix [A] as one group are taken, then the equations obtained at each frequency are divided into several groups. This is shown in figure 6.5.

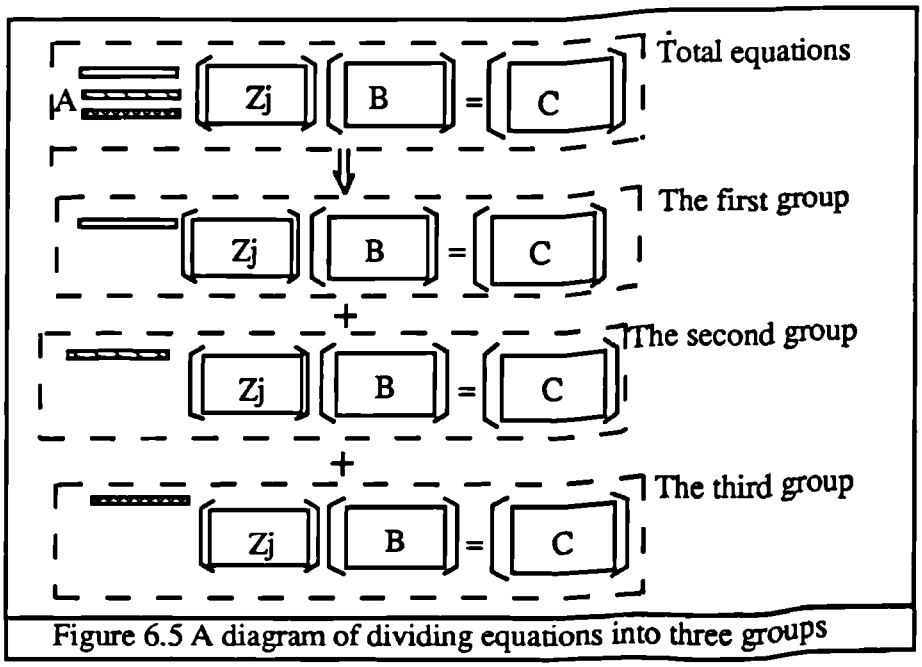

Figure 6.5 A diagram of dividing equations into three groups

§6.7.2 Numerical Illustration

§6.7.2.1 Description of the System Studied

The system considered is very similar to that used in §6.6. The substructure system is exactly the same, but to make the joint more complicated, the joint element has the same mass matrix as the beam element, i.e. the joint element is exactly the same as the beam element. Therefore, the joint has a total of 48 unknowns (16 stiffness elements, 16 mass elements and 16 damping elements).

Based on the geometric symmetry of the joint element, it is assumed that the stiffness, mass and damping matrices have the following restricted form:

$$(K, M, D) = \begin{bmatrix} a & c & e & d \\ c & b & -d & f \\ e & -d & a & -c \\ d & f & -c & b \end{bmatrix}$$

Therefore, each of the stiffness, mass and damping matrices have six independent unknowns and the total number of independent unknowns is 18.

The FRF data is assumed to be measured in a frequency range 100-1000Hz with a frequency increment of 30Hz.

It will be seen later that if equations (6.16-6.19) are used together, very good results are obtained for all the weighting methods. To illustrate the advantages of refined weighting methods (WBS & WBG) more clearly, only equation (6.16) is used in the second calculation.

§6.7.2.2 Methods for Presentation of Results

When two frequency points are used, one least-squares solution can be found; when the third frequency point is added, another least-squares solution is obtained, and so on. Although the accuracy of results obtained using all the measured frequency points can be used to evaluate different weighting methods, the change of the results during the accumulation of frequency points often gives a further insight to the problems in the different weighting methods.

For each frequency, there are three matrices (stiffness, mass and damping) and for N frequency points, 3×N matrices are formed. An attempt to present all the results can only cause confusion. One method of presenting the results is to plot a graph with one element in the identified results against frequency. However, one element may not necessarily be representative. In this section, a pair of factors is used to evaluate the accuracy of the results and efficiency of the method.

Upper triangular elements of an identified matrix (eg. a stiffness matrix) can be listed into a vector $V=\{v_1,v_2,...,v_n\}^T$ and if the corresponding vector for the exact results is $V_0=\{v_{01},v_{02},...,v_{0n}\}^T$, then a Joint Correlation Factor can be defined as:

$$JCF=\frac{(V^TV_0)^2}{\|V\|\|V_0\|} \tag{6.63}$$

If V and V_0 are perfectly correlated, (i.e. $V=V_0$), JCF=1; if V and V_0 are not correlated at all, then JCF=0. For the other cases, the JCF varies in a range [0,1]. A high JCF value may indicate accurate results. However, it is not always the case; if the magnitudes of elements in V vary greatly, the JCF will only be determined by the elements with large magnitudes. If one element is dominant, the JCF will be always close to one. To avoid this problem, relative values are used instead of the absolute values.

The Relative-Joint-Correlation-Factor is defined as:

$$RJCF=\frac{(U^TU_0)^2}{\|U\|\|U_0\|} \tag{6.64}$$

where $U=\{u_1,u_2,...,u_i,...u_n\}^T=\{\frac{v_1}{v_{10}},\frac{v_2}{v_{20}},..,\frac{v_i}{v_{i0}},..,..,\frac{v_n}{v_{n0}}\}^T$ and $U_0=\{1,1,..,..,1\}^T$

Usually, it is better to use the RJCF value to represent the accuracy of the identified results, unless there are some very small elements in the joint matrix; in this case, the RJCF value can be significantly affected by these small elements. However, because small elements in the joint matrix usually have little effect on the assembly, they can be ignored. If very small values are excluded from U and U_0, RJCF values give a good indication about the correlation between the identified and exact results.

Usually, good correlation between identified results and exact results indicates an accurate identification. However, if the identified results are proportional to the exact results, the RJCF value will be 1. To take this possibility into account, another Average-Relative-Value Factor can be defined:

$$ARVF=\frac{1}{n}\sum_{i=1}^{n}u_i \tag{6.65}$$

If the identified results are accurate, the ARVF should be close to 1.

The RJCF and ARVF are treated as a pair (RJCF, ARVF) to evaluate the accuracy of the identified results.

§6.7.2.3 Results and Discussion

Tables 6.6-6.8 show the identified results in the (RJCF,ARVF) pair using equations (6.16-6.19). The RJCF values for stiffness and mass matrices are higher than 98% (for

WBS and WBG, values of RJCF are higher than 99.5%), ARVF values for stiffness and mass fall in a range {0.99,1.01}, therefore, all the weighting methods yield very satisfactory results for stiffness and mass. The accuracy of the identified damping matrices are not as good as those of stiffness and mass, especially for the damping matrices using the WBS method with $\Delta<0.05$. However, when a proper Δ is chosen (eg. 0.05 or 0.1), the damping values identified are more accurate. The effects of Δ on the accuracy of the damping matrices using other weighting methods are not as significant as that on WBS methods. From the above results, it is known that when the measured data are sufficient, a proper choice of Δ value can improve the accuracy of the identified results slightly. However, since very good results have been obtained even using the WA or WB method, the choice of weighting methods is not very important.

Δ	0	0.02	0.05	0.1	0.2	0.3	0.4	0.5
WA	0.9962 0.9280	0.9960 0.9279	0.9960 0.9283	0.9960 0.9287	0.9960 0.9288	0.9962 0.9294	0.9975 0.9292	0.9978 0.9288
WB	0.9996 0.9829	0.9995 0.9853	0.9960 0.9871	1.0000 0.9978	0.9998 0.9900	0.9997 0.9904	0.9960 0.9900	0.9970 0.9923
WBG	0.9994 0.9984	0.9994 0.9986	0.9995 1.0000	0.9994 1.0010	0.9994 1.0020	0.9994 1.0030	0.9995 0.9957	0.9996 0.9983
WBS	0.9980 0.9866	0.9980 0.9853	0.9960 0.9949	0.9960 0.9934	0.9996 0.9937	0.9996 0.9946	0.9997 0.9951	0.9996 0.9935

Table 6.6 (RJCF,ARVF) pair for the stiffness matrices using equations (6.16-6.19)

Δ	0	0.02	0.05	0.1	0.2	0.3	0.4	0.5
WA	0.9860 0.9990	0.9863 0.9994	0.9864 1.0000	0.9866 1.0000	0.9865 1.0000	0.9871 0.9993	0.9900 0.9898	0.9903 0.9892
WB	0.9998 0.9764	0.9970 0.9895	0.9998 0.9970	1.0000 0.9977	0.9998 0.9922	0.9998 0.9913	0.9998 0.9829	0.9998 0.9888
WBG	0.9997 0.9896	0.9997 0.9899	0.9998 0.9982	0.9996 0.9789	0.9996 0.9790	0.9996 0.9794	0.9998 0.9810	0.9997 0.9822
WBS	0.9999 0.9842	0.9999 0.9835	0.9999 0.9835	0.9998 0.9834	0.9998 0.9838	0.9998 0.9842	0.9998 0.9854	0.9995 0.9749

Table 6.7 (RJCF,ARVF) pair for the mass matrices using equations (6.16-6.19)

Δ	0	0.02	0.05	0.1	0.2	0.3	0.4	0.5
WA	0.8960 0.9800	0.8964 0.9785	0.8959 0.9826	0.8972 0.9829	0.8969 0.9819	0.9022 0.9813	0.9094 0.9616	0.9087 0.9637
WB	0.9747 0.8842	0.8369 0.9475	0.8593 0.9577	0.8639 0.9875	0.8224 0.9337	0.8161 0.9313	0.8606 0.9520	0.8592 0.9553
WBG	0.8764 1.0790	0.8665 1.0600	0.9100 1.1260	0.9018 1.1240	0.8981 1.1210	0.8968 1.1210	0.9323 1.1020	0.9318 1.1072
WBS	0.5534 1.7480	0.5711 1.7380	0.9538 0.8436	0.9579 0.9712	0.9559 0.9699	0.9550 0.90690	0.9569 0.9613	0.9308 0.9649

Table 6.8 (RJCF,ARVF) pair for the damping matrices using equations (6.16-6.19)

If measured data are insufficient, however, different weighting methods can lead to a significant difference in the accuracy of the identified results. Tables 6.9-6.11 shows the identified results in the (RJCF,ARVF) pair using equation (6.16) only, the best results for each method are shown in **BOLD**. Table 6.12 shows the relative values of the best

identified results (the case shown in **BOLD** in Tables 6.9-6.11) with respect to the exact results using different weighting methods together with the exact values shown in the last column. It is obvious that the weighting methods (especially WBG and WBS) proposed in this section have clear advantages over the WA method in §6.5. When Δ=0, the WBG method yields the best results. However, if Δ is correctly chosen (eg. Δ=0.05), the results from the WBS method are the best.

	0	0.02	0.05	0.1	0.2	0.3	0.4	0.5
WA	**0.70,0.28**	0.70,0.28	0.70,0.28	0.70,0.28	0.69,0.27	0.70,0.28	0.62,0.25	0.71,0.30
WB	**0.64,0.43**	0.64,0.42	0.64,0.43	0.61,0.41	0.61,0.41	0.65,0.43	0.65,0.43	0.67,0.44
WBG	**0.91,1.10**	0.92,1.12	0.91,1.10	0.89,1.09	0.89,1.09	0.9,1.11	0.88,0.66	0.88,0.65
WBS	0.64,0.79	0.69,0.78	**0.99,0.98**	0.99,0.89	0.99,0.89	0.99,0.87	0.98,0.73	0.97,0.60

Table 6.9 (RJCF,ARVF) pair for the stiffness matrices using equation (6.16) only

Δ	0	0.02	0.05	0.1	0.2	0.3	0.4	0.5
WA	**0.76,0.64**	0.76,0.64	0.76,0.63	0.76,0.62	0.76,0.61	0.76,0.61	0.75,0.60	0.74,0.56
WB	**0.25,0.12**	0.24,0.12	0.25,0.12	0.18,0.10	0.17,0.09	0.12,0.08	0.09,0.07	0.88,0.08
WBG	**0.97,1.01**	0.97,1.03	0.97,1.05	0.97,1.00	0.97,1.00	0.97,1.01	0.98,0.67	0.98,0.66
WBS	0.54,0.81	0.55,0.83	**0.99,0.93**	0.99,0.86	0.99,0.86	0.99,0.84	0.98,0.68	0.94,0.56

Table 6.10 (RJCF,ARVF) pair for the mass matrices using equation (6.16) only

Δ	0	0.02	0.05	0.1	0.2	0.3	0.4	0.5
WA	**0.12,0.15**	0.12,0.16	0.11,0.16	0.11,0.16	0.61,0.15	0.10,0.16	0.09,0.13	0.11,0.15
WB	**0.52,0.39**	0.52,0.38	0.51,0.39	0.54,0.37	0.54,0.37	0.57,0.39	0.56,0.39	0.56,0.40
WBG	**0.71,1.21**	0.57,1.08	0.74,1.32	0.72,1.32	0.71,1.31	0.74,1.32	0.30,0.89	0.30,0.89
WBS	0.04,6.18	0.04,6.59	**0.65,0.64**	0.55,1.00	0.57,0.99	0.5,0.99	0.23,0.85	0.19,0.74

Table 6.11 (RJCF,ARVF) pair for the damping matrices using equation (6.16) only

	WA (Δ=0)	WB (Δ=0)	WBG(Δ=0)	WBS(Δ=0.05)	exact values
$k_j(1,1)$	0.29	0.44	0.79	1.02	662400
$k_j(1,2)$	0.49	0.75	1.32	0.91	99360
$k_j(1,3)$	0.38	0.39	1.56	0.92	-662400
$k_j(1,4)$	0.39	0.57	0.74	1.04	99360
$k_j(2,2)$	0.08	-0.16	1.03	1.01	19872
$k_j(2,4)$	-0.08	0.68	1.70	0.95	9936
$m_j(1,1)$	0.07	-0.10	1.16	0.88	0.50450
$m_j(1,2)$	0.86	0.29	0.96	1.00	0.02130
$m_j(1,3)$	1.25	-0.35	1.23	0.78	0.17470
$m_j(1,4)$	0.81	0.21	0.76	0.99	-0.01260
$m_j(2,2)$	0.545	0.28	1.07	0.95	0.00116
$m_j(2,4)$	0.74	0.23	1.03	0.93	-0.00090
$h_j(1,1)$	-0.27	0.62	0.87	0.67	662.400
$h_j(1,2)$	0.54	0.61	0.87	0.66	99.360
$h_j(1,3)$	1.00	-0.35	3.24	0.70	-662.400
$h_j(1,4)$	-0.28	0.86	0.49	1.36	99.360
$h_j(2,2)$	0.12	0.03	1.27	0.35	19.872
$h_j(2,4)$	0.35	0.36	1.84	-0.36	9.936

Table 6.12 The relative values of the identified results using different weighting methods

From tables 6.9-6.11, it can also be noted that Δ has little effect on the identified results for WA, WB and WBG methods for Δ<0.3, which indicates that the effects of equations with Δ<0.3 on WA, WB and WBG methods are actually negligible. This means that for these weighting methods, the information of many equations are not used sufficiently .

For the WBS method, it is clear that there is an optimum Δ; if Δ is too small, then the error levels in accumulated equations can be very high; if Δ is too large (Δ>0.4), much useful information is rejected, which leads to poor results. Table 6.13 shows the identified results in their relative values with respect to the exact results utilising the WBS method using different Δ values.

Δ	0.0	0.02	0.05	0.10	0.30	0.50	exact values
$k_j(1,1)$	0.54	0.62	1.02	0.86	0.84	0.64	662400
$k_j(1,2)$	1.55	1.45	0.91	0.94	0.91	0.68	99360
$k_j(1,3)$	1.43	1.31	0.92	0.94	0.91	0.63	-662400
$k_j(1,4)$	0.41	0.47	1.04	0.91	0.88	0.67	99360
$k_j(2,2)$	0.04	0.06	1.01	0.84	0.81	0.38	19872
$k_j(2,4)$	1.49	1.37	0.95	0.94	0.93	0.60	9936
$m_j(1,1)$	1.54	1.54	0.88	0.80	0.76	0.30	0.5045
$m_j(1,2)$	-0.42	-0.42	1.00	0.91	0.90	0.67	0.0213
$m_j(1,3)$	0.75	0.89	0.78	0.83	0.89	0.50	0.1747
$m_j(1,4)$	0.80	0.78	0.99	0.87	0.80	0.63	-0.0126
$m_j(2,2)$	1.62	1.64	0.95	0.89	0.86	0.61	0.0012
$m_j(2,4)$	0.35	0.41	0.93	0.90	0.91	0.63	-0.0009
$h_j(1,1)$	41.79	45.02	0.67	1.70	1.87	2.35	662.40
$h_j(1,2)$	-25.93	-28.47	0.66	-0.06	-0.18	-1.08	99.36
$h_j(1,3)$	-36.24	-38.82	0.70	0.14	-0.09	-1.28	-662.40
$h_j(1,4)$	24.66	27.10	1.36	2.16	2.18	2.34	99.36
$h_j(2,2)$	13.48	14.22	0.35	1.23	1.23	0.94	19.87
$h_j(2,4)$	-9.96	-10.99	-0.36	-1.56	-0.12	-0.46	9.94

Table 6.13 The relative values of the identified results with different Δ values using WBS method

The relation between Δ and the accuracy of the identified results can be further understood by studying the change of identified results with the frequency points. As shown in figure 6.6 and figure 6.7., the identified results change dramatically at some frequencies if Δ is small(eg. Δ=0), while the changes are less severe after the first few frequency points when Δ is large. The dramatic change of (RJCF,ARVF) pair values at a single frequency point indicates the effects of over-magnified erroneous equations. When erroneous equations are deleted (by choosing a greater Δ value), the changes of the (RJCF,ARVF) pair become less significant. When the Δ value is too large (of course it depends on the total available data, in this case Δ=0.5), the changes of the (RJCF,ARVF) pair are insignificant, however, in the frequency range measured, the (RJCF,ARVF) pair does not tend to converge to (1,1).

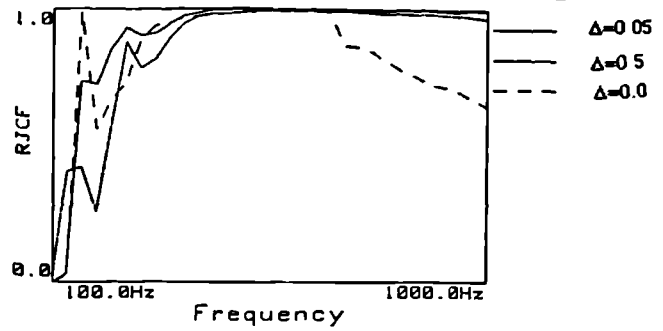

(a) RJCF values of the identified stiffness

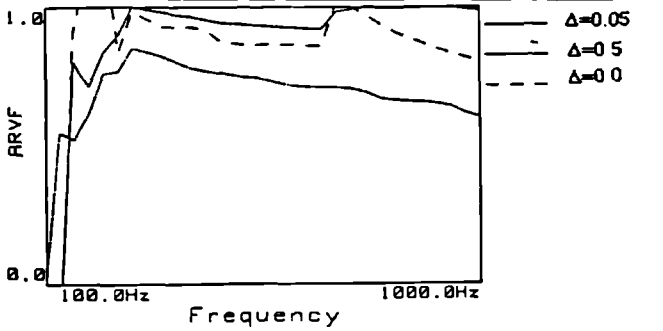

(b) ARVF values of the identified stiffness

Figure 6.6 (RJCF, ARVF) for the identified joint stiffness

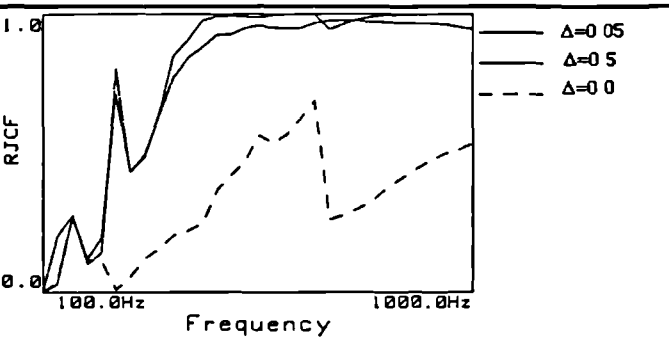

(a) RJCF values of the identified mass

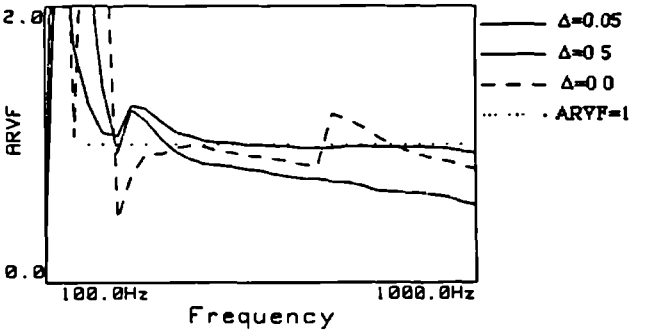

(b) ARVF values of the identified mass

Figure 6.7 (RJCF, ARVF) for the identified joint mass

As discussed above, when a proper Δ value is chosen, the WBS method yields the most accurate results. However, WBG should certainly have its application in joint identification. This is because the identified results from the WBG method are quite accurate if the amount of the measured data is not too small and the results are not so sensitive to the Δ value (in other words, the WBG method is more stable than the WBS

method). These properties can be very useful, because the real results are unknown in practice. If the identified results from both the WBG and WBS methods yield close agreement, the identified results are likely to be accurate.

§6.8 ACCURACY OF JOINT IDENTIFICATION

§6.8.1 The Basic Requirement for Accurate Identification of Joints

Several factors that affect the accuracy of the identification . have been studied in the last few sections. However, there is an additional decisive factor: the nature of the assembled system. Experience indicates that the accuracy of identification is significantly related to the system studied.

Recall equation (6.24) as:

$$[A][Z_j][B]=[C_1]-[C_2] \tag{6.24}$$

and denote the combined equations as

$$[A_3]\{y_1\}=\{b_3\} \tag{6.66}$$

To identify the joint parameters accurately, three basic conditions must be satisfied

1) the error levels in vector $\{b_3\}$ must be low,

2) the error levels in the matrix $[A_3]$ must be low, and

3) the matrix $[A_3]$ must be a well-conditioned matrix.

§6.8.2 Inaccurate Identification due to Not Satisfying Condition 1

If no element in the joint matrix (stiffness, mass and damping matrices) is known, the element in $\{b_3\}$ is a subtraction of the corresponding elements in matrices $[C_1]$ and $[C_2]$. If the magnitudes of elements in matrix $[C_1]$-$[C_2]$ are always much smaller than the element magnitudes of the matrices $[C_1]$ or $[C_2]$ over the available frequency range, the error levels in $\{b_3\}$ are much greater than error levels in $[C_1]$ or $[C_2]$. Therefore, the identified results will be very sensitive to errors in the measured data.

Matrices $[C_1]$ and $[C_2]$ are the measured FRF matrices of the assembly and substructures, which are only determined by the nature of the assembly and substructure systems. This indicates that even if the measured FRF data have the same levels of error, the accuracy of the identified results for different assembled structures can be significantly different.

In practice, difficulties arising from the condition $[C_1] \approx [C_2]$ in identification are often not a real problem, because $[C_1] \approx [C_2]$ only means that the joints are very soft and can simply be ignored. If the joint properties must be accurately identified, then one can use

the FRF data at low frequencies or reset the experimental rig. Some special considerations on experimental rig design will be discussed in §6.9

§6.8.3 Inaccurate Identification due to Not Satisfying Conditions 2 and 3

If several columns in the matrix [A] or several rows in the matrix [B] in equation(6.24) are approximately linearly dependent, the resultant $[A_3]$ matrix in equation (6.66) will be ill-conditioned. Consequently, the identified results are usually very sensitive to measurement errors. The results usually cannot be improved by using more frequency points or measured coordinates. This can be explained as follows:

Consider an equation generated from the αth row of matrix the [A] and the βth column of the matrix [B], the coefficients for z_{ik} and z_{jk} in the $[Z_j]$ matrix are $a_{\alpha i}b_{k\beta}$ and $a_{\alpha j}b_{k\beta}$ respectively. If the ith and the jth columns of matrix [A] happen to be approximately linearly dependent, then the coefficients of z_{ik} and z_{jk} (k=1 to n) will also be approximately linearly-dependent. In other words, the matrix $[A_3]$ constructed from [A] and [B] will still be an ill-conditioned matrix no matter how many frequency points or measured coordinates are selected.

If no restriction and transformation matrices are imposed, the elements in the resultant $[A_3]$ matrix are the products of the corresponding elements in matrices [A] and [B], therefore, the element in $[A_3]$ should have the same error levels as the element in matrix [A] and [B]. As a result, the condition $\underline{2}$ in §6.8.1 is usually satisfied.

If the $[A_3]$ matrix without imposing the restriction condition is ill-conditioned, then the restriction condition should be imposed. When a restriction matrix is imposed, the coefficients in the $[A_3]$ matrix will be the summation of several products, hence the error levels can be higher. Usually, an ill-conditioned matrix can always turn into a well-conditioned matrix by reducing the unknown numbers (an extreme case is to reduce the unknown number to one). However, because the error levels in $[A_3]$ can be high, the accuracy of the identified results may not necessarily be improved.

Columns and rows in the matrices [A] and [B] can be linearly dependent when the joint coordinates on the substructure system has little deformation, and/or the joint on the assembly has little deformation. In the first case, accuracy of the identified results can usually be improved by imposing the restriction condition; in the second case, however, the accuracy of the results will be very sensitive to the measurement errors even if the restriction matrix is imposed.

§6.8.4 Numerical Illustration

§6.8.4.1 Case C: Case Not Satisfying Condition 1 in §6.8.1

This case study illustrates the problems with very soft joints, therefore, condition 1 in §6.8.1 is not satisfied. The system studied is very similar to the system studied in §6.6.2 The substructures are exactly the same, but the the joint has only 1% of the stiffness of the joint in §6.6.2. For simplicity, the joint is assumed to have neither mass nor damping. Table 6.14 shows the identified relative stiffness in a frequency range 400-1000Hz with frequency increment 20Hz, the FRF data are polluted by 5% random errors. The results are very poor.(Case C1)

	k(1,1)	k(1,2)	k(1,3)	k(1,4)	k(2,2)	k(2,3)	k(2,4)	k(3,3)	k(3,4)	k(4,4)
case C1	-20.77	12.51	-1.06	1.98	-3.27	1.92	0.36	-35.03	14.82	-2.90
case C2	1.00	0.97	1.00	1.00	1.06	1.00	0.98	0.97	1.02	1.01

Table 6.14 Relative values of the identified results for case C

Figure 6.8 shows the receptance at coordinate 1 for the assembly and substructure systems. The difference between these two curves is so small that the effects of the joint can be ignored.

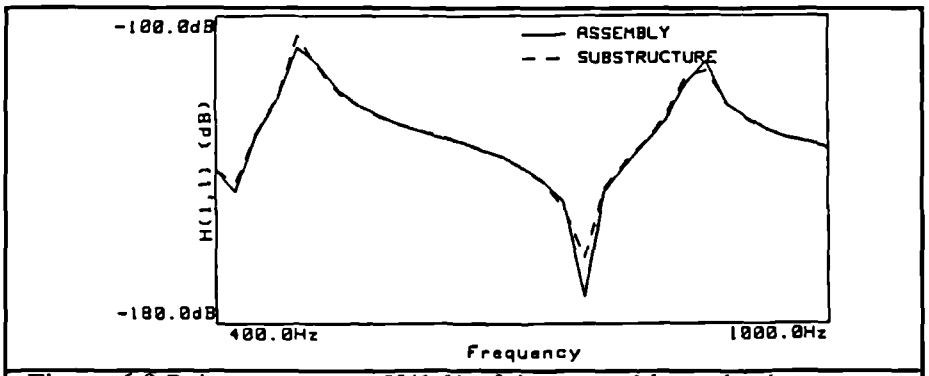

Figure 6.8 Point receptance H(1,1) of the assembly and substructure in a high frequency range

If the FRF data are measured at lower frequencies (1-50Hz), the difference between the FRFs of the substructure and assembly is enlarged as shown in figure 6.9. As expected, accurate results are found as shown in the second row of table 6.14. (Case C2)

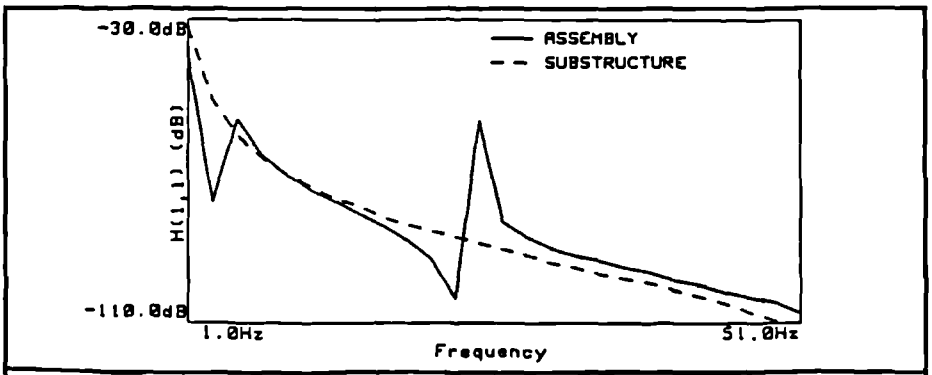

Figure 6.9 Point receptance H(1,1) of the assembly and substructure in a low frequency range

§6.8.4.2 Case D: Case Not Satisfying Conditions 3 in §6.8.1 and Results Can Be Improved by Imposing Proper Restriction Conditions.

A schematic diagram for the case studied in this section is shown in figure 6.10.

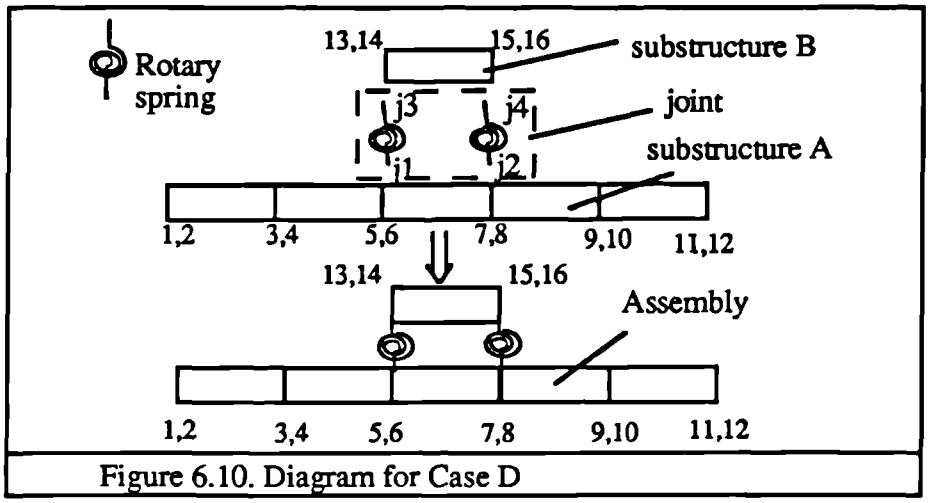

Figure 6.10. Diagram for Case D

The substructure A consists of five finite beam elements and substructure B consists of one beam element. The properties of the beam element (i.e. mass, stiffness and damping matrices) are exactly the same as those of the beam element in §6.6.1. Substructures A and B are coupled by 4 rotational coordinates 6, 8, 14 and 16 (corresponding to joint coordinate j_1, j_2, j_3 and j_4), hence the joint element is a 4×4 impedance matrix. The joint consists of two springs in the rotational direction and has no mass or damping. The stiffness of the two rotary springs of the joint element is 1987.2N.m/rad. The FRF data are assumed to be measured in the frequency range 40Hz to 500Hz with a frequency increment of 20Hz and polluted by 5% random errors. The impedance (stiffness) matrix is:

$$[Z_j]=\begin{bmatrix} x_1 & x_2 & x_3 & x_4 \\ x_2 & x_5 & x_6 & x_7 \\ x_3 & x_6 & x_8 & x_9 \\ x_4 & x_7 & x_9 & x_{10} \end{bmatrix}=\begin{bmatrix} 1987.2 & 0 & -1987.2 & 0 \\ 0 & 1987.2 & 0 & -1987.2 \\ -1987.2 & 0 & 1987.2 & 0 \\ 0 & -1987.2 & 0 & 1987.2 \end{bmatrix} \text{N.m/Rad}$$

The corresponding vector form of the joint elements is

$$\{z_j\}=\{x_1,x_2,x_3,x_4,x_2,x_5,x_6,x_7,x_3,x_6,x_8,x_9,x_4,x_7,x_9,x_{10}\}^T$$

In the first case (case D1), no other restriction condition except for the assumption of symmetry is imposed. The identified results are shown in table 6.15. The identified results are divided by the true stiffness k=1987.2N.m/Rad, therefore, the exact results should be 1, 0 or -1. It can be seen that except for elements x_1, x_2 and x_5, there are great discrepancies between the identified results and their true values. However, there is hardly any difference between the assembly FRFs regenerated from the identified joint

stiffness and noise-free substructure FRFs and the real FRFs of the assembly (figure 6.11). This means that the identified results do represent the effects of the joint.

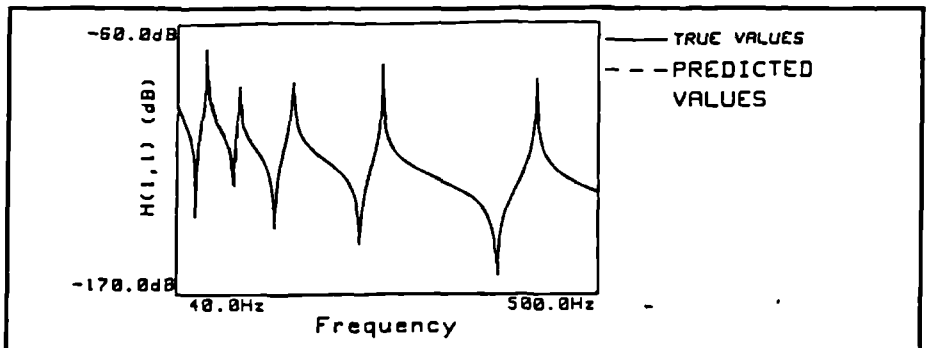

Figure 6.11 True receptance and predicted receptance from a "wrong" joint model

	$\frac{x_1}{k}$	$\frac{x_2}{k}$	$\frac{x_3}{k}$	$\frac{x_4}{k}$	$\frac{x_5}{k}$	$\frac{x_6}{k}$	$\frac{x_7}{k}$	$\frac{x_8}{k}$	$\frac{x_9}{k}$	$\frac{x_{10}}{k}$
exact	1.00	0.00	-1.00	0.00	1.00	0.00	-1.00	1.00	0.00	1.00
case D1	0.99	-0.03	-0.65	-0.36	1.05	-0.27	-0.73	-58.30	59.48	-58.58
case D2	0.99	-0.03	-1.00	0.00	1.05	0.00	-1.00	0.99	0.00	1.10
case D3	1.00	0.00	-1.00	0.00	1.00	0.00	-1.00	-4.15	5.04	-3.92

Table 6.15. Relative values of the dentified results for case D1, case D2 and case D3

To understand the problem of the large difference between the identified and the exact joint parameters, and the insignificant difference between the predicted and true dynamic characteristics of the assembly, consider an equation composed from one column in matrix [A] and one row in matrix [B]. Because substructure B is very short and light, the responses at points 14 and 16 are always close to each other. Consequently, one may write the row in matrix [A] as $\{a,b,c+\Delta_1, c+\Delta_2\}$ and the column in matrix [B] as $\{e,f,g+\Delta_3,g+\Delta_4\}^T$. where $\Delta_1,\Delta_2,\Delta_3$ and Δ_4 are second order terms compared with c and g and can contain high levels of measurement errors. The equation is

$$\{a,b,c+\Delta_1, c+\Delta_2\}\begin{bmatrix} x_1 & x_2 & x_3 & x_4 \\ x_2 & x_5 & x_6 & x_7 \\ x_3 & x_6 & x_8 & x_9 \\ x_4 & x_7 & x_9 & x_{10} \end{bmatrix}\begin{Bmatrix} e \\ f \\ g+\Delta_3 \\ g+\Delta_4 \end{Bmatrix} = h_1 - h_2 \qquad (6.67)$$

Rearranging equation (6.67) and ignoring the second order terms yields

$$aex_1+(af+be)x_2+(ag+ce)(x_3+x_4)+bfx_5+(bg+fc)(x_6+x_7)+cg(x_8+2x_9+x_{10})=h_1-h_2 \qquad (6.68)$$

It is clear that the coefficients of some elements such as x_3 and x_4 are approximately proportional (taking the neglected second order terms into account). Therefore, if no restriction condition is imposed, except for x_1, x_2 and x_5, the rest of the results will be

erroneous. However, the identified x_3+x_4, x_6+x_7 and $x_8+2x_9+x_{10}$ should be accurate. These deductions are verified from the identified results in table 6.15.

From equation (6.68), it can also be predicted that in order to ensure that the identified results are accurate, the maximum number of independent unknowns cannot exceed 6.

However, it is not true that if the unknown number is less than 6, accurate results are always obtained, or the smaller the number of unknowns, the higher the accuracy of the identified results. In the following examples, it will be shown that when improper restriction conditions are imposed, even if the total number of unknowns is less than 6, the identified results can still be erroneous.

Case D2: Assume

$$x_4=0, x_6=0, x_9=0, x_8=x_1 \qquad (6.69)$$

Substituting these restriction conditions into equation(6.68) leads to

$$(ae+cg)x_1+(af+be)x_2+(ag+ce)x_3+bfx_5+(bg+fc)x_7+cgx_{10}=h_1-h_2 \qquad (6.70)$$

All the coefficients are now independent, therefore, accurate results are expected.

Case D3: Assume $x_1, x_2, ..x_7$ are known, hence the total unknown number is only 3.

Substituting the restriction conditions into equation(6.68) yields

$$cgx_8+2cgx_9+cgx_{10}=h_1-h_2-aex_1-(af+be)x_2-(ag+ce)(x_3+x_4)-bfx_5-(bg+fc)(x_6+x_7) \qquad (6.71)$$

The coefficients on the left hand side of equation(6.71) are still linearly-dependent, therefore, the accuracy of the identified results is expected to be poor although the total number of the unknowns is less than 6.

Physically, this case is an example in which the interface part of one substructure is very "stiff" (the word "stiff" here means that the stiffness at the interface of the substructure is high enough so that the responses at the interface coordinates of the substructure become linearly-dependent). Because there is only a very small relative displacement between joint coordinates at the substructure, the two coordinates on the substructure interface can actually be approximately treated as the same coordinate. As a result, it makes little difference to the assembly response if a stiffness element (or a damping element) is connected to these coordinates on the rigid interface (eg. add a rotary spring between coordinates 14 and 16 in figure 6.10). Figure 6.12 shows another alternative for modelling the joint. Provided $k_1+k_3=k_2+k_4=1987.2$N/m, the properties of the assembly will be very similar to the assembly with a joint consisting of two rotary springs only. In other words, there can be several approximate ways to model the joint.

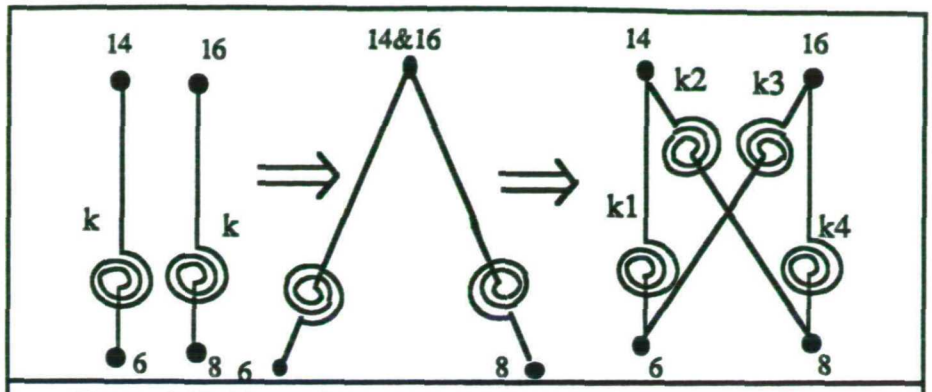

Figure 6.12 Alternatives to model the joint in case D

Although the joint can be modelled approximately in several ways, when the real joint changes (eg.the stiffness of the rotary springs changes), the characteristics of the assembly do change. For this kind of problem, if a physically sensible model is assumed (by imposing restriction to impedance matrix of the joint), the identified results are usually not sensitive to measurement errors.

§6.8.4.3 Case E: Case Not Satisfying Conditions 2 and 3 in §6.8.1 and Results Cannot be Improved by Imposing the Restriction Condition

Figure 6.13 shows a schematic diagram for case E. The substructure A has three beam elements and the substructure B has two. The stiffness of all the beam elements are the same as those in §6.6.2. The mass of beam elements of substructure A is also the same as those in §6.6.2, but the mass of the beam elements of substructure B is only 0.01 of the beam element. The damping of the substructure is assumed to be proportional and is 0.1% of the corresponding stiffness.The joint has no mass or damping. The frequency range is 100 to 400Hz with a frequency increment of 10Hz.

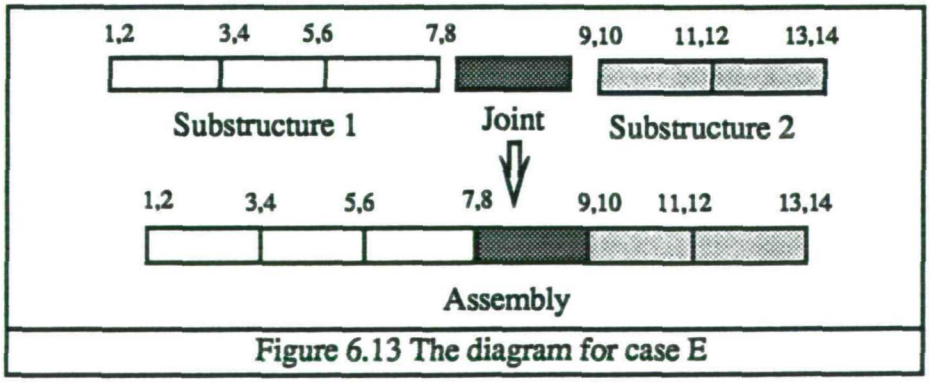

Figure 6.13 The diagram for case E

Because the substructure B is very light, the joint of the assembly will have little deformation if the assembly is excited. Therefore, a row in matrix [A] (which corresponds to the receptance related to coordinate 7,8,9 and 10) can be written as

$\{a,c+\Delta_1,b,c+\Delta_2\}$ where $c = \frac{b-a}{L} = \frac{b-a}{0.3}$, if a column in [B] is $\{d,e,f,g\}^T$, then any equation constructed from these rows and columns yields:

$$\{a,c+\Delta_1,b,\ c+\Delta_2\}\begin{bmatrix} x_1 & x_2 & x_3 & x_4 \\ x_2 & x_5 & x_6 & x_7 \\ x_3 & x_6 & x_8 & x_9 \\ x_4 & x_7 & x_9 & x_{10} \end{bmatrix}\begin{Bmatrix} d \\ e \\ f \\ g \end{Bmatrix} = h_1 - h_2 \qquad (6.72)$$

or $adx_1+(ae+(c+\Delta_1)d)x_2+(af+bd)x_3+(ag+(c+\Delta_2)d)x_4+(c+\Delta_1)ex_5+((c+\Delta_1)f+be)x_6$
$+((c+\Delta_1)g+(c+\Delta_2)e)x_7+bfx_8+(bg+(c+\Delta_2)f)x_9+(c+\Delta_2)gx_{10}=h_1-h_2$ (6.73)

The coefficients of x_5, x_7 and x_{10} (which are ce, cg+ce and cg respectively ignoring the second order terms) are approximately linearly dependent. Therefore, accurate results cannot be achieved. The identified results without restriction are shown in table 6.16 as case E1.

	K(1,1)	K(1,2)	K(1,3)	K(1,4)	K(2,2)	K(2,3)	K(2,4)	K(3,3)	K(3,4)	K(4,4)
case E1	0.37	0.38	0.42	0.30	0.56	0.39	0.01	0.34	0.29	0.42
case E2	0.68	0.68	0.68	0.68	0.68	0.68	0.68	0.68	0.68	0.68
case E3	1.09	1.01	1.00	1.00	1.01	1.01	1.03	1.01	1.01	1.01

where x_{ie}, i=1,...,10 are exact values of the joint element

Table 6.16. Relative values of the identified results of case E1, case E2 and case E3

Because the coefficients on the left hand side of equation (6.73) are approximately linearly dependent, one may try to improve the accuracy of the identified results by means of imposing some restrictions on the impedance matrix of the joint. The most effective restriction condition (if restriction has any effects) is to reduce the number of unknowns to one, i.e. to assume the joint impedance matrix has the form:

$$[Z_j]=\begin{bmatrix} 12 & 6L & -12 & 6L \\ 6L & 4L^2 & -6L & 2L^2 \\ -12 & -6L & 12 & -6L \\ 6L & 2L^2 & -6L & 4L^2 \end{bmatrix} y \qquad (6.74)$$

where L=0.3 and y is the only unknown

Substitution of equation (6.74) into equation (6.73) leads to the final equation:

$$\{(6Ld-6Lf+4L^2e+2L^2g)\Delta_1+(6Ld-6Lf+4L^2g+2L^2e)\Delta_2\}y=h_1-h_2 \qquad (6.75)$$

The significant terms (eg. ad) have cancelled each other out. Since Δ_1 and Δ_2 are two small values and can contain significant levels of measurement errors, the identified results are expected to be sensitive to errors.

The case with only one unknown is referred to as case E2. It can be seen that even if there is only one unknown, the identified results is still less than 70% of its true value.

Physically, this is a case that the joint stiffness is relatively high so that there is little deformation in the joint. Because the deformation at the joint is small, increasing or decreasing the stiffness usually makes little difference to the overall dynamic characteristics of the assembly. Consequently, a small change of FRFs of the assembly will mean a great change in the joint. Therefore, the identified results must be very sensitive to the measurement noise, and imposing a restriction will usually have little effect on improving the accuracy of the results.

To improve the accuracy of the identified results, it must be ensured that the joint has sufficient deformation. Usually, at higher frequencies, the deformation of the joint will increase, therefore, using FRFs at higher frequencies will be a natural choice to improve the accuracy of the identification.

If FRF data are available in a frequency range 600Hz to 1620Hz with a frequency increment 30Hz (case E3), the accuracy of the identified results can be improved. It can be noted from table 6.16 that even if no restriction is imposed for case E3, the accuracy of the identified results is much higher than the identified results from low frequency FRFs. For most elements, the error levels are only about 1%

The problem with using higher frequency FRF data is that it is not applicable to joints with characteristics which vary with frequency. In addition, there are practical limits on the frequency at which the FRF data can be accurately measured. Outside the limit, the measurement errors increase dramatically.

§6.8.5 Practical Considerations on Experimental Set-up for Accurate Identification

In §6.8.3 and §6.8.4, it is shown that if a joint has too small or too large deformation, the identified results can be inaccurate. It is also shown that the proper choice of frequency range can adjust the deformation levels. The main disadvantage in using the frequency range to adjust the deformation levels is that the joint property must be frequency independent. In addition, there is clear physical restriction in the frequency ranges that can be measured.

Actually, the joint deformation levels can also be controlled to some extent by using the correct experimental arrangement. In this section only the case with a stiff joint is illustrated, but the principle is also applicable to the case with a soft joint although opposite measures should be taken.

The structure studied is the same as case E. However, instead of having substructure B in a free-free condition, one end of the substructure B is clamped (i.e. substructure B becomes a cantilever beam). Two springs (one translational with stiffness 662400N/m and one rotary with stiffness 1987.2Nm/rad) are used to simulate the boundary condition at the clamped end of the substructure B. A schematic diagram for the system is shown in figure 6.14 as case F1.

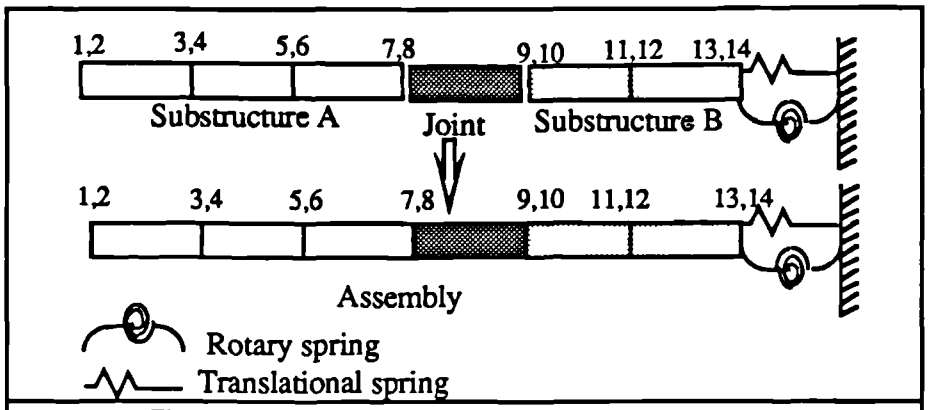

Figure 6.14 The diagram for case F1

The FRF data is assumed to be measured in the same frequency range (100-400Hz) with the same frequency increment (10Hz). The identified joint matrix is shown in table 6.17. It can be seen that the identified results are much more accurate than case E1.

	K(1,1)	K(1,2)	K(1,3)	K(1,4)	K(2,2)	K(2,3)	K(2,4)	K(3,3)	K(3,4)	K(4,4)
case F1	0.88	0.89	0.88	0.86	0.91	0.88	0.80	0.88	0.85	0.89
case F2	0.85	0.85	0.85	0.82	0.89	0.85	0.75	0.85	0.82	0.85
case F3	1.01	0.99	1.01	1.01	1.04	1.01	1.01	1.02	1.01	1.01

Table 6.17.Relative values of the identified joint parameters with special consideration on experimental arrangement

Another alternative method to increase the deformation at the joint is to add mass to the substructure B. If a 1 kg mass is added to the free end of the substructure B as shown in figure 6.15, the deformation at the joint will increase, therefore, the accuracy of the identified results is improved. The calculated results are shown in the second row of table 6.17 (as case F2).

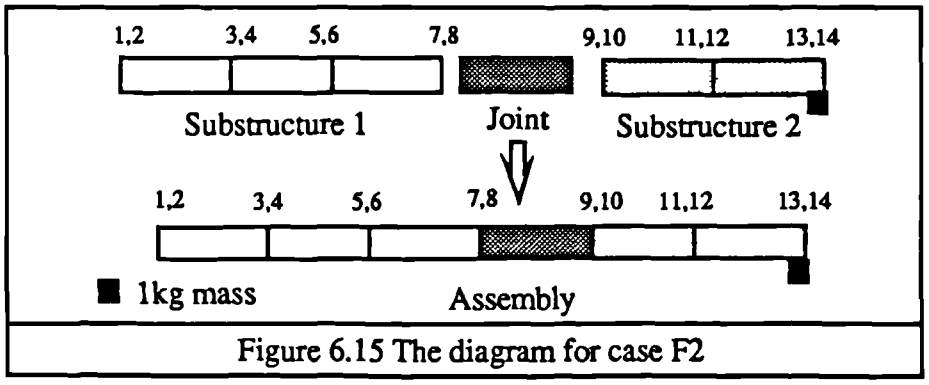

Figure 6.15 The diagram for case F2

If heavier masses are attached to the structure (say two 2kg masses are attached to coordinates 9 and 13 respectively as shown in figure 6.16(case F3), even more accurate results can be obtained. the results of case F3 are shown in table 6.17. It can be noted that the average error levels in the identified results is only about 1%.

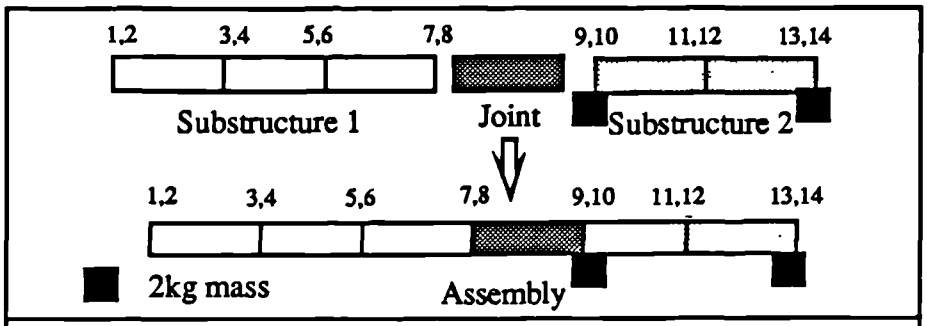

Figure 6.16 The diagram for case F3

§6.9 APPLICATION OF GENERALIZED COUPLING TECHNIQUES TO JOINT IDENTIFICATION

§6.9.1 Theory

It has been shown in the last section that if a joint deforms insignificantly, the identified results are usually very severely affected by various measurement errors in the FRF data. If a joint is very stiff, then the deformation of the joint will be insignificant no matter how the experiment is arranged, therefore, it is virtually impossible to identify this joint accurately. To make things worse, hard joints can affect the accuracy of identification of other effective joints (i.e. joints with sufficient deformation).

If a joint is very stiff, it may be reasonable to assume that the joint is completely rigid, the generalized coupling techniques can then be used to couple the substructures through the rigid joint first, then the coupled structure is treated as a new substructure, and the FRFs of this new substructure are used for identification. After the coupling, the hard joint is not involved in the identification process. If the rigid joint is massless, then the joint coordinates of the stiff joint can be completely deleted, otherwise, half the stiff joint coordinates should be retained to present the mass effects of the stiff joints.

Figure 6.17. shows the two steps for incorporation of coupling and joint identification techniques.

In Chapter 5, it is shown that due to the inconsistent errors, the errors in the predicted assembly response are usually magnified. The worst case is at the resonance frequencies of the substructure. Therefore, in the identification process, the FRFs at these frequencies should be excluded.

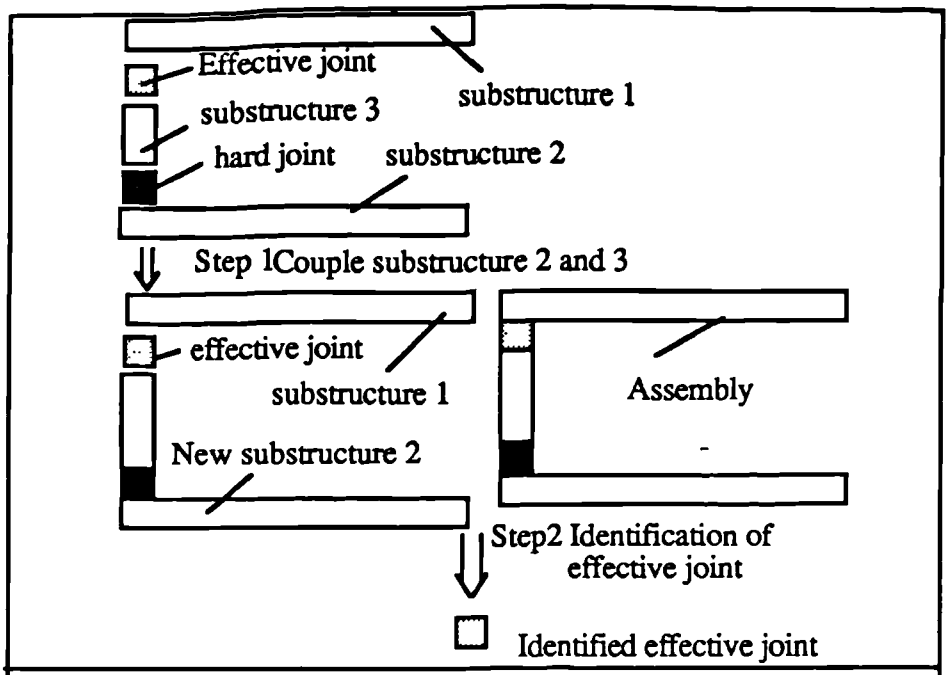

Figure 6.17 Two steps for the identification of effective joint properties

§6.9.2 Numerical Case Studies

Consider the beam system shown in figure 6.18.

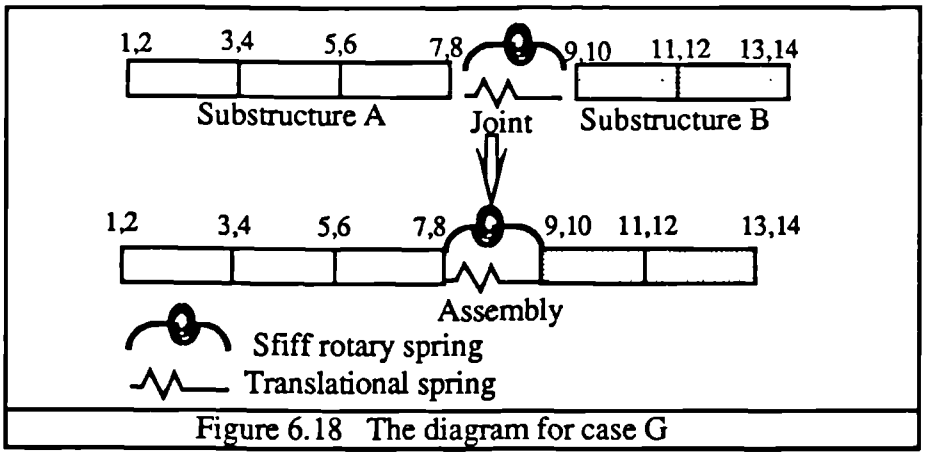

Figure 6.18 The diagram for case G

The substructures A and B are exactly the same as in §6.6.2, the joint element consists of two springs, one translational (662400 N/m) and one rotational (1987.2Nm/rad). The translational spring connects coordinates 7 and 9; the rotational spring connects coordinates 8 and 10. The FRF data are measured over a frequency range 100-500Hz with a frequency increment 20Hz and are polluted by 5% random noise. The joint matrix is assumed to have the form

$$[K_j]=\begin{bmatrix} x_1 & x_2 & 0 & 0 \\ x_2 & x_3 & 0 & 0 \\ 0 & 0 & x_4 & x_5 \\ 0 & 0 & x_5 & x_6 \end{bmatrix}$$

Five cases are studied and the identified stiffness in their relative values are shown in table 6.18. When no generalized coupling technique is applied, the accuracy of the identified joint element related to the rotary coordinates is poor, and the identified joint parameters in the translational direction are not very accurate either (even for the case with only two stiffness unknowns (case G3)). However, if generalized coupling techniques are applied and the FRFs at the resonance frequencies of the coupled substructure are excluded (Case G5), the accuracy of the identified results is improved significantly.

	$\frac{x_1}{k_1}$	$\frac{x_2}{k_1}$	$\frac{x_3}{k_1}$	$\frac{x_4}{k_2}$	$\frac{x_5}{k_2}$	$\frac{x_6}{k_2}$	Further Restriction	Resonant FRF	Coupling
CaseG1	4.8	-5.3	8.5	-2.3e-4	-2.6e-4	-2.8e-4	**********	yes	no
CaseG2	5.6	-5.2	9.4	-4.8e-4	-5.1e-4	-5.2e-4	**********	no	no
CaseG3	0.16	0.16	0.16	-3.5e-4	-3.5e-4	-3.5e-4	x_1-x_2=x_3,x_4=x_5=x_6	no	no
CaseG4	0.40	0.55	0.36	**	**	**	**********	yes	yes
CaseG5	0.93	1.04	0.82	**	**	**	**********	no	yes

Table 6.18 The identified joint parameters for a structure with both hard and effective joints

§6.10 THE EFFECTS OF CONSISTENT ERRORS, APPLICATION OF MODAL ANALYSIS TECHNIQUES AND SELECTION OF FREQUENCY POINTS

In Chapter 5, it is shown that using modal analysis, the effects of inconsistent errors can be eliminated, and in most cases, the accuracy of the predicted assembly results can be significantly improved. Therefore, it would be a natural extension to introduce modal analysis in the joint identification.

If modal analysis is applied, the inconsistent errors are eliminated. However, the consistent errors will be retained, and sometimes, consistent errors may be introduced during the modal analysis. Therefore, it is necessary to study the effects of consistent errors on the accuracy of the identification, if the modal analysis technique is to be introduced in the joint identification.

When random error is introduced, the FRF is polluted proportionally, i.e. the error in any FRF at any frequency does not exceed a small bound (say 5%). However, if there are consistent errors, the resonance frequency can be shifted slightly. At frequencies close to the resonance frequency, the error levels in the the FRFs can be much more significant. Therefore, the frequencies close to (both the substructure and the assembly) the resonance frequencies should not be used in the joint identification.

To illustrate the effects of consistent errors, consider the system in §6.6.1 again. Instead of having random errors, 5%, 1% and 1% errors are used to pollute the mode shape, natural frequency and modal damping respectively, the other parameters used are exactly the same as that of case A in §6.6.2. Figure 6.19 and figure 6.20 show the first elements

of the identified stiffness against the frequency and table 6.19 shows the identified stiffness element in their relative values. It is noted that if all the frequency points are used (case H1), the accuracy of the identified results ' very poor; and if the FRFs close to resonance frequencies are excluded(case H2), the accuracy of the results is improved significantly. It is also noted that if all the frequency points are used in the identification, there is a dramatic change at around 570Hz in the identified stiffness. This frequency corresponds to one of the substructure natural frequencies. The change is much less significant when these frequency points are excluded. The significant change in the identified results along the frequency axis clearly indicates the effects of the consistent errors. Checking the identified results along the frequency axis gives a good indication whether some of the frequency points should be excluded.

	K(1,1)	K(1,2)	K(1,3)	K(1,4)	K(2,2)	K(2,3)	K(2,4)	K(3,3)	K(3,4)	K(4,4)
case H1	6.178	-1.16	-0.39	1.41	1.73	1.80	6.87	2.70	0.43	1.10
case H2	2.66	0.38	0.88	1.03	1.18	1.12	0.88	1.79	0.68	1.02

Table 6.19 The relative values of the identified joint parameters from data contaminated by consistent errors.

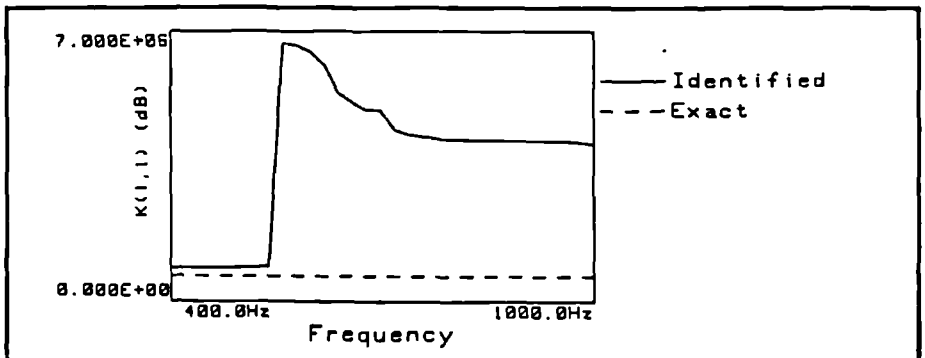

Figure 6.19 The identified stiffness $K_j(1,1)$ using the FRF data contaminated by consistent errors (including FRFs at resonances)

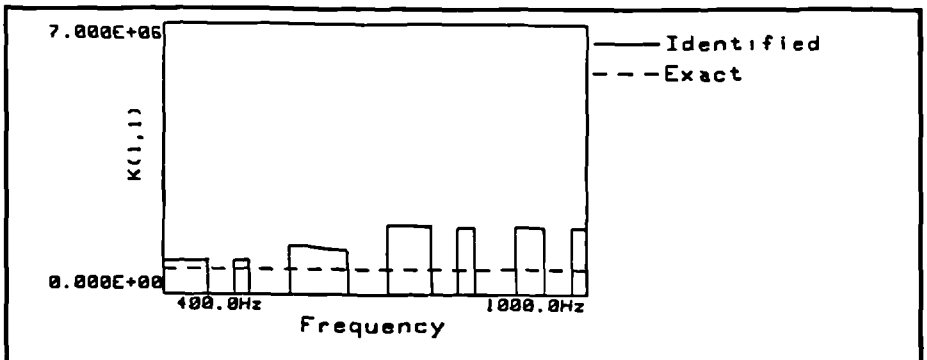

Figure 6.20 The identified stiffness $K_j(1,1)$ using the FRF data contaminated by consistent errors (excluding FRFs at resonances)

The above results indicate that the consistent errors can have significant effects on the joint identification. Unfortunately, the consistent errors cannot be eliminated from modal analysis. Indeed, because of the effects of the modes outside the measured frequency range, the levels of the consistent errors can actually be higher. If applying modal

analysis can eliminate random errors, but does not introduce consistent errors, the accuracy of the identified results should be improved, but if consistent errors are introduced during the application of the modal analysis techniques, then the accuracy of the results can be worse. In summary, the modal analysis techniques must be used with great caution.

§6.11 THE BASIC STRATEGY IN DEALING WITH JOINT MASS

In the foregoing sections, various factors that affect the accuracy of the identification have been discussed. Using the formulae proposed, it is possible to identify the stiffness, mass and damping matrices uniquely. Experience indicates that much more FRF data are required to identify both mass and stiffness matrices of the joint than that required for the identification of the stiffness matrix only. This is because both stiffness and mass contributed to the impedance element of the joint, and it is the impedance of the joint that affects the assembly response.

In practice, the mass of the joint is usually not significant, and it can often be modelled simply and accurately (sometimes simply by weighting). If the mass of the joint can be evaluated, the mass properties of the joint should be used as some known parameters in the identification process rather than to identify both the stiffness and mass matrices together.

§6.12 JOINT IDENTIFICATION WITH INACCESSIBLE ASSEMBLY JOINT COORDINATES

§6.12.1 Direct Solution

Sometimes, the joint coordinates are not accessible after the structure has been assembled, i.e. for assembly, the only available receptance matrix is $[H_{nn}]$. Therefore, the formulae derived (equations(6.16-19)) cannot be used directly, other formulae are required.

Multiplying both side of equation (6.16) by the matrix $[H_{ba}]^+$ leads to

$$[H_{nj}][Z_j]=([H_{aa}]-[H_{nn}])\,[H_{ba}]^+ \tag{6.76}$$

Substituting equation (6.76) in equation (6.17) yields

$$[H_{nj}]=[H_{ab}]-([H_{aa}]-[H_{nn}])[H_{ba}]^+[H_{bb}] \tag{6.77}$$

Equation(6.77) shows that the matrix $[H_{nj}]$ can be found from the matrix $[H_{nn}]$ and the receptance matrix of the substructure.

Substituting equation (6.77) back into equations (6.16) yields

$$\{[H_{ab}]-([H_{aa}]-[H_{nn}])[H_{ba}]^{+}[H_{bb}]\}[Z_j][H_{ba}]=[H_{aa}]-[H_{nn}] \qquad (6.78)$$

Equation (6.78) at different frequencies can be combined together in the way already discussed in §6.4

However, if the receptance matrix is polluted by measurement errors, the matrix $[H_{nj}]$ calculated from equation(6.77) can contain much higher error levels than that in other sub-matrices, therefore, the identified joint properties from equation (6.78) are usually found to be very sensitive to measurement errors.

§6.12.2 Solution Using Indirect Iterative Methods

§6.12.2.1 General

Identification using equation(6.78) is a direct method. However, the joint properties can also be identified using the indirect iterative method. Recall equation(6.12)

$$[H_{nn}]=[H_{aa}]-[H_{ab}]([I]+[Z_j][H_{bb}])^{-1}[Z_j][H_{ba}] \qquad (6.12)$$

Matrix $[H_{nj}]$ is not required in this equation. Equation (6.12) is effectively the same as the coupling equation in Chapter 5. From Chapter 5, it is known that when the substructure data are polluted by random errors, the predicted assembly response using equation (6.12) will usually not be smooth, but at frequencies other than the substructure natural frequencies, the discrepancy between the predicted and real assembly response is usually not significant. This clearly indicates that equation(6.12) is still approximately correct at frequencies other than the substructure natural frequencies. Therefore, the [Zj] matrix identified from equation(6.12) should be more accurate than that identified from equation(6.77). The problem with equation(6.12) is that it is nonlinear and it cannot be solved directly. Therefore, iterative methods must be used.

The methods which have been applied to solve equation(6.12) are function minimization methods [85](which includes the Patten Search method, the DFP method, the Powell method and the Steepest Descent method) and the Newton-Raphson method[2] (Which is actually also a function minimization method). It is found that the Newton-Raphson method (or the sensitivity analysis) is more efficient than the function minimization methods. Only this method is described in the next section.

§6.12.2.2 Application of the Newton-Raphson method

The aim of joint identification is to minimise the difference between the measured and predicted assembly response. To use the Newton-Raphson method, a vector is constructed:

$$\{F\}=\begin{Bmatrix}\{\text{real}(h_m-h_p)\}\\ \{\text{imag}(h_m-h_p)\}\end{Bmatrix} \tag{6.79}$$

where h_m and h_p are the predicted and measured receptance elements between different coordinates and at different frequencies.

The following iteration process is used:

$$\{y^{(k+1)}\}=\{y^{(k)}\}+[J(y^{(k)})]^{+}\{F(y^{(k)})\} \tag{6.80}$$

or to avoid overshooting

$$\{y^{(k+1)}\}=\{y^{(k)}\}+\beta[J(y^{(k)})]^{+}\{F(y^{(k)})\} \tag{6.81}$$

where

$$[J(y^{(k)})]=\frac{\partial F}{\partial y^{(k)}} \tag{6.82}$$

is the Jacobian (or the sensitivity matrix), and β is a scaling factor on the modification

The converged solution from equation(6.81) is the least-squares solution for equation (6.79), i.e.

$$\|F(\{y\})\|\rightarrow \text{minimum} \tag{6.83}$$

One method to determine the β value is to use 1D minimization [85] so that

$$\|F(\{y^{(k)}\}+\beta[J(y^{(k)})]^{+}\{F(y^{(k)})\})\|\rightarrow \text{minimum} \tag{6.84}$$

Experience shows that this approach is not necessary. The 1D minimization can itself be expensive. Instead of 1D minimization, the following approach may be adopted

First set $\beta=1$ and if

$$\|F(\{y^{(k)}\}+\beta[J(y^{(k)})]^{+}\{F(y^{(k)})\})\| < \|F(\{y^{(k)}\})\| \tag{6.85}$$

then update $\{y^{(k)}\}$ with $\{y^{(k+1)}\}$, otherwise, set $\beta=\frac{\beta}{5}$ and repeat the checking process until equation(6.85) is satisfied.

The analytical Jacobian matrix is usually not available, therefore, a finite difference approximation is used as

$$J_{ij}=\frac{\partial F_i}{\partial y_j}=\frac{F_i(y+\Delta y_j)-F(y-\Delta y_j)}{2\delta y_j} \tag{6.86}$$

$$\text{where } \delta y_j=\begin{cases} 10^{-6} & \text{if } |p_j| < 10^{-4} \\ 10^{-6}\,|p_j| & \text{if } |p_j| \geq 10^{-4} \end{cases} \tag{6.87}$$

To reduce the effects of numerical errors, the unknowns are so scaled that the difference between the unknowns does not exceed the order of 10^2.

§6.12.2.3 Computation Consideration and Weighting

There can be practical difficulties in direct application of the algorithm discussed in §6.12.2.2, especially when the code is run on a small computer. For the Jacobian matrix, the number of rows is the product of the number of the elements at each frequency ($N_{size}(N_{size}+1)$) taking the symmetry of $[H_{nn}]$ and the real and imaginary parts of $[H_{nn}]$ into account, and the number of the frequency points. i.e.

$$N_{row}=N_{freq}N_{size}(N_{size}+1) \tag{6.88}$$

$$N_{col}=k_0 \tag{6.89}$$

where N_{row} and N_{col} are the number of rows and columns of the Jacobian, N_{freq} and N_{size} are the numbers of the frequency points and the size of the matrix $[H_{nn}]$, and k_0 is the number of unknowns.

It is noted from equation (6.88) and (6.89) that the size of the Jacobian can be significant.

Equation(6.80) is the least-squares solution for

$$[J(y_i)]\{\Delta y_i\}=F(y_i) \tag{6.90}$$

where $\{\Delta y_i\}=\{y_{i+1}\}-\{y_i\}$

In §6.5, it is known that the solution for equation (6.80) can be found through its sub-matrix operations. Let

$$[J(y_i)]=\begin{bmatrix}[J_0(\omega_1)]\\ [J_0(\omega_2)]\\ \vdots\\ [J_0(\omega_i)]\\ \vdots\\ [J_0(\omega_n)]\end{bmatrix} \text{ and } \{F(y_i)\}=\begin{Bmatrix}\{F_0(\omega_1)\}\\ \{F_0(\omega_2)\}\\ \vdots\\ \{F_0(\omega_i)\}\\ \vdots\\ \{F_0(\omega_n)\}\end{Bmatrix} \qquad (6.91,6.92)$$

where $[J_0(\omega_i)]$ and $\{F_0(\omega_i)\}$ are the sub-matrix and sub-vector at frequency ω_i

Then the solution is

$$\{\Delta(y_i)\} =\Big[\sum_{i=1}^{n} \alpha_i^2[J_0(\omega_i)]^T[J_0(\omega_i)]\Big]^{-1} \sum_{i=1}^{n} \left(\alpha_i^2[J_0(\omega_i)]^T\{F_0(\omega_i)\}\right) \qquad (6.93)$$

where α_i is the weighting at each frequency.

If $\alpha_i=1$, the direct solution is obtained. An alternative is to set $\alpha_i=\frac{1}{\|J_0(\omega_i)\|}$, which effectively means that all the frequency points are of the same importance.

It should be noted that the weighted equation(6.93) gives the weighted least-squares solution, i.e.

$$\|F\|=\sum_{i=1}^{n}\alpha_i^2\|F_0(\omega_i)\| \qquad (6.94)$$

The weighting is essential to ensure convergence to the true solution.

§6.12.2.4 Selection of Frequency

The measured FRFs at some frequencies should not be used, this is mainly due to the following reasons:

1) At the substructure natural frequencies, the predicted assembly response from coupling can be significantly affected by the measurement noise. This has been discussed in Chapter 5.(§5.9).

2) The FRFs at some frequencies can cause local minima and the solution will converge to these local minima rather than the true joint values.

Consider the following two examples:

Figure 6.21 shows three FRFs. Curve B is clearly closer to curve C (the true value) than curve A (initial estimation). However, the value of the objective function of curve B will actually be greater than that of curve A, because one frequency point (ω_3) coincides with the natural frequency of the curve B, hence the differences between curves B and C are significant. Therefore, the frequencies between the predicted and true resonance frequencies should be excluded in the identification process.

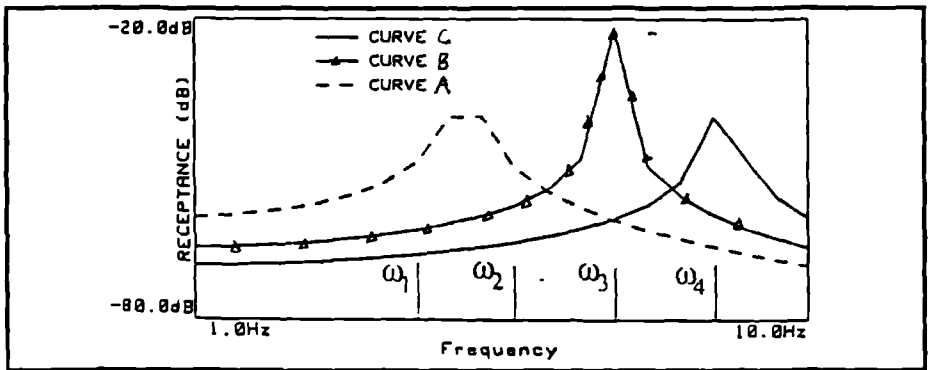

Figure 6.21 An example of possible local minima caused by including FRFs between the true and predicted resonances.

Another possible case for the local minima is that one natural frequency of the predicted assembly is closer to another natural frequency of the real assembly as shown in figure 6.22. When ω_{B2} approaches its true value ω_{A2}, the value of the objective function can actually increase. In this case, the FRFs between ω_{A1} and ω_{B2} should not be used in the iteration process until the predicted ω_{B2} is sufficiently close to ω_{A2}.

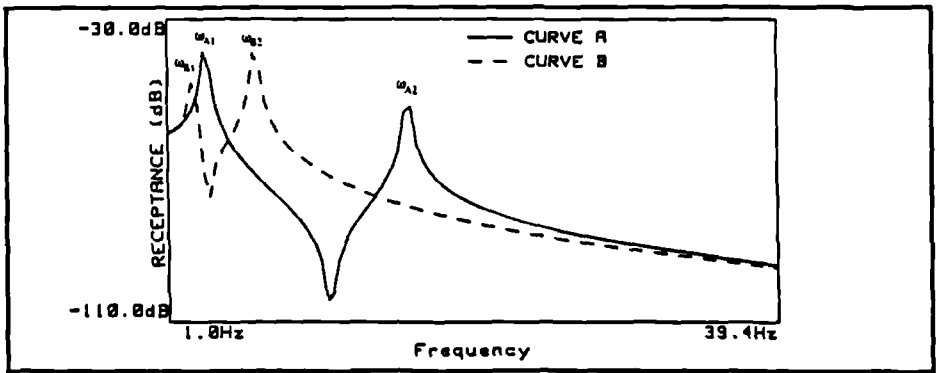

Figure 6.22 An example of possible local minima because the predicted resonance is closer to a different resonance of the true assembly

The above two cases can cause local minima, however, these are often not the only cause of local minima. However, different sets of data usually have different local minima (or at least some of the local minima are different). Therefore, if the frequency points are chosen randomly for each iteration after some of the frequencies are deleted as discussed in the forgoing paragraph, the convergence can usually be improved. Experience shows that selection of the frequency and imposition of weighting can actually be of utmost

importance for the iterative method. Without proper choice of frequency points, the algorithm usually does not lead to the true solution.

§6.12.3 Numerical Illustration

The system used in this section is exactly the same as the system studied in §6.6.1, but $[H_{nj}]$ is not available and the joint has no damping. The symmetry of the stiffness matrix is imposed and hence the total number of unknowns is 10.

Recall equations (6.77)(6.13):

$$[H_{nj}]_p=[H_{ab}]_m-([H_{aa}]_m-[H_{nn}]_m)[H_{ba}]_m^+[H_{bb}]_m \qquad (6.77)$$

$$[H_{nj}]_p=[H_{ab}]_m([I]+[Z_j][H_{bb}]_m)^{-1} \qquad (6.13)$$

where $[\ ]_p$ and $[\ ]_m$ represent the predicted and measured receptance matrices. When the receptance matrices are free of measurement errors, exact results are found from both equations(6.77)(6.13). . However, this is not the case when the measured receptance matrices are polluted by 5% random errors. Figure 6.23 and figure 6.24 show the first element of the predicted assembly receptance ($[H_{nj}(1,1)]_p$) from equations(6.77)(6.13) with exact $[Z_j]$ when the receptance matrices are polluted by 5% random errors. It is noted that the predicted results from equation(6.77) are significantly different from the real values, while results from equation(6.13) are reasonable except at some frequency points which are close to one of the substructure resonance frequencies.

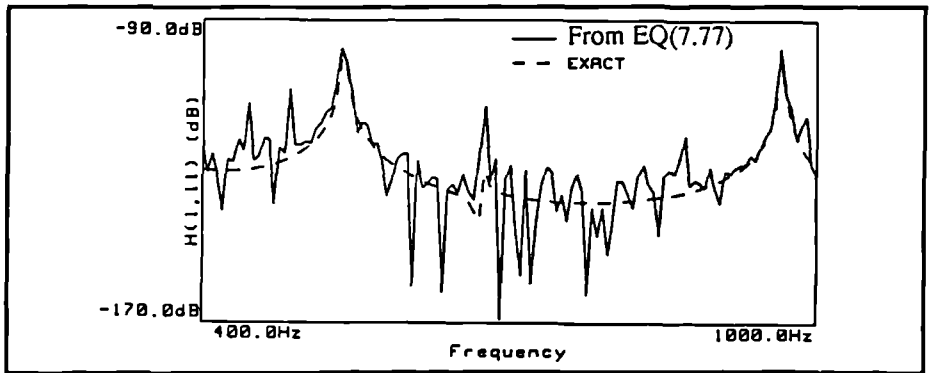

Figure 6.23 Predicted assembly response using direct identification

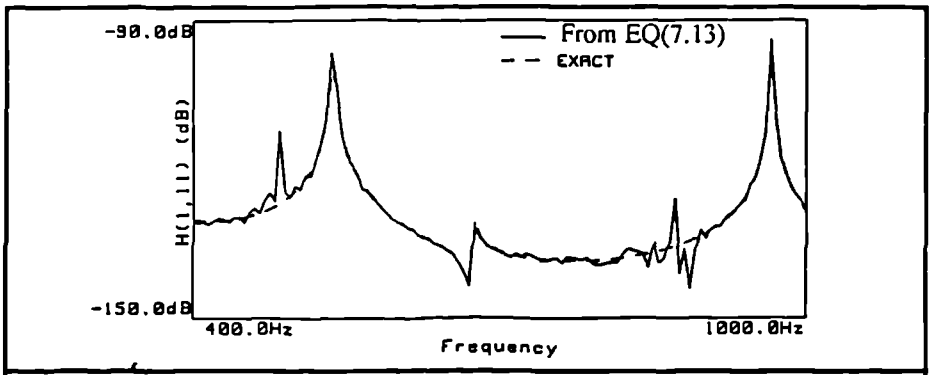

Figure 6.24 Predicted assembly response using iterative identification

Table 6.20 shows the identified results using equation(6.78). As expected, when there is no error in the measured data, exact results are identified, however, when the measured data are polluted with 5% random noise, the accuracy of the identified results is too poor to have any practical use.

	K(1,1)	K(1,2)	K(1,3)	K(1,4)	K(2,2)	K(2,3)	K(2,4)	K(3,3)	K(3,4)	K(4,4)
Case H3	0.37	0.62	-14.56	7.34	-0.19	9.08	-6.98	-0.10	2.29	-1.47

Table 6.20 The relative values of the identified results from the direct solution

To use equation(6.12), an initial estimate has to be made. The initial joint stiffness matrix is generated from a beam element with L=0.25m, w=0.07m, h=0.015m, E=2.07E11N/m^2 and ρ=7547 kg/m^3.

Figure 6.25 shows the real assembly receptance and the predicted assembly response with the initial estimation in equation(6.12) and the relative stiffness values of the initial estimation is shown in the first row of table 6.21.

	K(1,1)	K(1,2)	K(1,3)	K(1,4)	K(2,2)	K(2,3)	K(2,4)	K(3,3)	K(3,4)	K(4,4)
Initial	4.73	3.94	4.73	3.94	3.28	3.94	3.28	4.72	3.94	3.28
1st iteration	-3.03	1.35	2.95	-3.16	0.54	1.50	0.68	2.82	3.06	-1.91
2nd iteration	-3.46	1.60	5.40	-3.04	0.51	-0.21	1.02	-1.66	4.53	-2.23
5th iteration	-0.59	-0.45	5.88	-1.89	1.08	-1.00	0.68	-4.55	5.09	-2.18
10th iteration	3.87	0.06	0.98	2.07	1.62	-0.15	0.61	-1.40	1.43	0.47
12th iteration	2.80	0.42	0.87	1.82	1.48	0.32	0.79	-0.43	1.13	0.746
15th iteration	1.13	0.80	0.83	0.99	1.16	1.19	1.01	1.18	0.98	1.03
16th iteration	1.00	1.00	1.00	1.00	1.00	1.00	1.00	1.00	1.00	1.00

Table 6.21The relative values of the iteration results during iteration(noise free)

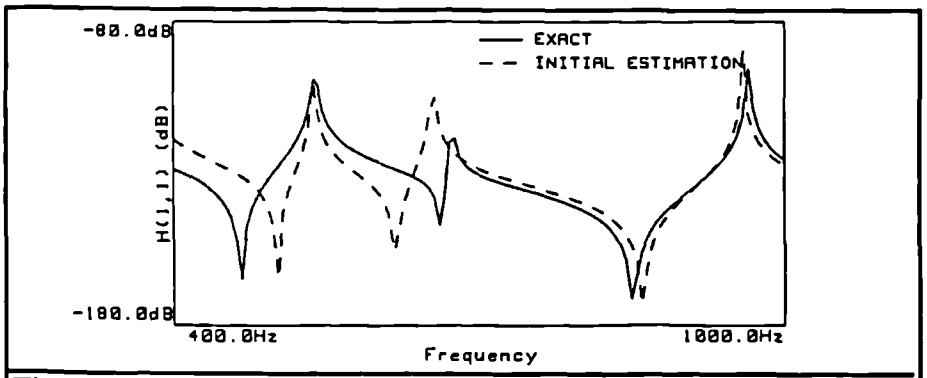

Figure 6.25 Predicted assembly response from initial estimated joint parameters

If no weighting or no selection of frequency points are applied, and even if the receptance matrices are noise free, the results do not converge to their true values.

When weighting is applied and some frequency points deleted using the method discussed in §6.12.2.4, the results converge to the true solution. Table 6.22 shows some

identified results during the iteration process and figure 6.26 shows the values of the objective function against the number of iterations; the frequency increment is 20 Hz.

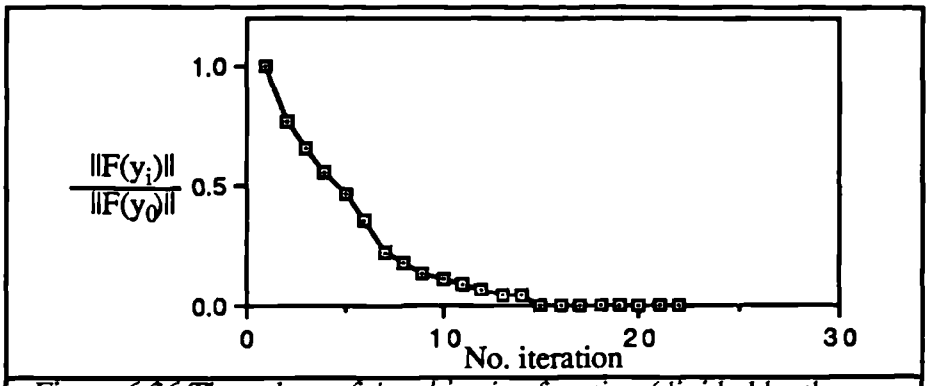

Figure 6.26 The values of the objective function (divided by the value of the objective function of the initial estimation) against the number of iterations (no measurement errors)

When the receptance matrices are polluted with random noise (5%), the selection of the frequency points becomes more critical and more frequency points around the resonance frequencies of the substructures should be excluded. To compensate for these additional frequency points round the resonance of the substructures, a smaller frequency increment (5Hz) is used. Table 6.22 show some of the identified results during the iteration process. The values of the objective function against the number of iterations is shown in figure 6.27. It is noted that the results are less sensitive to the measurement errors than the direct solution. Figure 6.28 shows the regenerated FRFs using the identified joint parameter and the noise-free FRF data. Although the errors in the identified element can exceed 40%, the difference between the predicted and true assembly response is not significant.

	K(1,1)	K(1,2)	K(1,3)	K(1,4)	K(2,2)	K(2,3)	K(2,4)	K(3,3)	K(3,4)	K(4,4)
Initial	4.73	3.94	4.73	3.94	3.28	3.94	3.28	4.72	3.94	3.28
1st iteration	3.22	3.26	4.33	2.46	2.21	3.05	2.39	4.24	3.66	2.20
2nd iteration	1.93	2.80	4.02	1.13	1.44	2.43	1.75	3.93	3.45	1.18
5th iteration	-0.79	2.21	3.36	-0.17	-0.31	0.74	0.39	2.83	2.78	-1.47
10th iteration	-0.63	1.03	2.68	-0.98	0.64	1.40	0.11	-0.54	3.34	-1.26
12th iteration	0.17	0.99	1.31	2.54	0.77	1.52	0.41	1.41	1.50	0.270
15th iteration	0.67	1.02	1.11	0.76	0.74	1.30	0.33	1.32	1.19	0.50
17th iteration	1.40	1.07	0.71	1.43	0.63	1.09	0.11	1.42	0.70	0.79
20th iteration	1.41	1.10	0.75	1.44	0.61	1.04	0.14	1.35	0.71	0.79
22th iteration	1.40	1.10	0.75	1.44	0.61	1.04	0.14	1.37	0.71	0.79

Table 6.22 The relative values of the iteration results during iteration(5% random error)

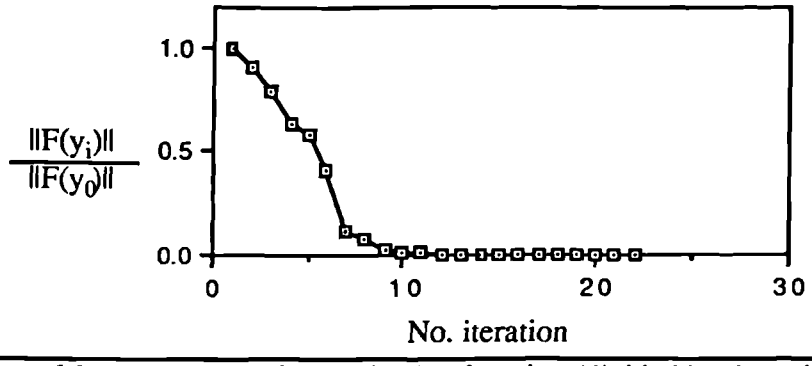

Figure 6.27 The values of the objective function (divided by the value of the objective function of initial estimation) against the number of iterations (5% random error)

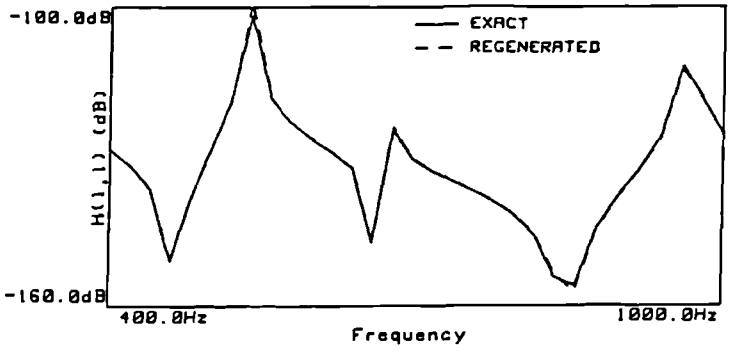

Figure 6.28 Predicted assembly response from the identified joint parameters and substructure FRFs

§6.13 CONCLUSIONS

The joint identification techniques are very important in the study of the joint behaviour and its effects on the overall structure. It is believed that in order to develop techniques for the nonlinear joint identification techniques, the techniques on the linear joint identification must be fully understood; some nonlinear joints, if the experiment is carried out with some control, can be approximately modelled by linear joints.

It is believed that the FRF joint identification techniques can be extended to the nonlinear joint identification (see Chapter 7). Compared with the joint identification method using modal data, the FRF joint identification methods are not well-developed. In this chapter, the FRF joint identification techniques have been investigated systematically.

Two new direct identification algorithms have been developed. Method one is found to be superior to method two. It is shown that unlike the coupling techniques in Chapter 5, the accuracy of the identified joint parameters are heavily related to the identification formulae used.

It is shown that information obtained at one frequency may not be enough to extract an accurate joint model from contaminated experimental data. In order to identify the accurate results, it is suggested that all the information available should be used together. Because the joint impedance parameters can be frequency-dependent, they must be transferred to frequency-independent parameters through a transformation matrix. It is also shown that in order to retain the physical properties of the joint (eg. the symmetry of the impedance matrix) and reduce the number of unknowns, a restriction matrix should be imposed. Restriction techniques are very effective in improving the accuracy of the identified results, especially when there is not suffucient data available. The mass of the joint is usually not significant and is not difficult to model. Accordingly, it is suggested that the mass of the joint should be calculated first and treated as a known parameter in the identification. The identified stiffness of the joint are usually more accurate.

The frequency range and the measured coordinates are two important factors which can affect the accuracy of the identified joint parameters significantly. A sufficiently wide frequency range and sufficiently well-spaced coordinates should be measured. In contrast, the total number of frequency points is not so critical, very small frequency increments and very closely located coordinates are not necessary and hence they are not suggested in the identification.

In order to use the available information effectively, the equations obtained at different frequencies and different coordinates should be properly scaled. Several weighting techniques are proposed. The WA and WB methods tend to weight the FRFs at different frequencies with the same importance while the WBG and WBS methods not only weight

the FRFs at different frequencies, but at different coordinates too. When the measured data are limited, it is strongly suggested that the WBS and/or WBG methods should be used. The use of WBS methods must be incorporated with an elimination process to delete erroneous equations.

The accuracy of the identified joint is found to be heavily dependent on the effects of the joint on the structure. If a small change in the joint will cause a significant change in the predicted response of the assembly, then the joint can be accurately identified; otherwise, the identified joint may not be accurate. Three cases in which the identified joint parameters are sensitive to measurement errors are discussed.

1) a very soft joint so that the assembly and substructure response are similar.

2) a very hard joint so that the response at the joint coordinates are linearly-dependent.

3) a very hard substructure interface so that the response on the interface is linearly-dependent.

Proper restriction can improve the accuracy of the identified joint parameters significantly in case 3, but restriction techniques are usually not effective in case 1 and case 2.

The selection of a proper frequency range can improve the conditions in identification, i.e. a lower frequency range for the soft joint and a higher frequency range for the stiff joint.

It is also shown that the carefully designed rig can improve the accuracy of the identified joint parameters significantly. The rule of thumb is that the joint should be situated so that when the structure is excited, the joint deforms in a proper range.

When the joint is very stiff, it is usually not possible to identify the stiff joint. However, if there is some other joints to be identified, these joint parameters can be significantly affected by the measurement errors in the FRFs at the stiff joint. It is suggested that the generalised techniques developed in Chapter 5 can be used to couple the coordinates related to the stiff joint first, then the joint identification algorithm can be applied only to the rest of the joints.

In most cases, random errors are used to simulate the measurement errors. However, it is shown that the effects of consistent errors can be much more significant in identification than the random errors. It is found that the FRFs at resonance are mostly affected, therefore, they should be excluded in the identification process. It is also shown that the significance of the consistent errors can usually be investigated by studying the variation of the averaged results with frequency.

In practice, after the structure is assembled, it may not be possible to measure the FRFs at the joint. The case when the FRFs at the assembled joint is inaccessible is investigated.

It is shown that a small modification to method one can be made so that a direct solution can be found with the absence of the FRFs at the assembled joint. However, it is found that this direct solution is very sensitive to measurement errors. Therefore, it is not recommended.

An alternative is to solve a set of nonlinear identification equations using the Newton-Raphson algorithm. A memory saving algorithm is proposed so that the Newton-Raphson algorithm can be used on a computer with a small memory. In dealing with the nonlinear identification equations, the most important thing is that there should be no local minima between the estimation and the true solution. It is found that imposing weighting is very effective in eliminating some of the local minima. In order to avoid the local minima, the frequency points used in identification should be properly selected. It is shown that the weighting and selection of the frequency points are extremely important in the iterative identification.

The main disadvantage for the iterative identification method is that it can be computationally expensive. It is also necessary to have a reasonable initial estimation of the solution.

CHAPTER 7

EXPERIMENTAL CASE STUDIES

§7.1 INTRODUCTION

In this chapter, the generalized coupling and joint identification techniques developed in Chapter 5 and Chapter 6 are applied to real structures. Two experimental rigs have been used.

Rig one was a linear structure consisting of two aluminium beams. A rigid joint and a flexible joint were used separately to connect the two beams together. Both the coupling and the joint identification techniques are applied. It is found that for the assembly with the rigid joint, it is appropriate to ignore the flexibility of the joint, i.e to predict the assembly response simply by applying the coupling technique; for the assembly with the flexible joint, however, the properties of the joint must be considered, i.e. joint identification techniques must be applied.

Rig two was effectively a nonlinear structure. Two beams were first connected together through linear bolts to form a substructure system. At the middle of the two beams, a friction joint was formed by using two aluminium pieces. The clamping force at the friction joint was so controlled that slip was allowed under excitation. The characteristics of the structure is "linearised" by controlling the relative displacement at the joint. The equivalent stiffness and damping are identified. The friction joint parameters (such as the friction limit) are then extracted from the variation of the equivalent stiffness and damping against the magnitude of the relative displacement at the joint.

§7.2 EXPERIMENTAL CASE STUDY ONE -- LINEAR STRUCTURE

§7.2.1 Test Structure

The diagrams of the substructure and the assembly systems are shown in figure 7.1 .The test structure consisted of two aluminium beams with the same rectangular cross section 2.54×1.27 cm^2($1\times\frac{1}{2}$ in^2). One beam had a length of 102cm, the other was 91cm long.

Two joint elements have been used separately to connect the two beams to form two assemblies. One joint element was a rectangular aluminium piece (Joint A); the other consisted of two aluminium pieces and a steel shell element cut from a $\frac{1}{2}$ inch BSW nut

(Joint B). Figure 7.1 also shows photographs of these two joint elements. The steel shell element was used to introduce flexibility of the joint B.

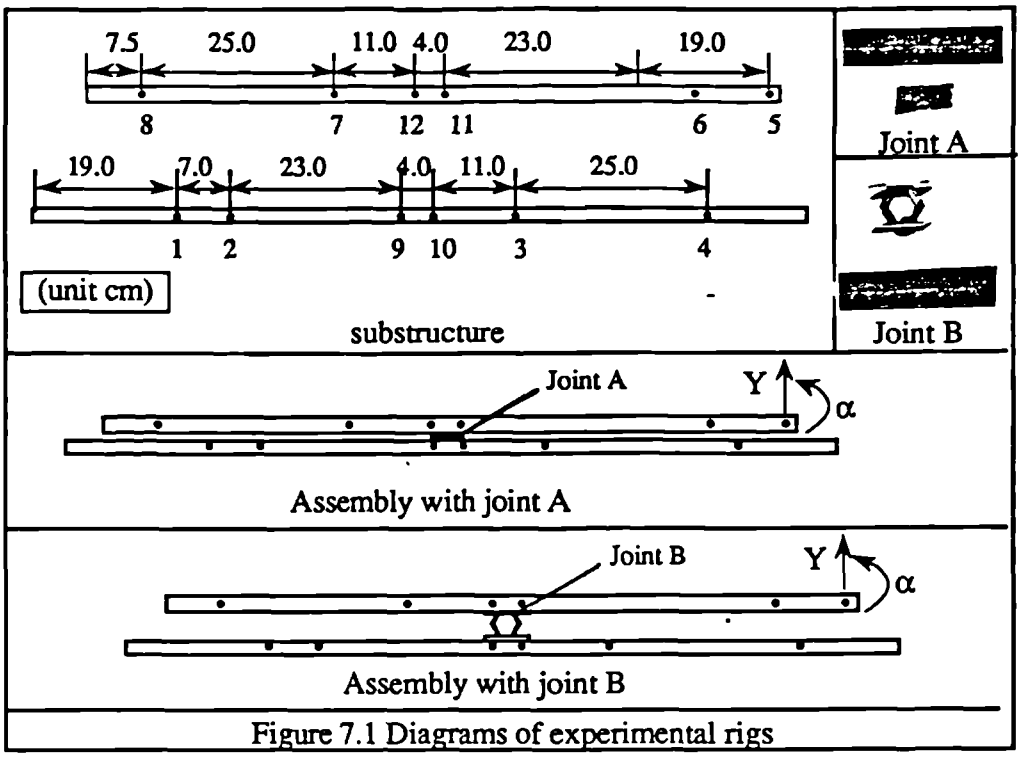

Figure 7.1 Diagrams of experimental rigs

§7.2.2 Measurement

The structure was suspended by using two soft strings (to simulate the free-free boundary condition) and excited perpendicular to the line of the beam by an instrumented hammer (B&K type 8202) . The force was measured by a force gauge (B&K type 8200) installed at the end of the hammer; the response of the structure was detected using an accelerometer (B&K type 8303). The mass of the accelerometer was about 3g, hence the effect of its mass on the structure was negligible.

The signals of the force and response were sent to two charge amplifiers (B&K type 2626) which turned the charge signals into suitable voltage signals. These voltage signals were then sent to a dual channel spectral analyser (B&K 2034). The analysed data in the analyser (FRF data) were then sent to a microcomputer (HP 9816) and stored in floppy discs for further analysis. A schematic diagram for the experimental setup is shown in figure 7.2.

Before doing any measurement, the overall measurement arrangement was calibrated using the ratio-calibration technique [1].

To avoid the leakage problem, an exponential window and a rectangular window were applied to the response and the force signals respectively.

Six coordinates were measured at each beam, hence twelve coordinates were measured on

the assembly as shown in figure 7.1. The point receptance was measured by positioning the accelerometer at the opposite side as the excitation on the beam as shown in figure 7.2. Because the thickness of the joint A was smaller than the height of the accelerometer, no point receptance of the assembly with joint A was measured

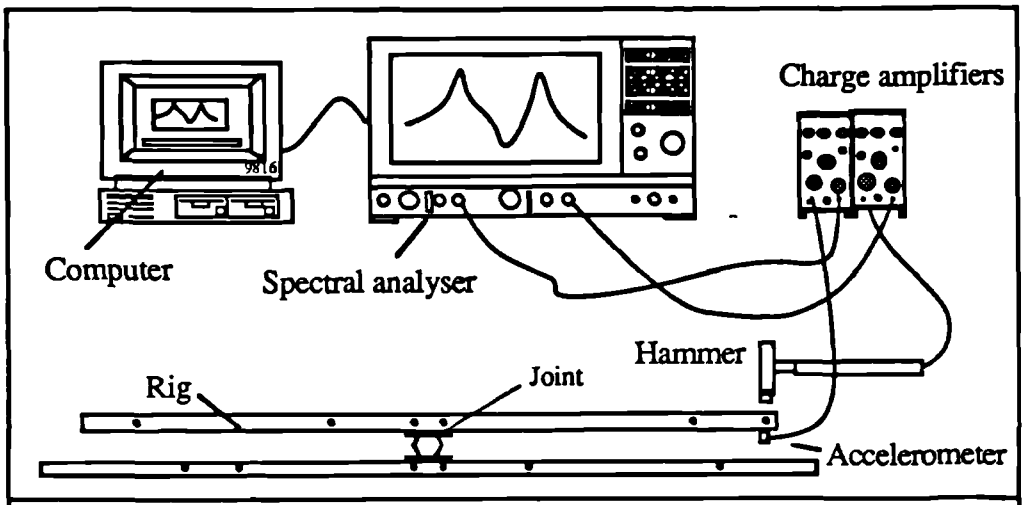

Figure 7.2 A diagram of the experimental set up for experiment one

§7.2.3 Modelling of the Joint

Because of the symmetry of the beam structure and excitation, the structure could only vibrate in one translational direction and one rotational direction (Y and α in figure 7.1).

The joint was assumed to have four translational DOFs, two DOFs were connected to the long beam and the other two connected to the short beam as shown in figure 7.1. Because the mass of joint A and B were insignificant(2.5g for joint A and 12.4g for joint B), the effects of the joint mass were ignored.

Since the joint was modelled with four coordinates and other coordinates were chosen for convenience, only the responses in the Y direction were measured.

§7.2.4 Modal Analysis

The FRFs at coordinates 1, 9, 10, 11 and 12 were analysed by using the available modal data extracting program <<MODENT>> [106]. The modal data were first extracted from each FRF and the extracted modal data were then forced to be consistent by making small adjustments. The modal properties outside the measured frequency range could not be extracted. To compensate for the effects of the modes outside the measured frequency range, residual terms[1] were included.

Typical FRFs regenerated from the modal data are shown in figure 7.3

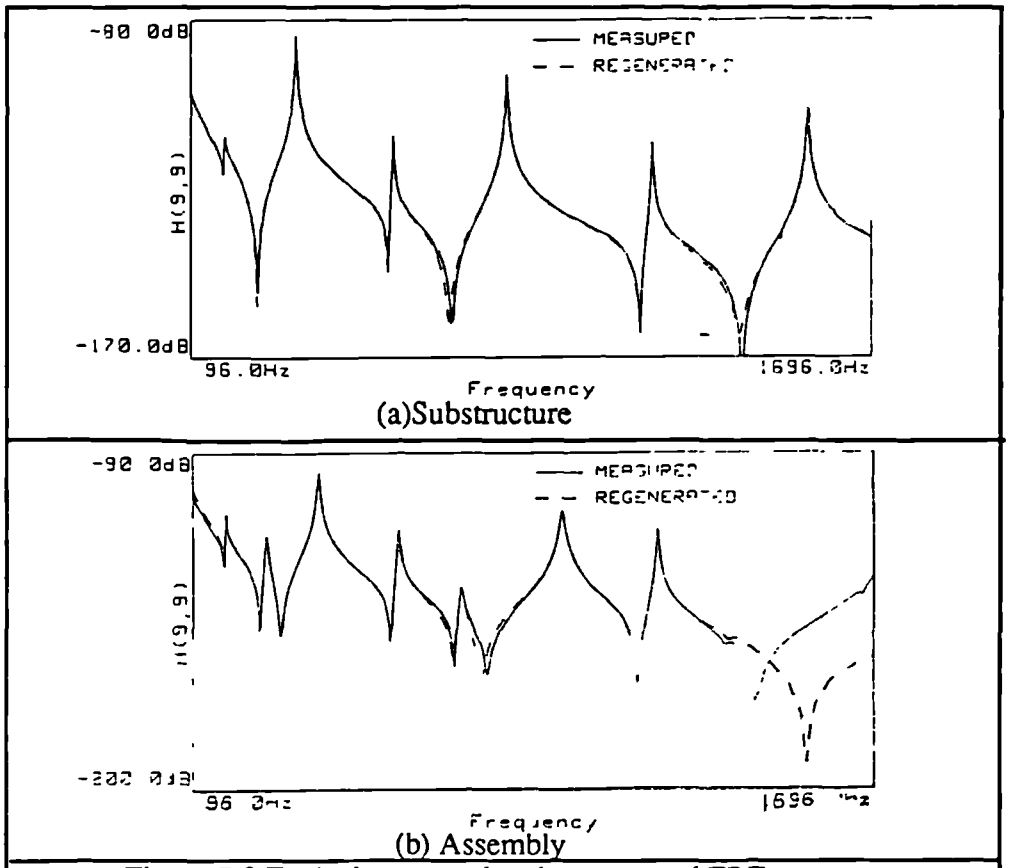

Figure 7.3 Typical measured and regenerated FRFs

§7.2.5 Prediction of the Assembly Response Using Generalized Coupling Techniques

Figure 7.4a and figure 7.5a show the predicted FRFs of the assemblies obtained from the measured substructure FRFs by using coupling techniques. The predicted FRFs are not smooth. Some peaks are observed at the frequencies corresponding to the resonances of the substructures. This is clearly due to the effects of inconsistent errors, which has been discussed in Chapter 5.

For the assembly with joint A, apart from these pseudo resonance peaks, the overall shape of the predicted FRFs match the measured counterpart very well; the resonances of the assembly are also well-predicted. However, for the assembly with joint B, the difference between the predicted and measured FRFs of the assembly is much more significant, particularly at high frequencies.

Figure 7.4b and figure 7.5b show the predicted assembly response obtained from the regenerated substructure FRFs (from the extracted modal data). The predicted FRF are now smooth and the magnitude of the pseudo resonance peaks are greatly reduced and

become insignificant (e.g. a pseudo resonance peak can be noted between the third and

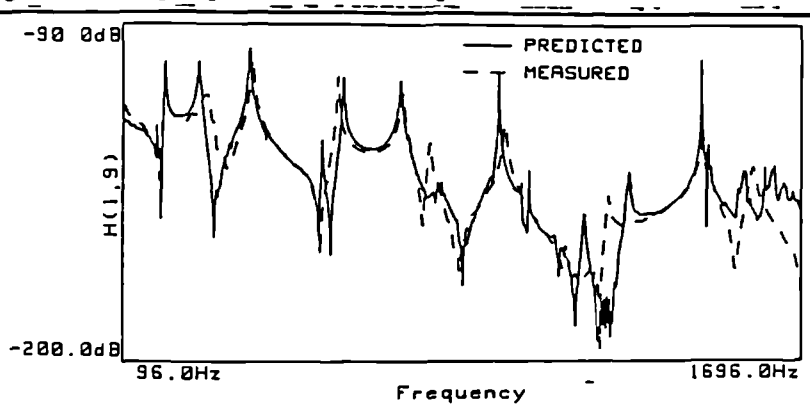

(a) From measured substructure FRFs

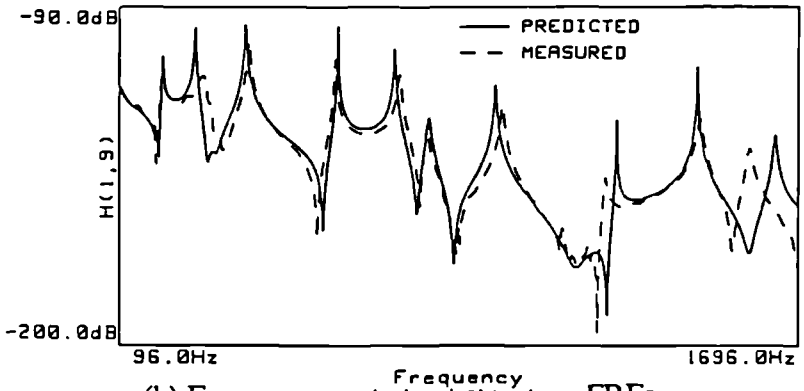

(b) From regenerated substructure FRFs

Figure 7.4 Coupling results for the assembly with joint A

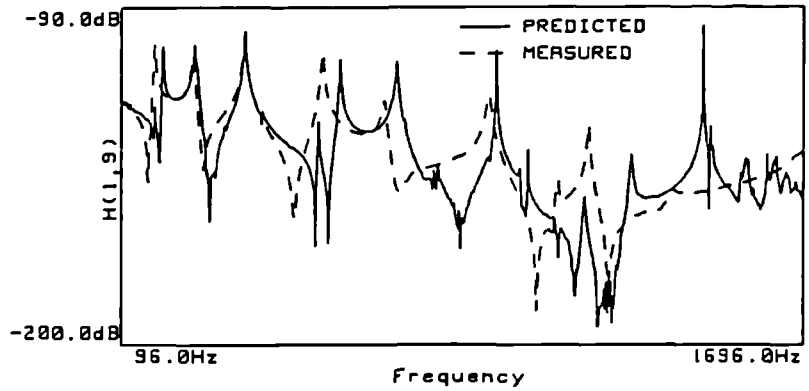

(a) from measured substructure FRF

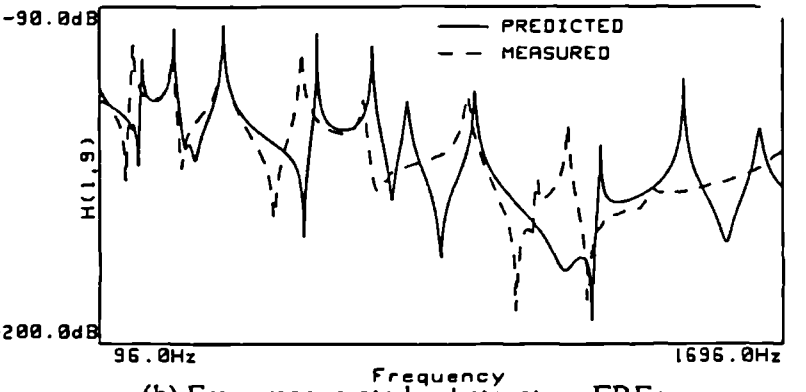

(b) From regenerated substructure FRFs

Figure 7.5 Coupling results for the assembly with joint B

fourth measured resonance frequencies in figure 7.4a, but the peak can not be observed in figure 7.4b). Again, the FRFs of the assembly with joint A are satisfactorily predicted, but the predicted FRFs of the assembly with joint B are still significantly different from the real ones.

For the assembly with joint A, some of the predicted resonance frequencies are lower than the measured resonance frequencies as they should be, these difference between resonance frequencies must be caused by measurement errors. The magnitudes of the difference between the predicted and the measured resonance frequencies for the overestimated and underestimated resonances are similar; therefore, the difference between the predicted FRFs around under-estimated frequencies and their measured counterparts can also be caused by measurement errors. Since the difference between the predicted and measured response can be caused by measurement errors, it may not be appropriate to try to identify a joint.

For the assembly with joint B, the predicted response is significantly different from the measured one, particularly at high frequencies. The predicted resonance frequencies from coupling are overestimated, which means that the stiffness of the joint is also overestimated. Clearly, joint identification techniques should be applied.

The results in this section also demonstrate that modal analysis techniques are very effective in eliminating inconsistent measurement errors. Accordingly, modal analysis techniques are recommended for the applications of coupling techniques. Since the predicted resonance frequencies from measured substructure FRFs and from regenerated substructure FRFs are similar as shown in table 7.1, and the assembly FRFs predicted from regenerated substructure FRFs are much smoother, the regenerated substructure FRFs are used to predict the assembly FRFs in the next few sections.

No.of Natural frequency	A I (Hz)	A II (Hz)	A III (Hz)	B I (Hz)	B II (Hz)	B III (Hz)
1	196	196	198	176	196	198
2	286	272	270	266	272	270
3	402	390	390	390	390	390
4	606	620	614	576	620	614
5	760	754	746	722	754	746
6	822	858	826	962	980	826
7	994	980	978	1188	1178	978
8	1238	1282	1262	1378	1284	1262
9	1462	1458	1456		1458	1456
10	1582	1566	1642	-	1628	1640

NB:
A I Measured natural frequency of the assembly A
A II Predicted natural frequency of the assembly A from the measured substructure FRFs
A III Predicted natural frequency of the assembly A from the regenerated substructure FRFs

B I Measured natural frequency of the assembly B
B II Predicted natural frequency of the assembly B from the measured substructure FRFs
B III Predicted natural frequency of the assembly B from the regenerated substructure FRFs

Table 7.1 Predicted and measured resonance frequency for assembly A and assembly B

§7.2.6 Results of Joint Identification

§7.2.6.1 Identification Using Measured FRFs Directly

Unlike the theoretical case study, the exact properties of a joint to be identified are not known in the experimental study. Therefore, the accuracy of the identified results can only be evaluated by means of deduction.

If the joint properties are accurately identified, the response of the assembly must be accurately predicted from the substructure FRFs and the identified joint parameters. In addition, the identified results from using different data sets should be close to each other; and because the joint is approximately symmetric in its geometry, the stiffness and damping matrices should be close to the following form

$$[K]=\begin{bmatrix} A & B & C & D \\ B & A & D & C \\ C & D & A & B \\ D & C & B & A \end{bmatrix} \tag{7.1}$$

Three cases were studied for each joint by using different data sets. In the first case, all the data are used (12 coordinates and frequency range 96-1696Hz). For the assembly with joint A, equations(6.16)(6.17) were used, and for the assembly with joint B, equations(6.16-6.19) were used; in the second case, all the coordinates were used, but only the FRFs within the frequency range 800-1696Hz were used; in the third case, only

parts of the data were used (for assembly with joint A, equation(6.16) was used and for the assembly with joint B, equation(6.19) was used).

Different weighting methods have been applied, it is found that all the weighting techniques yield similar results, but if no weighting is applied, the accuracy of the results is poor.

The cases including and excluding the resonance frequencies have also been calculated and the difference between these two is insignificant, indicating that the effects of consistent errors are insignificant.

Because of the similarity of the identified results obtained from using different weighting techniques and from using data including and excluding resonance frequencies, only the identified results from the WBG method using all the frequency points are presented.

The identified results are shown in table 7.2 and table 7.3. It can also be noted that deduction from the geometry symmetry of the joint (equation(7.1)) is satisfied. In addition, the results from different data sets are similar. Therefore, the identified results are likely to be accurate if the predicted assembly FRFs match the measured ones.

Case A1

$$[K]=\begin{bmatrix} 3.94 & -1.74 & -4.06 & 1.76 \\ -1.74 & 3.58 & 2.08 & -3.81 \\ -4.06 & 2.08 & 4.01 & -1.86 \\ 1.76 & -3.81 & -1.86 & 3.83 \end{bmatrix} \times 10^7 \text{N/m} \quad [D]=\begin{bmatrix} 1.32 & -1.42 & -2.50 & 2.12 \\ -1.42 & 2.63 & 1.18 & -2.26 \\ -2.50 & 1.18 & 3.29 & -2.20 \\ 2.12 & -2.26 & -2.20 & 2.94 \end{bmatrix} \times 10^6 \text{N/m}$$

Case A2

$$[K]=\begin{bmatrix} 4.38 & -1.43 & -4.53 & 1.47 \\ -1.43 & 3.71 & 1.92 & -4.02 \\ -4.53 & 1.92 & 4.31 & -1.46 \\ 1.47 & -4.02 & -1.46 & 4.00 \end{bmatrix} \times 10^7 \text{N/m} \quad [D]=\begin{bmatrix} 1.23 & -1.69 & -2.70 & 2.32 \\ -1.69 & 2.54 & 1.59 & -2.35 \\ -2.70 & 1.59 & 3.05 & -2.36 \\ 2.32 & -2.35 & -2.36 & 3.47 \end{bmatrix} \times 10^6 \text{N/m}$$

Case A3

$$[K]=\begin{bmatrix} 3.98 & -1.59 & -4.07 & 1.60 \\ -1.59 & 3.60 & 1.92 & -3.83 \\ -4.07 & 1.92 & 3.98 & -1.71 \\ 1.60 & -3.83 & -1.71 & 3.90 \end{bmatrix} \times 10^7 \text{N/m} \quad [D]=\begin{bmatrix} 1.06 & -1.24 & -1.93 & 1.45 \\ -1.24 & 2.09 & 1.19 & -1.81 \\ -1.93 & 1.19 & 1.96 & -1.70 \\ -1.45 & -1.81 & -1.70 & 2.61 \end{bmatrix} \times 10^6 \text{N/m}$$

Table 7.2 Identified results for joint A

Case B1

$$[K]=\begin{bmatrix} 2.74 & 1.53 & -1.93 & -1.98 \\ 1.53 & 2.89 & -2.18 & -2.33 \\ -1.93 & -2.18 & 2.57 & 1.48 \\ -1.98 & -2.33 & 1.48 & 2.88 \end{bmatrix} \times 10^6 \text{N/m} \quad [D]=\begin{bmatrix} 2.44 & 1.64 & -1.21 & -1.56 \\ 1.64 & 2.61 & -2.30 & -2.34 \\ -1.21 & -2.30 & 2.14 & 1.56 \\ -1.56 & 2.34 & 1.56 & 2.67 \end{bmatrix} \times 10^5 \text{N/m}$$

Case B2

$$[K]=\begin{bmatrix} 2.78 & 1.77 & -2.29 & -2.12 \\ 1.77 & 3.11 & -2.42 & -2.44 \\ -2.29 & -2.42 & 2.86 & 1.51 \\ -2.12 & -2.44 & 1.51 & 3.18 \end{bmatrix} \times 10^6 \text{N/m} \quad [D]=\begin{bmatrix} 2.19 & 1.88 & -1.85 & -1.86 \\ 1.88 & 2.33 & -1.30 & -2.21 \\ -1.85 & -1.30 & 2.43 & 1.46 \\ -1.86 & -2.21 & 1.46 & 1.32 \end{bmatrix} \times 10^5 \text{N/m}$$

Case B3

$$[K]=\begin{bmatrix} 3.08 & 1.68 & -1.79 & -2.39 \\ 1.68 & 2.68 & -2.44 & -2.02 \\ -1.79 & -2.44 & 2.52 & 1.65 \\ -2.39 & -2.02 & 1.65 & 2.70 \end{bmatrix} \times 10^6 \text{N/m} \quad [D]=\begin{bmatrix} 3.10 & 1.92 & -3.12 & -1.07 \\ 1.92 & 3.24 & -8.64 & -3.88 \\ -3.12 & -8.64 & 2.21 & 1.79 \\ -1.07 & -3.88 & 1.79 & 2.33 \end{bmatrix} \times 10^5 \text{N/m}$$

Table 7.3 Identified results for joint B

Figure 7.6 and figure 7.7 show the predicted FRFs of the assembly with joint A and joint B respectively.

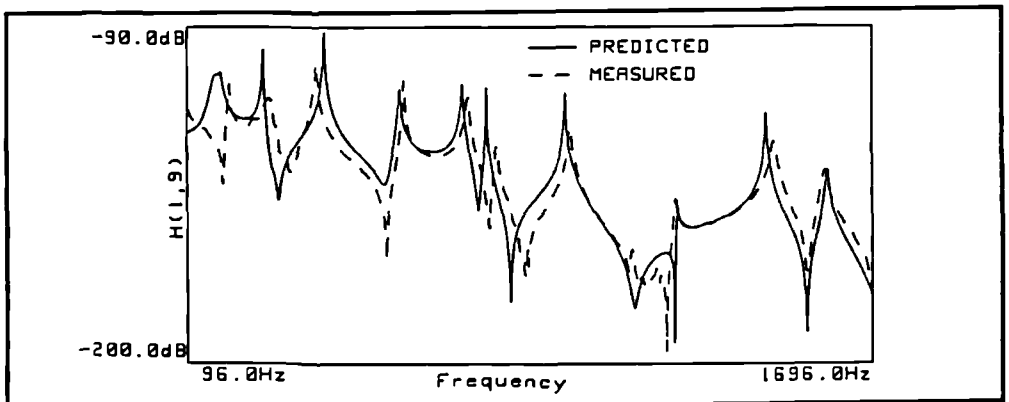

Figure 7.6 Predicted FRF for the assembly with joint A

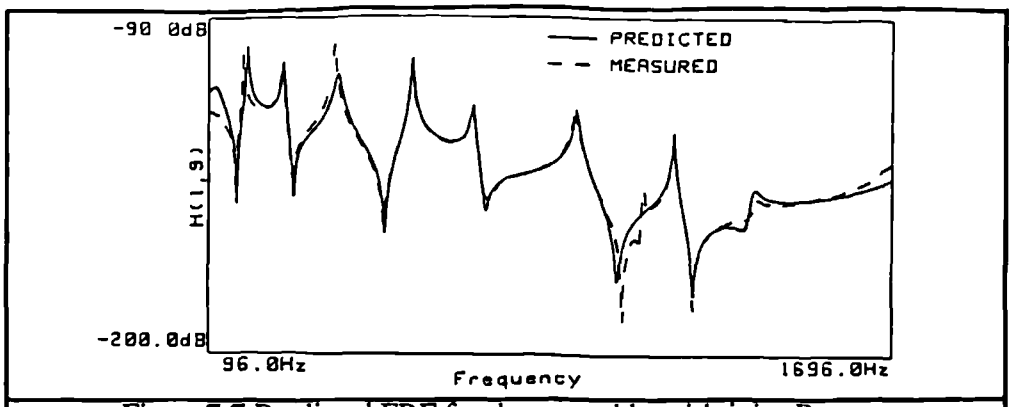

Figure7.7 Predicted FRF for the assembly with joint B

For the assembly with joint A, the accuracy of some predicted resonance frequencies is improved (e.g. the last resonance frequency), while others slightly deteriorate. But overall, it is difficult to claim that the accuracy of the predicted FRFs of the assembly is improved by considering the flexibility of the joint.

For the assembly with joint B, however, the accuracy of the predicted assembly FRFs is significantly improved by considering the joint effects. Not only the resonance frequencies are accurately predicted, but the overall shape of the predicted FRFs also matches the measured one accurately.

The accurate prediction of the resonance frequencies means that the stiffness matrix is accurately predicted. However, a nice fit on the measured FRFs does not necessarily mean that the damping properties of the joint are accurately identified, this is because an exponential window has been applied to the response signal in the experiment, which effectively introduces artificial damping into the FRFs, since the damping information in the substructure FRFs of the substructures and assembly are not correct, the damping identified cannot be correct either. Actually, because the artificial damping is applied to the whole system, (i.e. the substructures are heavily damped due to artificial damping), the change of the FRFs of the assembly due to change of the joint damping is insignificant as can be seen in §7.2.6.3

§7.2.6.2 Joint Identification Using Regenerated FRF Data.

In this section, the effects of applying modal analysis techniques on the measured FRFs are studied. The FRFs regenerated from the modal data are used.

Table 7.4 shows the identified joint parameters and figure 7.8 shows a regenerated FRF. The regenerated assembly FRF does not match the real assembly FRF as well as in the last section (Case B1), and the property of physical symmetry of the joint is not well-preserved.

Case B4

$$[K]=\begin{bmatrix} 4.49 & 1.86 & -2.98 & -3.04 \\ 1.86 & 1.60 & -2.75 & -2.41 \\ -2.98 & -2.75 & 3.46 & 2.05 \\ -3.04 & -2.41 & 2.05 & 3.07 \end{bmatrix} \times 10^6 \text{N/m} \quad [D]=\begin{bmatrix} -0.76 & 3.58 & -3.28 & -1.06 \\ 3.58 & 1.03 & -2.05 & -8.83 \\ -3.28 & -2.05 & 3.06 & 3.70 \\ -1.06 & -8.83 & 3.70 & 3.53 \end{bmatrix} \times 10^5 \text{N/m}$$

Case B5

$$[K]=\begin{bmatrix} 2.68 & 1.04 & -2.37 & -1.57 \\ 1.04 & 3.04 & -2.21 & -1.62 \\ -2.37 & -2.21 & 6.44 & -1.74 \\ -1.57 & -1.62 & -1.74 & 5.66 \end{bmatrix} \times 10^6 \text{N/m} \quad [D]=\begin{bmatrix} 2.19 & 1.88 & -1.85 & -1.86 \\ 1.88 & 2.33 & -1.30 & -2.21 \\ -1.85 & -1.30 & 2.43 & 1.46 \\ -1.86 & -2.21 & 1.46 & 1.32 \end{bmatrix} \times 10^5 \text{N/m}$$

Table 7.4 Identified results for joint B by using the regenerated FRF data

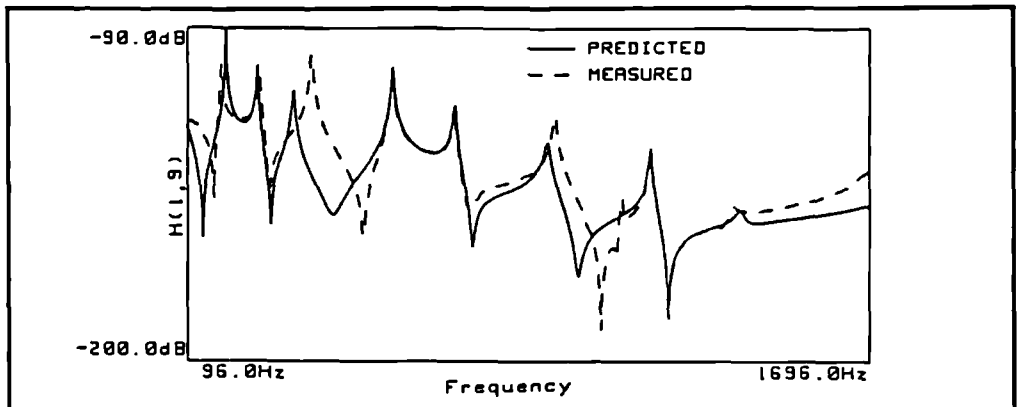

Figure7.8 Predicted FRF for the assembly with joint B
(joint identified with the regenerated FRF data at all the frequencies)

The problem in using regenerated FRF data is that although it is possible to extract some modal parameters for FRFs so that the regenerated FRFs match the raw FRF accurately, it is very difficult to obtain a set of consistent modal data to regenerate all the FRF data, accurately particularly for the assembly.

Usually, it is found that the worst parts of regenerated FRFs is at the two ends of the frequency range (i.e. around 96 Hz or 1696Hz) due to the effects of the modes outside the measured frequency range. If the FRFs at these frequencies are excluded, the accuracy of the identified results can be improved to some extent. The identified results from the regenerated FRFs (excluding the frequency points at both ends) are shown in table 7.4 as case B5 and the regenerated FRF of the assembly is shown in figure 7.9. It can be noted that although the accuracy of identified results is improved, it is still not as accurate as those using the measured FRFs directly.

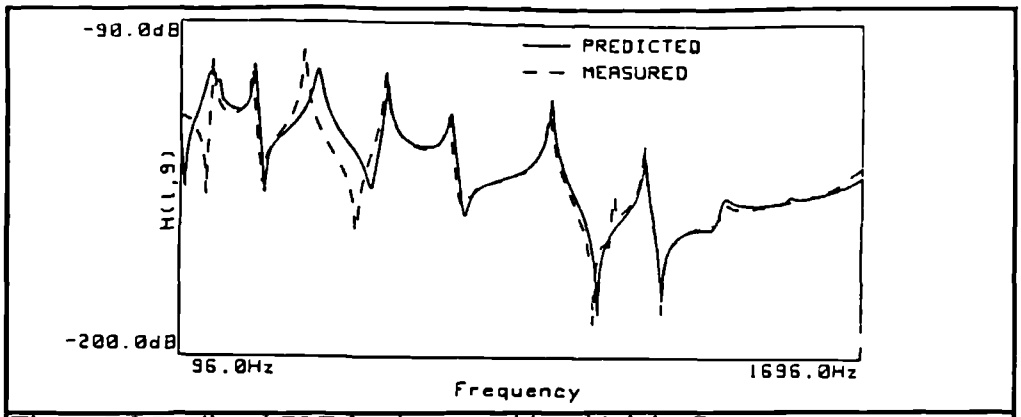

Figure 7.9 Predicted FRF for the assembly with joint B
(joint identified with the regenerated FRF data at selected frequencies)

The results in this section clearly agree with the conclusion drawn in Chapter 6. Although, it may be hasty to conclude that the application of modal analysis techniques will reduce the accuracy of joint identification, the applications of modal analysis in joint identification are severely limited due to the difficulty in obtaining a set of consistent and accurate modal data. Since the effects of inconsistent errors on identification are not as severe as on coupling, the modal analysis technique, which is mainly effective in eliminating inconsistent errors in the measurement data, is not as suitable for joint identification as for coupling.

§7.2.6.3 Joint Identification Using the Iterative Method

In this section, iterative joint identification techniques are investigated. The FRFs of the assembly are assumed to be inaccessible. The condition of physical symmetry of the joint (i.e. equation(7.1)) is used which reduces the independent joint parameters from 20 to 8.

The initial estimation on the joint parameters is shown in the first column of table 7.5 and the identified results after 11 iterations are shown in the second column. The predicted assembly FRFs from the initial estimation of the joint and identified joint parameters are shown in figure 7.10 and figure 7.11 respectively. From the second row of table 7.5 and figure 7.11, it can be deduced that the joint stiffness is accurately identified. For the identified damping, however, the diagonal terms are negative and cannot be realistically correct. However, since the regenerated FRF fit the measured FRFs accurately, the effects of the joint damping on the assembly are insignificant (at least after artificial damping has been introduced).

Initial estimation

$$[K]=\begin{bmatrix} 10.00 & 0.00 & -5.00 & -5.00 \\ 0.00 & 10.00 & -5.00 & -5.00 \\ -5.00 & -5.00 & 10.00 & 0.00 \\ -5.00 & -5.00 & 0.00 & 10.00 \end{bmatrix} \times 10^6 \text{N/m} \quad [D]=\begin{bmatrix} 10.00 & 0.00 & -5.00 & -5.00 \\ 0.00 & 10.00 & -5.00 & -5.00 \\ -5.00 & -5.00 & 10.00 & 0.00 \\ -5.00 & -5.00 & 0.00 & 10.00 \end{bmatrix} \times 10^3 \text{N/m}$$

Identified results

$$[K]=\begin{bmatrix} 2.46 & 1.42 & -1.83 & -2.05 \\ 1.42 & 2.46 & -2.05 & -1.83 \\ -1.83 & -2.05 & 2.46 & 1.42 \\ -2.05 & 1.42 & -1.83 & 2.46 \end{bmatrix} \times 10^6 \text{N/m} \quad [D]=\begin{bmatrix} -2.74 & 0.29 & 3.92 & -1.31 \\ 0.29 & -2.74 & -1.31 & 3.92 \\ 3.92 & -1.31 & -2.74 & 0.29 \\ -1.31 & 3.92 & 0.29 & -2.74 \end{bmatrix} \times 10^5 \text{N/m}$$

Table 7.5 Identified results for joint B by using iterative joint identification method

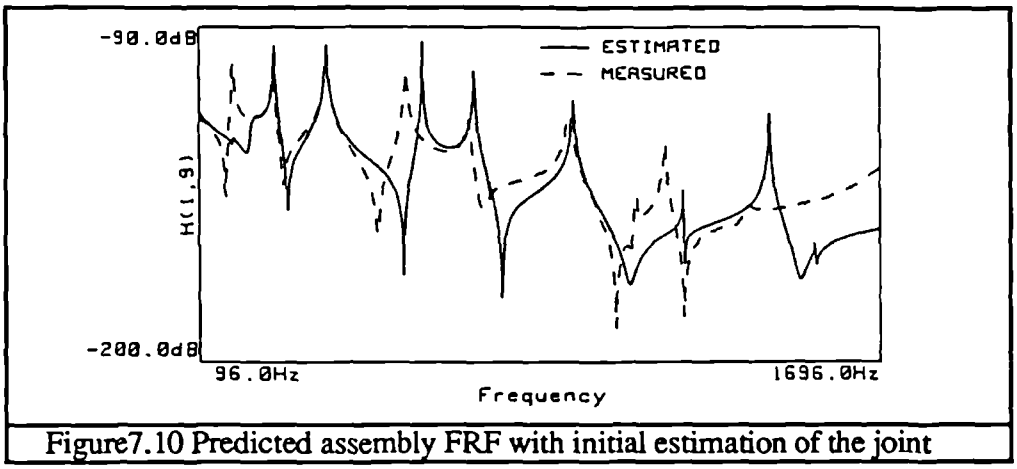

Figure7.10 Predicted assembly FRF with initial estimation of the joint

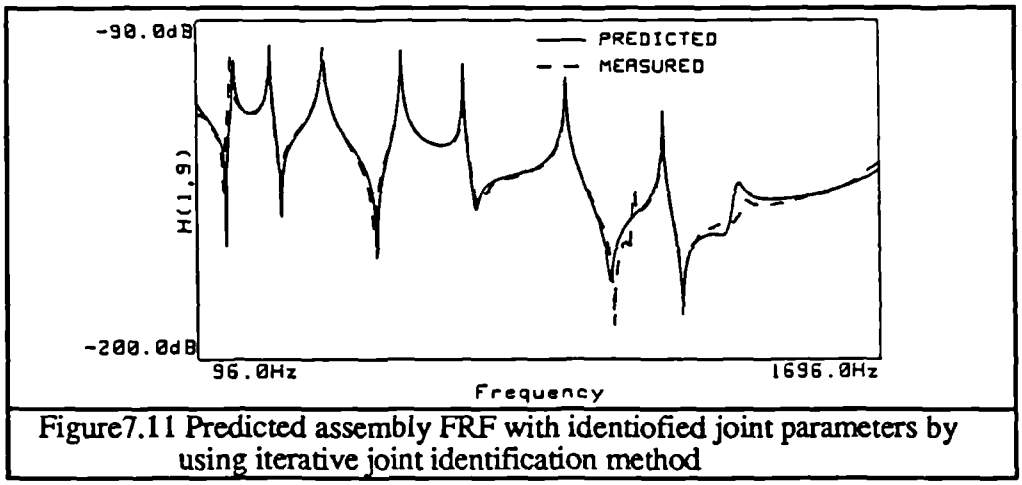

Figure7.11 Predicted assembly FRF with identiofied joint parameters by using iterative joint identification method

§7.2.6.4 Concluding Remarks

From the above studies, it is clearly that joint identification techniques (both direct and iterative methods) developed in Chapter 6 are appropriate for practical applications. It is also shown that the joint identification techniques should be applied to obtain the joint

with sufficient flexibility; for very stiff joints, joint identification may not be appropriate.

An additional feature for the experimental study is reviewed, that being artificial damping introduced during the experimental process (i.e. windowing effects). Due to the effects of artificial damping, joint damping cannot be identified accurately.

Modal analysis techniques have proved to be effective in predicting the assembly response from substructures (and joint). However, due to the possible consistent errors introduced during the modal analysis process, it is shown experimentally that modal analysis techniques may not be appropriate for joint identification. The potential danger in using modal analysis techniques in joint identification should always be born in mind.

§7.3 EXPERIMENTAL CASE STUDY TWO -- A STRUCTURE WITH A NONLINEAR FRICTION JOINT ATTACHED

§7.3.1 Experimental Rig

The purpose of this case study is to investigate the possibility and limitation of application of the joint identification techniques on a nonlinear friction joint.

The substructure system in this study consisted of two mild steel beams as shown in figure 7.12a. One beam was 104 cm long and had a rectangular section 5.08×0.95cm^2 ($2\times\frac{3}{8}$ in^2), the other was 91.5cm long and had a rectangular section 2.54×1.27cm^2 ($1\times\frac{1}{2}$ in^2). Two beams were connected together at both ends by using two steel rods (14cm in length and 0.4cm in diameter); the distance between the two beams was 9.1cm.

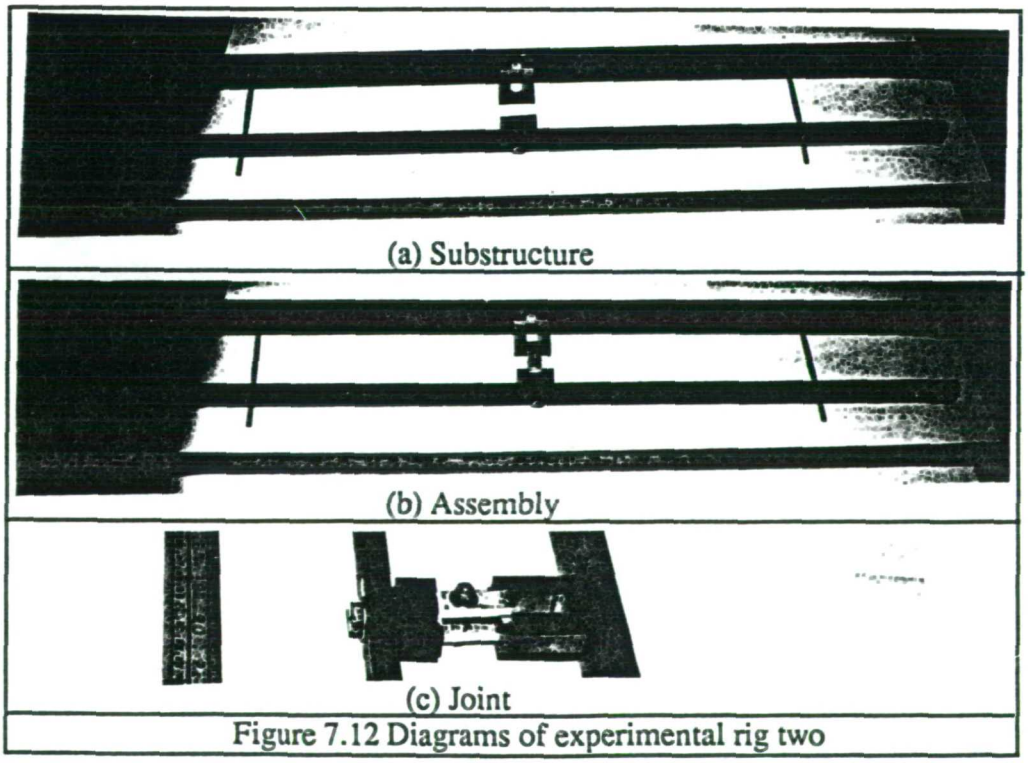

(a) Substructure

(b) Assembly

(c) Joint

Figure 7.12 Diagrams of experimental rig two

Two steel blocks (shown in figure 7.12a) were clamped to the middle of the two beams by using two $\frac{1}{4}$ inch BSW bolts. These two steel blocks were cut from the same steel bar and machined together, and hence they had the same thickness. The top and bottom surfaces of the blocks were ground. Two small aluminium pieces were clamped to the steel blocks to form two friction joints (figure 7.12b). The contact surfaces of the aluminium pieces were polished with abrasive paper, the contact surface at each end of the aluminium piece was approximately 24 mm^2(12mm×2mm). The two pieces were clamped by a bolt 0.9cm from one end (figure 7.12c), therefore, the normal pressure at one joint was approximately double the pressure at the other. Slip could only occur at one joint, accordingly, the other joint could be considered as parts of the substructure. Only the effects of the joint where slip could occur was studied.

§7.3.2 Measurement Equipment

Because the properties of a friction joint depend on the response at the joint, control of the experimental process is essential. Probably the simplest properties of a nonlinear joint in the spatial domain are the equivalent stiffness and damping. As discussed in Chapter 4, the equivalent stiffness and damping are only meaningful when the structure is excited by a sinusoidal force. Therefore, sine sweep excitation was applied, the measurement set up was slightly different from the setup in §7.2.2 as follows:

The structure was also suspended by using two soft strings. A sinusoidal signal was generated in a frequency analyser (Solartron type 1254), the signal was amplified in a power amplifier (GW type ss30) and sent to a shaker (GOODMANS type V50MK) to excite the structure. In order to apply excitation only in the direction intended, a push rod, which is rigid in the direction of the excitation and relatively flexible in all other directions, was used to connect the shaker and the structure (more detailed discussion on the push rod can be found in [1]). The force and the response signals were detected by a force gauge (B&K type 8200) and two accelerometers (B&K type 8303), amplified in charge amplifiers (B&K type 2626) and sent back to the analyser for processing. The processed data (FRF) were transferred to a microcomputer(HP 9816) and stored in floppy discs for further procesing. A schematic diagram is shown in figure 7.13.

To simplify the properties of the joint (which is discussed in the next section), the excitation was only applied to the mid-points of the two beams. The responses at the middle of the two beams were measured.

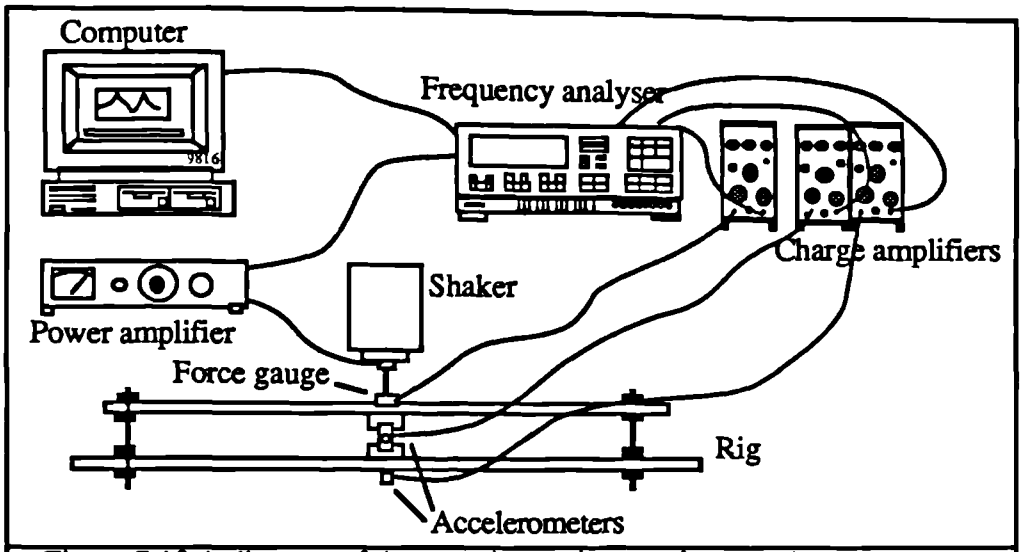

Figure 7.13 A diagram of the experimental set up for experiment two

§7.3.3 Model of the Friction Joint

Because of the symmetry of the structure and the excitation, the response of the mid-point of the beam was dominated by motion in the direction perpendicular to the beams (i.e. rotation is negligible). Therefore, the joint was modelled by a single dimension connection between the mid-points of the two beams. Because slip could only occur at one joint, the mass of the two small aluminium pieces and the bolts were considered as parts of the substructure, therefore, the joint has no mass. For a 2DOF massless joint, the dynamic characteristics can be modelled by a spring and a damper and the corresponding stiffness and damping matrices are

$$[K_j]=\begin{bmatrix} 1 & -1 \\ -1 & 1 \end{bmatrix}k_j \tag{7.2}$$

$$\text{and } [D_j]=\begin{bmatrix} 1 & -1 \\ -1 & 1 \end{bmatrix}d_j \tag{7.3}$$

Accordingly, a 2DOF massless joint only has two unknowns k_j and d_j.

§7.3.4 Control of the Relative Displacement Level

In order to use the joint identification techniques developed in the last chapter, the structure must be either linear or linearised. If the relative displacement at the joint is approximately sinusoidal and the magnitude of the relative displacement of the joint is constant, the equivalent stiffness and damping of the joint are constant too. Then the whole structure becomes linear (or the structure is linearised)

The responses were measured by accelerometers, therefore, the signal measured was acceleration. However, if a response is approximately sinusoidal, the displacement can be calculated from the acceleration:

$$x = -\frac{1}{\omega^2}a \qquad (7.4)$$

where x and a are the displacement and acceleration respectively, and ω is the angular frequency of the response.

Therefore, the relative displacement can be kept as constant by keeping the magnitude of $\frac{a_1-a_2}{\omega^2}$ constant (where subscripts 1 and 2 denote the coordinates at the two ends of the joint respectively). Control of relative displacement was achieved by employing a microcomputer (HP 9816) controlled feed back loop as shown in figure 7.14. The basic strategy of the control is based on a physical observation that increase of excitation level increases the magnitude of the relative displacement. The magnitude of the relative displacement could usually be controlled within a variation of 1% in the experiment.

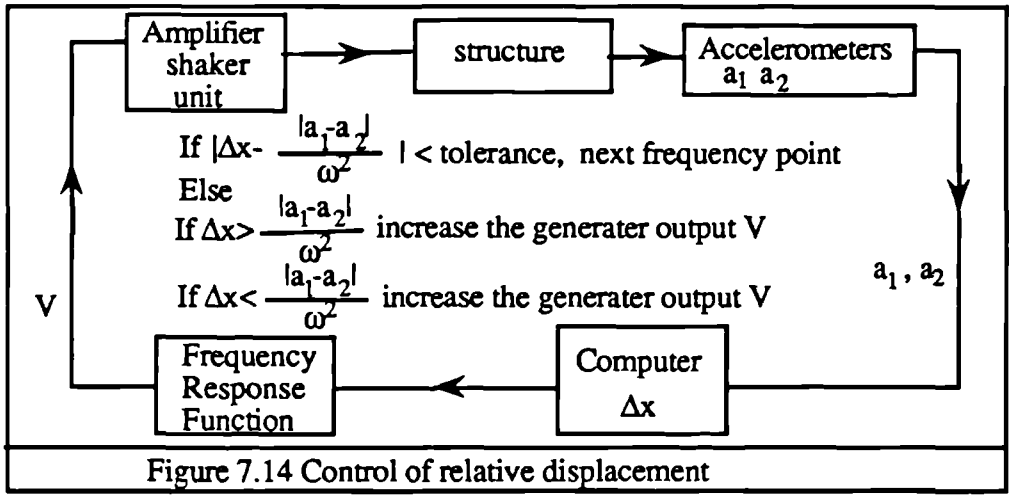

Figure 7.14 Control of relative displacement

§7.3.5 Control of the Clamping Force at the Friction Joint

The normal force applied to the friction joint is an important parameter. The clamping force is applied by using a specially made tool as shown in figure 7.15a. The elongation of the spring corresponds to the clamping force and is recorded.

The relation between the elongation of the spring and normal clamping force at the friction joint interface was calibrated by using a dead weight as shown in figure 7.15b. The spring elongation at which the nut just slips corresponds to a normal force equal to the weight.

The actual friction limit corresponding to a clamping force can be measured directly with a static measurement set up as shown in figure 7.15c. The maximum tangential force which can be applied is the friction limit.

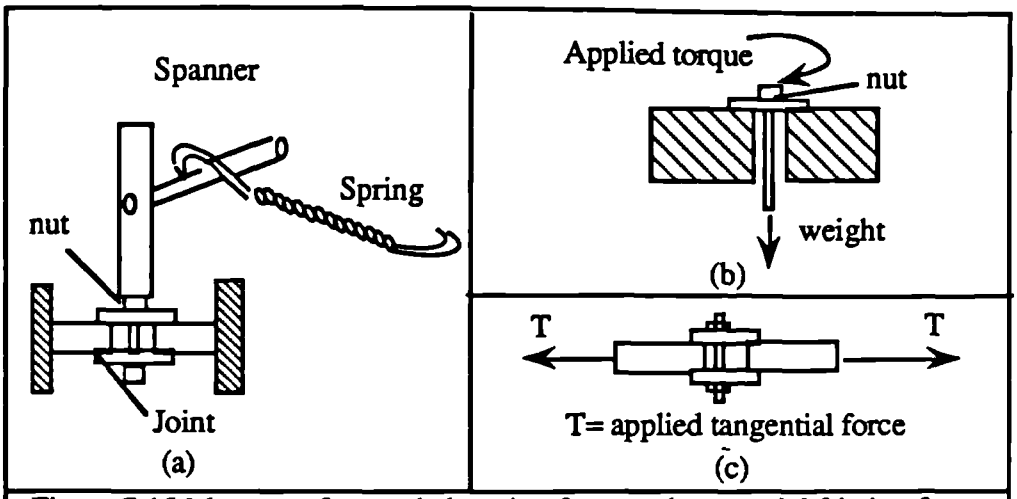

Figure 7.15 Measure of normal clamping force and tangential friction force

§7.3.6 Identification Formulation

The direct joint identification technique (equations(6.16-6.19) in Chapter 6) can be used for the identification, however, it is found that the responses at the two ends of the joint are very close when the joint is clamped, therefore, direct solution yields very poor results.

Because the joint only has two unknowns, the indirect iteration technique is applied. Recall equation(6.15)

$$[H_{jj}]=[H_{bb}]([I]+[Z_j][H_{bb}])^{-1} \tag{6.15}$$

and denote

$$[H_{jj}]=\begin{bmatrix} h_{jj}(1,1) & h_{jj}(1,2) \\ h_{jj}(2,1) & h_{jj}(2,2) \end{bmatrix}=\begin{bmatrix} h_1 & h_3 \\ h_3 & h_2 \end{bmatrix} \tag{7.5}$$

$$[H_{bb}]=\begin{bmatrix} h_{bb}(1,1) & h_{bb}(1,2) \\ h_{bb}(2,1) & h_{bb}(2,2) \end{bmatrix}=\begin{bmatrix} h_a & h_c \\ h_c & h_b \end{bmatrix} \tag{7.6}$$

$$h=\frac{1}{k_j+id_j} \tag{7.7}$$

Substituting equations(7.5-7.7) into equation(6.15) and rearranging yields

$$\begin{cases} h_1=\dfrac{h_a h_b+h_a h-h_c^2}{h_a+h_b-2h_c+h} \\ h_2=\dfrac{h_a h_b+h_b h-h_c^2}{h_a+h_b-2h_c+h} \\ h_3=\dfrac{h_a h_b+h_c h-h_c^2}{h_a+h_b-2h_c+h} \end{cases} \tag{7.8-7.10}$$

In the experiment, to avoid introducing measurement errors due to disconnection and re-

connection of the shaker, the assembled structure was only excited at one point (i.e. point 1, the mid-point of the long beam), hence only h_1 and h_3 were measured. The objective function used was

$$f(k_j,d_j)=\sum_{i=1}^{n}\{h_1(\omega_i)-\frac{h_a(\omega_i)h_b(\omega_i)+h_a(\omega_i)h-h_c^2}{h_a(\omega_i)+h_b(\omega_i)-2h_c(\omega_i)+h}\}^2+\{h_3(\omega_i)-\frac{h_a(\omega_i)h_b(\omega_i)+h_c(\omega_i)h-h_c^2}{h_a(\omega_i)+h_b(\omega_i)-2h_c(\omega_i)+h}\}^2 \quad (7.11)$$

where n is the frequency number used in minimisation and ω_i is the angular frequency.

To use the concept of equivalent stiffness and damping, the responses have to be close to sinusoidal, therefore, the assembly has to be excited at a frequency close to its resonance. Unfortunately, the magnitude of the FRFs at the resonance are usually significantly affected by measurement errors.

From equation(7.11), the resonance frequency of the assembly is the frequency when $h_a(\omega_i)+h_b(\omega_i)-2h_c(\omega_i)+h$ is a minimum. At frequencies close to the resonance frequency of the assembly, it is found that the magnitude of $h_a(\omega_i)+h_b(\omega_i)-2h_c(\omega_i)$ is much smaller than the magnitudes of h_a, h_b or h_c, therefore, $h_a(\omega_i)+h_b(\omega_i)-2h_c(\omega_i)$ can contain very high levels of errors. When h is small compared with $h_a(\omega_i)+h_b(\omega_i)-2h_c(\omega_i)$, the identified results can be completely affected by the measurement errors.

There is an alternative to equation (7.11) which makes the identified results less sensitive to measurement errors. When the joint is very tightly clamped, the flexibility of the friction joint may be ignored, in other words, the response of the assembly can be generated by rigid-coupling two coordinates at the two ends of the friction joint (i.e. h=0). Hence

$$h_{1r}=h_{3r}=\frac{h_ah_b-h_c^2}{h_a+h_b-2h_c} \quad (7.12)$$

Therefore

$$h_a+h_b-2h_c=\frac{h_ah_b-h_c^2}{h_{1r}}=\frac{h_ah_b-h_c^2}{h_{3r}} \quad (7.13)$$

Since $h_a+h_b-2h_c$ from equation (7.13) is not calculated by subtraction between quantities with similar magnitudes, it is less sensitive to measurement errors.

The average of h_{1r} and h_{3r} can be used to represent the rigid coupled assembly, hence

$$h_a+h_b-2h_c=\frac{2(h_ah_b-h_c^2)}{h_{1r}+h_{3r}}=\delta H \quad (7.14)$$

Substituting equation (7.14) into (7.8-7.11) yields

$$\begin{cases} h_1 = \dfrac{h_a h_b + h_a h - h_c^2}{\delta H + h} \\ h_2 = \dfrac{h_a h_b + h_b h - h_c^2}{\delta H + h} \\ h_3 = \dfrac{h_a h_b + h_c h - h_c^2}{\delta H + h} \end{cases} \qquad (7.15\text{-}7.17)$$

$$f(k_j,d_j)=\sum_{i=1}^{n}\{h_1(\omega_i) - \frac{h_a(\omega_i)h_b(\omega_i)+h_a(\omega_i)h-h_c^2}{\delta H(\omega_i)+h}\}^2+\{h_3(\omega_i) - \frac{h_a(\omega_i)h_b(\omega_i)+h_c(\omega_i)h-h_c^2}{\delta H(\omega_i)+h}\}^2 \qquad (7.18)$$

equations(7.15-7.17) is less sensitive to the effects of measurement errors, however, because of the assumption on which it is based, it can still be erroneous when the deformation at the joint is small.

Another problem in the identification is the damping. The substructure has been found to have very low damping. However, the imaginary parts of the receptance at off resonance frequencies are much greater than they should be (which can be seen in the next section). Since the damping in the assembly mainly arises from microslip at the joint interface, the damping effects from other damping sources is believed to be negligible. Therefore, the substructure FRFs can be approximated as real quantities. To make the FRFs real quantities, the sign of the real part of the measured FRF is considered as the sign of the processed FRF, and the magnitude of the measured FRF as the magnitude of the processed receptance, i.e.

$$h_{pro}=\text{Sign}(\text{real}(h_m))\,|\,h_m\,| \qquad (7.19)$$

where subscript "pro" and "m" represent the processed and measured FRF respectively.

After the equivalent stiffness and damping at different relative displacement levels were identified, they were used to identify the joint parameters (e.g. a,b and k for the new microslip element in Chapter 2). The Pattern search method(see Chapter 2) is employed and the objective function used is

$$f(a,b,k)=\sum_{i=1}^{n}\frac{(k_j(i)-k_p(i))^2+(d_j(i)-d_p(i))^2}{(k_j^2(i)+d_j^2(i))} \qquad (7.20)$$

where i corresponds to the different relative displacement, subscripts j and p represent the states of quantities identified from FRF data and regenerated from a microslip model respectively; a,b k are parameters to define the new microslip element in Chapter 2.

§7.3.7 Experimental Results and Discussion

Because of imperfections in the rig and errors in the excitation position and direction, rotation also occurred at the mid-points of the beams. The rotation at the mid-points of the beams became more significant at high frequencies. Accordingly, only the frequencies around the first assembly resonance were used for identification.

Figure 7.16 shows a Nyquist plot and a damping plot of an FRF corresponding to the assembly with relative displacement 0.88mm and clamping force 200N. The plot is effectively a circle and the damping plot is effectively flat. This means that the FRF effectively corresponds to a linear structure. The other FRFs are measured with smaller relative displacement and are closer to the FRFs from a linear structure. Consequently, the condition of using linear identification techniques is satisfied.

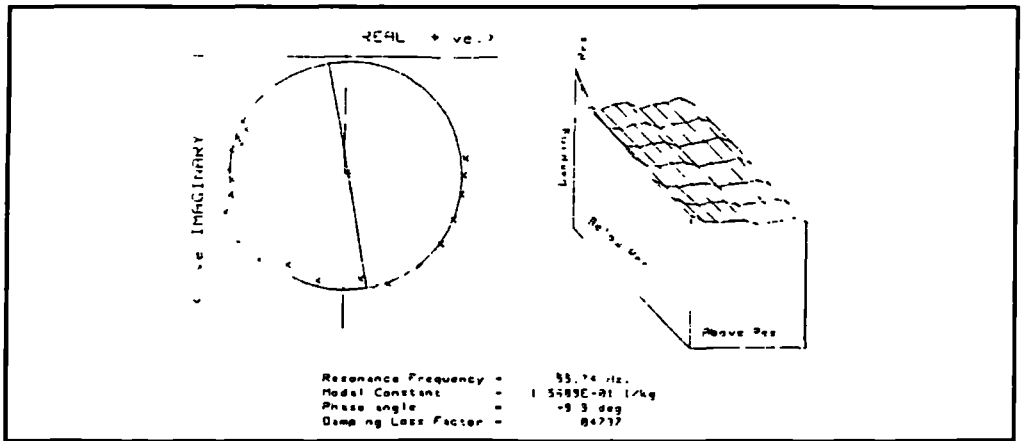

Figure 7.16 Nyquist and damping plots of an FRF on rig two with relative displacement 0.8mm

Figure 7.17 shows the predicted assembly response by using the coupling technique. A significant feature of the predicted response is that damping of the assembly is greatly overestimated (0.124% for the measured FRF and 0.403% for the predicted FRF). The results clearly indicate that the damping properties of the substructure are overestimated in the FRFs. Therefore, in the following analysis, the technique discussed in the last section is used to make the substructure FRFs real quantities.

Figure 7.18 shows the identified equivalent stiffness and damping under the clamping force 200N by using equation(7.11). Figure 7.19 shows the regenerated assembly FRFs from the substructure FRFs and identified theoretical model of the joint (with their measured counterparts). It can noted that the regenerated FRFs fit the measured FRFs very well. However, this does not necessarily mean the identified results are accurate.

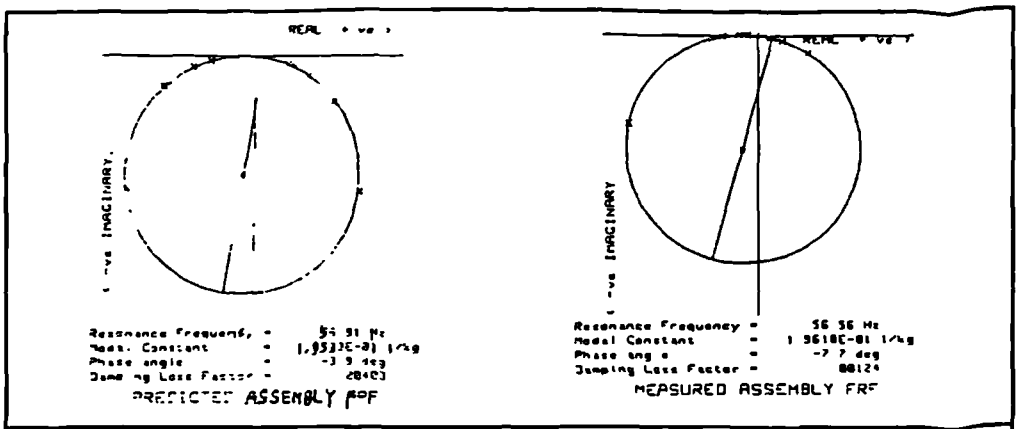

Figure 7.17 Nyquist plots of predicted and measured FRF of the assembly with a tighly fastened joint

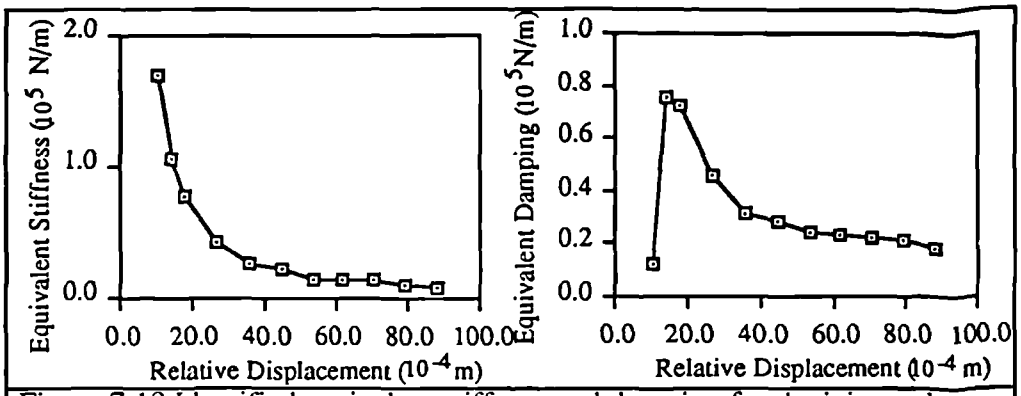

Figure 7.18 Identified equivalent stiffness and damping for the joint under 200N clamping force

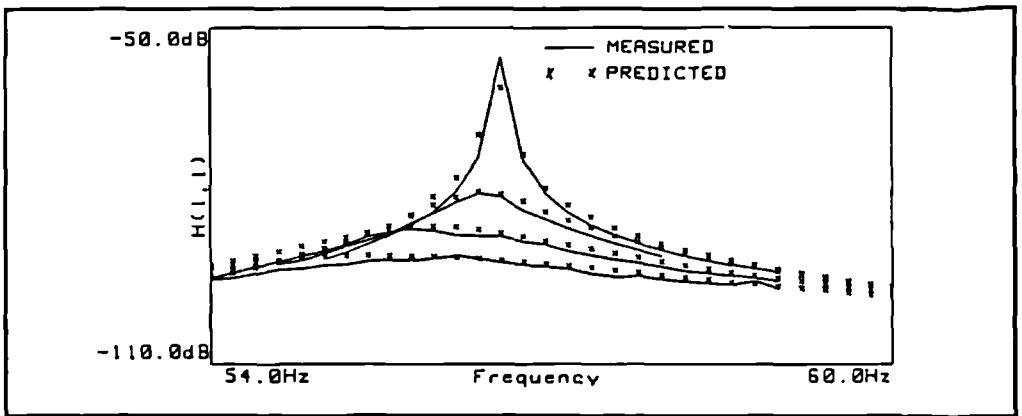

Figure 7.19 Predicted and measured assembly FRFs of the assembly

In Chapter 6, it has been shown that what can be identified is the difference between the two systems (i.e. the substructure and the assembly systems), including the difference caused by the measurement errors. If the identified results are very sensitive to the measurement errors, the identified results are likely to be inaccurate. To study the effects of measurement errors on the identified results, the substructure FRFs are perturbed; in the first case, the measured h_a is multiplied by a constant 1.03 , h_b and h_c by a constant 0.97; in the second case, h_a is multiplied by a constant 0.97, and h_b and h_c by 1.03. (3% error is chosen because the variation of the different measurements on the same FRFs is about 0.3dB, the sign of the errors are so chosen that they cause the greatest shift in

$h_a+h_b-2h_c$).The identified results for the joint with clamping force 200N are shown in figure 7.20 and extracted joint friction joint parameters are shown in table 7.6. The identified equivalent stiffness and damping from two perturbed cases are significantly different when the relative displacement is small. The effects of the measurement errors can also be noted from the coupling results as shown in figure 7.21; the predicted resonance frequency of the assembly is very sensitive to the measurement errors.

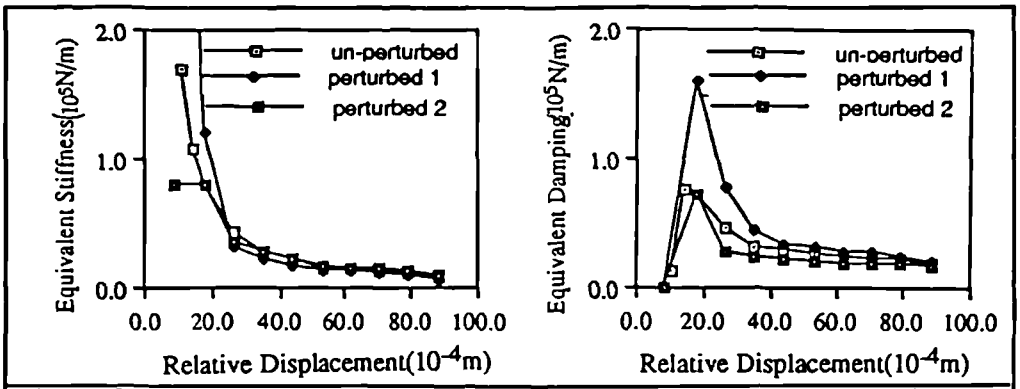

Figure 7.20 Identified equivalent stiffness and damping from perturbed substructure FRFs

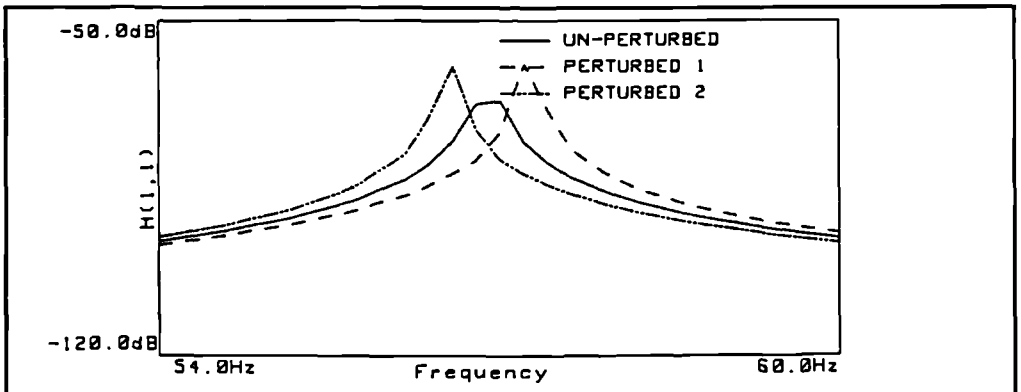

Figure 7.21 Predicted assembly response from perturbed substructure FRF data

	k ($\times 10^6$N/m)	a ($\times 10^{-7}$m)	b	T_{max} (N)
Un-perturbed data	3.20	2.35	4.32	13.0
perturbed data 1	7.66	1.09	4.39	15.3
perturbed data 2	2.00	1.94	5.09	12.4

Table 7.6 Effects of measurement errors on the extracted friction joint parameters

However, from table 7.6, the friction limits for the three cases are not significantly different; the variation is about 2.5N. This seems to indicate that the properties of the friction joint with a large displacement range have been preserved. This can also be noted from figure 7.20 that the difference from the three cases becomes insignificant as relative displacement increases.

The alternative identification method(equation(7.18)) has also been used; the identified equivalent stiffness and damping are insensitive to the small perturbations in the measured FRF data. Figure 7.22 and figure 7.23 show the identified equivalent stiffness and damping corresponding to clamping forces of 200N and 264N. The parameters of the new microslip element extracted from the identified equivalent stiffness and damping data are shown in table 7.7, and the regenerated equivalent stiffness and damping curves are also shown in figure 7.22 and figure 7.23. The friction model fits the identified equivalent stiffness and damping well when the relative displacement is large, however, a big discrepancy exists when the relative displacement is small. Because of the assumption on which equation(7.18) is based, the equivalent stiffness and damping with very small relative displacement cannot be identified accurately. Therefore, the discrepancy may not neccessary mean that the extracted friction model is inaccurate.

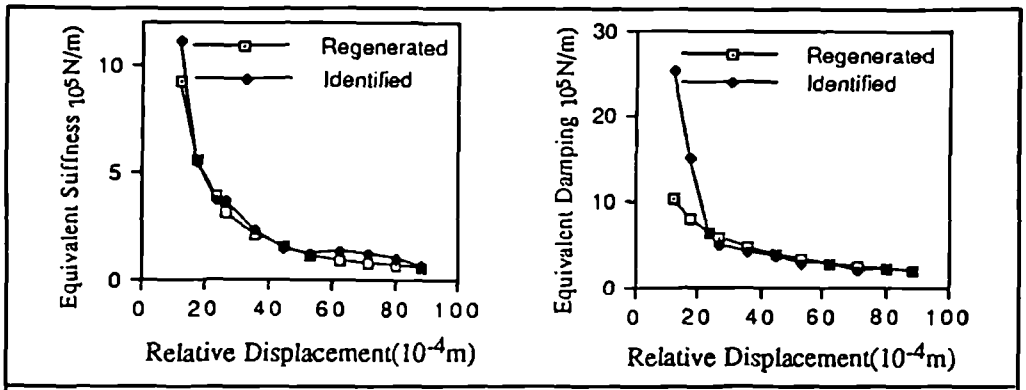

Figure 7.22 Identified equivalent stiffness and damping for the joint under 200N clamping force using the modified identification technique

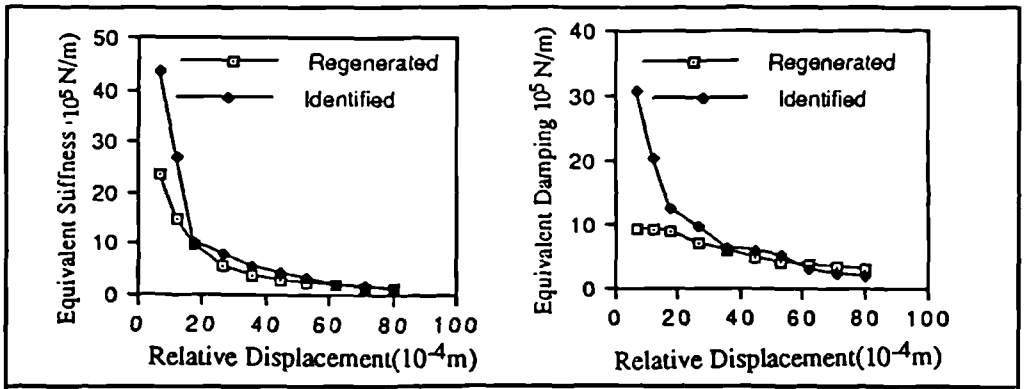

Figure 7.23 Identified equivalent stiffness and damping for the joint under 264N clamping force using the modified identification technique

Clamping force (N)	k ($\times 10^6$N/m)	a ($\times 10^{-7}$m)	b	T_{max} (N)
200	8.20	1.07	4.27	14.46
264	6.46	1.98	4.21	20.33

Table 7.7 Identified theoretical model for the friction joint under 200N and 264N

From table 7.7, it can also also noted that the friction limit corresponding to clamping forces of 200N and 264N are 14.5N and 20.0N respectively. The friction limit under 200N clamping force is similar to those identified in table 7.6.

The friction limit corresponding to clamping forces of 200N and 264N are about 16N and 22N with variations of about 5N in the static experimental test. The theoretically identified friction limits from the microslip model are within the variation of experimental test and are slightly under estimated. However, the static test was carried out after the dynamic test. During the dynamic test, surface damage was observed. It is believed that the damaged surface should have higher friction limits than the undamaged one.

The above results indicate that the properties of the friction joint in the large relative displacement range can be identified with reasonable confidence, but joint identification techniques are less satisfactory to apply to the friction joint in the small relative displacement range (microslip).

§7.3.8 Concluding Remarks

Joint identification techniques have been successfully applied to identify a nonlinear friction joint with large relative displacement. In order to linearise the behaviour of the nonlinear joint, the relative displacement has to be controlled as a constant, which can be achieved by means of a feedback control with the aid of a microcomputer. An approximately linear behaviour was observed by inspecting the Nyquist plot of the measured assembly response.

To use the principle of equivalent stiffness and damping, the FRFs close to the resonance frequency of the assembly must be used, but at these frequencies, the joint identification is sensitive to measurement errors. The contradictory requirement for use of linearisation of the joint and joint identification leads to inaccurate results for the joint with small relative displacement.

Another major shortcoming with the linearisation technique is that the technique is only applicable to structures with one joint. Further research on development of the nonlinear joint identification techniques is necessary.

CHAPTER 8

CONCLUSIONS

§8.1 MODELLING FRICTION JOINTS

It is believed that the establishment of an accurate model for a friction joint is of the utmost importance in effective utilisation of joints for controlling the vibration of engineering structures. Lack of progress in the application of friction joints for vibration control is believed to be due to lack of progress in friction joint modelling. In most engineering structures, friction joints are often tightly fastened so that nonlinear problems caused by these joints can be avoided, and in the mean time, the damping levels at these joints are also reduced to their minima.

The load-deformation relationship of a friction joint in both the normal and tangential directions is not linear. However, the relationship in the normal direction becomes effectively linear after a pre-load and can be considered as linear in most applications, while the relationship in the tangential direction is always nonlinear and energy is dissipated when a cyclic load is applied. Consequently, modelling a friction joint in the tangential direction is more difficult and also more important than in the normal direction. The load-deformation relation is investigated in this thesis. For the first time, two different types of microslip mechanisms are distinguished; the first is macro-microslip which is effective only at a large flexible interface, the second is micro-microslip which is caused by the effects of uneven asperities and has significant effects even at a very small interface area. It is shown that macro-microslip can often be modelled satisfactorily by the classic stress analysis technique and/or finite element method. However, the method to model the property of micro-microslip is still underdeveloped. Due to the complexity of the micro-microslip mechanism, it is suggested that the identification approach is more realistic for the establishment of the theoretical model for a friction joint than the prediction approach. A new generalised micro-microslip model is proposed. It is shown experimentally that the new model is superior in representing the micro-microslip behaviour of real friction joints to other published models.

The new micro-microslip model can be used in conjunction with the classic stress analysis technique or the finite element method to yield a realistic joint model which includes the effects of both the micro-microslip and macro-microslip mechanisms.

§8.2 PREDICTION OF RESPONSE OF STRUCTURES CONTAINING JOINTS

If the properties of a structure (including the properties of all the joints) are known, it is of interest to know what the response will be if the structure is subjected to an excitation. If the structure is linear, the response of a structure can usually be found using Duhamel integration or the Step-by-step Time-domain Integration method(STI). If a structure is nonlinear, it is believed that the STI method is the only possible way to calculate the transient response.

A problem with the STI method is the computation cost. It has been shown that if a very small time interval is used, accurate results can usually be achieved. However, if a relatively large time interval is used, some algorithms remain stable, while others become unstable, and the numerical results become unbounded or physically meaningless. Except for the limit of stability, the computation cost can be significantly different at each time step; some algorithms are direct and others are iterative (indirect). For the indirect method, some involve matrix inversion at each iteration, while for other methods, the matrix inversion only needs to be calculated once for several time steps or for all the time steps. Several integration algorithms have been discussed and two computationally efficient algorithms are suggested for calculating the response of a structure containing nonlinear friction joints; one is direct and the other is iterative. A new start-up procedure using an iterative algorithm (Algorithm One) is suggested for the direct algorithm (Algorithm Two) to overcome the disadvantages of the commonly used start up procedure.

Very high initial stiffness of the joint can cause problems in integration for both of the suggested algorithms. It is found that reduction of the initial stiffness to a reasonable level can often improve the accuracy of the numerical results.

In order to reduce the computation cost, the size of the problem should be reduced if possible. The size of the problem can often be reduced by using the linear transformation technique. It is found that the free-modes obtained from the linear system without joints form a representative subspace for the condensation.

Another difficulty in the application of STI for a structure containing joints is to calculate the force corresponding to a deformation at the joint. Two algorithms based on Masing's rule have been developed for calculation of the friction force from the relative displacement. The algorithms are simple to program and computationally efficient.

Although the STI method is the only method to calculate the transient response of a nonlinear structure, in many cases, the steady-state response of a nonlinear structure can be obtained by other means. These methods become important when the cost of the STI

method is significant. If a structure is lightly damped, the transient response can last for a significantly long period, when the size of the structure is also significant, the computation cost to calculate the steady-state response can be prohibitively expensive. Therefore, alternative cheap methods to calculate the steady state response are in great demand.

The most commonly used method is the Harmonic Balance method, however, it has very significant disadvantages. To overcome the shortcoming of the HB method, a new Higher order Harmonic Balance method(HHB) is developed. FRF data are used so that the number of unknowns can be significantly reduced. Although the principle of the new method is simple, it has not received wide application because of the difficulty in obtaining a converging solution. A new incremental approach is proposed, and linear and quadratic approximations are proposed for the new estimation in the incremental process.

The new HHB method is very accurate and efficient. These advantages become more significant when the size of the system is significant. It is believed that calculation of accurate steady-state response of a real engineering structure may no longer be an expensive job with the development of the HHB method.

§8.3 PREDICTION OF PROPERTIES OF THE STRUCTURE AFTER COUPLING

In chapter 5, commonly used coupling techniques are investigated and four criteria are set to evaluate a coupling method; it is shown that these methods are either not mathematically generalised or not physically generalised. A new coupling method which is both physically and mathematically generalised has been developed. The method is also computationally efficient. Based on the new method, a more effective coupling algorithm (MTC) is proposed; the MTC algorithm requires no matrix inversion operation and can save the computation cost for up to 30%. The new algorithm is also simpler and easier to program than any other coupling methods.

The modal analysis technique is widely used for eliminating measurement errors so as to improve the accuracy of the properties of the predicted assembly. However, it is shown that results thus obtained should still be treated with care. Application of modal analysis techniques can eliminate some of the measurement errors, but in the meantime, may introduce some errors to the processed data. The effects of the remaining errors are very difficult to detect. The joint is often blamed for the discrepancy between the predicted and real response of the assembly, but in fact, the real cause may well be the effects of the measurement errors. Unfortunately, this simple truth is often neglected. In Chapter 5, this point is emphasised with the results of numerical case studies.

It is shown that the effects of measurement errors on the accuracy of the predicted assembly response can be significantly magnified under some circumstances. The new coupling algorithm is found to be more effective in detecting these circumstances. Although it is not possible to eliminate the effects of the measurement errors completely, it is possible to evaluate the reliability of the predicted assembly response with the help of the new coupling algorithm.

§8.4 IDENTIFICATION OF JOINT PROPERTIES FROM DYNAMIC TESTS

It is believed that an understanding about the identification of linear joints has significant importance in the development of techniques for nonlinear joint identification. On the other hand, linear joint identification techniques are also of interest for the study of the friction joint, since a friction joint with high level clamping force or with low level excitation is effectively linear.

FRF joint identification methods are studied. It is believed that the principle of most FRF joint identification methods can be extended for nonlinear joint identification. In theory, what can be identified is the difference between the substructure and assembly systems. Due to the effects of measurement errors, identification of an exact joint model is impossible, thus the identified joint model can only be an approximation by some means to minimise the difference between the two systems. Based on different means of minimisation, various identification methods have been developed. It is shown in chapter 6 that unlike the coupling problem, the accuracy of the identified results from different methods is significantly different. Thus, effort should be devoted to developing an identification method which is insensitive to measurement errors.

It is found that if more information is used, the accuracy of the identified results can be improved. Accordingly, a good identification method should utilise the available information fully, i.e. available data should be used together in identification and the measured coordinates should be well spaced and measured FRFs should cover a sufficiently wide frequency range. Apart from using more measured data, it is also found that the accuracy of the identified results can be improved significantly by using the available information effectively. Several weighting methods have been developed to achieve this purpose. The accuracy of the identified results can also be improved by imposing some constraint conditions.

Apart from the levels of measurement errors, the accuracy of the identified results is significantly related to the nature of the joint. It is shown that both very stiff and very soft joints are difficult to identify accurately. Rigid joint components can also cause difficulty in identification, but the difficulty can often be overcome by imposing constraints on the joint model. It is further shown that some difficulties in identification can be overcome by

carefully designing the experimental structure, sometimes it simply means to clamp or to free some parts of the structure. If a joint is very stiff, it is not recommended to try to identify it; the assembly response from rigid coupling is often more accurate than that assembled from the substructures and the identified joints. It is also indicated that replacement of some stiff joints by rigid joints can often improve the accuracy of the identification on other effective joints.

In some cases, some of the FRF data at a joint may be difficult to measure after the structure is assembled. A new iterative method is proposed in chapter 6. The main shortcoming for the iterative method is that the results may converge to some values (local minima) other than the true solution. Accordingly, some efforts are spent in eliminating these local minima by choosing proper measured data and proper weighting of the available information.

Experimental results indicate that the joint identification techniques developed in this thesis can be applied to real structures

§8.5 SUGGESTION FOR FURTHER STUDIES

Extensive research work on the establishment of joint models and the prediction of dynamic properties of a fabricated structure has been carried out in this thesis. The work completed so far forms a good basis for further development. Some general suggestions for possible further studies are summarised as follows:

1) Establishment of the theoretical model for a joint

Due to the limited period available, the joint identification methods have only been applied to a simple beam structure. Applications to more complicated engineering structures are recommended.

The new microslip element developed in Chapter 2 has been proved realistic and representative. However, since the parameters of a new element based joint model must be identified by experimental means, development of nonlinear joint identification techniques is necessary. In Chapter 7, the iterative identification methods together with the HB principle have been applied to identify a nonlinear joint, due to contradictory requirement on identification and harmonic balance techniques, the application of the above technique is severely limited. However, it is believed that the principles of the iterative identification method in Chapter 6 and the Higher order Harmonic Balance method in Chapter 4 may be combined to yield a new nonlinear joint identification method. Since there is no contradictory requirement from the iterative identification method and the HHB method, the limitation of the method used in Chapter 7 may be overcome.

2) Prediction of the response of a structure containing nonlinear joints

In chapter 3, it has been shown that for Algorithm One, the most important thing is to achieve convergence at each time step. The convergence is largely determined by the property of the matrix $[\hat{K}_1]$ in equation (3.27). It may be worthwhile to investigate new algorithms for constructing the matrix$[\hat{K}_1]$. The efficiency of Algorithm One may be improved significantly if a proper $[\hat{K}_1]$ can be determined.

The time interval for Algorithm Two has to be extremely small to yield accurate results if the initial stiffness of the joints is very high. The reason for this is that the local stiffness of the joint can be much smaller than the initial stiffness at some time points, which causes very large effective parameter a_e at these time points. If the magnitudes of the elements in the $[K_r]$ matrix at these points are reduced, the effective parameter a_e can be reduced too, hence a greater time interval Δ may be used for the same accuracy.

3) New research field

Without establishing a theoretical model, friction joints may still be used for vibration reduction. The basic idea is as follows:

Under an excitation, the response of the structure can be altered by changing the clamping force at a joint. If the clamping force is changed in such a way that the response is a minimum, then the vibration of the structure can be significantly reduced.

Using this approach, the property of a joint is not required, in other words, the joint can be treated as a 'black box'. A microcomputer may be used for adjusting the clamping force to its optimum value to minimise the response of a structure by using function minimisation techniques (e.g. the Newton-Raphson method).

APPENDIX A: PROOF OF MASING'S RULE

Assume that the relation between force and deformation (or deformation and force) of a joint in initial loading is

$$u=f(F) \text{ or } F=g(u) \qquad \text{A.1}$$

and the area that slipped is

$$A=A(u) \qquad \text{A.2}$$

If the initial tangential load is applied in the opposite direction, the distribution of the slip region at the interface of the joint is exactly the same as that when a positive force is applied, but in the opposite direction. Therefore, the total deformation will be the same as the positive loading, but in the opposite direction, hence

$$u=-f(-F) \text{ or } F=-g(-u) \qquad \text{A.3}$$

For the unloading, one can consider it as applying an additional force F_u-F_i after the initial load F_i is applied. If the friction force at the interface is considered as an external force, then the rest of the joint is linear and the principle of superposition holds.

The direction of the additional force F_u-F_i is opposite to the direction of the initial loading force F_i and hence causes some of the slipped area to slip in the opposite direction. However, the reversed slip can only occur at the area where the shear stress changes from the positive friction limit to the negative friction limit, this is equivalent to a change in the shear stress from zero to double the negative friction limit. Therefore, for the additional force F_u-F_i, the friction coefficient is effectively doubled. In order to generate the same slip area in the reversed direction as in the initial loading, the magnitude of the reversed force must be doubled. Since both external force and shear stress in the slipped area are doubled the additional deformation must be doubled too.

Therefore:

$$\frac{u_{rev}}{2} = -f(-\frac{F_{rev}}{2}) \qquad A.4$$

Since $u_{rev} = u_u - u_i$ and $F_{rev} = F_u - F_i$, A.5&A.6

Substitution of equation(A.5) into (A.4) leads to.

$$\frac{u_u - u_i}{2} = -f(-\frac{F_u - F_i}{2}) \qquad A.7$$

Hence

$$u_u = u_i - 2\, f(\frac{F_i - F_u}{2}) \qquad A.8$$

When the unloading level reaches the level of initial loading, i.e. $F_u = -F_i$ or $F_u - F_i = -2F_i$ the initial slipped area is completely and exactly reversed, therefore, further unloading is the same as initial loading in the opposite direction, hence

$$u_u = -f(-F_u) \qquad A.9$$

For the reloading process to F_r, one can consider the process as applying an additional force $F_r - F_u$ in the positive direction. When the magnitude of $F_r - F_u$ increases, the reversed slipped area will be reversed back and applying the same principle as unloading, hence

$$\frac{u_r - u_u}{2} = f(\frac{F_r - F_u}{2}) \qquad A.10$$

$$\text{or } u_r = u_u + 2\, f(\frac{F_r - F_u}{2}) \qquad A.11$$

When the reversed slipped area during unloading is exactly reversed, the stress distribution as the interfaces will be exactly the same as the initial loading, therefore, further reloading will be exactly the same as initial loading. Hence

$$u_r = f(F_r) \qquad A.12$$

It can be noted that if $|u_u| < |u_i|$, the deformation to completely reverse the slipped area during unloading should satisfy

$$u_r - u_u = -(u_u - u_i) \qquad A.13$$

therefore

$$u_r = u_i \qquad A.14$$

If $|u_u|>|u_i|$, the slipped area in initial loading is completely reversed and slip can also occur in the additional area during unloading, therefore, the reloading can be considered as the 'unloading' to the real unloading, hence, to reverse the slipped area in unloading,

$u_r=|u_u|$. A.15

APPENDIX B

CALCULATION OF EQUIVALENT STIFFNESS AND DAMPING

If displacement is

$$x=x_0 \cos\theta \qquad \text{B.1}$$

the unloading and reloading force can be expressed as:

$$F_u=F_0 - 2f\left(\frac{x_0(1-\cos\theta)}{2}\right) \qquad \text{B.2}$$

$$F_r= -F_0 + 2f\left(\frac{x_0(1+\cos\theta)}{2}\right) \qquad \text{B.3}$$

then the equivalent stiffness is

$$k=\frac{1}{\pi x_0}\int_0^{\pi} F_u \cos\theta\, d\theta+\int_{\pi}^{2\pi} F_r \cos\theta\, d\theta$$

$$= -\frac{4}{\pi x_0}\int_0^{\pi} f\left(\frac{x_0(1-\cos\theta)}{2}\right) \cos\theta\, d\theta \qquad \text{B.4}$$

and equivalent damping is

$$d=-\frac{1}{\pi x_0}\left(\int_0^{\pi} F_u \sin\theta d\theta+ \int_{\pi}^{2\pi} F_r \sin\theta d\theta\right)$$

$$=\frac{8}{\pi x_0^2}\left(\int_0^{x0} f(x)dx - \frac{F(x_0)x_0}{2}\right) \qquad \text{B.5}$$

APPENDIX C

RELATION BETWEEN RC AND GRC METHODS

For two structure coupling,

$$[H_{bc}]=[H_{cb}]=[0] \qquad \text{C.1}$$

$$[H_{aa}]=\begin{bmatrix} {}_{A}H_{ii} & 0 \\ 0 & {}_{B}H_{ii} \end{bmatrix} \qquad \text{C.2}$$

$$[H_{ab}]=\begin{bmatrix} 0 \\ {}_{B}H_{im} \end{bmatrix} \qquad \text{C.3}$$

$$[H_{ac}]=\begin{bmatrix} {}_{A}H_{im} \\ 0 \end{bmatrix} \qquad \text{C.4}$$

$$[H_{bb}]=[{}_{B}H_{mm}] \qquad \text{C.5}$$

$$[H_{cc}]=[{}_{A}H_{mm}] \qquad \text{C.6}$$

Substituting equation C.1-6 into equation (5.36) yields:

$$\begin{bmatrix} {}_{A}H_{nn} & {}_{AB}H_{nn} \\ {}_{AB}H_{nn} & {}_{B}H_{nn} \end{bmatrix}=\begin{bmatrix} {}_{A}H_{ii} & 0 \\ 0 & {}_{B}H_{ii} \end{bmatrix}-\begin{bmatrix} -{}_{A}H_{im} \\ {}_{B}H_{im} \end{bmatrix}({}_{A}H_{mm}+{}_{B}H_{mm})^{-1}\begin{bmatrix} -{}_{A}H_{im} \\ {}_{B}H_{im} \end{bmatrix}^{T} \qquad \text{C.7}$$

$$\begin{bmatrix} {}_{A}H_{nj} \\ {}_{B}H_{nj} \end{bmatrix}=\begin{bmatrix} {}_{A}H_{im} \\ 0 \end{bmatrix}+\begin{bmatrix} -{}_{A}H_{im} \\ {}_{B}H_{im} \end{bmatrix}({}_{A}H_{mm}+{}_{B}H_{mm}])^{-1}[{}_{A}H_{mm}] \qquad \text{C.8}$$

$$[H_{jj}]=[{}_{A}H_{mm}]-[{}_{A}H_{mm}]({}_{A}H_{mm}+{}_{B}H_{mm}])^{-1}[{}_{A}H_{mm}] \qquad \text{C.9}$$

Equations (C.7)(C.8)and (C.9) can be written in a more compact form as

$$\begin{bmatrix} {}_{A}H_{nn} & {}_{A}H_{nj} & {}_{AB}H_{nn} \\ {}_{A}H_{jn} & H_{jj} & {}_{B}H_{jn} \\ {}_{AB}H_{nn} & {}_{B}H_{nj} & {}_{B}H_{nn} \end{bmatrix}=\begin{bmatrix} {}_{A}H_{ii} & {}_{A}H_{im} & 0 \\ {}_{A}H_{mi} & {}_{A}H_{mm} & 0 \\ 0 & 0 & {}_{B}H_{ii} \end{bmatrix}-\begin{bmatrix} {}_{A}H_{im} \\ {}_{A}H_{mm} \\ -{}_{B}H_{im} \end{bmatrix}({}_{A}H_{mm}+{}_{B}H_{mm}])^{-1}\begin{bmatrix} {}_{A}H_{im} \\ {}_{A}H_{mm} \\ -{}_{B}H_{im} \end{bmatrix}^{T} \qquad \text{C.10}$$

which is exactly the same as the RC formulae

APPENDIX D
NUMBER OF MULTIPLICATION FOR MATRIX INVERSION USING GAUSSIAN-ELIMINATION METHOD

Gaussian-elimitation is an algorithm which turns an extended matrix [A: I] into a matrix [I: B] through linear combination of rows in the extended matrix. The matrix [B] is the inverse of the matrix [A].

Figure 5.1 shows sub-stages of the elimination process and the number of multiplications required at each stage.

The total number of mutiplications N is the sum of the multiplication at each step, hence

$$N=\sum_{i=1}^{m-1}\{2(m-i)(m+1)\}+m^2$$

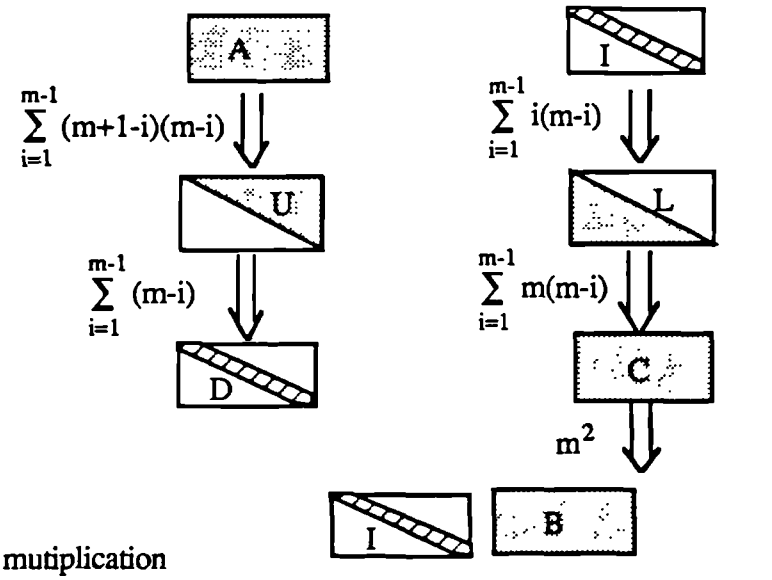

Tatol mutiplication

$$N=m^2+\sum_{i=1}^{m-1}(m+1-i)(m-i)+\sum_{i=1}^{m-1} i(m-i)+\sum_{i=1}^{m-1} m(m-i)+\sum_{i=1}^{m-1}(m-i)$$

$$=m^2+\sum_{i=1}^{m-1} 2(m+1)(m-i)$$

NB: A -- the matrix to be inverted
B -- the inverse of matrix A
U -- a upper triangular matrix
L -- a lower triangular matrix
C -- a full size matrix
D -- a diagonal matrix

Figure D.1 A schematic diagram for the number of multiplications required to invert a matrix

REFERENCES

[1] Ewins, D J
"Modal analysis:Theory and Practice"
Research Studies Press LTD, John Wiley&SONS INC, 1985.

[2] Bathe, K J
"Finite Element Procedures in Engineering Analysis"
Prentice-Hall. 1982

[3] Beards, C F
"The Damping of Structural Vibration by Controlled Interfacial Slip in Joints"
An ASME publication, 81-DET-86.

[4] Ren, Y
"Damping in Structural Joints"
M.Sc Thesis. Imperial College, London University, 1988.

[5] Earles, S W E and Mott, N
"A Response Predication and Optimisation of a Frictionally Damped Structure"
The 13th International MTD&R Conference, Manchester University, September, 1972. Paper 43.

[6] Earles, S W E and Mansoor, F S
"Frictional Damping applied to a Cantilevel-beam Structure: A Theoretical and Experimental Response Comparison".
Int. J. Mach. Tool. Des. Res, Vol.14, pp111-124, 1974

[7] Williams, E J and Earles, S W E
"Optimization of the Response of Frictionally Damped Beam Type Structures with Reference to Gas Turbine Compressor Blading"
Journal of Engineering for Industry. ASME, Vol. 76 pp471-476, 1974.

[8] Beards, C F and Neroutspoulos, A A
"The Control of Structural Vibration by Frictional Damping in Electro-discharge Machined Joints"
An ASME publication, NO.79-DET-79.

[9] Beards, C F and Imam, I M A
"The Damping of Plate Vibration by Interfacial Slip Between Layers".
International Journal of Machine Tool Design and Research, Vol.18, pp131-137. 1978

[10] Beards, C F and Williams, J L
"The Damping of Structural Vibration by Rotational Slip in Joints"
Journal of Sound and Vibration, Vol.53(3), pp333-340, 1977.

[11] Beards, C F and Woowat, A
"The control of frame vibration by friction damping in joints"
An ASME publication, 83-DET-76,1983

[12] Beards, C F
"Some Effects of Interface Preparation on Frictional Damping in Joints"
Int. J. Mach. Tool. Des. Res, Vol.15, pp77-83, 1975.

[13] Beards, C F and Robb, D A
"The Use of Frictional Damping to Control the Vibration of the Plates in Structures".
International Conference on Recent Advances in Structural Dynamics, Southampton, England. pp749-760, July, 1980.

[14] Dowell, E H and Schwartz, H B
"Forced Response of a Cantilever Beam with a Dry Friction Damper Attached, Part I: Theory"
Journal of Sound and Vibration, Vol.91(2), pp255-267, 1983

[15] Dowell, E H and Schwartz, H B
"Forced Response of a Cantilever Beam with a Dry Friction Damper Attached, Part II: Experiment"
Journal of Sound and Vibration, Vol.91(2), pp269-291, 1983.

[16] Menq, C H, Bielak, J and Griffin, J H
"The Influence of Microslip on Vibratory Response, Part I: A New Microslip Model"
Journal of Sound and Vibration. Vol.107(2), pp279-293, 1986.

[17] Menq, C H, Griffin, J H and Bielak J
"The Influence of Microslip on Vibratory Response, Part II: A Comparison with Experimental Results"
Journal of Sound and Vibration. Vol. 107(2), pp295-307, 1986

[18] Cuschieri, J M and Desai, V R.
"Friction Damping due to Interfacial Slip"
Proceedings of the 3nd International Conference on Recent Advance in Structural Dynamics, pp449-458, 1988

[19] Jones, D I G and Muszynska, A
"Effect of Slip on Response of a Vibrating Compressor Blade"
An ASME publication, 77-WA/GT-3. 1977.

[20] Martins, J A C, Oden, J T and Simone, F M F
"A Study of Static and Kinetic Friction"
International Journal of Engineering Science, No.1, pp29-91, 1990

[21] Den Hartog, J P
"Forced Vibrations with Combined Coulomb and Viscous Friction"
Journal of Applied Mechanics, ASME, APM-53-9, pp107-115, 1931.

[22] Yeh, G C K
"Forced Vibrations of a Two-degree of Freedom System with Combined Coulomb and Viscous Friction"
J.Acoust. Soc. Am, Vol. 39, pp14-24, 1966

[23] Levina, Z M
"Research on the Static Stiffness of Joints in Machine Tools"
Proceedings of the 8th International. MTDR Conference. pp737-758,
University of Manchester Sept, 1967.

[24] Mindlin, R D, Masan, W P, Omer, T F, and Dereiswicz, H
"Effects of an Oscillating Tangential Force on the Contact Surfaces of Elastic Spheres"
Proceedings of the 1st US National Congress on Applied Mechanics, pp203-208, 1951.

[25] Goodman, L E and Brown, C B
"Energy Dissipation in Contact Friction: Constant Normal and Cyclic Tangential Loading"
Journal of Applied Mechanics, ASME, Vol. 32, pp17-22, 1962.

[26] Earles, S W E and Philpot, M G
"Energy Dissipation at Plane Surfaces in Contact"
Journal of Mechanical Engineering Science, Vol.9, No2, pp86-97, 1967.

[27] Dekoninck, C
"Deformation Properties of Metallic Contact Surfaces of Joints under the Influence of Dynamic Tangential Loads".
Int J. Mach. Tool Des. Res, Vol.12, pp193-199, 1972.

[28] Masuko, M, Ito, Y and Fujmoto, C
"Behaviour of the Horizontal Stiffness and the Micro-sliding on the Bolted Joint under the Normal Pre-load"
The 12th International MTDR Conference, University of Manchester, paper 1007, September, 1971

[29] Masuko, M, Ito, Y and Koizumi, T
"Horizontal Stiffness and Micro-slip on a Bolted Joint Subjected to Repeated Tangential Static Loads"
Bulletin of the JSME. Vol. 17, No 113. pp1494-1501, 1974

[30] Rogers, P F and Boothroyd, G
"Damping at Metallic Interfaces Subjected to Oscillating Tangential Loads"
Journal of Engineering for Industry, ASME. Vol.97, pp1087-1093, 1975

[31] Kirsanova, V N
"The Shear Compliance of Flat Joints"
Machines &Tooling Vol. XXXVIII. pp30-34, 1967.

[32] Burdekin, M, Back, N and Cowley, A
"Experimental Study of Normal and Shear Characteristics of Machined Surfaces in Contact"
Journal of Mechanical Engineering Science. Vol.20, No.3, pp129-132, 1978.

[33] Bell, R and Burdekin, M
"A study of the Stick-slip Motion of Machine Tool Feed Drives"
Proc Instn Mech Engrs. Vol.184. Pt.1. No.30. pp543-555, 1969-70.

[34] Padmanabhan, K K and Murty, A S R
"Damping in structural Joints Subjected to Tangential Loads"
Proc Instn Mech Engrs. Vol. 205. pp121-129, 1991

[35] Villanueva-Leal, A and Hinduja, S
"Modelling the Characteristics of Interface Surfaces by the Finite Element Method".
Proc Instn Mech Engrs, Vol.198c. No.4, pp9-23, 1984

[36] Vinogradov, O G and Pivovarov, I
"Vibrations of a System with Nonlinear Hysteresis"
Journal of Sound and Vibration. Vol.111(1). pp145-152, 1986

[37] Pivovarov.I and Vinogradov.O.G
"One Application of Bouc's model for Non-linear Hysteresis"
Journal of Sound and Vibration. Vol 118(2).pp209-216, 1987

[38] Wen, Y K
"Method for Random Vibration of Hysteretic Systems"
Journal of the Engineering Mechanics Division. ASCE. No EM2. pp249-263, 1976.

[39] Oden, J T and Pires, E B
"Nonlocal and Nonlinear Friction Laws and Variational Principles for Contact Problems in Elasticity"
Journal of Applied Mechanics, ASME. Vol.50, pp67-76, 1983.

[40] Srinivasan, A V and Cassenti, B N
"A Nonlinear Theory of Dynamic Systems with Dry Friction Forces"
Journal of Engineering for Gas Turbines and Power, ASME. Vol.108, pp525-530, 1986

[41] Pian, T H H and Hallowell, F C
"Structural Damping in a Simple Built-up Beam"
Proceedings of the 1st US National Congress on Applied Mechanics, pp97-102, 1951

[42] Mindlin, R D and Deresiewicz, H
"Elastic Spheres in Contact under Varying Oblique Forces"
Journal of Applied Mechanics, ASME. Vol.20, pp327-344, 1953

[43] Pian, T H H
"Structural Damping of a Simple Built-up Beam with Riveted Joints in Bending"
Journal of Applied Mechanics, Vol.24, pp35-38, 1957

[44] Iwan, W D
"On a Class of Models for the Yielding Behaviour of Continuous and Composite Systems"
Journal of Applied Mechanics, ASME, Vol.64, pp612-617, 1967

[45] Metherell, A F and Diller, S V
"Instantaneous Energy Dissipation Rate in a Lap Joint-uniform Clamping Pressure".
Journal of Applied Mechanics, ASME. Vol.65, pp123-128, 1968

[46] Ungar, E E
"The Status of Engineering Knowledge Concerning the Damping of Built-up Structures"
Journal of Sound and Vibration, Vol.26(1), pp141-154, 1973

[47] Richardson, R S H and Nolle, H
"Energy Dissipation in Rotary Structural Joints"
Journal of Sound and Vibration. Vol. 54(4), pp577-588, 1977

[48] Burdekin, M, Cowley, A and Back, N
"An Elastic Mechanism for the Micro-Sliding Characteristics between Contacting Machined Surfaces"
Journal of Mechanical Engineering Science. Vol.20, No.3, pp121-127, 1978.

[49] Shoukry, S N
"A Mathematical Model for the Stiffness of Fixed Joints Between Machine Parts"
Proceedings of the NUMETA '85 Conference, pp851-858, Swansea, 1985.

[50] Shoukry, S N
"Assessment of Frictional Damping in Tangentially Loaded Metallic Interfaces"
Proceedings of the3rd International Conference on Recent Advances in Structural Dynamics, pp437-448, University of southampton, 18-22 July 1988.

[51] Menq, C H
"Modeling and Vibration Analysis of Friction Joints"
Journal of Vibration, Acoustics, Stress, and Reliability in Design, ASME. Vol.111, pp71-76, 1989

[52] Iwan, W D
"The Steady-State Response of a Two-degree-of-freedom Bilinear Hysteretic System"
Journal of Applied Mechanics, ASME, Vol.62. pp151-156, 1965.

[53] Dowell, E H
"The Behaviour of a Linear, Damped Modal System with a Non-linear Spring-mass-dry Friction Damper System Attached"
Journal of Sound and Vibration. Vol.89(1). pp64-84, 1983

[54] Ferri, A A and Dowell, E H
"The Behaviour of a Linear, Damped Modal System with a Non-linear Spring-mass-dry Friction Damper System Attached, Part II"
Journal of Sound and Vibration. Vol.101(1). 55-74, 1985.

[55] Dowell, E H
"Component Mode Analysis of a Simple Non-linear, Non-conservative System",
Journal of Sound and Vibration. Vol.80(2). pp233-246, 1982

[56] Sinha, A and Griffin, J H
"Stability of Limit Cycles in Frictionally Damped and Aerodynamically Unstable Rotor Stages"
Journal of Sound and Vibration, Vol.103(3), pp341-356, 1985

[57] Menq, C H and Griffin, J H
"A comparison of Transient and Steady State Finite Element Analyses of the Forced Response of a Frictionally Damped Beam"
Journal of Vibration, Acoustics, Stress, and Reliability in Design, ASME, Vol.107, pp19-25, 1985.

[58] Menq, C H, Griffin, J H and Bielak, J
"The Forced Response of Shrouded Fan Stages"
Journal of Vibration, Acoustics, Stress, and Reliability in Design, ASME, Vol.108, pp50-55, 1986

[59] Menq, C H, Griffin, J H and Bielak, J
"The Influence of a Variable Normal Load on the Forced Vibration of a Frictionally Damped Structure"
Journal of Engineering for Gas Turbines and Power, ASME, Vol.108, pp300-305, 1986

[60] Griffin, J H and Menq, C H
"Friction Damping of Circular Motion and Its Implication to Vibration Control"
Journal of Vibration, Acoustics, Stress, and Reliability in Design, ASME, Vol.113, pp225-229, 1991.

[61] Menq, C H and Chidamparma, P
"Friction Damping of Two Dimensional Motion and Its Application in Vibration Control"
Journal of Sound and Vibration, Vol.144(3), pp427-447, 1991.

[62] Anderson, J R and Ferri, A A
"Behaviour of a Single-degree-of-freedom System with a Generalised Friction Law"
Journal of Sound and Vibration, Vol.140(2), pp287-304, 1990.

[63] Pierre, C, Ferri, A A and Dowell, E H
"Multi-harmonic Analysis of Dry Friction Damped Systems Using an Incremental Harmonic Balance Method"
Journal of Applied Mechanics, ASME, Vol.52, pp958-964, 1985.

[64] Ferri, A A and Dowell, E H
"Frequency Domain Solutions to Multi-degree-of-freedom, Dry Friction Damped Systems"
Journal of Sound and Vibration, Vol.124(2), 207-224, 1988.

[65] Cameron, T M and Griffin, J H
"An Alternating Frequency/Time Domain Method for Calculating the Steady-state Response of Nonlinear Dynamic Systems"
Journal of Applied Mechanics, ASME, Vol. 56, pp149-154, 1989.

[66] Pratt, T K and Williams, R
"Non-linear Analysis of Stick-slip Motion"
Journal of Sound and Vibration, Vol.74(4), pp531-542, 1981.

[67] Muszynska, A and Jones, D I G
"On Tuned Bladed Disk Dynamics:Some Aspects of Friction Related Mistuning"
Journal of Sound and Vibration, Vol.86(1), pp107-128, 1983.

[68] Shaw, S W
"On the Dynamic Response of a System with Dry Friction"
Journal of Sound and Vibration, Vol.108(2), pp305-325, 1986.

[69] Vinogradov, O
"Effect of Frequency on Losses in a Dry Friction Joint"
The DAMPING 89 conference, pp2-10, Florida, U.S.A, February 1989.

[70] Dweib, A H and D'Souza, A F
"Self-excited Vibrations Induced by Dry Friction, Part 1: Experimental Study",
Journal of Sound and Vibration, Vol.137(2), pp163-175, 1990.

[71] Dweib, A H and D'Souza, A F
"Self-excited Vibrations Induced by Dry Friction, Part 2: Stability and Limit-cycle Analysis"
Journal of Sound and Vibration, Vol.137(2), pp177-190, 1990.

[72] Paranjpe, R S
"Dynamic Analysis of a Valve Spring with a Coulomb-friction Damper"
Journal of Mechanical Design, ASME, Vol.112, pp509-513, 1990

[73] Cheng, S P and Perkins, N C
"The Vibration and Stability of a Friction-Guided Translating String"
Journal of Sound and Vibration, Vol.144(2), pp281-292, 1991.

[74] Thomson, W T
"Analog Computer for Nonlinear System with Hysteresis"
Journal of Applied Mechanics, ASME, Vol.24, pp245-247, 1957.

[75] Jones, D I G
"Recent Advances in Structural Damping"
Proceeding of the 3nd International Conference on Recent Advances in Structural dynamics, pp409-428, 1988.

[76] Thornley, G H, Connolly, R, Barash, M and Koenigsberger, F
"The Effect of Surface Topography Upon the Static Stiffness of Machine Tool joints".
Int. J. Mach. Tool. Des. Res. Vol.5. pp57-74, 1965.

[77] Herrera.I
"Dynamic Models for Masing Type Materials and Structure."
Boletin Sociedad Mexicana De Ingenieria Sismica, Vol.3, pp1-8, 1965

[78] Whiteman, I R
"On the Deviation of the Stress-strain Diagram from a Statistical Approach".
Aerospace Engineering Vol.21, pp56-57&69-73, 1962

[79] Mindlin.R.D
"Compliance of Elastic Bodies in Contact"
Journal of Applied Mechanics. ASME. Vol.16, pp259-268, 1949.

[80] Goodman.L.E and Klumpp.J.H
"Analysis of Slip Damping With Reference to Turbine-Blade Vibration."
Journal of Applied Mechanics. ASME.Vol.23, pp421-429, 1956

[81] Meirovitch.L
"Elements of Vibration Analysis"
Macmillan, 1975

[82] Timoshenko, S, Young, D H and Weaver, J R W
"Vibration Problem in Engineering"
John Wiley & Sons Inc, 1974

[83] Greenwood.J.A
"Surface Modelling in Tribology"
Published in "Applied Surface Modelling" Ed by Creasy.C.F.M and Craggs.C.
Ellis Horwood Limited, 1990.

[84] Brent.R.P
"Algorithms for Minimization without Derivations".
Englewood Cliffs, 1973.

[85] Press, W H, Flannery, P B, Teukolsky, S A and Vetterling, W T
"Numerical Recipes ".
Cambridge University Press, 1988

[86] Hitchins, D
"Finite Element Methods for Structural Dynamics".
Short course note, Imperial College, London SW7, 2AZ. 19-20th June, 1989.

[87] Houbolt.J.C
"A Recurrence Matrix Solution for the Dynamic Response of Elastic Aircraft".
Journal of Aeronautical Science. Vol.17, pp540-550&594, 1950.

[88] Wilson.E.L, Farhoomand.I and Bathe.K.J
"Nonlinear Dynamic Analysis of Complex Structure".
International Journal of Earthquake Engineering and Structural Dynamics. Vol.1. pp241-252, 1973

[89] Newmark.N.M
"A Method of Computation for Structural Dynamics".
A.S.C.E, Journal of Engineering Mechanical Division. Vol.85, pp67-94, 1959

[90] Macneal, R H
"NASTRAN Theoretical Manual."
The Macneal-Schwendler Corporation, 1972

[91] Guyan, R J
"Reduction of Stiffness and Mass Matrices"
AIAA, Vol.3, p380, 1965

[92] Yao, M S
"Linear and Geometrically nonlinear structural dynamic analysis using reduced basis finite element technique"
Ph.D thesis, Imperial College, London University, 1990

[93] Ewins, D J and Imregun, M
"State-of-the-Art Assessment of Structural Dynamic Response Analysis Methods(DYNAS)"
Shock and Vibration Bulletin, Vol. 56, pp59-90, 1986.

[94] Minorsky, N
"Nonlinear Oscillations"
Robert E. Krieger Publishing Company. Florida. 1988

[95] Lau, S L and Cheung, Y K
"Amplitude Incremental Variational Principle for Nonlinear Vibration of Elastic Systems"
Journal of Applied Mechanics, ASME, Vol.48, pp959-964, 1981.

[96] Lau, S L, Cheung, Y K and Wu, S Y
"A Variable Parameter Incrementation Method for Dynamic Instability of Linear and Nonlinear Elastic Systems".
Journal of Applied Mechanics, ASME, Vol.49, pp849-853, 1982.

[97] Cheung, Y K and Chen, S H
"Application of the Incremental Harmonic Balance Method to Cubic Non-linearity Systems".
Journal of Sound and Vibration, Vol.140(2), pp273-286, 1990.

[98] Cooley, J W, Lewis, P and Welch, P
"Historical notes on the Fast Fourier Transform"
IEEE Transactions on Audio and Electroacoustics, Vol.AU-15, pp76-79, 1967

[99] Urgueira, A P V
"Dynamic Analysis of Coupled Structures Using Experimental Data"
Ph.D thesis, Imperial College, London University, 1989.

[100] Hurty.W.C
"Dynamic Analysis of Structural Systems Using Component Modes"
AIAA Journal, Vol.3(4), pp678-685, 1965

[101] Craig.R.R and Bampton.M.C.C
"Coupling of Substructures for Dynamic Analysis"
AIAA Journal, Vol.6(7), pp1313-1319, 1968

[102] Hou.S
"Review of Modal Synthesis Techniques and a New Approach"
Shock and Vibration Bulletin, Vol.40 (4), pp25-39, 1969

[103] Imregun.M, Robb.D.A and Ewins.D.J
"Structural Modification and Coupling Dynamic Analysis Using Measured FRF Data"
The 5th IMAC, pp1136-1141, 1987

[104] Tsai, J S and Chou, Y F
"The Jdentification of Dynamic Characteristics of a Single Bolt Joint"
Journal of Sound and Vibration, Vol. 125(3), pp487-502, 1988

[105] Newland, D E
"An Introducation to Random Vibration and Spectral Analysis"
Longman, New York, 1984.

[106] Robb, D A
"User's Guide to Program MODENT"
Dynamic section, Dept of Mech. Eng, Imperial College, London, U.K.

[107] Otte, D, Leuridan, J, De Vis, D Grangier, H and Aquilina, R
"Coupling of Structure Using Measured FRFs by means of SVD Based Data Reduction Techniques"
The 8th IMAC, Florida. pp213-220. 1990

[108] Penrose, R
"A Generalized Inverse for Matrices" Pro.Camb.Phil.Sco Vol.51, pp406-413, 1955.

[109] Penrose, R
"On Best Approximate Solutions of Linear Matrix Equations"
Proc.Camb.Phil.Soc, Vol.52, pp17-19, 1956

[110] Huckelbridge, A A and Lawrence, C
"Identification of Structural Interface Characteristics using Component Mode Synthesis".
Journal of Vibration, Acoustic, Stress and Reliability in Design. ASME Vol.111. pp140-147, 1989.

[111] Carneiro, S H S and Arruda, J R F
"Updating Mechanical Joint Properties Based On Experimentally Determined Modal Parameters"
The 8th IMAC. pp1169-1175, 1990.

[112] Wang, J H and Liou, C M
"Experimental Substructure Synthesis with Special Consideration of Joint Effect"
The International Journal of Analytical and Experimental Modal Analysis, Vol.5(1), pp1-12, January 1989.

[113] Hong, S W and Lee, C W
"Identification of Linearised Joint Structural Parameters By Combined Use of Measured and Computed Frequency Responses"
Mechanical Systems and Signal Process, Vol.5(4), pp267-277, 1991

[114] Lin, R M and Ewins, D J
"Modal Updating Using FRF Data"
Proc. the 15th International Seminar on Modal Analysis, pp141-162, K.U.Leuven, Belgium, Sept 1990.

[115] Friswell, M I and Penny, J E T
"Updating Model Parameters Directly from Frequency Response Data"
The 8th IMAC, pp843-849, 1990

[116] Isenberg, J
"Progressing from Least Squares to Bayesian Estimation"
An ASME publication, No. 79-WA/DSC-16, 1979.